School of Life Sciences
University of Nottingham

Investigating the Roles of the Gliovasculature and Neuroinflammation on Secondary Pain in Peripheral Inflammation

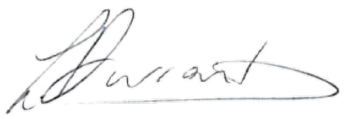
Alexandra Durrant

Thesis submitted to the University of Nottingham for the degree of Doctor of Philosophy

January 2021

Declaration

I, Alexandra Margaret Durrant, confirm that the work presented in this thesis was carried out in accordance with the requirements of the University's Regulations and Code of Practice for Research Degree Programs, and that it has not been submitted for any other academic award. I confirm that the work and views demonstrated in this thesis are my own. Where information has been derived from other sources, I confirm this has been indicated in the thesis.



8th Jan 2021

Name

Date

Abstract

Rheumatoid Arthritis (RA) is an autoimmune disease that results in inflammation, damage, pain and stiffness in joints. Patients with RA often complain of pain despite inflammation being well managed, or pain in areas with no associated inflammation or damage. This is referred to as secondary or referred pain, and is a hallmark of central sensitisation. As well as neuronal hyperactivity in the dorsal horn of the spinal cord, there is glial activation and neuroinflammation, both of which are thought to contribute to central sensitisation and the resulting chronic pain. Neural endothelial cells are key components of blood-neural barriers, such as the Blood Spinal Cord Barrier (BSCB), and of the Neurovascular Unit (NVU). There is evidence of BSCB disruption in chronic pain conditions like inflammatory arthritis, and there is an emerging role of neural endothelial cells in contributing to central sensitisation and chronic inflammatory pain.

In this thesis, secondary pain was induced through intra-articular Complete Freund's Adjuvant (CFA), and the gliovascular response and contribution was investigated through histology, knockdown of endothelial cell-specific Vascular Endothelial Growth Factor Receptor (VEGF-R)2, and pharmacological inhibition of VEGF-R2 and/or Tumour Necrosis Factor α (TNFα). Additionally, single cell *in vivo* electrophysiology was employed to investigate the neural response to TNFα, and *in vitro* studies investigated Human Brain Microvascular Endothelial Cell (HBMEC) responses to TNFα and Vascular Endothelial Growth Factor (VEGF)-A_{165}a.

Peripheral inflammation induced robust secondary pain, which was neither prevented or reversed with VEGF-R2 or TNFα inhibition. However, a combination of both VEGF-R2 and TNFα inhibition partially reversed established secondary pain. Peripheral inflammation also led to astrocyte activation in the dorsal horn of the spinal cord. Endothelial-specific VEGF-R2 knockout prevented secondary pain development and associated gliovascular alterations (Beazley-Long et al. 2018b). Using analysis techniques developed in this thesis, astrocyte activation was found to be specific to the spinal dorsal horn vasculature. Additionally, TNFα caused an increase in expression of adhesion molecules by and Human Monocyte-like Cells (THP-1) binding to HBMECs. Exogenous intrathecal TNFα had no impact on spinal dorsal horn neuronal signalling, which was attributed to technical issues.

In conclusion these results indicate the gliovasculature, in particular astrocytes and endothelial cells, undergoes activation in chronic inflammatory pain and central sensitisation. They also support the hypothesis that endothelial cells are involved in maintaining chronic pain through their activation by inflammatory mediators and subsequent downstream signalling on glial cells and neurones.

Acknowledgements

Firstly I would like to thank my supervisors, Lucy Donaldson and Nick Beazley-Long. Lucy, your unending support has helped me to continue my PhD journey on several occasions, and you have given me confidence in both my work and myself. You are an inspiration to me both as a professional and as a woman. Thank you. Nick, in no uncertain terms you saved my PhD by agreeing to become my supervisor. Your help and friendship have meant so much to me over the past years and I will miss being desk-mates and running-partners (and hearing you talk work *ad infinitum*).

I will always be grateful to Gareth Hathway for his support and guidance early in my PhD, without his help I would not have started my PhD journey. Thanks must go to Vicky Chapman for her help in early studies and for her continued support in preclinical meetings throughout my project. Also thanks to Dave Bates for his expertise and advice. To Devi Sagar for incredible support and expert guidance in electrophysiology studies. Thank you to Ian Ward and those at SLIM for their help with histology preparations, even if I had to listen to Radio 2 endlessly. Ian Devonshire, Mark Trussell and everyone at BSU, thank you for your help with my *in vivo* work.

I am eternally grateful to everyone who created an amazing work environment and helped me to complete my PhD. I was fortunate enough to be supported by incredible post-docs: James Burston, Steve Woodhams, Pete Gowler, Katie Hodge, Fernanda Lopes and Andy Benest. I can't name everyone who supported me through my studies and enriched my time here but special thanks go to Emma Dayman, Amanda Lillywhite, Zoe Smith, Charles Greenspon, Emma Battell, Matt Swift, and Laura Humphrys. To everyone else in the Hathway-Chapman and Donaldson-Bates labs, you may not be individually named here but I will always be grateful for your love and support.

I would like to thank those who funded me including the BBSRC, the University of Nottingham, the Guarantors of Brain, IASP, ecopa, and the British Microcirculation Society. Without their financial support my work and experience would not have been what it was. I must also thank those who made my experience outside of my PhD so valuable. Thank you to IntoUniversity who provided me with an excellent PIP opportunity during my studies, and to Coach Ray Ricketts who always believed in me.

Lastly, but in no means least, I need to thank my incredible family, patient husband and awesome child (and also my beautiful, stupid dog). Steve, you have supported me from the beginning and put up with so much. I can't put into words how much you and your love mean to me. Lyla, you are hilarious and have perfectly completed my time studying. I love you all, thank you.

Publications

Durrant, A. M., Swift, M. N., and Beazley-Long, N. (2018). 'A role for pericytes in chronic pain?' *Current opinion in supportive and palliative care*, 12(2), 154-161.

Beazley-Long, N., **Durrant, A. M.**, Swift, M. N., and Donaldson, L. F. (2018). 'The physiological functions of central nervous system pericytes and a potential role in pain.' *F1000Research*, 7.

Beazley-Long, N., Moss, C. E., Ashby, W. R., Bestall, S. M., Almahasneh, F., **Durrant, A. M.**, Benest, A.V., Blackley, Z., Ballmer-Hofer, K., Hirashima, M., Hulse, R.P., Bates, D.O., and Donaldson L.F. (2018). 'VEGFR2 promotes central endothelial activation and the spread of pain in inflammatory arthritis.' *Brain, Behavior, and Immunity*.

Conference Abstracts and Awards

Conference Abstracts

Alexandra Durrant, Nicholas Beazley-Long, and Lucy Donaldson. 'Investigating The Contribution Of VEGFR2 and TNFα In The Maintenance Of Inflammatory Pain And The Associated Spinal Glio-Vascular Response.' Oral presentation at: British Microcirculation Society 69^{th} Annual Meeting; Essex, UK. April 2019.

Alexandra Durrant, Catherine Moss, Nicholas Beazley-Long, and Lucy Donaldson. 'Targeting VEGFR2 can Reverse Established Secondary Inflammatory Pain and Prevent the Associated Glio-Vascular Response.' Poster Presentation at: IASP — 17^{th} World Pain Congress; Boston, USA. September 2018.

Awards

British Microcirculation Society Student Assistance Scheme 2019

University of Nottingham Graduate School Travel Prize 2018

Guarantors of Brain Travel Award 2018

BBSRC Strategic Skills Award 2016

ecopa Travel Grant for the FRAME Training School 2016

List of Abbreviations

ABC ATP-Binding Cassette

AIA Antigen-Induced Arthritis

AMPA α-Amino-3-Hydroxy-5-Methylisoxazole-4-Propionate

AMT Adsorptive-Mediated Transcytosis

AP-1 Activator protein 1

ASIC Acid Sensing Ion Channel

ATF-3 Activating Transcription Factor-3

ATP Adenosine Triphosphate

BBB Blood Brain Barrier

BBSRC Biotechnology and Biological Sciences Research Council

BDNF Brain Derived Neurotrophic Factor

BFE Binary Feature Extraction

BNB Blood Nerve Barrier

BSA Bovine Serum Albumin

BSCB Blood Spinal Cord Barrier

BSU Biomedical Support Unit

Calcein-AM Calcein Acetoxymethyl

CCL2 C-C motif Chemokine Ligand 2

CD11b Cluster of Differentiation-11b

CD14 Cluster of Differentiation-14

CD31 Cluster of Differentiation-31

CD68 Cluster of Differentiation-68

cDNA Complementary Deoxyribonucleic Acid

CFA Complete Freund's Adjuvant

CGRP Calcitonin Gene-Related Protein

CHCS Classic Heterosynaptic Central Sensitisation

CIA Collagen-Induced Arthritis

CIPN Chemotherapy-Induced Peripheral Neuropathy

CNS Central Nervous System

COX Cyclooxygenase

CSF Cerebrospinal Fluid

CXCL1 C–X–C Chemokine Ligand 1

dATP Deoxyadenosine Triphosphate

dCTP Deoxycytidine Triphosphate

DEPC Diethyl Pyrocarbonate

dGTP Deoxyguanosine Triphosphate

DMARD Disease Modifying Anti-Rheumatic Drug

DMSO Dimethyl Sulfoxide

DNA Deoxyribonucleic Acid

DNase Deoxyribonuclease

dNTPs Deoxynucleotide Triphosphates

DRG Dorsal Root Ganglion

dTTP Deoxythymidine Triphosphate

dTTP Dithiothreitol

EAE Experimental Autoimmune Encephalomyelitis

EB Evans Blue

ecopa European Consensus-Platform for Alternatives

EDTA Ethylenediaminetetraacetic Acid

EGTA Ethylene Glycol-bis(β-aminoethyl ether)-N,N,N',N'-Tetraacetic Acid

EP4 Prostaglandin E2 receptor 4

F Filial

FBS Foetal Bovine Serum

GABA Gamma-Aminobutyric Acid

GAPDH Glyceraldehyde 3-Phosphate Dehydrogenase

GFAP Glial Fibrillary Acidic Protein

HBMEC Human Brain Microvascular Endothelial Cell

HUVEC Human Umbilical Vein Endothelial Cell

i.p. Intraperitoneal

IASP International Association for the Study of Pain

IB4 Plant Lectin Isolectin B4

IBA-1 Ionized Calcium Binding Adaptor Molecule-1

ICAM-1 Intracellular Adhesion Molecule-1

IFNγ Interferon γ

IgG Immunoglobulin G

IL Interleukin

IL-1β Interleukin-1β

IL10R Interleukin-10 Receptor

IL1R1 Interleukin-1 Receptor-1

IL6R Interleukin-6 Receptor

IntDen Integrated Density

IP Prostaglandin I2 Receptor

JAK Janus Kinase

JAM Junctional Adhesion Molecule

L Lumbar Section

LCN2 Lipocalin-2

LPS Lipopolysaccharide

LTP Long-Term Potentiation

M-MLV Moloney Murine Leukemia Virus Reverse Transcriptase

MAPK Mitogen-Activated Protein Kinase

MCP1 Monocyte Chemoattractant Protein 1

MEA Multi Electrode Array

MEM Minimum Essential Medium

mGluR Metabotropic Glutamate Receptor

MIA Monosodium Iodoacetate

MMP Matrix Metalloproteinase

MND Motor Neurone Disease

mRNA Messenger Ribonucleic Acid

MS Multiple Sclerosis

NADPH Nicotinamide Adenine Dinucleotide Phosphate

Nav Voltage-Gated Sodium Channel

NF-κB Nuclear Factor Kappa-Light-Chain-Enhancer of Activated B Cells

NGF Nerve Growth Factor

NMDA N-Methyl-D-Aspartate

NRP1 Neuropilin-1

NSAID Non-Steroidal Anti-Inflammatory Drug

NVU Neurovascular Unit

OA Osteoarthritis

Oligo-dT Oligo Deoxythymine

p Passage

PAG Periaqueductal Grey

PBS Phosphate Buffered Solution

PBS-Tween Phosphate Buffered Saline-Tween

PCR Polymerase Chain Reaction

PD Post-Discharge

PDGFR-β Platelet Derived Growth Factor Receptor-β

PECAM-1 Platelet and Endothelial Cell Adhesion Molecule-1

PFA Paraformaldehyde

PG Prostaglandin

PGE2 Prostaglandin E2

PGI2 Prostaglandin I2

PMSF Phenylmethylsulfonyl Fluoride

PTGIS Prostaglandin I2 Synthase

RA Rheumatoid Arthritis

RECA-1 Rat Endothelial Cell Antigen-1

RIPA Radio-Immunoprecipitation Assay Buffer

RMT Receptor-Mediated Transcytosis

RNA Ribonucleic Acid

RNase Ribonuclease

ROI Region of Interest

RPE Retinal Pigment Epithelium

RPMI-1640 Roswell Park Memorial Institute-1640 Medium

RT Reverse Transcriptase

RVM Rostroventral Medulla

S100 S100 Calcium-Binding Protein

SD Standard Deviation

SDS Sodium Dodecyl Sulfate

SDS-PAGE Sodium Dodecyl Sulfate–Polyacrylamide Gel Electrophoresis

SerpinA3N Serine Protease Inhibitor A3N

SGC Satellite Glial Cell

SLC Solute Carrier

SLIM School of Life Sciences Imaging

SpD Sprague Dawley

SR Serine/Arginine

SRSF1 Serine/Arginine Splicing Factor 1

SRSF2 Serine/Arginine Splicing Factor 2

STAT3 Signal Transducer and Activator of Transcription-3

TBS Tris Buffered Saline

TBS-Tween Tris Buffered Saline-Tween

TEER Transendothelial Electrical Resistance

THP-1 Human Monocyte-like Cells

TJ Tight Junction

TLR Toll-Like Receptor

TNFR Tumour Necrosis Factor Receptor

TNFα Tumour Necrosis Factor α

TrkA Tropomyosin Receptor Kinase A

TRP Transient Receptor Potential

TRPA1 Transient Receptor Potential cation channel subfamily A member 1)

TRPC Transient Receptor Potential Canonical

TRPM Transient Receptor Potential cation channel subfamily M

TRPM8 Transient Receptor Potential cation channel subfamily M member 8

TRPV Transient Receptor Potential cation channel subfamily V

TRPV1 Transient Receptor Potential cation channel subfamily V member 1

VCAM-1 Vascular Cell Adhesion Molecule-1

VEGF Vascular Endothelial Growth Factor

VEGF-R Vascular Endothelial Growth Factor Receptor

VMpo Ventromedial Posterior Nuclei

VP Ventral Posterior Nuclei

vWF von Willebrand Factor

WDR Wide Dynamic Range

WU Wind-Up

ZEB-1 Zinc Finger E-Box Binding Homeobox-1

ZO-1 Zona Occludens-1

Table of Contents

Abbreviations vi

1 Introduction 1
- 1.1 Rheumatoid Arthritis . . . 1
  - 1.1.1 Animal Models of Inflammatory Pain/Arthritis . . . 2
  - 1.1.2 Measuring Pain in Animal Models . . . 3
- 1.2 The Nociceptive Pathway . . . 4
  - 1.2.1 Nociceptive Fibres . . . 4
  - 1.2.2 Transducer Receptor Subtypes . . . 5
  - 1.2.3 The Dorsal Root Ganglion . . . 5
  - 1.2.4 The Dorsal Horn of the Spinal Cord . . . 6
  - 1.2.5 Ascending Pathways . . . 8
  - 1.2.6 Descending Control . . . 8
  - 1.2.7 Peripheral and Central Sensitisation . . . 10
- 1.3 The Blood-Neural Barriers . . . 16
  - 1.3.1 The Blood-Nerve Barrier . . . 18
  - 1.3.2 Migration Across Blood-Barriers . . . 18
  - 1.3.3 Barrier Alterations during Nociception . . . 20
  - 1.3.4 Measuring Alterations in the Neurovascular Unit . . . 25
  - 1.3.5 VEGF . . . 27
- 1.4 Aims and General Hypothesis . . . 29

2 Materials & Methods 32
- 2.1 Introduction . . . 32
- 2.2 In Vivo Procedures . . . 32
  - 2.2.1 Animal Usage . . . 32
  - 2.2.2 Nociceptive Surgical Procedures . . . 33
  - 2.2.3 Drug Dosing . . . 35
  - 2.2.4 Behavioural Tests . . . 36
  - 2.2.5 Tissue Processing . . . 37
  - 2.2.6 Immunofluorescence . . . 38
  - 2.2.7 Spinal Electrophysiology . . . 38
- 2.3 In Vitro Procedures . . . 42
  - 2.3.1 The Monocyte Attachment Assay . . . 43
  - 2.3.2 Immunofluorescence . . . 43
  - 2.3.3 Western Blotting . . . 44
  - 2.3.4 RNA Isolation and cDNA Generation . . . 45
  - 2.3.5 PCR . . . 45
  - 2.3.6 Absorbance Assay . . . 46

2.4 Statistical Analysis . . . 46

3 Optimisation of In Vivo Immunofluorescence Analyses 47
3.1 Introduction . . . 47
3.2 Materials & Methods . . . 49
3.2.1 Experimental Animals . . . 49
3.2.2 Induction of Peripheral Inflammation . . . 49
3.2.3 Induction of Osteoarthritis . . . 50
3.2.4 Pain Behaviour . . . 51
3.2.5 Histology . . . 51
3.2.6 Immunofluorescence Analysis . . . 51
3.2.7 Statistical Analysis . . . 55
3.3 Results . . . 55
3.3.1 Behavioural Data . . . 55
3.3.2 Validation of Analysis Techniques . . . 57
3.3.3 Astrocyte Activation . . . 62
3.4 Discussion . . . 64

4 VEGF-A and TNFα in the Development and Maintenance of Inflammatory Pain 67
4.1 Introduction . . . 67
4.2 Materials & Methods . . . 72
4.2.1 Experimental Animals . . . 72
4.2.2 Blinding . . . 73
4.2.3 Experimental Design . . . 74
4.2.4 Induction of Peripheral Inflammation . . . 76
4.2.5 Pain Behaviour . . . 77
4.2.6 Inhibition of TNFα and VEGF-R2 . . . 77
4.2.7 Immunofluorescence . . . 78
4.2.8 Immunofluorescence Analysis . . . 79
4.2.9 Cell Culture . . . 80
4.2.10 The Monocyte Attachment Assay . . . 82
4.2.11 Absorbance Assay . . . 84
4.2.12 Statistical Analysis . . . 84
4.3 Results . . . 84
4.3.1 Study 1: Prophylactic Inhibition of VEGF-Receptors and TNFα in Acute Inflammatory Arthritis . . . 84
4.3.2 Study 2: Therapeutic Inhibition of VEGF-Receptors and TNFα in Chronic Inflammatory Arthritis . . . 98
4.3.3 The Central Astrocytic Response to Peripheral Inflammation and the Effect of TNFα Inhibition . . . 101
4.3.4 Study 3: Refined Arthritis Model and Inhibition of VEGF-Receptors and/or TNFα in Chronic Inflammatory Arthritis . . . 108

4.3.5 Differences Between CFA Regimens . . . 124
4.3.6 The Central Gliovascular Alterations in Response to CFA were Prevented in VEGF-R2 KO Mice . . . 128
4.4 Discussion . . . 132
4.4.1 The Effect of VEGF-R2 and/or TNFα Inhibition on Pain . . . 132
4.4.2 Spinal Gliovascular Alterations after CFA . . . 135
4.4.3 Differences in CFA Regimens . . . 139
4.4.4 Limitations . . . 141
4.4.5 Conclusion . . . 143

5 In Vitro Models of Endothelial Cell Activation Using VEGF-A and TNFα 146
5.1 Introduction . . . 146
5.2 Materials & Methods . . . 150
5.2.1 Cell Culture . . . 150
5.2.2 The Monocyte Attachment Assay . . . 150
5.2.3 Immunofluorescence . . . 152
5.2.4 Western Blotting . . . 152
5.2.5 cDNA Generation and Amplification . . . 153
5.2.6 Statistical Analysis . . . 153
5.3 Results . . . 154
5.3.1 The Monocyte Attachment Assay Can Be a Useful Tool to Study Functional Endothelial Responses to Inflammatory Molecules . . . 154
5.3.2 Commercially Available HBMECs Do not Express Typical Endothelial Markers . . . 161
5.4 Discussion . . . 164

6 Spinal Electrophysiology as a Model of Neuroinflammation Using TNFα 170
6.1 Introduction . . . 170
6.2 Materials & Methods . . . 171
6.2.1 Experimental Animals . . . 171
6.2.2 Drugs . . . 172
6.2.3 In Vivo Spinal Electrophysiology . . . 172
6.2.4 Data Analysis . . . 175
6.3 Results . . . 175
6.3.1 Characteristics of WDR Neurones . . . 175
6.3.2 Intrathecal TNFα has No Effect on Spinal WDR Firing . . . 175
6.4 Discussion . . . 176

7 General Discussion and Conclusion 182
7.1 Human Translation . . . 188
7.2 Future Studies . . . 189
7.3 Conclusion . . . 190

Bibliography 190

A Appendices 225
A.1 PIP Reflective Statement 225
A.2 COVID19 Impact Statement 227
A.3 Macros 236
A.3.1 CD31-associated GFAP 236
A.3.2 Laminin-associated GFAP 238
A.3.3 Laminin Overlay on GFAP or ICAM-1 241
A.3.4 RECA-1-associated GFAP 243
A.3.5 RECA-1-associated ZEB1 245
A.3.6 RECA-1-associated ZEB1 Nuclei 247
A.3.7 Cell Coverage 249

List of Figures

1.1 The Dorsal Horn of the Spinal Cord. 6
1.2 Ascending and Descending Nociceptive Tracts. 9
1.3 Classic Heterosynaptic Central Sensitisation vs LTP 12
1.4 Components of the Neurovascular Unit and Endothelial Junctions 17
1.5 Components of the Blood-Nerve Barrier 19
1.6 Barrier Disruptions in Chronic Pain 22
1.7 VEGF-A Splicing Variants 28
1.8 Summary of Thesis Investigation Aims 31

3.1 GFAP and CD31 Immunofluorescence in the Dorsal Horn of the Spinal Cord after Peri-articular CFA in the Mouse 52
3.2 Vessel-Overlay GFAP Analysis 53
3.3 Vessel Lumina are Included in the ROI Overlay Method 54
3.4 Astrocytes Extend Away From the Neurovascular Unit 55
3.5 Vessel-Associated GFAP Structures Are Included in the Overlap Extraction Method 56
3.6 Nociceptive Behaviour after Carrageenan or MIA 57
3.7 Nociceptive Behaviour after Peri-Articular CFA 58
3.8 Validation of Vessel-GFAP Overlay Analysis Technique in the Mouse CFA Model 59
3.9 Validation of Vessel-GFAP Overlap Extraction Analysis Technique in the Mouse CFA Model 60
3.10 GFAP and CD31 Immunofluorescence in the Dorsal Horn of the Spinal Cord after Peri-articular CFA 61
3.11 Global GFAP Intensity after Carageenan or MIA 62
3.12 GFAP and CD31 Immunofluorescence after Carrageenan or MIA 63

4.1 Timeline for Prophylactic VEGF-R Inhibition (Study 1) 74
4.2 Timeline for Therapeutic VEGF-R Inhibition (Study 2) 75
4.3 Timeline for Therapeutic VEGF-R Inhibition (Study 3) 75
4.4 Timeline for Mouse Endothelial Cell VEGF-R2 Knockout 76
4.5 Example of a von Frey Stimulus-Response Curve 78
4.6 Representative Images of Overlay vs Overlap Analysis Techniques 81
4.7 Identification Criteria of Endothelial Cell Nuclei 82
4.8 Criteria for CD68-Positive Cell Counting in the DRG 83
4.9 Weight Bearing and Swelling after Acute Peripheral Inflammation 85
4.10 GFAP in the Dorsal Horn of the Spinal Cord 2 Days after Acute Peripheral Inflammation 86

4.11 Representative Images of GFAP Immunofluorescence after Acute CFA in the Spinal Cord . . . 87
4.12 Correlation of Knee Diameter vs. GFAP Signal in the Spinal Cord 2 Days after Peripheral CFA . . . 88
4.13 CD31 vs Laminin Signal in the Dorsal Horn . . . 89
4.14 Dorsal Horn Microglial CD11b Fluorescence after Acute Peripheral Inflammation . . . 90
4.15 Percentage of CD11b-Positive Microglial Structures in Sections after CFA 91
4.16 Dorsal Horn ICAM-1 Fluorescence after Acute Peripheral Inflammation . 92
4.17 Representative Images of ICAM-1 Immunofluorescence after Acute CFA in the Spinal Cord . . . 93
4.18 Deep Vessel Area in the Spinal Cord after Acute Peripheral CFA . . . 94
4.19 Representative Images of CD68-Positive DRG Neurones in Test and Control Antibody Tissue . . . 95
4.20 CD68 Fluorescence and Positive Cell Count in the DRG after Acute Peripheral Inflammation . . . 96
4.21 Representative Images of CD68 Immunofluorescence in the DRG after Acute CFA . . . 97
4.22 Behavioural Data after Peripheral CFA . . . 99
4.23 Change in Mechanical Threshold from Day 3 after Intra-Articular CFA . . 100
4.24 Monocyte Attachment Assay using Experimental PTK787 . . . 101
4.25 GFAP in the Spinal Cord 10 days after Peripheral CFA . . . 102
4.26 Representative Images of GFAP Signal in the Spinal Cord 10 days after Peripheral CFA . . . 103
4.27 Correlation of Knee Diameter vs. GFAP Signal in the Spinal Cord 10 Days after Peripheral CFA . . . 104
4.28 CD11b and ICAM-1 Fluorescence in the Spinal Cord 10 days after Peripheral CFA . . . 105
4.29 Representative Images of CD11b Signal in the Spinal Cord 10 days after Peripheral CFA . . . 106
4.30 Representative Images of ICAM-1 Signal in the Spinal Cord 10 days after Peripheral CFA . . . 107
4.31 Deep Vessel Area in the Spinal Cord 10 days after Peripheral CFA . . . 108
4.32 Behavioural Data after Low Dose Peripheral CFA . . . 109
4.33 Change in Mechanical Threshold from Day 3 after Low Dose Intra-Articular CFA . . . 110
4.34 GFAP Signal in the Spinal Cord 10 days after Low Dose Peripheral CFA . 111
4.35 Representative Images of GFAP Signal in the Spinal Cord 10 days after Low Dose Peripheral CFA . . . 112
4.36 Correlation of Knee Diameter vs. GFAP Signal in the Spinal Cord 10 Days after Low Dose Peripheral CFA . . . 113

4.37 Representative Images of Superficial Vs Deep Segregation in the Spinal Cord . . . 114
4.38 Higher Powered GFAP Signal in the Spinal Cord 10 days after Low Dose Peripheral CFA . . . 114
4.39 Representative Images of GFAP Signal in the Superficial Dorsal Horn of the Spinal Cord 10 days after Low Dose Peripheral CFA . . . 115
4.40 Representative Images of GFAP and ICAM-1 Signal in the Deep Dorsal Horn of the Spinal Cord after Peripheral CFA (50µg) . . . 116
4.41 Vessel-Associated GFAP Signal in the Spinal Cord after Peripheral CFA (50µg) . . . 117
4.42 CD11b Signal in the Spinal Cord 10 days after Low Dose Peripheral CFA 118
4.43 Representative Images of CD11b Signal in the Spinal Cord 10 days after Low Dose Peripheral CFA . . . 119
4.44 High Powered ICAM Signal in the Spinal Cord 10 days after Peripheral Low Dose CFA . . . 120
4.45 Vessel Area in the Spinal Cord 10 days after Low Dose Peripheral CFA . . 121
4.46 Immunofluorescence of ZEB-1 Signal in the Spinal Cord 10 days after Low Dose Peripheral CFA . . . 122
4.47 Representative Images of ZEB-1 Signal in the Spinal Cord after Peripheral CFA (50µg) . . . 123
4.48 Area of Nuclear-ZEB-1 Signal in the Spinal Cord 10 days after Low Dose Peripheral CFA . . . 124
4.49 Comparison of Knee Diameter, Weight Bearing and von Frey Data Between Three CFA Regimes . . . 125
4.50 Comparison of Late Glial Changes Between Two CFA Regimes . . . 126
4.51 Representative Images of Late Glial Changes Between Two CFA Regimes 127
4.52 Pain Behaviour after Endothelial Cell VEGF-R2 KO . . . 129
4.53 GFAP in the Spinal Cord after Peri-Articular CFA . . . 130
4.54 Representative Images of GFAP Signal in the Spinal Cord after Peri-Articular CFA . . . 131
4.55 Sex Differences in Spinal Astrocyte Response after Peri-Articular CFA in the Mouse . . . 132
4.56 Correlation of Cartilage Damage vs. Knee Diameter at Day 10 . . . 141

5.1 THP-1s Adhere to Fibronectin Coating . . . 151
5.2 Monocyte Attachment to High Passage HBMECs after TNFα . . . 154
5.3 TNFα-Induced Monocyte Binding to HBMECs can be Reduced with the Addition of an ICAM-1 Blocking Antibody . . . 156
5.4 Monocyte Fluorescence after TNFα or VEGF-A_{165}a Treatment on ScienCell HBMECs . . . 157
5.5 HBMEC Coverage is Not Dependent on Treatment . . . 158
5.6 Representative Images of HBMEC Coverage after TNFα or VEGF-A_{165}a Treatment . . . 159

5.7 The Addition of an ICAM-1 Blocking Antibody does not Reduce Monocyte Binding to ScienCell HBMECs 160
5.8 Endothelial Cell Western Blot after TNFα or VEGF-A_{165}a Treatment 161
5.9 Brain Microvascular Endothelial Cell (High Passage) PCR after TNFα or VEGF-A_{165}a Treatment 162
5.10 Brain Microvascular Endothelial Cell (Low Passage) PCR after TNFα or VEGF-A_{165}a Treatment 163

6.1 Electrophysiology Setup 173
6.2 Electrophysiology Study Timeline 174
6.3 Spinal Electrophysiology Responses to Intrathecal TNFα or Vehicle 176
6.4 Fibre-Specific Responses to Intrathecal TNFα 177
6.5 Area under the Curve of Fibre-Specific Responses to Intrathecal TNFα . 178

7.1 Acute Inflammatory Pain Signalling in the Periphery and Spinal Cord . . 183
7.2 Receptors and Transmitters in Acute Inflammatory Pain Signalling in the Spinal Cord 184
7.3 The Contribution of the Gliovasculature to Chronic Inflammatory Pain Signalling in the Periphery and Spinal Cord 185
7.4 Receptors and Transmitters Involved in the Gliovasculature's Contribution to Chronic Inflammatory Pain Signalling in the Spinal Cord 186

List of Tables

1.1 Summary of Barrier Disruptions and Consequences in Painful Conditions 24

2.1 Details of Primary Antibodies 39
2.2 Details of Secondary Antibodies 39

3.1 Animal Numbers for In Vivo Method Development Pilot Studies 50
3.2 Details of Antibodies and Probes for In Vivo Method Development 51

4.1 Animal Numbers for In Vivo Studies 73
4.2 Details of Primary Antibodies for In Vivo Studies 79
4.3 Details of Secondary Antibodies for In Vivo Studies 79
4.4 Approximate Spinal Cord Locations 85
4.5 PTK787 Activity 100
4.6 Summary of In Vivo Experimental Findings 144
4.7 Summary of Effect of CFA Dose on Experimental Outcomes 145

5.1 Details of Primary Antibodies for In Vitro Studies 152
5.2 Details of Secondary Antibodies for In Vitro Studies 152
5.3 Sequence of PCR Primers 153
5.4 Summary of HBMEC Experimental Responses 168
5.5 Summary of HBMEC Expression 169

6.1 Characteristics of Recorded Cells 175

1 | Introduction

The ability of an organism to detect painful or noxious stimuli through the nociceptive system is an essential survival mechanism as it helps to protect against damage. There is a distinction between *pain* and *nociception*, with the former defined as the "unpleasant sensory and emotional experience associated with ... actual or potential tissue damage" (Raja et al. 2020), whereas the latter refers to the detection and signalling of noxious stimuli. If actual damage occurs, the nociceptive system and resulting acute pain alerts the organism so it can protect the site of injury until wound healing has been completed. However, in some cases, pain can persist past healing, and can lead to reduced quality of life and significant economic costs (Smith and Torrance 2012). It is difficult to accurately state the prevalence of chronic pain in a population, but it has been estimated that up to 20% of adults have chronic pain (Goldberg and McGee 2011).

Persistent pain lasting for 3 or more months in humans is defined as chronic pain (Treede et al. 2019), and peripheral and central nociceptive signalling alterations are key in driving this chronic pain (Latremoliere and Woolf 2009). Constant activation of the nociceptive pathway can cause both neuronal and glial cell alterations within the Central Nervous System (CNS), leading to increased sensitivity (allodynia) and enhanced pain (hyperalgesia) (Gosselin et al. 2010; Costigan et al. 2009b; Latremoliere and Woolf 2009).

Glial cells primarily play a role in protecting neurones by maintaining the CNS microenvironment, and are aided by the presence of anatomical barriers such as the Blood Brain Barrier (BBB) and Blood Spinal Cord Barrier (BSCB). These barriers are pivotal in controlling entry of molecules and cells into the CNS (Salter and Beggs 2014), but under neuropathic (involving nerve damage) and inflammatory conditions, barrier integrity can become compromised to allow infiltration of non-neuronal cells and molecules. These blood-borne cells can, along with glial cells, release substances that can directly sensitise, activate, and even injure neurones (Varatharaj and Galea 2016).

1.1 Rheumatoid Arthritis

Rheumatoid Arthritis (RA) is a chronic autoimmune condition that affects the joints and causes inflammation, pain and stiffness. To manage the inflammation, patients are first offered conventional Disease Modifying Anti-Rheumatic Drugs (DMARDs) which suppress the immune system (National Institute for Health and Care Excellence 2018). However, this is not always enough to alleviate associated pain as many patients can complain of pain during periods of low inflammation or in areas with no inflammation (known as referred or secondary pain) (Boyden et al. 2016). In order to develop treat-

ments to successfully alleviate this pain, determining the reason why patients with little or no inflammation still experience pain is vital. In RA and other chronic pain conditions, there are central changes in nociceptive signalling at both spinal and supraspinal levels (Boyden et al. 2016; Walsh and McWilliams 2014), which may be attributed to activated glial cells/neuroinflammation (Flores Bjurström et al. 2020; Jung et al. 2020; Albrecht et al. 2018). As well as this, central endothelial cells may be involved in contributing to glial activation and neuroinflammation (and therefore nociceptive signalling) through endothelial release of inflammatory molecules and infiltration of blood-borne cells and molecules (DosSantos et al. 2014; Radu et al. 2013; Zlokovic 2011). For example, patients with RA show signs and markers of endothelial dysfunction, and have an increased risk of cardiovascular diseases (Chimenti et al. 2015; Steyers and Miller 2014). Circulating inflammatory molecules, such as Tumour Necrosis Factor α (TNFα) and Vascular Endothelial Growth Factor (VEGF), that are increased in RA (Totoson et al. 2016; Wei et al. 2015; Nakahara et al. 2003) have the potential to 'activate' endothelial cells to release inflammatory factors, decrease tight junction protein expression and increase adhesion molecule expression, therefore increasing permeability (Chimenti et al. 2015; Steyers and Miller 2014).

1.1.1 Animal Models of Inflammatory Pain/Arthritis

As there are obvious practical and ethical obstacles in researching human diseases, animal and cell models can be used to investigate disease mechanisms. There are several models of RA, including Collagen-Induced Arthritis (CIA) and Antigen-Induced Arthritis (AIA), in which arthritis is induced by immunising the animal with collagen or an injected antigen (for example methylated bovine serum albumin) respectively (Asquith et al. 2009). These models use Complete Freund's Adjuvant (CFA) as an adjuvant to enhance the immune response, but a single peri-articular injection of CFA alone is sufficient to induce arthritis (Donaldson et al. 1993; Grubb et al. 1988). CFA is composed of heat-killed *Mycobacterium tuberculosis* suspended in mineral oil and activates Toll-Like Receptor (TLR)4 and TLR2 on macrophages and dendritic cells to initiate a reliable inflammatory response (Faridgohar and Nikoueinejad 2017; Stils 2005; Billiau and Matthys 2001). As mentioned above, peri-/intra-articular injection can induce chronic monoarthritis that is localised to the joint, making it a useful model that can avoid systemic changes induced by other polyarthritic inflammatory models (Zhang and Ren 2011; Donaldson et al. 1993; Butler et al. 1992). However, higher doses of CFA are able to induce contralateral effects (Donaldson et al. 1993), meaning it can be easily exploited to investigate particular disease mechanisms. Animals with CFA-induced arthritis demonstrate localised swelling and a reduction in affected hind-leg use, which peaks after 48-72hr and begins to return to normal over 10 days (Beazley-Long et al. 2018b; Donaldson et al. 1993). There is also sustained joint damage and a decrease in hindpaw mechanical pain threshold that can spread to the contralateral paw (Beazley-Long et al. 2018b; Neugebauer et al. 2007).

Whilst not classically regarded as an inflammatory arthritis, the role of inflammation and the immune system in Osteoarthritis (OA) progression is becoming more evident (Chow and Chin 2020; Woodell-May and Sommerfeld 2020). OA is a joint disease that is characterised by cartilage erosion, osteophyte formation (bony outgrowths), synovitis (synovial inflammation), neurovascular invasion and pain (Glyn-Jones et al. 2015; Thakur et al. 2014). Intra-articular Monosodium Iodoacetate (MIA) is used as a common animal model and induces OA by disrupting cellular glycolysis, leading to chondrocyte cell death and rapid joint degeneration (de Sousa Valente 2019). The early stage in MIA-induced OA is predominantly mediated by inflammation, and the later stage by substantial structural alterations in the joint (and a possible neuropathic component) as a result of inflammation and chondrocyte cell death (de Sousa Valente 2019). The MIA model is rapid and reliable with a well-characterised pain phenotype (that has a biphasic profile that manifests 1-3 days post-injection (Pitcher et al. 2016)), which can be easily manipulated with MIA dose (de Sousa Valente 2019).

As a purely inflammatory model of pain, subcutaneous injections of inflammogens can be used, for example CFA or λ-carrageenan. The latter is an experimental inflammogen that induces an acute and robust inflammatory response through binding to Interleukin (IL)-8 and activating immune cells, leading to the release pro-inflammatory molecules (Chan et al. 2017; Sokolova et al. 2016; Radhakrishnan et al. 2003). When injected into the hindpaw, there is redness, swelling, altered hind-limb weight bearing and hyperalgesia that can last <1 week (Coulthard et al. 2003; Hargreaves et al. 1988).

1.1.2 Measuring Pain in Animal Models

Measuring pain in animal models can be difficult as animals are generally unable to let us know the amount of pain they are in. Therefore, *in vivo* studies measure "pain-like" behaviours to give an indication of pain (Deuis et al. 2017). The most commonly used method in pre-clinical (and clinical) research for determining pain thresholds is the von Frey hair test. This method uses monofilaments with different bending forces to determine the mechanical threshold that elicits a painful response. A single monofilament is applied to the surface of the skin until it bends, exerting a determined force. In pre-clinical models, baseline thresholds are determined, and after injury, if the threshold for eliciting a painful response (for example licking or withdrawing the paw) decreases, then the animal is experiencing allodynia (pain from previously non-painful stimuli) (Deuis et al. 2017). Mechanical hypersensitivity can be used as an indication of central changes within the nociceptive pathway. For example, in arthritis models, injury is induced and limited to the knee, and so a reduction in pain thresholds in the hindpaw is indicative of secondary/referred pain and therefore of central sensitisation (Malfait et al. 2013; Woolf 2011). Thermal thresholds can also be measured, for example using Hargreave's method of thermal hyperalgesia that uses paw withdrawal latencies to heat exposure to determine thermal thresholds (Hargreaves et al. 1988). However, compared von Frey tests, these methods can be more expensive and more difficult

to perform. Weight bearing measurements detect the difference in weight borne by affected and unaffected hindlimbs, and therefore may be used to asses joint function (O'Brien et al. 2017). Because the animal is at rest and pain is not evoked through a stimulus, it may be a measure of static or spontaneous pain (O'Brien et al. 2017).

1.2 The Nociceptive Pathway

1.2.1 Nociceptive Fibres

The nociceptive system is a complex network of peripheral, spinal, and supra-spinal neurones and centres. In the periphery, nociceptive fibre cell bodies reside in the Dorsal Root Ganglion (DRG) and a bifurcating projection extends to both the spinal cord and the skin or viscera. Individual fibres are encapsulated by the perineurium in bundles, and groups of these bundles are surrounded by the epineurium to form spinal nerves (Weerasuriya and Mizisin 2011). These bundles can contain both afferent (sensory neurones) and efferent (motorneurones or sympathetic neurones) fibres, and supporting vascular and structural components.

Of the afferent sensory neurones, there are three main types: thick, fast myelinated Aβ fibres; thin, moderate-speed myelinated Aδ fibres; and small, non-myelinated and therefore slow C fibres (Millan 1999). Nociceptor size and conduction volume are not reported here as they vary depending on species (Djouhri and Lawson 2004) and age (Fitzgerald 1985). All three fibre types can encode noxious stimuli, and although Aβ fibres were classically regarded as non-nociceptive only, a subset of Aβ fibres are nociceptive (Djouhri and Lawson 2004).

There are three types of noxious stimuli that can be encoded by nociceptors: thermal, mechanical, and chemical. C fibres can encode all these modalities, with the majority of them being polymodal (Wooten et al. 2014), Aδ mechanical and/or thermal, and Aβ mechanical (McGlone and Reilly 2010; Djouhri and Lawson 2004). Aδ fibres can be divided into Type I and Type II high threshold A-mechano-heat nociceptors. Type I can respond to mechanical and chemical stimuli and have high thermal thresholds, whereas Type II have higher mechanical threshold but lower thermal threshold (Basbaum et al. 2009). During tissue damage, Type I fibres can be sensitised, resulting in a lower threshold for thermal activation (Broeke et al. 2016). Additionally, there are a subset of C fibres that are not normally activated by thermal or mechanical stimuli (termed "silent nociceptors"), but during tissue injury these nociceptors become sensitised to these modalities (Prato et al. 2017), contributing to peripheral sensitisation (see Section 1.2.7).

Aδ and C fibres can also be divided into two subtypes: peptidergic and non-peptidergic (Lawson et al. 1997). Peptidergic C fibres express substance P, Calcitonin Gene-Related Protein (CGRP) and Tropomyosin Receptor Kinase A (TrkA) receptors, which bind Nerve Growth Factor (NGF). NGF is important during development for neuronal survival but

also mediates pain signalling through these TrkA receptors (Kumar and Mahal 2012). Non-peptidergic C fibres express Isolectin B4 and purigenic Adenosine Triphosphate (ATP)-gated P2X receptors. P2X receptors, and notably P2X3 subunit-containing receptors, are activated by ATP, which can be released during inflammation, and are involved in both pain processing during inflammation and peripheral sensitisation (Bernier et al. 2018; North 2004). There is overlap between these two populations and there are significant differences across species (Lallemend and Ernfors 2012; Ernsberger 2009).

1.2.2 Transducer Receptor Subtypes

Noxious stimuli modalities are transduced and encoded through activation of different receptors on free nerve endings of the nociceptor terminals. One of the most well studied receptor families are the Transient Receptor Potentials (TRPs), which encompasses a number of different subtypes, including the vanilloids (Transient Receptor Potential cation channel subfamily V (TRPV)) and melastatins (Transient Receptor Potential cation channel subfamily M (TRPM)). Transient Receptor Potential cation channel subfamily V member 1 (TRPV1) was one of the first discovered nociceptive receptors, and is a non-selective K+, Na+ and Ca2+ cation channel that is activated by capsaicin, other endogenous ligands such as protons and lipids (Patwardhan et al. 2010), and heat (>43˚C) to produce a burning sensation (Caterina et al. 1997). CFA can enhance capsaicin-activated TRPV1 nociceptive responses in the DRG (Gu et al. 2018). TRPM8 is conversely activated by innocuous cooling and lowering the temperature to the noxious cold range (McKemy 2007). Acid Sensing Ion Channels (ASICs) are present on terminals and cell bodies of nociceptors and are activated by protons (i.e. a reduction in pH) (Wemmie et al. 2013).

Tactile stimuli are generally encoded by low-threshold mechanoreceptors that are highly specialised secondary cell structures, for example Pacinian corpuscles that detect mechanical deformation (Adrian and Umrath 1929). Transient Receptor Potential cation channel subfamily A member 1) (TRPA1), and potentially the Transient Receptor Potential Canonical (TRPC) channel family, are also important in low and high threshold mechanosensation (Chen et al. 2020; Kerstein et al. 2009), as well as Piezo1 and Piezo2 (Coste et al. 2010). Low threshold stimuli are generally benign, for example innocuous pressure or skin stretch, whereas high threshold stimuli are harmful and noxious (Roudaut et al. 2012). TRPA1 can be activated by multiple agonists (Meents et al. 2019), and so is generally considered to be a universal sensitiser channel (Donaldson and Beazley-Long 2016).

1.2.3 The Dorsal Root Ganglion

As mentioned above, the DRG contain the cell bodies of nociceptive fibres and sit adjacent to the spinal cord. DRG neurone soma membranes are excitable (Wall and Devor 1983) and can affect nociceptive transmission through neurotransmitters and gap junction signalling (Du et al. 2017; Huang et al. 2010; Onda et al. 2002). Therefore, some

sensory processing can occur in the DRG prior to modulation in the dorsal horn of the spinal cord. Under normal circumstances, nociceptive signals from the periphery can bypass the DRG, but sensory processing within the DRG may play an important role during chronic pain states (Liem et al. 2016).

1.2.4 The Dorsal Horn of the Spinal Cord

Primary afferent neurones terminate in the dorsal horn of the spinal cord, which is the area responsible for initial sensory processing within the spinal cord. It is anatomically divided into regions or laminae dependent on neuronal size and density (Peirs et al. 2020), with primary afferent fibres terminating in different locations depending on their type. C and Aδ fibres terminate superficially in lamina I and II, whereas Aβ largely terminate in lamina II to IV (Koch et al. 2018; Benarroch 2016; Todd 2010) (see Figure 1.1).

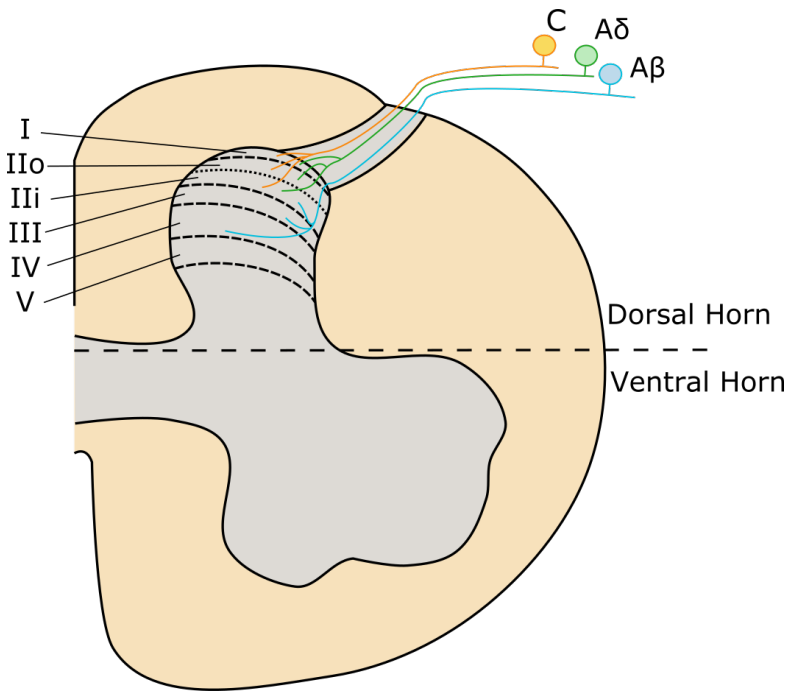


Figure 1.1: Nociceptive neurones terminate in different laminae of the dorsal horn of the spinal cord.

Within the dorsal horn, primary afferent fibres can terminate onto interneurones that stay within the dorsal horn, or projection neurones that extend towards the brain (Todd 2017; Benarroch 2016). It is the excitability of these second order cells that determines whether nociceptive signals are relayed to supra-spinal nuclei in the brain for further processing, for example intensity/location and the subjective feeling of pain (Dostrovsky and Craig 2013). Wide Dynamic Range (WDR) neurones primarily reside in lamina V of the dorsal horn and receive direct input from Aβ and Aδ fibres, and indirect input from C fibres (Basbaum et al. 2009). Therefore, these cells respond to a variety of stimuli and are often used in electrophysiological recordings to monitor the excitability of the dorsal horn.

The excitability of the dorsal horn is determined by interneurone and glial signalling, as well as functional changes in peripheral nociceptors and central projection neurones that occur during peripheral and central sensitisation (Koch et al. 2018; Ji et al. 2018; Millan 1999). Interneurones are a diverse population of excitatory and inhibitory neurones (Todd 2017) that have been implicated in chronic pain states (Koch et al. 2018). Altered interneurone signalling and dorsal horn excitability can also unmask previously silent A fibre circuits that are thought to contribute to allodynia and hyperalgesia in inflammatory pain (Torsney 2019). As well as dorsal horn excitability being determined by surrounding cells, projections from supra-spinal centres can also regulate spinal processing and pain sensitivity through descending control (see Section 1.2.6).

1.2.4.1 Non-Neuronal Cells of the Dorsal Horn

There are a multitude of other cells within the dorsal horn that contribute to nociceptive signalling (Millan 1999). Microglia are macrophage-like cells that are considered to be the resident immune cells of the CNS and are responsible for regulating homeostasis and maintaining physiological conditions in the CNS (Salter and Beggs 2014; Kettenmann et al. 2011). They are highly ramified when in a resting state and scan their environment with motile processes (Kettenmann et al. 2011). When activated, microglia lose their ramified phenotype and become motile and amoeboid in appearance (Kettenmann et al. 2011). Astrocytes are the most abundant cell type in the CNS, and are a diverse population that are organised into non-overlapping domains (Ji et al. 2019; Miller 2018; Sofroniew and Vinters 2010). Like microglia, astrocytes can become activated or 'reactive', where they lose this organisation and undergo hypertrophy and proliferation (Ji et al. 2019; Miller 2018; Sofroniew and Vinters 2010). Both astrocytes and microglia play a role in acute pain signalling (Chen et al. 2018b; Chiang et al. 2012), and astrocytes have been shown to contribute to nociceptive signalling during homeostasis, as down-regulation of connexin 43 (a main astrocyte gap junction that allows intercellular communication) results in allodynia (Morioka et al. 2018; Ohara et al. 2008). Both can become activated after insults (Miller 2018; Hansen and Malcangio 2013; Ji et al. 2013; Calvo and Bennett 2012; Sofroniew and Vinters 2010). As well as in acute pain processing, both microglia and astrocytes have been heavily implicated in the initiation and maintenance of chronic pain (Ji et al. 2013) (see Section 1.2.7.1).

Immune cells, such as macrophages/monocytes and T-cells, present in the dorsal horn (and DRG) also play an important role in pain regulation through their release of inflammatory molecules (Ji et al. 2016; Grace et al. 2014).

1.2.4.2 Neurotransmitters of the Dorsal Horn

Glutamate is the main excitatory neurotransmitter in pain transmission, and all primary afferents release glutamate in the dorsal horn (Broman et al. 1993). Glutamate can activate the ionotropic α-Amino-3-Hydroxy-5-Methylisoxazole-4-Propionate (AMPA), N-Methyl-D-Aspartate (NMDA) and kainate receptors, and the Metabotropic Glutamate

Receptors (mGluRs). As well as acute signalling, AMPA, NMDA and mGluR are important in facilitating chronic pain states through central sensitisation (see 1.2.7). Kainate receptors are responsible for decreasing the amount of glutamate released by nociceptor pre-synaptic terminals (Lucifora et al. 2006). GABA (Gamma-Aminobutyric Acid) is found in interneurones in the dorsal horn and, with glycine, is one of the major inhibitory neurotransmitters in nociceptive signalling (Enna and McCarson 2006).

1.2.5 Ascending Pathways

Nociceptive information is integrated within the dorsal horn by second order neurones, which project to supra-spinal centres in the brain. Projection to supra-spinal levels depends on the excitability of these cells, which is determined by the microenvironment and signalling by other cells. Two main ascending nociceptive pathways they follow are the spinothalamic tract and the spinoparabrachial tract (see Figure 1.2).

Spinothalamic neurones project from laminae I and V to thalamic nuclei, such as the Ventromedial Posterior Nuclei (VMpo) and Ventral Posterior Nuclei (VP) (Dostrovsky and Craig 2013). The VMpo projects to the insular cortex to process the subjective feeling of pain, whereas neurones from the VP project to the somatosensory cortex to process pain location and intensity (Dostrovsky and Craig 2013). Spinoparabrachial neurones project to the parabrachial area in the midbrain, and then to the amygdala and the ventromedial hypothalamus, which are also involved in generating the emotional aspects of pain (Basbaum et al. 2009).

1.2.6 Descending Control

Supra-spinal centres are also able to regulate spinal processing and pain sensitivity through descending control (see Figure 1.2). The main regions responsible for this descending modulation are the midbrain Periaqueductal Grey (PAG) and the Rostroventral Medulla (RVM) in the brainstem. These areas coordinate information from the spinal cord and several brain areas, including the limbic system, the hypothalamus, and the prefrontal cortex, and project to the dorsal horn to influence excitability (Neugebauer et al. 2004; Parry et al. 2002; Fields et al. 1991). Activation of the PAG can indirectly produce analgesia (Praag and Frenk 1991) via signalling to the RVM which then bi-directionally signals to the dorsal horn (see Figure 1.2). The RVM has two classes of neurones referred to as 'ON cells' or 'OFF cells' (Heinricher and Fields 2013). ON cells have a tonic pro-nociceptive influence, whereas OFF cells have a tonic inhibitory effect (Chen and Heinricher 2019). Non-selective activation of the RVM results in analgesia, but selective activation of ON cells can cause hyperalgesia (Neubert et al. 2004) and activation of OFF cells can produce anti-nociception (Heinricher et al. 2010; Hentall et al. 1984).

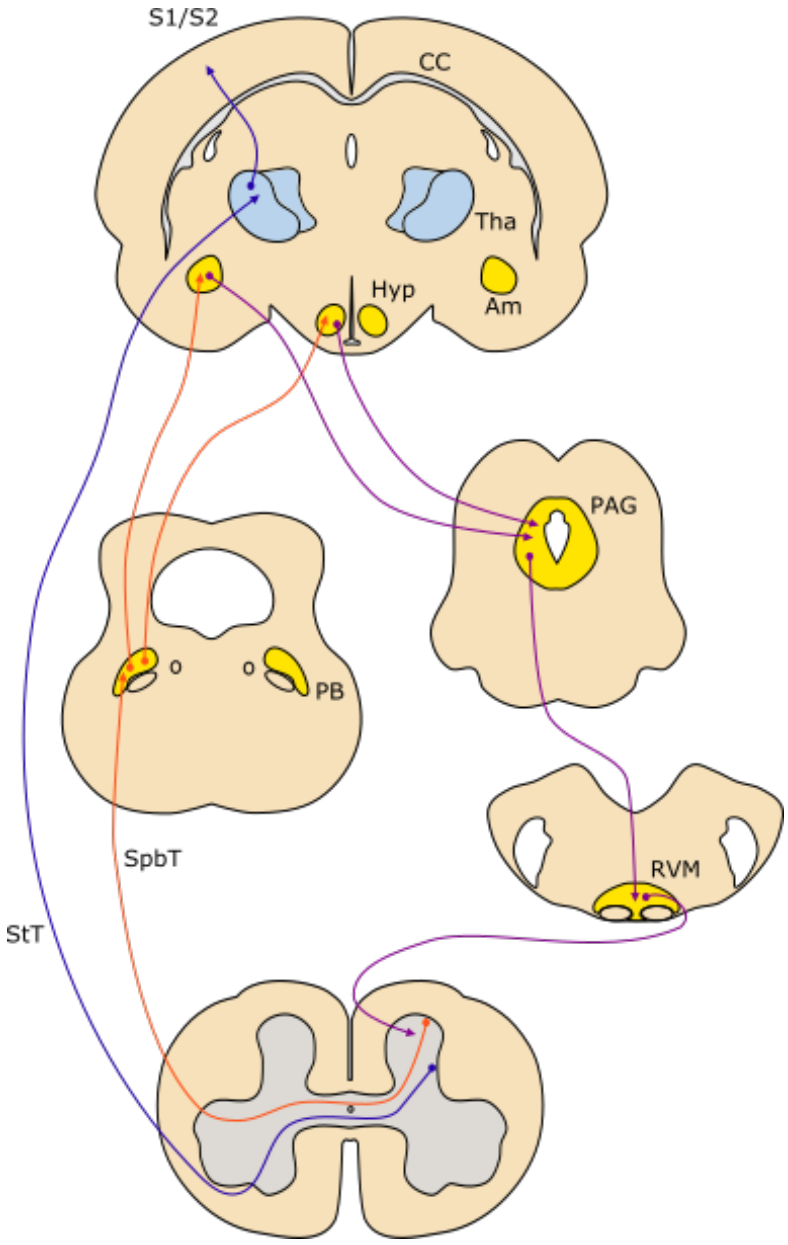


Figure 1.2: Ascending and descending nociceptive tracts. **Ascending tracts**: Blue, Spinothalamic tract (StT); Orange, Spinoparabrachial tract (SpbT). **Descending tract**: Purple. **PB**: Parabrachial area. **Hyp**: Hypothalamus. **Am**: Amygdala. **Tha**: Thalamus. **CC**: Corpus Callosum. **S1/S2**: Somatosensory cortex 1/2. **PAG**: Periaqueductal Grey. **RVM**: Rostroventral Medulla. (Adapted from Hunt and Mantyh 2001).

1.2.7 Peripheral and Central Sensitisation

Acute pain is a useful mechanism that helps to protect an organism from harm. Nociceptors are activated by either potentially or actually damaging stimuli (mechanical, thermal, or chemical) and the nociceptive pathway is engaged (see above). This allows the organism to reflexively then consciously remove itself from the source of the noxious stimulus and protect the damaged area whilst wound healing occurs. However, when pain persists, it is considered non-useful, debilitating chronic pain (defined as pain for longer than 3 months in humans (Treede et al. 2019)). In chronic pain conditions, in particular in chronic inflammation such as RA, nociceptors can become sensitised in a process called 'peripheral sensitisation' resulting in lower activation thresholds and enhanced nociceptive responses (McWilliams and Walsh 2017; Gangadharan and Kuner 2013). Sensitisation occurs due to chemical mediators released by nociceptors (for example Substance P (Chen et al. 2007)) and/or immune cells (for example TNFα and Prostaglandin E2 (PGE2) (Walsh and McWilliams 2014; Julius 2001)) modulating receptor and channel activity and therefore nociceptor terminal excitability (Gangadharan and Kuner 2013). For example, PGE2 activation of Prostaglandin E2 receptor 4 (EP4) (which incidentally is involved in RA disease progression (McCoy et al. 2002)) initiates phosphorylation of TRPV1 to lower its activation threshold and of Voltage-Gated Sodium Channels (Navs) to increase terminal excitability (Lin et al. 2006; Julius 2001). Activation of receptors by inflammogens can also initiate increased expression of pronociceptive proteins; for example, TrkA activation by NGF promotes increased TRPV1 and Nav1.8 expression (Fang et al. 2005; Ji et al. 2002). Additionally, NGF can unmask mechanosensation in previously silent nociceptors via the disinhibition of the mechanically-gated ion channel, Piezo2 (Prato et al. 2017). Peripheral sensitisation has an important role in contributing to chronic inflammatory pain, as demonstrated by NGF inhibition being effective at providing analgesia in OA through the reversal of NGF-mediated peripheral sensitisation (Khan et al. 2021; Schnitzer and Marks 2015). Furthermore, drugs that suppress PGE2 production (Non-Steroidal Anti-Inflammatory Drugs (NSAIDs), aspirin) through Cyclooxygenase (COX) inhibition are common and effective analgesics for pain conditions (Kroenke et al. 2009; Ashburn and Staats 1999).

This increased nociceptive input from sensitised and activated peripheral nociceptors can alter nociceptive signalling within the CNS, for example through increased glutamate, substance P and Brain Derived Neurotrophic Factor (BDNF) release at central terminals (Latremoliere and Woolf 2009; Ji et al. 2003), which can strengthen synapses and augment the post-synaptic responses. This occurs due to the initiation of phosphorylation of AMPA receptors, NMDA receptors and Kv4.2 potassium channels, and insertion of new AMPA receptors into the membrane (see Figure 1.3, right). PGE2 can directly activate post-synaptic neurones, but it is also able to activate pre-synaptic PGE2 receptors to increase transmitter release (Ji et al. 2003). Spinal PGE2 can also reduce glycinergic inhibition in the superficial dorsal horn (see Zeilhofer et al. 2012, review). This results in central sensitisation and hyperexcitable nociceptive circuits, leading to

enhanced functionality and signalling to supra-spinal centres. For example, there are several changes that occur to spinal WDR neurones that increase their sensitivity: previously nociceptive-specific neurones can convert to WDR neurones which then respond to both noxious and innocuous stimuli; temporal Wind-Up (WU) can occur (where repeated innocuous stimuli result in progressive increases in responses); and their receptive fields can increase (Latremoliere and Woolf 2009). These neuronal changes are also accompanied by glial cell activation, which can also contribute to hyperexcitability of the dorsal horn (see Section 1.2.7.1). Due to both peripheral and central sensitisation, subthreshold innocuous inputs are also able to contribute to nociceptive signalling, which results in the hyperalgesia and allodynia phenomena (Torsney 2019; Latremoliere and Woolf 2009). There may be several triggers responsible for central sensitisation, but a leading theory is through Classic Heterosynaptic Central Sensitisation (CHCS) (see Figure 1.3). Heterosynaptic facilitation occurs when activity and signalling in one set of synapses on a neurone spreads and augments activity in other, non-activated synapses on the same neurone (Latremoliere and Woolf 2009).

In chronic pain, pain can also present in areas that are outside of the original injury site (known as secondary or referred pain), which is indicative of central changes in the nociceptive pathway (McWilliams and Walsh 2017). This phenomenon is the result of cellular and molecular changes in central nociceptive circuits in central sensitisation (Latremoliere and Woolf 2009). Disinhibition of previously blocked pathways, possibly excitatory interneurones, may result in this referred pain (Torsney 2019; Sandkühler 2013).

Other mechanisms of central sensitisation are WU and spinal Long-Term Potentiation (LTP), which, unlike CHCS, are homosynaptic (see Figure 1.3 for summary). During WU, there is a cumulative increase in action potentials in response to a train of repeated low frequency C fibre stimulation (<5Hz) (Mendell and Wall 1965). The $Mg2+$ block is removed from NMDA receptors due to the summation of synaptic potentials, which increases glutamate sensitivity and therefore action potential response (Ji et al. 2003). This phenomenon however is short-lasting and reversible, and so is unlikely to be responsible for chronic pain. In people with OA, a similar phenomenon occurs where repeated mechanical stimuli can lead to increased pain responses, i.e. there is augmentation of temporal summation, but the time-course is longer than that of WU and it is yet not fully understood (Khan et al. 2021). Spinal LTP is similar to hippocampal LTP and occurs in response to high-frequency stimulation (~100Hz) to cause an increase in excitatory postsynaptic potentials (Ji et al. 2003). However, C fibres are physiologically unable to fire at the high intensity needed to induce LTP (Ji et al. 2003), and so LTP is unlikely to be responsible for central sensitisation.

1.2.7.1 Glial Activation in Central Sensitisation

Both astrocytes and microglia react to trauma and disease within the central nervous system, and undergo morphological and phenotypical alterations. Glia are termed to

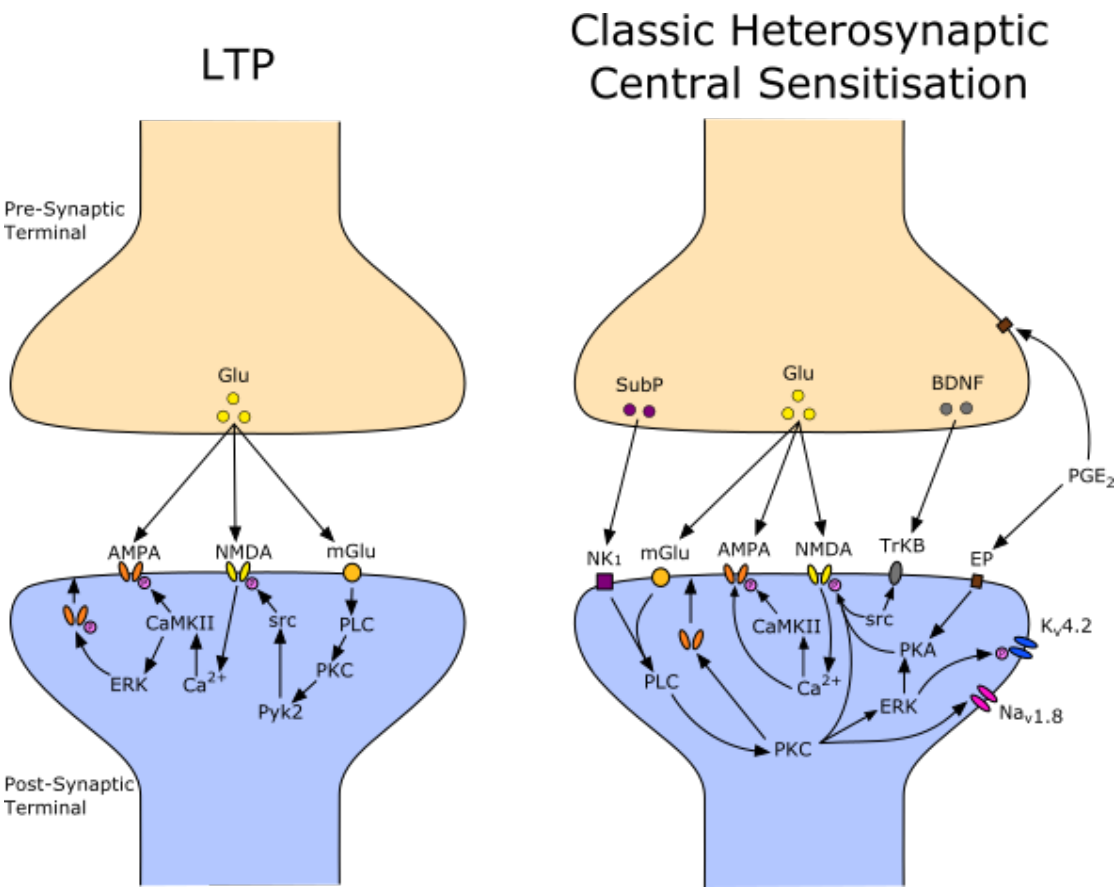


Figure 1.3: LTP (long term potentiation) occurs physiologically in hippocampal CA1 neurones, and is integral for learning and memory. Glutamate activates NMDA receptors to allow calcium influx, which induces CaMKII activation and leads to phosphorylation and expression of new of AMPA receptors. Src activation also leads to phosphorylation of NMDA receptors. Classic Heterosynaptic Central Sensitisation occurs in dorsal horn spinal neurones. Nociceptors release Substance P, Glutamate and BDNF to initiate phosphorylation of AMPA receptors, NMDA receptors and Kv4.2 potassium channels. New AMPA receptors are expressed and inserted into the membrane, and Nav1.8 channels are modulated. PGE2 can also activate pre-synaptic EP receptors to increase transmitter release. Adapted from Ji et al. (2003). **AMPA**: α-amino-3-hydroxy-5-methylisoxazole-4-propionate receptors; **BDNF**: brain-derived neurotrophic factor; **CaMKII**: Ca2+/calmodulin-dependent protein kinase II; **EP**: PGE2 receptor; **ERK**: extracellular-regulated kinase; **Glu**: glutamate; **Kv4.2**: voltage-gated potassium ion channel subunit 4.2; **mGlu**: metabotropic glutamate receptors; **Nav1.8**: voltage-gated sodium ion channel subunit; **NK1**: Neurokinin 1 receptor; **NMDA**: N-methyl-D-aspartate receptors; **PGE2**: prostaglandin E2; **PKA**: cAMP-dependent; **PKC**: Ca2+/phospholipid-dependent protein kinase C; **PLC**: phospholipase C protein kinase A; **Pyk2**: Protein tyrosine kinase 2; **src**: proto-oncogene tyrosine-protein kinase src; **SubP**: substance P; **TrKB**: tyrosine kinase receptor B.

be 'activated' or in a 'reactive state' after such events. As well as during trauma, glia can become activated from increased neuronal activity (Biber et al. 2007), which is a hallmark of central sensitisation (Latremoliere and Woolf 2009). Both microglial and astrocytic activation have been implicated in acute and chronic pain conditions (for reviews see Ji et al. 2019; Li et al. 2019; Tsuda 2019; Chen et al. 2018b; Inoue and Tsuda 2018; Ji et al. 2013; Ji and Suter 2007). Additionally, activated glial cells/neuroinflammation has been detected in painful conditions in humans (Flores Bjurström et al. 2020; Jung et al. 2020; Albrecht et al. 2018; Kosek et al. 2018).

Quiescent microglia are a heterogeneous population (Hammond et al. 2019) and are highly ramified, but take on an amoeboid appearance with short cellular processes when activated (Suzumura et al. 1991). In this activated state, microglia can release pro- and anti-inflammatory cytokines/chemokines, and can become phagocytic or antigen-presenting (Town et al. 2005). These pro-inflammatory mediators can go on to activate and sensitise neurones (Chen et al. 2018b; Calvo and Bennett 2012; Ji et al. 2013), and can activate endothelial cells, for example microglial-derived TNFα can induce COX-2 and Prostaglandin I2 Synthase (PTGIS) expression in endothelial cells (Kanda et al. 2017). Activation of TLRs and chemokine/cytokine receptors, and subsequent downstream p38 Mitogen-Activated Protein Kinase (MAPK) and Matrix Metalloproteinase (MMP)9 signalling, are involved in activating microglia (Kawasaki et al. 2008a; Ji and Suter 2007; Town et al. 2005).

Microglia have been shown to be essential for LTP (Zhou et al. 2019), and in terms of chronic pain development, microglia have been shown to be involved in many, but not all, painful conditions (Ji et al. 2019). For example, inhibiting the microglial p38 MAPK pathway reduces pain symptoms after traumatic nerve injury but not Chemotherapy-Induced Peripheral Neuropathy (CIPN) (Luo et al. 2018; Taves et al. 2015). Depletion of microglia at early (2 weeks) and late (3 months) stages after nerve injury also reversed hypersensitivity (Echeverry et al. 2017). The authors attributed early phase hypersensitivity to microglial release of pro-inflammatory cytokines and chemokines, and the late stage to BDNF release (Echeverry et al. 2011). There are, however, significant sex differences in the microglial response to chronic pain (Mapplebeck et al. 2016). For example, spinal microglial expression of TLR4 (and $P2X_4$ receptors (Sorge et al. 2015)) was involved in inflammatory and nerve injury-induced hypersensitivity in male mice but not in female mice, despite both sexes expressing comparable levels of TLR4 (Sorge et al. 2011). Additionally, inhibition of several microglial-neuronal signalling molecules (p38 MAPK and BDNF) reversed neuropathic pain in male mice only (Sorge et al. 2015). In both neuropathic and inflammatory pain, microglia were not found to be involved in mechanical hypersensitivity in female mice but were in male mice (Chen et al. 2018a; Taves et al. 2015; Sorge et al. 2015). T-cell involvement appears to be more important than microglial activation in female mice (Raoof et al. 2018; Rosen et al. 2017). In T-cell (and B-cell) deficient mice, neuropathic and inflammatory pain in both sexes is reduced with microglial inhibitions (Sorge et al. 2015), suggesting that female mice use the male

microglial-dependent pain pathway in the absence of T-cells. Female T-cell deficient mice that received splenocyte transfer (and therefore adopted T-cells) were rendered insensitive to analgesia produced by microglial inhibition in inflammatory pain (Sorge et al. 2015). The authors suggest the differences are due to testosterone effects on Peroxisome Proliferator Activated Receptors (PPARs) in T-cells (Sorge et al. 2015) affecting their ability to mediate hypersensitivity via interferon-γ release after transmigration into the CNS in pain.

Microglial reactivity appears to precede astrocyte activation, and may actually induce astrogliosis (Ji et al. 2019; Gao and Ji 2010; Kawasaki et al. 2008a). However, selective astrocyte activation can cause microglial activation (Nam et al. 2016), demonstrating extensive cross-talk between these two populations.

Astrocytes, too, are a highly heterogeneous cell population, and so not surprisingly they demonstrate a varied gene expression during reactive astrogliosis that is dependent on injury type (Miller 2018; Liddelow et al. 2017; Zamanian et al. 2012). It has been proposed that astrocytes have differing activation states, and can fall into broadly pro-inflammatory 'A1' and pro-regenerative 'A2' states depending on their phenotypic expression (Liddelow et al. 2017). This nomenclature follows the idea that macrophages and microglia can exist in pro-inflammatory 'M1' and anti-inflammatory 'M2' states, although this microglia/macrophage polarisation has been disputed (Hammond et al. 2019; Ransohoff 2016). It is likely that astrocytes (and microglia) exist in a more complex array of phenotypes during pathology (Hammond et al. 2019; Ji et al. 2019), but in chronic pain conditions the specific phenotype of astrocyte reactivity is yet to be determined. Resting astrocytes are organised into non-overlapping domains, and A1-like reactive astrocytes lose this organisation (Ji et al. 2019; Sofroniew and Vinters 2010), release a milieu of cytokines, and can induce neuronal cell death (Liddelow et al. 2017; Ikeda et al. 2012). It is widely accepted that astrocytes undergo activation and phenotypic changes as a result of peripheral insults, with early studies demonstrating increased expression of Glial Fibrillary Acidic Protein (GFAP) after peripheral nerve injury (Garrison et al. 1991). Activation of astrocytes has been attributed to, among others, Activator protein 1 (AP-1), Janus Kinase (JAK)/Signal Transducer and Activator of Transcription-3 (STAT3), Nuclear Factor Kappa-Light-Chain-Enhancer of Activated B Cells (NF-κB), MAPK and MMP2 signalling (Giovannoni and Quintana 2020; Brenner et al. 2019; Kawasaki et al. 2008a).

Astrocytes themselves have the capacity to induce hypersensitivity and pain in naive rats. For example, experimental downregulation of connexin 43, which is a key gap junction protein that allows intercellular communication between spinal astrocytes (Xing et al. 2019), caused allodynia in rodents (Morioka et al. 2018; Ohara et al. 2008). Additionally, optogenetic stimulation of astrocytes can induce rapid mechanical hypersensitivity and microglial activation in rats (Nam et al. 2016). Release of TNFα and C-C motif Chemokine Ligand 2 (CCL2) from astrocytes can also cause hyperalgesia (Gao et al. 2010; Menetski et al. 2007; DeLeo et al. 2000), and inhibiting STAT3, which drives

proliferation of astrocytes, and therefore preventing their proliferation after nerve injury reduces pain (Tsuda et al. 2011). It is clear then that astrocytes have a pivotal role in pain transmission and contribute to pain pathology, but although extensively studied in neuropathic pain and inflammatory pain (Ji et al. 2019; Li et al. 2019; Ji et al. 2013), their relationship with the Neurovascular Unit (NVU) in chronic pain development/maintenance is yet to be fully established. Glial cells, and astrocytes in particular, are key components of the NVU and are heavily involved in the physiological functioning of the BBB and BSCB (see Section 1.3). If there is activation of glial cells in painful conditions, this may have downstream effects on barrier permeability and the neuronal environment due to infiltrating blood-borne cells and molecules. What specifically happens to astrocytes and other glial cells in the proximity of bloody vessels? What happens to the BSCB in painful conditions, especially in inflammatory arthritis, and are alterations in function a consequence or cause of glial activation in chronic pain? There have been very few recent reviews explicitly discussing the contribution of the central NVU to chronic pain (Durrant et al. 2018; Beazley-Long et al. 2018a; Dos-Santos et al. 2014; Radu et al. 2013; Willis et al. 2008), despite BBB/BSCB disruption being a well-known phenomenon during pain states (Sauer et al. 2017; Xanthos et al. 2012; Echeverry et al. 2011; Beggs et al. 2010; Huber et al. 2005; Huber et al. 2002; Huber et al. 2001).

1.2.7.2 Neuroinflammation

Neuroinflammation is the localised inflammation that occurs within the CNS after trauma, autoimmunity, neurodegeneration or infection. It is characterised by glial activation, production of inflammatory molecules (such as TNFα, Interleukin-1β (IL-1β) and IL6), increased BBB/BSCB permeability and immune cell infiltration into the neural parenchyma (Ji et al. 2018; Becher et al. 2016). Although not exclusive to painful conditions, neuroinflammation occurs in many of these conditions, such as stroke, brain injury, chemotherapy-induced pain, and arthritis (Ji et al. 2018). It has been suggested that pain-induced glial activation causes neuroinflammation, which can drive central sensitisation through further glial activation and release of cytokines/chemokines (and other factors) that sensitise neurones (Ji et al. 2019; Ji et al. 2018; Ji et al. 2016; Grace et al. 2014; Koyama 2014; Gao et al. 2010; Menetski et al. 2007; DeLeo et al. 2000).

Of the inflammatory molecules involved in neuroinflammation, TNFα is a key cytokine. It is released by cells within the NVU such as astrocytes, microglia, and pericytes, and has been implicated in chronic pain development and maintenance (Ji et al. 2018; Rustenhoven et al. 2017; Becher et al. 2016; Leung and Cahill 2010). TNFα can enhance glutamate-induced excitatory currents in neurones (Kawasaki et al. 2008b), induce glial activation (Koyama 2014), and cause reduced endothelial tight junction expression and increased BBB/BSCB permeability (Zhang et al. 2019; Daniels et al. 2014; Förster et al. 2008; Didier et al. 2003; Mark and Miller 1999). It can also induce the release of further inflammatory molecules such as IL6, IL-1β and VEGF-A by glial cells and endothelial cells

(Zhang et al. 2019; Lee et al. 2017; Varatharaj and Galea 2016; Ji et al. 2013), making it an important mediator in neuroinflammation and the gliovascular-neuronal axis.

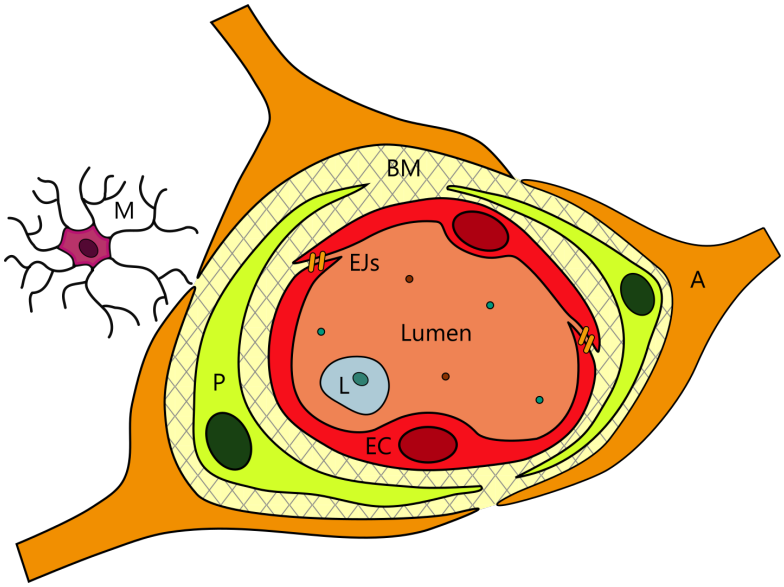
1.3 The Blood-Neural Barriers

Glial and resident immune cells act to protect normal physiological functioning of neurones by maintaining the correct microenvironment within the CNS. Physical barriers, such as the BBB and BSCB (and the Blood Nerve Barrier (BNB), see Section 1.3.1), are responsible for limiting cell and molecular access into the CNS through specialised intercellular junctions and transporters within components of the NVU. The NVU consists of endothelial cells, the basement membrane that surrounds blood vessels, pericytes, astrocytes, and microglia, which serve structural and functional purposes (see Figure 1.4).

Development of the BBB/BSCB begins with the elimination of fenestrations in endothelial cells to form an endothelial monolayer that is connected via specialised junctions (Zhao et al. 2015a; Alvarez et al. 2011) (see Figure 1.4b). Transporters, ion channels and junctions expressed by endothelial cells are the main component of the BBB/BSCB as they restrict the access of cells and molecules into the CNS parenchyma (Abbott et al. 2010). Oxygen and carbon dioxide can freely diffuse across the endothelium, as well as <400Da lipophilic molecules and those that form <6 hydrogen bonds (Zhao et al. 2015a; Abbott et al. 2010). There are several transporters expressed in endothelial cells that transport small molecules from the blood into the CNS and vice versa, but there are mechanisms available to allow specific macromolecules to cross endothelial cells through endocytosis (Abbott et al. 2010) (see Section 1.3.2). Adherens junctions, including cadherins, Platelet and Endothelial Cell Adhesion Molecule-1 (PECAM-1) also known as Cluster of Differentiation-31 (CD31), and nectin, span the intercellular gap and interact with catenin scaffolding proteins to connect endothelial cells to each other, and provide structural support for formation of tight junctions (Figure 1.4b) (Zhao et al. 2015a; Abbott et al. 2010). The tight junction proteins occludin and the claudins (1, 3, 5, 12), as well as Junctional Adhesion Molecules (JAMs), also span this gap to link with the Zona Occludens-1 (ZO-1) scaffolding and regulatory proteins (Abbott et al. 2010) (Figure 1.4b).

Pericytes ensheath endothelial cells (Figure 1.4a) to provide structural stability to vessel walls, and help to regulate cerebral blood flow, vessel diameter, and BBB/BSCB permeability (Winkler et al. 2011). It has also been shown that pericyte recruitment is necessary in normal barrier formation and maintenance (Daneman et al. 2010). Astrocyte association with blood vessels is also necessary in the formation of tight junctions and activity of transporters in endothelial cells (Obermeier et al. 2013; Abbott et al. 2010). Astrocytes can directly alter barrier permeability (Argaw et al. 2012), and as they also signal with neurones (Barros et al. 2018; Gee and Keller 2005), they may be involved in coordinating neuronal and barrier functions. Indeed, increased neu-

(a) The Neurovascular Unit (NVU)



(b) Endothelial Junctions

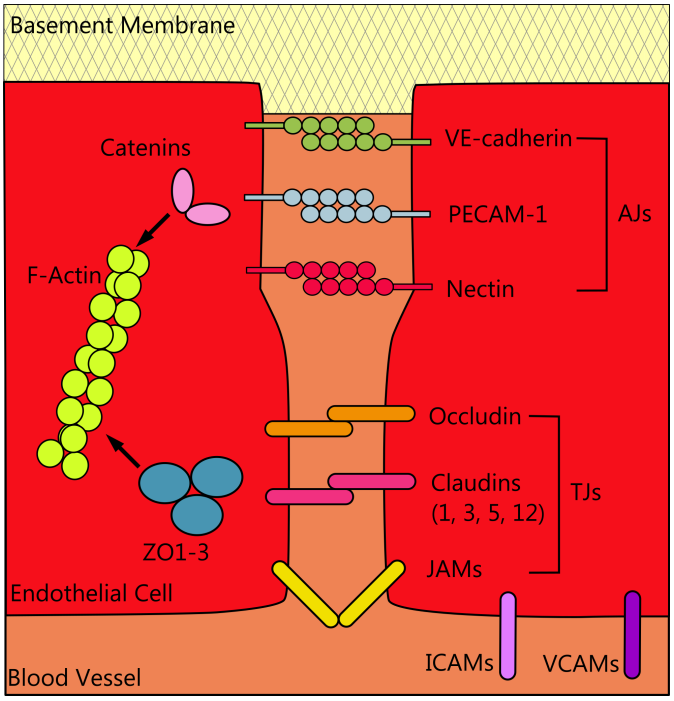


Figure 1.4: Components of the Neurovascular Unit (NVU) and endothelial junctions at the blood-spinal cord barrier. **A**: Astrocyte endfoot; **AJs**: Adhesion junctions; **BM**: Basement membrane; **EC**: Endothelial cell; **EJs**: Endothelial junctions; **ICAMs**: Intracellular adhesion molecules; **JAMs**: Junctional adhesion molecules; **P**: Pericyte; **TJs**: Tight junctions; **VCAMs**: Vascular cell adhesion molecules; **ZO**: Zona occludens. Adapted from Beazley-Long et al. (2018a) and Zhao et al. (2015b).

ronal activity signals to astrocytes to increase blood flow (Attwell et al. 2010), and so this gliovascular-neuronal axis already exists. Microglia, too, are implicated in barrier induction, maintenance and function (Carvalho da Fonseca et al. 2014; Abbott et al. 2010). Glial activation has implications for both neuronal state and barrier permeability, and so their involvement in development of chronic pain and associated barrier disruptions should be investigated. I hypothesised that glia, in particular astrocytes, actively contribute to the disruption of blood-barriers after inflammatory pain (see Figure 1.6), and that this disruption is involved in driving development and maintenance of chronic pain.

There are several important differences between the BSCB and the BBB, such as decreased expression of tight-junction proteins and adherens junction proteins in the BSCB (and therefore increased permeability to tracers and cytokines), and glycogen deposits in the superficial vessels of the spinal cord that are not normally found in brain microvessels (Radu et al. 2013; Sharma 2005).

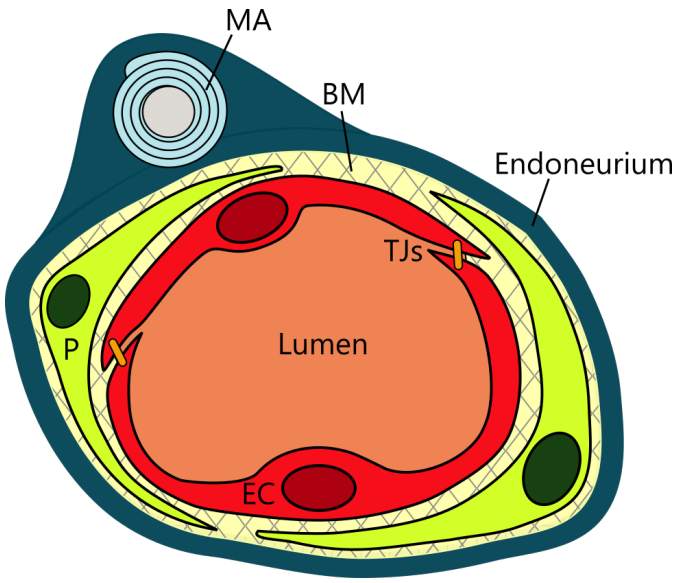
1.3.1 The Blood-Nerve Barrier

The peripheral nerve has its own distinct blood-barrier, called the Blood Nerve Barrier (BNB). The multilayered perineurium surrounds bundles of myelinated and non-myelinated fibres and endoneurial blood vessels, and is composed of specialized epithelioid myofibroblast cells. These cells form tight junctions, adherens junctions and gap junctions, which act as a diffusion barrier (Reinhold and Rittner 2017). The endothelial cells of endoneurial vessels themselves are also joined by tight junctions, involving tight junction proteins such as occludin and VE-cadherin (see Figure 1.5), and a multitude of other intercellular junctional complex molecules (Ubogu 2020), making up the BNB. The BNB is regarded as the second most restrictive microvascular tissue barrier after the BBB/BSCB.

1.3.2 Migration Across Blood-Barriers

There are several mechanisms that regulate transport across endothelial cells: passive diffusion; ATP-Binding Cassette (ABC) transporters; Solute Carriers (SLCs); vesicular-based transport; and leukocyte passage. Passive diffusion can be achieved by molecules that are lipid soluble, less than 450Da in size, have a low polar surface area, and form less than 6 hydrogen bonds (Abbott et al. 2010). The active ABC transporters are able to intercept some lipid soluble molecules and pump them back out of endothelial cells into the blood (Abbott et al. 2010). SLCs allow transport of necessary polar molecules such as glucose and amino acids across the endothelium (Zhang et al. 2002). Large molecules can be transported via Receptor-Mediated Transcytosis (RMT) or Adsorptive-Mediated Transcytosis (AMT), which rely on receptor activation (RMT) and cationic molecules interacting with binding sites (AMT) to initiate endocytosis (Abbott et al. 2010).

(a) Endoneurial Vessels



(b) BNB Endothelial Junctions

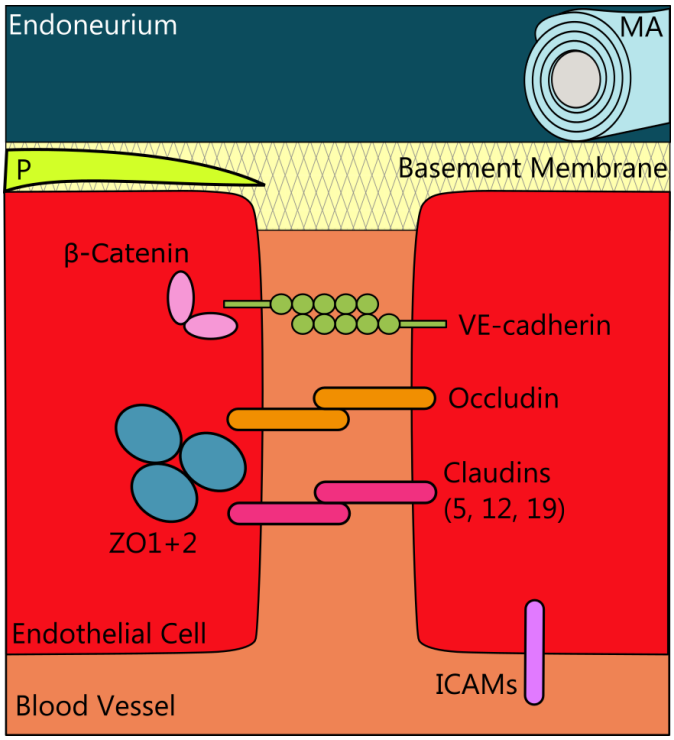


Figure 1.5: Components of the Blood-Nerve Barrier (BNB). The BNB is made up of endoneurial endothelial cells, pericytes and the basement membrane **(a)**. Endothelial tight junctions at the BNB **(b)**. **AJs**: Adhesion junctions; **BM**: Basement membrane; **EC**: Endothelial cell; **EJs**: Endothelial junctions; **ICAMs**: Intracellular adhesion molecules; **JAMs**: Junctional adhesion molecules; **MA**: Myelinated axon; **P**: Pericyte; **TJs**: Tight junctions; **ZO**: Zona occludens. Adapted from Richner et al. (2019).

Peripherally circulating leukocytes are also able to cross the BBB and BSCB either through (transceullular) or between (paracellular) endothelial cells (Wittchen 2009) via interaction with endothelial adhesion molecules, such as Intracellular Adhesion Molecule-1 (ICAM-1) and Vascular Cell Adhesion Molecule-1 (VCAM-1). First, ligands expressed on leukocytes interact with selectins on endothelial cells, which increase exposure of leukocytes to endothelial chemokines. These chemokines can activate leukocyte integrins to cause a conformational change and increase leukocyte binding (Lawson and Wolf 2009). Leukocytes then migrate along and firmly attach to the endothelium through binding to ICAM-1, which initiates either transcellular or paracellular migration (Reglero-Real et al. 2012; Lawson and Wolf 2009). ICAM-1 and VCAM-1 are constitutively expressed in low levels on the endothelial cell surface, and are upregulated during inflammation (Reglero-Real et al. 2012; Dustin et al. 1986).

1.3.3 Barrier Alterations during Nociception

If barriers fail to function properly, there is an opportunity for blood-borne molecules and cells to infiltrate the CNS parenchyma and disrupt the carefully maintained microenvironment. These molecules and cells have the potential to directly activate glia and neurones, possibly contributing to changes in neuronal excitability and the maintenance of chronic pain states (Wieseler-Frank et al. 2005). During some pain states the BSCB can become compromised (Varatharaj and Galea 2016; Radu et al. 2013; Willis et al. 2008) (see Figure 1.6 and Table 1.1 for summary). In fact, C fibre activation alone can cause generalised extravasation of serum proteins into brain and spinal cord tissue (Beggs et al. 2010), and so clearly chronic pain conditions (with sustained nociceptor activation) such as RA are at risk of compromised barriers.

Although well documented in pain conditions such as nerve injury and subcutaneous peripheral inflammation, it is not clear what happens after chronic inflammatory pain states like RA, and exactly whether, and if so then *how*, nociception and primary afferent activation can compromise the BSCB. As mentioned above, glia signal with both neurones and endothelial cells, so may be paramount in orchestrating neuronal-induced barrier permeability, or endothelial-induced neuronal activation. Microglial activation was not required for increased BSCB permeability after nerve injury (Echeverry et al. 2011), and so perhaps astrocyte activation is more important here. Additionally, it is not known whether a compromised NVU contributes to the hypersensitivity seen in chronic pain and whether it is involved in the development and/or maintenance of central sensitisation. In other words, is barrier permeability merely a consequence of sustained and chronic pain, or does it have a role in setting up and maintaining central sensitisation and chronic pain? We have started to answer these unknowns by investigating the gliovasculature in experimental inflammatory arthritis (Beazley-Long et al. 2018b). We demonstrated a role of endothelial cells in chronic pain development and associated glial activation through disrupting Vascular Endothelial Growth Factor Receptor (VEGF-R)2 signalling, but more work is needed to fully understand the role of

the microvasculature and BSCB (Beazley-Long 2019).

Alterations in the normal functioning of the BSCB can involve changes in anatomy that can be observed histologically, for example endothelial damage and tight junction alterations, or a change in function at the molecular level, for example up-regulation of endothelial transporters and cytokine production (Varatharaj and Galea 2016). The alterations documented below (see Section 1.3.4) are a combination of both, but it is important to note that if anatomical changes are absent, molecular changes might still occur.

It is also important to note that alterations in barrier integrity and gliovascular activation will not only have implications for pain signalling, but will also have an impact on the access of drugs into the CNS. Drug delivery into the CNS can be difficult due to the highly selective nature of the BBB/BSCB, which can either be problematic when trying to treat CNS disorders or beneficial and neuroprotective when treating peripheral disorders. There is a risk that periods of BBB/BSCB instability caused by pain states may also allow access to the CNS of neurotoxic drugs that are usually restricted to the periphery, meaning there is the potential for them to access and damage nervous tissue.

Activation of the Bradykinin-2 receptor has been shown to rapidly and transiently cause the BBB to become more permeable through disengagement of tight junctions and assist drug delivery into the CNS (Borlongan and Emerich 2003). Bradykinin is increased during and after inflammation and nerve injury (Abbott et al. 2006; Levy and Zochodne 2000; Petersen et al. 1998; Dray and Perkins 1993), suggesting there is a potential for uncontrolled infections and insults to cause the BBB/BSCB to become more permeable to pharmaceuticals. Claudin-5 also seems to be important in restricting access of small molecules (<800Da) across the BBB/BSCB without altering structural morphology (Nitta et al. 2003), and claudin-5 expression has been shown to be altered during pain states (Campos et al. 2008; Brooks et al. 2005), although there are conflicting reports as to whether claudin-5 increases or decreases. The implication of undesirable drug access to central tissue during different pain states has not been greatly considered but it is clearly important in regards to patient safety. Conversely, enhanced CNS access to drugs during pain states may actually be beneficial in terms of drug treatment effectiveness.

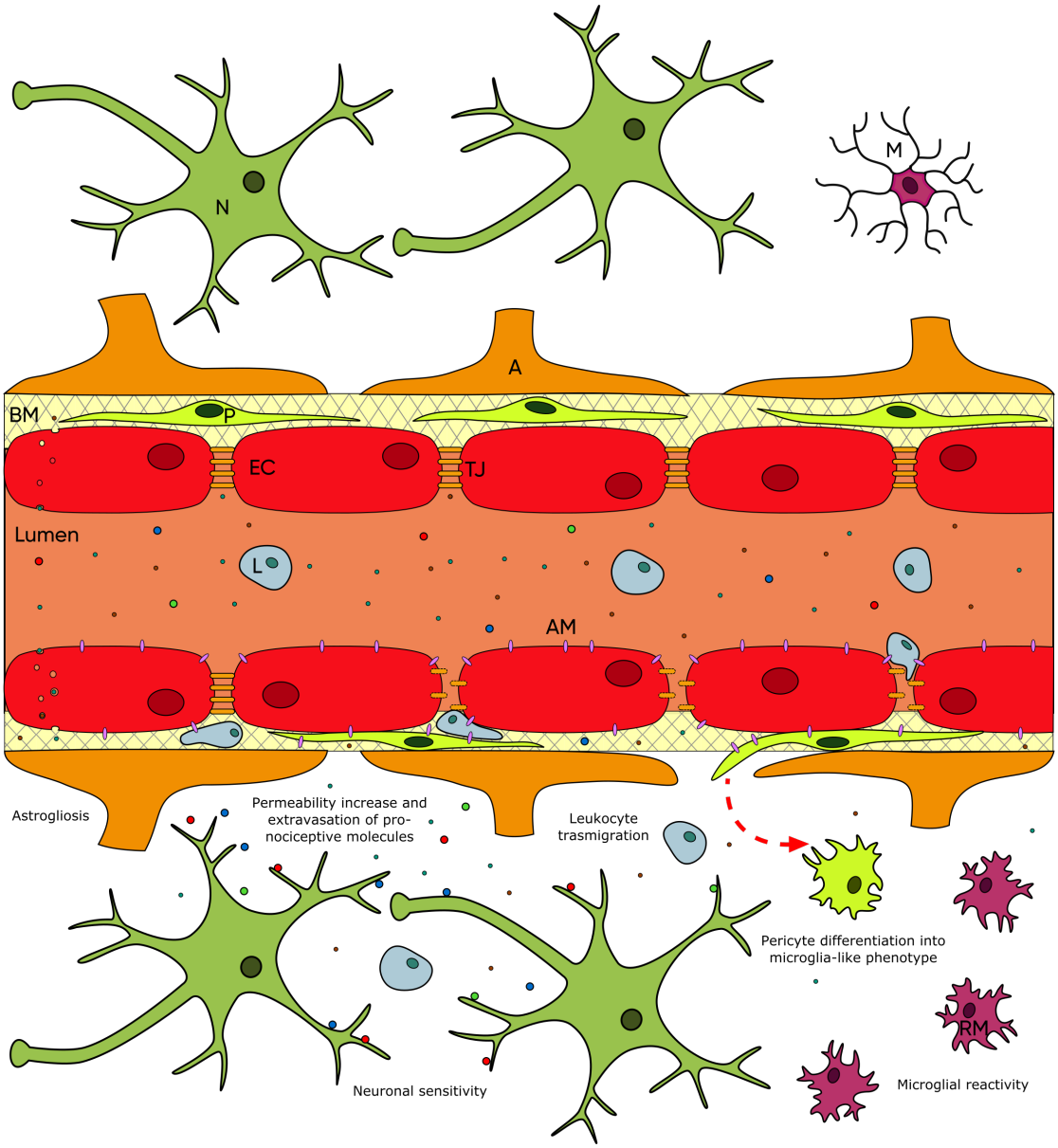


Figure 1.6: Barrier disruptions that can occur during chronic pain. In the top half of the figure, the blood spinal cord barrier is maintained by glial and endothelial cells, and prevents extravasation of blood-borne molecules and cells. The bottom half of the figure demonstrates barrier disruptions that can occur in painful conditions, including increased molecule extravasation, leukocyte transmigration, and glial activation. **A**: Astrocyte endfoot; **AM**: Adhesion molecules; **BM**: Basement membrane; **EC**: Endothelial cell; **EJs**: Endothelial junctions; **L**: Leukocyte; **M**: Myelin; **N**: Neurone; **P**: Pericyte; **RM**: Reactive microglia; **TJ**: Tight junctions. Adapted from Durrant et al. (2018).

Model		Barrier Disruption?		Immune Cell Transmigration?
		Location (BBB/BSCB/BNB)	Assay	
Nerve Injury	PSNL	BSCB,[1] BNB[2]	Evans blue,[1] Sodium Fluorescein,[1,2] Plasma protein extravasation,[1,2] Tight junction alterations[1,2]	SC monocyte infiltration,[1] SC lymphocyte infiltration,[1] Sciatic nerve macrophage infiltration[2]
	CCI	BSCB,[3,4] BBB[3]	Evans blue,[3,4] Horseradish Peroxidase,[3] Sodium fluorescein[4], Tight junction alterations[4]	
	SNI	BSCB[3,4]	Evans blue,[3] Horseradish Peroxidase,[3] Tight junction alterations[4]	SC CD3+/CD4+ T-cell infiltration[5]
	SNL	BSCB[6]	Plasma protein extravasation[6],	SC CD3+/CD4+ T-cell infiltration[7,8]
Chemical Induced-Pain	Capsaicin (peri-neural)	BSCB[3]	Evans blue[3]	
Peripheral Inflammation	Carageenan (intra-plantar)	BBB,[9–11] BSCB[12]	Evans blue,[9] [14C]-sucrose,[9–11] Tight junction alterations,[9–12] Plasma protein extravasation[12]	PMN infiltration in frontal and parietal cortices and thalamus[13]
	CFA (intra-plantar/intra-articular)	BBB[9,14,15]	Evans blue,[9] [14C]-sucrose,[9,14,15] Tight junction alterations[9,14,15]	ICAM-1+ SC vessels,[16] CD11b+ SC microvascular cells[16]
	Formalin (intra-plantar)	BBB[9]	Evans blue,[9] [14C]-sucrose,[9] Tight junction alterations[9]	

(Continued on next page page)

(Continued from previous page)

Diabetic Neuropathy	STZ	BNB,[17] BSCB,[18] BBB[19,20]	Evans blue,[17–19] [3H]-inulin,[19] [14C]-sucrose,[19,20] Tight junction alterations,[18] Alterations in NVU morphology[20]	
CIPN	Paclitaxel	BNB[21]		DRG CD3+ T-Cell infiltration[21]
Migraine	Cortical Spreading Depression	BBB[22]	Evans blue,[22] Tight junction alterations[22]	
Multiple Sclerosis	EAE	BSCB[23]	Evans blue,[23] Tight Junction alterations[23]	SC PBMC infiltration[23]
	LPC	BSCB[24]	Evans blue,[24] Fluorescent-cadaverine,[24] Plasma protein extravasation,[24] Tight junction alterations[24]	

CCI: Chronic constriction injury; **CIPN**: Chemotherapy induced peripheral neuropathy; **CFA**: Complete Freund's adjuvant; **DRG**: Dorsal root ganglion; **EAE**: Experimental autoimmune encephalomyelitis; **FC**: Flow cytometry; **IHC**: Immunohistochemistry; **LPC**: Lysophosphatidylcholine; **PBMC**: Peripheral blood mononuclear cell; **PMN**: Polymorphonuclear neutrophils; **PSNL**: Partial sciatic nerve ligation; **SC**: Spinal cord; **SNI**: Spared nerve injury; **SNL**: Spinal nerve ligation; **STZ**: Streptozotocin. **1**, Echeverry et al. Echeverry et al. 2011; **2**, Lim et al. 2014; **3**, Beggs et al. 2010; **4**, Sauer et al. 2017; **5**, Costigan et al. 2009a; **6**, Gordh et al. 2006; **7**, Cao and DeLeo 2008; **8**, Sweitzer et al. 2002; **9**, Huber et al. 2001; **10**, Huber et al. 2002; **11**, Campos et al. 2008; **12**, Xanthos et al. 2012; **13**, Huber et al. 2005; **14**, Brooks et al. 2005; **15**, Brooks et al. 2006; **16**, Beazley-Long et al. 2018b; **17**, Hulse et al. 2015; **18**, Ved et al. 2018; **19**, Huber et al. 2006; **20**, Salameh et al. 2016; **21**, Krukowski et al. 2016; **22**, Gursoy-Ozdemir et al. 2004; **23**, Bennett et al. 2010; **24**, Muramatsu et al. 2015.

Table 1.1: Summary of barrier disruptions and consequences in painful conditions.

1.3.4 Measuring Alterations in the Neurovascular Unit

There are many ways to identify barrier breakdown, but the simplest way is through detection of extravasation of blood serum proteins into the spinal cord parenchyma. To do this, exogenous substances that would not normally cross the BSCB, for example sodium fluorescein, horseradish peroxidase, or tagged Albumin, are intravenously injected into the animal prior to sacrifice, and the amount of substance found in the CNS can be quantified to give an indication of barrier integrity (Saunders et al. 2015). Additionally, these exogenous substances are different sizes, and so depending on what can extravasate gives further evidence of the extent of barrier breakdown (Saunders et al. 2015). Experimental inflammatory conditions such as CFA, carrageenan, and Experimental Autoimmune Encephalomyelitis (EAE) have demonstrated increased extravasation of central vessels to exogenous substances (Varatharaj and Galea 2016; Wu et al. 2016; Banks 2015; Argaw et al. 2009; Brooks et al. 2005; Huber et al. 2001). It should be noted that plasma protein extravasation can increase with increased blood flow (Bates 2010), and there are caveats to using extravasation of exogenous proteins, such as Evans Blue and horseradish peroxidase to measure barrier integrity, that need to be considered when interpreting results (Saunders et al. 2015). For example, Evans blue does exclusively bind to plasma albumin, and may actually be free (i.e. not bound to plasma proteins) meaning detection of the dye in the CNS does not equate with albumin extravasation (Saunders et al. 2015). In some rat strains, horseradish peroxidase may cause degranulation of mast cells and induce release of histamine and serotonin, which can affect permeability (Saunders et al. 2015).

Another way to study barrier integrity is by looking at changes within components of the NVU, which may be responsible for the increased infiltration of exogenous substances into the CNS. Spinal cord endothelial cells form the walls of blood vessels and are the first line of defence in the NVU, so their proper functioning has an impact on barrier efficacy. By observing changing levels of expression of tight junction proteins after insults, barrier health can be inferred. For example, expression levels of occludin, ZO-1 and claudin-5 can be detected through Western Blotting or immunohistochemistry (Lim et al. 2014; Huber et al. 2001). Similarly to BSCB leakage, experimental nerve injury and inflammation have been shown to alter the expression of tight junction proteins such as ZO-1 (Varatharaj and Galea 2016; Wu et al. 2016; Lim et al. 2014).

Investigating adhesion molecules and other NVU cell proteins, such as GFAP and Cluster of Differentiation-11b (CD11b), can also shed light on barrier functioning. A summary of studies investigating barrier disruption and immune cell transmigration in painful conditions can be found in Table 1.1.

1.3.4.1 Endothelial Cell and Glial Activation

Adhesion molecules such as ICAM-1 and VCAM-1 are constitutively expressed in low levels on the endothelial cell surface and are involved in leukocyte migration (Reglero-

Real et al. 2012; Dustin et al. 1986). ICAM-1 is upregulated in activated endothelial cells by cytokines during inflammation and initiates trans-endothelial migration (Lawson and Wolf 2009; Dustin et al. 1986) either through transcellular or paracellular mechanisms (Reglero-Real et al. 2012; Wittchen 2009). ICAM-1 disruption, either through knock-down or antibody blockade, impairs migration even though adhesion is unaffected (Wittchen 2009), demonstrating its crucial role in diapedesis. Therefore it is conceivable that an increase in ICAM-1 expression would cause an increase in leukocyte migration. There has been little research conducted in ICAM-1 expression in the context of pain, but ICAM-1 has been shown to be increased in the brain, spinal cord and DRG after inflammatory pain (Beazley-Long et al. 2018b; Huber et al. 2005). As ICAM-1 has a role in extravasation, it is an interesting research avenue in the field of barrier disruption associated with painful conditions.

Immune cells infiltrating into the CNS and DRG parenchyma have been detected in nerve injury, inflammatory pain and experimental arthritis (Raoof et al. 2018; Jochmann et al. 2015; Echeverry et al. 2011). These infiltrating immune cells contribute heavily to neuroinflammation and glial activation, and can sensitise and damage neurones (Raoof et al. 2018; Becher et al. 2016; Grace et al. 2014). Although no infiltrating immune cells were detected by my colleagues in inflammatory arthritis (Beazley-Long et al. 2018b), there was an increase in both spinal cord and DRG ICAM-1-positive vessels, which may indicate that immune cells may have been detected at later timepoints. Nevertheless, infiltrating immune cells play an important role in neuroinflammation and central sensitisation, and monitoring their access to the neural parenchyma is important when investigating the gliovasculature and chronic pain.

Interestingly, Echeverry and colleagues (2011) found that bone marrow-derived monocytes/macrophages migrated into spinal cord parenchyma and differentiated into microglia after nerve injury. Additionally, when microglia were depleted at the time of nerve injury, early BSCB permeability to Evans blue still occurred (Echeverry et al. 2011), and hypersensitivity was only partially reversed, suggesting barrier alterations and leakage contributes to development of chronic pain. As hypersensitivity was partially reversed with microglial depletion, they are therefore also important in the gliovascular-neuronal axis that exists in chronic pain. In support of this, in spinal nerve injury, reactive microglia release TNFα, which acts on endothelial cells to induce COX-2 and Prostaglandin I2 Synthase (PTGIS) expression (Kanda et al. 2017). The authors propose that subsequent neuronal-endothelial signalling via Prostaglandin I2 Receptor (IP) and Prostaglandin I2 (PGI2) contributes to the generation of neuropathic pain, highlighting the importance of microglial cells and downstream endothelial signalling in the development and maintenance of chronic pain.

CD11b is the ligand for ICAM-1, and has been found to be upregulated in microglia in chronic pain conditions, including in inflammatory pain (Ji et al. 2013), making it an ideal candidate for investigating the microglial response in chronic pain conditions. Recently, Haruwaka and colleagues (2019) showed that some microglia helped to maintain the

BBB through claudin-5 expression in early inflammation, but in sustained inflammation microglia phagocytosed astrocytic end-feet and increased BBB permeability (Haruwaka et al. 2019). Astrocytes are clearly important in this gliovascular-neuronal axis (Ji et al. 2019), and their increased expression of GFAP during activation can also be monitored to investigate their response to inflammatory pain (Eng and Ghirnikar 1994). Additionally, activated astrocytes have been shown to be involved in BBB breakdown through their release of VEGF-A acting on endothelial cells (Argaw et al. 2012; Argaw et al. 2009; Argaw et al. 2006), highlighting their role in the gliovascular-neuronal axis. Interestingly though, ablation of astrocytes or their endfeet had limited impact on BBB function (Kubotera et al. 2019; Schreiner et al. 2015; Tsai et al. 2012). Nevertheless, these studies may question whether astrocytes are essential to barrier maintenance, but the role of astrocytes in barrier *modulation* is still well-established (Osipova et al. 2018; Abbott et al. 2006).

1.3.5 VEGF

VEGF is a subfamily of proteins that are involved in the formation of blood and lymphatic vessels. Of the 5 members, VEGF-A has the most evidence for being involved in the physiological functioning of endothelial cells, including angiogenesis, migration and proliferation. There are several isoforms of VEGF-A, which result from alternative splicing of the *Vegfa* gene (see Figure 1.7). Splicing is controlled by several RNA binding Serine/Arginine (SR) proteins, such as Serine/Arginine Splicing Factor 1 (SRSF1) and Serine/Arginine Splicing Factor 2 (SRSF2), and occurs at major sites on exons 6 and 7 and at exon 8 (Peach et al. 2018). Splicing at exon 8 can result in anti-angiogenic VEGF-A_{xxx}b isoforms, rather than prototypical angiogenic VEGF-A_{xxx}a, where xxx refers to the number of amino acids in the mature protein sequence (Peach et al. 2018; Bates et al. 2002). VEGF-Ax is the newest identified isoform and results from extended translation and includes both the 8a and 8b sequences (Peach et al. 2018). The VEGF-A_{165} isoform is the most widely studied and its two variants, VEGF-A_{165}a and VEGF-A_{165}b, have generated interest in the pain field as they have seemingly opposite effects on pain. After nerve injury, VEGF-A_{xxx}a is upregulated compared to VEGF-A_{xxx}b, and by blocking the splicing of VEGF-A_{xxx}a to favour VEGF-A_{xxx}b, neuropathic pain can be reduced (Hulse et al. 2014; Hulse et al. 2016). Additionally, exogenous VEGF-A_{165}a exacerbates neuropathic pain whereas VEGF-A_{xxx}b reverses pain (Hulse et al. 2016; Hulse et al. 2014). As well as with nerve injury-induced pain, the development of secondary inflammatory pain can be prevented with VEGF-A_{165}b (Beazley-Long et al. 2018b).

VEGF-A and all its isoforms activate VEGF-Rs 1 and 2, but VEGF-R2 appears to mediate many of its actions (Peach et al. 2018). VEGF-R1 shows decreased activity upon VEGF-A binding, and so was thought to be a decoy receptor and negative modulator of VEGF-R2 (Peach et al. 2018), although there is now evidence to show VEGF-R1 has an independent functional role (Weddell et al. 2018). Both VEGF-R1 and VEGF-R2 have been implicated in chronic pain (Qiu et al. 2020; Lee et al. 2019; Beazley-Long et al.

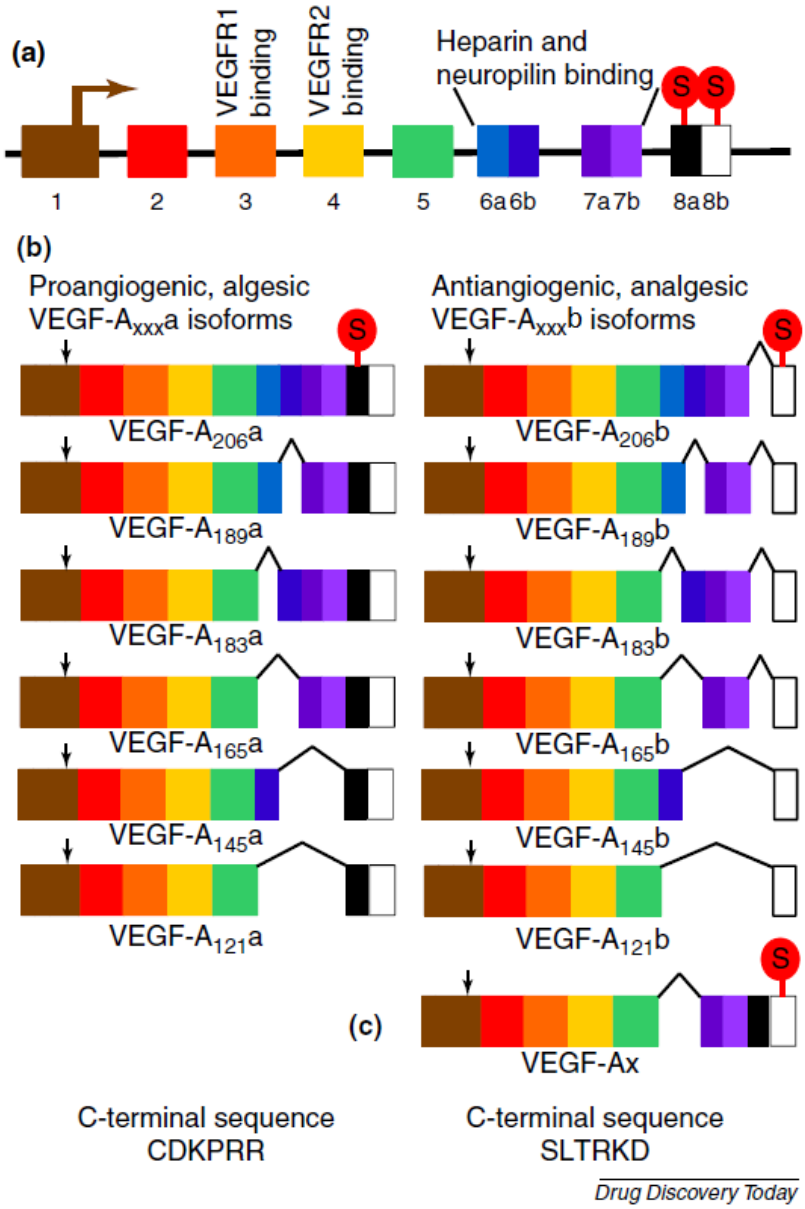


Figure 1.7: Splicing variants of the *VEGFA* gene. **(a)** Structure of the *Vegfa* gene with translational start (arrow) and stop codons (red circles). **(b)** VEGF-A$_{xxx}$a and VEGF-A$_{xxx}$b (xxx refers to the amino acid number of the mature protein) splice variants of *Vegfa*. **(c)** VEGF-Ax is the newest isoform that has been identified. From Donaldson and Beazley-Long (2016).

2018b; Hulse et al. 2016; Selvaraj et al. 2015; Hulse et al. 2014; De Bandt et al. 2003).

Alterations in VEGF-A signalling have been demonstrated in several diseases, including both OA and RA (Hamilton et al. 2016; Llorián-Salvador and González-Rodríguez 2018), but specific mechanisms of its contribution in the CNS to the development and maintenance of chronic pain are still unclear. In the periphery, VEGF-A is one of the main factors responsible in arthritis for angiogenesis, swelling, synovial thickening, neurovascular invasion and inflammation, and can directly stimulate nociceptors (Hamilton et al. 2016; Llorián-Salvador and González-Rodríguez 2018). In the CNS, VEGF-A increases BBB permeability (Argaw et al. 2012; Croll et al. 2004; Proescholdt et al. 1999; Dobrogowska et al. 1998) and can induce experimental neurovascular angiogenesis (Croll et al. 2004; Proescholdt et al. 1999; Dobrogowska et al. 1998). One emerging hypothesis of VEGF-A's central contribution to chronic pain is that VEGF-A signalling in spinal endothelial cells can encourage endothelial activation, leading to BBB/BSCB permeability and downstream glial alterations. These could ultimately lead to neuronal sensitivity and increased pain signalling. This is supported by the study from our lab (Beazley-Long et al. 2018b) as blockade of VEGF-A signalling both systemically (with pharmacological VEGF-R inhibition) and specifically in endothelial cells (with inducible endothelial cell VEGF-R2 knockdown) in murine models of inflammatory monoarthritis prevented the development of secondary hyperalgesia.

As well as VEGF-A's role in pain, it has a well-established contribution to endothelial signalling and BBB/BSCB functioning (Argaw et al. 2012; Croll et al. 2004; Proescholdt et al. 1999; Dobrogowska et al. 1998). It has been linked to the gliovascular-neuronal axis as neurones can activate astrocytes and cause them to release VEGF-A, which acts on endothelial cells to disrupt the BBB (Li et al. 2014; Argaw et al. 2012; Argaw et al. 2009; Argaw et al. 2006). VEGF-A and its receptors are clearly important in nociceptive signalling and the relationship between neurones, astrocytes, and endothelial cells, and both require more investigation to fully understand their role. Further discussion of VEGF-A can be found in Chapter 4.

1.4 Aims and General Hypothesis

In chronic pain conditions, there is central sensitisation, glial activation and neuroinflammation (Ji et al. 2018; Millan 1999). Activated glial cells (and infiltrating immune cells) can further sensitise neurones through enhanced pre-synaptic neurotransmitter release and increased post-synaptic transmission (Figure 1.8) (Ji et al. 2019; Ji et al. 2016; Tsuda et al. 2013; Ji et al. 2013). There is also central endothelial activation and BSCB disruption demonstrated by increased permeability and changes in endothelial cell tight junction and adhesion junction expression (DosSantos et al. 2014; Radu et al. 2013; Willis et al. 2008). However, there are still some gliovascular unknowns in chronic inflammatory pain development/maintenance that this thesis aimed to investigate (Figure 1.8):

1. What is the role of endothelial cells?
2. What is the role of the astrocyte-endothelial cell relationship?
3. Is there increased immune cell binding to the neural endothelium and increased trafficking into the parenchyma?
4. What are the roles of TNFα and VEGF-A on the gliovasculature and neuronal signalling?

Peripheral inflammation can lead to secondary pain, which may be due to glial activation, neuroinflammation, and BSCB disruption. I hypothesised signalling between the gliovasculature, notably between endothelial cells and astrocytes, can drive central sensitisation and contribute to chronic pain development/maintenance. I hypothesised this is mediated by two key inflammatory mediators, VEGF-A and TNFα.

This was explored experimentally by:

- Developing histological analysis techniques that specifically probe the NVU to detect gliovascular changes in rodents (Chapter 3).
- Inducing inflammatory arthritis in rodents, and inhibiting VEGF-R2 and/or TNFα function to measure effects on pain behaviour and gliovascular alterations (Chapter 4).
- Using Human Brain Microvascular Endothelial Cells (HBMECs) to investigate their functional response to TNFα and VEGF-A application (Chapter 5).
- Measuring WDR neurone responses to noxious stimuli after TNFα application (Chapter 6).

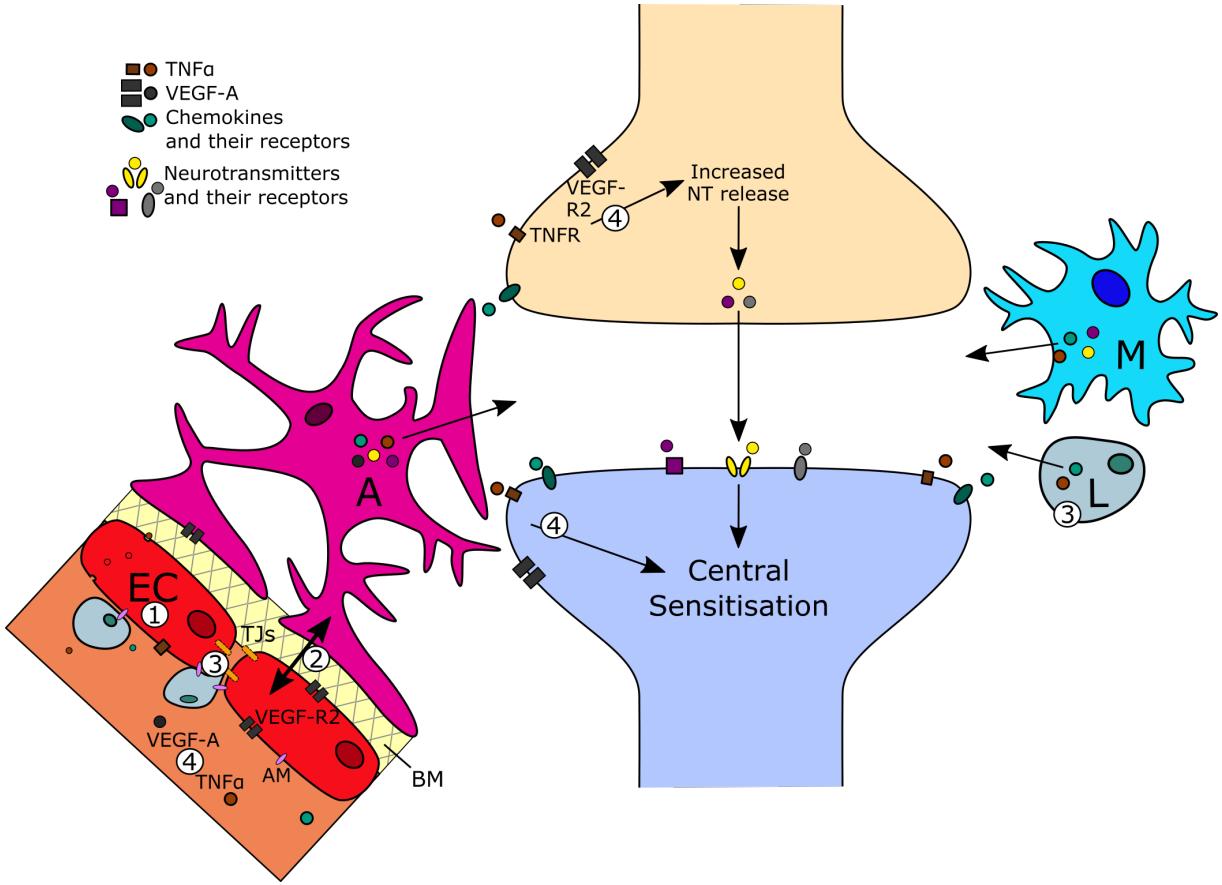


Figure 1.8: In chronic pain conditions, there is central sensitisation, glial activation and neuroinflammation. Activated glial cells and infiltrating immune cells can enhance nociceptive signalling through release of gliotransmitters and inflammatory molecules that both increase pre-synaptic neurotransmitter release and post-synaptic transmission. There is also blood-spinal cord barrier (BSCB) disruption and endothelial activation demonstrated by increased BSCB permeability, increased adhesion molecule expression and immune cell trafficking into the parenchyma, and decreased tight junction expression. However, there are still some gliovascular unknowns in chronic inflammatory pain development/maintenance that this thesis aimed to investigate: what is the role of endothelial cells (**1**) and of the endothelial-astrocyte relationship (**2**); is there increased immune cell binding and increased trafficking (**3**); what are the roles of TNFα and VEGF-A on the gliovasculature and neuronal signalling (**4**)? **A**: astrocyte; **AM**: adhesion molecules; **BM**: basement membrane; **EC**: endothlial cell; **L**: leukocyte; **M**: microglia; **NT**: neurotransmitter; **TJs**: tight junctions; **TNFα**: tumour necrosis factor α; **TNFR**: tumour necrosis factor receptor; **VEGF-A**; vascular endothelial growth factor-A; **VEGF-R2**: vascular endothelial growth factor receptor 2.

2 | Materials & Methods

2.1 Introduction

This chapter provides an overview of the methodologies used throughout this thesis to generate data for results chapters. More detailed methods relevant to the results will be given in each chapter to provide more information.

2.2 In Vivo Procedures

2.2.1 Animal Usage

All experiments and procedures were performed in accordance with the Animals (Scientific Procedures) Act (1986; 2012) and were authorised by the UK Home Office. All studies were designed to minimise suffering and distress, and appropriate endpoints and severity limits were set out before the study commenced. Animals were habituated by myself prior to any behavioural or surgical procedures being carried out, and on the day of pain behavioural testing, animals were acclimatised for 15-20 min prior to testing.

Experiments were carried out on adult (≥175g) male Sprague Dawley (SpD) or Wistar rats (Charles River, UK). The oestrus cycle in females causes hormone fluctuations that may interact with pain signalling and experimental outcomes (Becker et al. 2005a; Craft et al. 2004), and so male rats were used due to time constraints and because the work carried out in this thesis was early work within the gliovascular-pain field. Once robust results and conclusions have been drawn from male rats, the same outcomes in female rats should be measured, especially since there are sex differences in the neuroimmune modulation of pain (Rosen et al. 2017) and Rheumatoid Arthritis (RA) course and severity (Vollenhoven 2009). Experiments involving transgenic mice (*vegfr2*$^{fl/fl}$ Tie2CreER^{T2}, see (Beazley-Long et al. 2018b) and 2.2.3.1) were carried out on both male and female adult mice.

Rats were group-housed (3-4 per cage) in conventional or individually-ventilated cages and mice were group-housed in individually ventilated cages (3-4 per cage), and animals maintained in a 12 hour light/dark cycle at 22˚C and 55% humidity with access to food and water *ad libitum*. Animals were allocated to treatment groups using the standard = RAND() function in Microsoft Excel or by an independent investigator. Sample size was calculated (`http://powerandsamplesize.com/Calculators/Compare-2-Means/2-Sample-Equality`) for each experiment using data from previous experiments and will be specified in relevant chapter methods.

All treatment groups and experimental conditions were blinded. An independent in-

vestigator allocated animals to treatment groups and shared the blinding code with a second independent investigator to help with drug dosing. Drugs were prepared by me but drawn up into syringes by an independent investigator so I was unaware of the drug being injected. For pain behaviour, an independent investigator randomly placed animals into the relevant behaviour boxes so I was unaware of which cage (or treatment group) animals were from. Tissue processing and immunofluorescence was also carried out on blinded sections, and animals and treatment groups were only unblinded after image analysis using the blinding code.

2.2.2 Nociceptive Surgical Procedures

2.2.2.1 Anaesthesia

Isoflurane (Abbott Laboratories, Kent, UK) was chosen as an anaesthetic as inhalation causes a continuous depth of anaesthesia that can be easily adjusted during surgery. Animals were anaesthetised with 3% isoflurane vaporized (Burtons, Kent, UK) in 100% Oxygen using an induction box until the automatic righting reflex ceased. Animals were then transferred to a heat mat (Harvard Apparatus, UK) and connected to a nose cone with a non-rebreathable tubing system. Fluo Vac (Harvard Apparatus, Massachusetts, U.S.A) was used as an active extraction system to remove exhaled gasses via an aldasorber (Pioneer, Kent, U.K). Pressure was controlled by 0-4 bar multistage gas ARC multistage regulators, and flow rate was maintained by Platon glass variable flow meters. Animals were allowed to recover in dedicated cages before returning to their home cage.

2.2.2.2 Intraplantar Carrageenan Model

λ-Carrageenan (2%, Sigma-Aldrich) was prepared by immersing carrageenan in 0.9% saline (NaCl) and placing the solution in a water bath at 50°C for 24 hours. The solution was then agitated and kept at room temperature prior to use. 2% carrageenan was chosen as this concentration has been used in previous studies to produce acute pain responses in the rat (Chakrabarty et al. 2011; Loram et al. 2007; Hua et al. 2005). Vehicle used was 0.9% sodium chloride (NaCl). Induction of inflammation was carried out by Dr Emma Dayman. SpD rats were anaesthetised with 3% isoflurane as described above and maintained in 2% isoflurane delivered via a face mask in the same gas mixture. Once areflexic (confirmed by the pedal reflex), the left hindpaw was disinfected using chlorhexidine gluconate 4% surgical scrub (Hydrex®) and received a subcutaneous injection of 100μL of 2% (w/v) of carrageenan or saline using a 25-gauge; 16-mm needle (Becton, Dickinson and Company Ltd, Ireland, 300600) attached to a 1ml hypodermic syringe (Terumo, New Jersey, U.S.A). Animals were housed in conventional cages, and severe limping and spontaneous vocalisation were monitored for the duration of the study.

2.2.2.3 Intra-articular MIA Model

Monosodium Iodoacetate (MIA) (Sigma-Aldrich, Germany) was dissolved in 0.9% NaCl to obtain a final concentration of 2mg/50µL. MIA inhibits NADPH and chrondrocyte metabolism to cause rapid degeneration in joint integrity, and at a dose of 2mg has been shown to induce peripheral nerve injury (Thakur et al. 2012). SpD rats were anaesthetised with 3% isoflurane as described above and maintained in 2.5% isoflorane delivered via a face mask in the same gas mixture. Once areflexic (confirmed by the pedal reflex), the left knee was shaved with hair clippers and the leg was disinfected with chlorhexidine gluconate 4% surgical scrub (Hydrex®). The left paw was extended and the base of the patella located, and using a 0.5mL microsyringe, 50µL of MIA or saline were injected through the infra-patella ligament into the knee joint. To prevent posterior leakage, only 2/3 of the needle was inserted. Induction of arthritis was performed by Dr James Burston. Animals were housed in conventional cages and monitored for the duration of the study.

2.2.2.4 Intra-articular CFA Model

Complete Freund's Adjuvant (CFA) was chosen to induce inflammatory monoarthritis as it a well-established model that induces a long-lasting and robust response (Donaldson et al. 1993). CFA is composed of heat-denatured *mycobacterium tuberculosis* suspended in mineral oil, which allows a sustained antigen release and causes an innate immune response (Billiau and Matthys 2001). More information on CFA dosage will be discussed in Chapter 4. CFA was either purchased from Sigma-Aldrich (1mg/mL, F5881) or prepared by resuspending heat-denatured *mycobacterium tuberculosis* (UK Ministry of Agriculture Fisheries and Food, now known as DEFRA, UK) in mineral oil (2mg/mL), sonicated for 1 hr and and filtered (40µm pore size). Control animals received no injection but underwent anaesthesia and shaving of the knee. This is because the oil vehicle and the injection process itself can cause joint damage and inflammation, confounding results.

Wistar rats were anaesthetised with 3% isoflurane as described above and maintained in 2% isoflurane delivered via a face mask in the same gas mixture. Once areflexic (confirmed by the pedal reflex), the right knee was shaved with hair clippers and the leg was disinfected with chlorhexidine gluconate 4% surgical scrub (Hydrex®). The right paw was extended and the base of the patella located, and using a 25-gauge; 16-mm needle needle, 50 or 100µL of CFA (2mg/mL or 1mg/mL to give a final dose of 50 or 100µg) was injected through the infra-patella ligament into the knee joint (tibiofemoral). To prevent posterior leakage, only 2/3 of the needle was inserted. A 25-gauge needle was used as a tighter gauge was too small for the oil to pass through. Shams were anaesthetised and shaved but received no injection. Animals were housed in individually-ventilated cages (two-tier), and gait and hind-leg use were monitored for the duration of the study.

2.2.2.5 Peri-articular CFA Model

In mice, the tibiotarsal (ankle) joint was targeted as a model of inflammatory arthritis. Mice received a subcutaneous, unilateral peri-articular injection of CFA on both sides of the joint. This induces robust inflammatory response that mimics arthritis (Chillingworth and Donaldson 2003). CFA was purchased from DEFRA and prepared in-house at 2mg/mL in mineral oil as described above.

The following procedures were carried out by Dr Nick Beazley-Long. Transgenic male and female mice (*vegfr2*$^{fl/fl}$ Tie2CreER^{T2}, see (Beazley-Long et al. 2018b)) were anaesthetised with 3% isoflurane as described above and maintained in 2% isoflurane delivered via a face mask in the same gas mixture. Once areflexic (confirmed by the pedal reflex), the right leg was shaved and disinfected, and mice received 2 x 80µg CFA in 40µL oil, on either side of the tibiotarsal joint (unilateral). Shams were anaesthetised and shaved but received no CFA injection, and were age/sex matched. Animals were housed in individually-ventilated cages (single-tier) with other non-induced transgenic mice to prevent tamoxifen cross-contamination, and gait and hind-leg use were monitored for the duration of the study.

CFA vehicle was not injected into control animals because the oil and injection itself are sufficient to cause inflammation, therefore confounding the interpretation of results.

2.2.3 Drug Dosing

2.2.3.1 Induction of Endothelial Cell VEGF-R Knockout in Transgenic Mice

Inducible endothelial *vegfr2* knockout mice were produced by crossing mice that were homozygous for the Vascular Endothelial Growth Factor Receptor (VEGF-R)2 gene with floxP sites either side of exon 1 (*vegfr2*$^{fl/fl}$) (Albuquerque et al. 2009) with Tie2CreER^{T2} mice [European Mutant Mouse Archive EM:00715] (Forde et al. 2002). All mice used were confirmed homozygous for the VEGF-R2-loxP transgene (*vegfr2*$^{fl/fl}$) and either heterozygous or wild-type for Tie2CreER^{T2}. Filial (F)3/F4 female and male mice were used.

Tamoxifen (Sigma, T5648) was dissolved in ethanol then diluted in autoclaved sunflower oil (vehicle: 10% ethanol and 90% oil) (Acharya et al. 2011). Five daily doses of tamoxifen (1mg/100µL Intraperitoneal (i.p.)) or vehicle (volume/route-matched) were administered to either Tie2CreER^{T2}-positive or Tie2CreER^{T2}-negative mice as a control for actions of tamoxifen prior to induction of inflammation.

2.2.3.2 Pharmaceutical VEGF-R Antagonism

Animals were dosed via i.p. injection of PTK787 (15mg/kg, AdooQ BioScience LLC, USA, A10967 or Selleckchem, USA, S1101)) and/or Etanercept (5.5mg/kg, Enbrel®, Pfizer Limited, UK) in Phosphate Buffered Solution (PBS) or saline vehicle. Drug doses and

regimes were based on previous published studies (Boettger et al. 2008; Beazley-Long et al. 2018b). PTK787 was first dissolved in either sterile PBS or saline vehicle at 3.75mg/mL to give a final dose of 15mg/kg. If in PBS, the solution was heated to 60˚C, vortexed, sonicated (1 hr) and filtered (40µm pore size) to ensure no clumps remained in the solution. Heating, vortexing, sonication and filtering were not needed if PTK787 was dissolved in saline. Etanercept was diluted in sterile PBS or saline to 1.375mg/mL to give a final dose of 5.5mg/kg.

2.2.3.3 Prophylactic Dosing

To investigate whether VEGF-R are involved in the development of chronic pain, animals were dosed with PTK787 for one week prior to induction of inflammation. Animals received an injection i.p. of PTK787 (15mg/kg), etanercept (5.5mg/kg) or vehicle (PBS, equivalent volume per body weight) 7 and 4 days prior to inflammation.

2.2.3.4 Therapeutic Dosing

Animals were first dosed with vehicle (PBS or saline, i.p.) for one week prior to inflammation to allow animals to habituate to dosing. Once mechanical hypersensitivity was confirmed at 3 days, animals were dosed i.p. with PTK787 (15mg/kg) and/or etanercept (5.5mg/kg), or vehicle (saline or PBS, equivalent volume per body weight) 3 and 7 days or 3, 6 and 9 days post-inflammation. A group of animals were dosed at induction of inflammation (day 0) as a positive control, as this regime has previously been shown to prevent the development of secondary pain (Beazley-Long et al. 2018b).

2.2.4 Behavioural Tests

2.2.4.1 Weight-Bearing Asymmetry

Weight distribution across both limbs, to determine weight-bearing asymmetry, was detected using an Incapacitance Tester (Linton Instrumentation, UK) to assess pain behaviour prior to and after induction of nociception. Animals were placed in an angled plexiglass chamber (Medical Engineering Unit, University of Nottingham) and hindpaws centred on individual pressure sensors that measured the average force (in grams) over 3 sec. Three recordings were made, and results displayed as the difference in weight borne between ipsilateral and contralateral hindpaws. Alternatively, weight-bearing is displayed as percentage of weight borne on the ipsilateral side using the following formula:

(average weight borne on ipsilateral / total weight borne on both limbs) * 100

2.2.4.2 Mechanical Hypersensitivity

Mechanical thresholds are a useful technique to detect allodynia by observing painful withdrawal responses from von Frey monofilaments (Touch Test® Sensory Evaluators)

that have different bending forces (0.16, 0.6, 1, 2, 4, 8, 15, 26, and 60g). Animals were placed in transparent plastic boxes with mesh flooring (Medical Engineering Unit, University of Nottingham), and were allowed to acclimatise before testing. Mechanical sensitivity was assessed by measuring the threshold at which the hindpaw withdrew from mechanical punctate stimuli (calibrated von Frey monofilaments). Each von Frey monofilament was applied perpendicular to the plantar surface of the ipsilateral and contralateral hindpaws 3 times for a period of 3 seconds each. If no withdrawal response was seen, the next highest hair was applied; if a response was seen, a lower hair was applied until no response was elicited. This is known as the up-down paradigm (Chaplan et al. 1994) and results displayed as the lowest monofilament (i.e. the threshold) to elicit a response.

Alternatively, mechanical sensitivity was assessed by determining the force that evoked paw withdrawal at 50% of stimulations from von Frey monofilaments. Each von Frey hair was applied to the plantar surface of the ipsilateral and contralateral hindpaws 5 times for a period of 3 seconds each, and the number of times the paw was withdrawn was counted. It should be noted that the 5 repetitions were not carried out at once as the paw may become desensitised - each paw received 2 applications then other rats were tested before returning to the first rat for 2 more applications, retesting other rats, and then repeating the final application. If a response was detected, a lower hair was applied until no response was elicited. Then hairs increased in force until a response was elicited 100% of the time. The proportion of withdrawal responses was plotted against the log of the bending force, and a stimulus-response curve was generated to determine the 50% withdrawal response. A positive response to a monofilament was classified as a quick withdrawal of the paw or a flinch, which may or may not be accompanied by licking or shaking of the paw.

2.2.4.3 Knee Diameter

In order to monitor and record swelling, ipsilateral and contralateral knee diameters were recorded using callipers. Three recordings were taken in each session and the average recorded.

2.2.5 Tissue Processing

At the end of each study, animals were euthanised by overdose of sodium pentobarbitone (i.p., 60 mg/ml) and transcardially perfused with saline, with or without 1U heparin, then 4% Paraformaldehyde (PFA) in 0.1M PBS. Heparin helps to prevent the blood from clotting during perfusion. To perform the transcardial perfusion, once animals were areflexic (confirmed by pedal reflex and blink reflex), the chest cavity was opened and blunt needle attached to a cannula and connected to the perfusion apparatus was inserted into the left ventricle of the still-beating heart. An incision was made in the right atrium and animals were transcardially perfused at a pressure of 80-100mmHg with 300mL saline (with or without 1U heparin) followed by 300mL 4% PFA. Spinal cords

were dissected, kept in 4% PFA overnight and maintained in 30% sucrose with 0.02% w/v sodium azide (Sigma-Aldrich, UK) for free-floating immunofluorescence. Alternatively, for slide-mounted immunofluorescence, spinal columns were collected, kept in 4% PFA overnight, then spinal cords and Dorsal Root Ganglion (DRG) Lumbar Section (L) 3-5 were collected and cryo-protected in 30% sucrose for 3-4 days until being stored whole at -80˚C.

2.2.6 Immunofluorescence

Antibodies used are detailed in Table 2.1 and Table 2.2. Primary host-matched Immunoglobulin G (IgG) antibody controls were used. For slide-mounted immunofluorescence, spinal cords were cut at or just above the thickest part of the lumbar area and cut rostrally up the spinal cord, allowing the areas of the spinal cord innervated by the knee and foot to be investigated. 40µm (20µm in mice, performed by Dr Nick Beazley-Long) spinal cord sections and 20µm DRG sections were cut using a cryostat and thaw-mounted on slides (SuperFrost® Plus, VWR). Sections were wrapped in film and maintained at 4˚C until immunofluorescence performed. Alternatively, for free-floating immunofluorescence, spinal cords were marked for the contralateral side using a needle, and the thickest part of the lumbar area was sectioned using a freezing microtome (Leica, SM2010R) at 40µm. Dry ice was used to freeze and mount the tissue onto the stage, and the blade was frozen before the slicing. Sections were collected in 24-well plates filled with 30% sucrose solution with 0.02% w/v sodium azide, wrapped in film and stored at 4°C until use. Free-floating immunofluorescence was performed on 40µm sections before being mounted onto gelatinised glass microscope slides.

Sections were washed in PBS + 0.2 or 0.3% Triton-X-100, and blocked for 1 hour in 5% BSA + 10% Foetal Bovine Serum (FBS) in 0.1, 0.2 or 0.3% Triton-X-100 in PBS. Primary antibodies were then applied overnight in the same block then washed in PBS + Triton-X-100 whilst being gently agitated. Secondary antibodies were applied for 4 hours in block then sections were washed again. With free-floating immunofluorescence, sections were gently agitated during antibody incubations. Sections were then mounted onto slides if needed and coverslipped using Fluoroshield™ mounting medium (Sigma-Aldrich, F6182) then sealed with nail varnish. Sections were imaged on a confocal microscope (Leica TCS SPE, Leica Microsystems). Images were analysed using FIJI Image J software (National Institutes of Health, USA) as described in 3 with or without the additional BioVoxxel plugin (BioVoxxel, Germany).

2.2.7 Spinal Electrophysiology

In order to gain an understanding of neuronal responses to inflammatory mediators, spinal electrophysiology was carried out on SpD rats. The method used here measures the activity of single Wide Dynamic Range (WDR) neurones in response to noxious stimuli and in the presence of the inflammatory mediator, Tumour Necrosis Factor α (TNFα).

Identifies	Antibody	Host	Supplier	Product Number	Working Concentration
Microglia	CD11b	Mouse	BIO-RAD	MCA275GA	2µg/ml
Vascular Endothelial Cells	CD31	Goat	R&D Systems	AF3628	2µg/ml
Monocytes/Macrophages	CD68	Rabbit	abcam	ab125212	1µg/ml
Astrocytes	GFAP	Goat	abcam	ab53554	1µg/ml
Astrocytes	GFAP	Mouse	ThermoFisher	MS-1376-P	0.2µg/ml
Astrocytes	GFAP	Rabbit	abcam	ab7260	1µg/ml
ICAM-1	ICAM-1	Mouse	ThermoFisher	MA5407	2µg/ml (IF/WB) 100ng/ml (MA)
Vascular Basement Membrane	Laminin	Rabbit	Novus Bio	NB300-144	2µg/ml
Vascular Endothelial Cells	RECA-1	Mouse	ThermoFisher	HIS52	1µg/ml
ZEB-1	ZEB-1	Rabbit	Santa Cruz	sc-515797	2µg/ml
VEGF-R2	VEGF-R2	Rabbit	Cell Signalling Technology	2479	1:200
Actin Filaments	β-actin	Goat	Santa Cruz	sc1615	0.5µg/ml
-	IgG	Rabbit	LS Bio	LS-C109222	matched*
-	IgG	Mouse	Novus Biologicals	NBP1-97019	matched*

CD11b: cluster of differentiation 11b; **GFAP**: glial fibrillary acidic protein; **ICAM-1**: intracellular adhesion molecule-1; **IF**: For use in immunofluorescence; **MA**: For use in monocyte attachment assays; **RECA-1**: rat endothelial cell antigen-1; **VEGF-R2**: vasculare endothelial growth factor receptor 2; **WB**: Western blotting; **ZEB-1**: Zinc finger E-box-binding homeobox 1. ***** IgG concentration was matched to the relevant primary antibody concentration.

Table 2.1: Details of primary antibodies

Target	Host	Fluorophore	Supplier	Product Number	Working Concentration
α-Goat	Chicken	AF® 488	Invitrogen	A21467	1µg/ml
α-Mouse	Donkey	AF® 488	Invitrogen	R37114	2 drops/1mL
α-Goat	Donkey	AF® 555	Invitrogen	A21432	1µg/ml
α-Mouse	Donkey	AF® 555	Invitrogen	A21202	1µg/ml
α-Rabbit	Donkey	AF® 555	Invitrogen	A31572	1µg/ml
α-Rabbit	Donkey	CF™ 633	Sigma	SAB4600132	1µg/ml
α-Rabbit	Donkey	IRDye® 680RD	LI-COR	926-68073	0.2µg/ml
α-Mouse	Donkey	IRDye® 800CW	LI-COR	926-32212	0.2µg/ml
α-Goat	Donkey	IRDye® 680CW	LI-COR	926-68074	0.2µg/ml
F-Actin	Phalloidin-conjugate	AF® 488	ThermoFisher	A12379	1:500
Hoeschst-543334		-	Sigma	-	1µg/ml

AF: Alexa Fluor®; **CF**: CruzFluor™

Table 2.2: Details of secondary antibodies

See Figure 6.1 in Chapter 6 for an overview of the animal setup for spinal electrophysiology.

2.2.7.1 Electrode Etching and Glass-Coating

In order to record from spinal cord dorsal horn neurones, tungsten wire electrodes were used and manufactured in our laboratory using methods adapted from Bullock and others (Bullock et al. 1988). 4cm lengths of tungsten wire (Harvard Apparatus, Kent, UK) were taped around a brass chuck, with 2.5cm projecting beyond the end, and attached to the arm of an etching unit (Medical Engineering, University of Nottingham, UK). Both the chuck and a carbon electrode were lowered into a KNO_2 (13.22M) bath solution, and a current of 250mA was passed through the electrodes while the chuck rotated at 5rpm. This caused the electrodes to taper into a point as the tungsten at the ends is removed via electrolysis. Etching was carried out until the current dropped to 200mA.

The exposed metal was insulated with a glass coating by dropping the etched wire into a glass capillary tube blunt end first (with one end of the tube stoppered with plasticine). The tube was clamped in an electrode pulling unit (Medical Engineering, University of Nottingham, UK) and heated in order to melt the glass. The electrode was pulled down by gravity, causing it to be coated in glass. In order to expose the end of the tungsten tip, the end of the electrode was inserted into a bead of melted borax heated by a cauterising heating element. The heating element was turned off, causing the borax to cool and retract from the electrode tip, which removed the glass and exposed the tip.

2.2.7.2 Electrophysiology Recording

Spinal WDR neurone activity was recorded using the assembled electrode and the signal was amplified and recorded using a Neurolog system. A Neurolog headstage (NL100AK) mounted the electrode, which was grounded to the animal and frame using crocodile clips. Animal-related background was removed from spinal nerve activity recordings with the pre-amplifier. Amplification was set to 2K and the signal was amplified through an AC-DC Amp (NL106) and filtered through low and high-pass filters (NL125; bandwidth 0.8-1.5kHz) to remove background and mains supply noise and leave only the neuronal signal. Signal to noise ratio was typically 4:1.

The signal was sent through an oscilloscope (Tektronix TDS210) to visualise the neuronal responses, an audioamp (NL120s) to provide an auditory cue, and a spike trigger module (NL201) that counted action potentials of a specified height through adjustment of a window discriminator. A CED1401 microprocessor converted spinal neuronal input to a digital signal, and captured with Spike 2.0 version 6.05 (Cambridge Electronic Design, Cambridge, UK).

2.2.7.3 Laminectomy Surgery

Animals were placed in an induction box and anaesthetised with 3% isoflurane (Abbott Laboratories, Kent, UK) vaporised in 33% nitrous oxide and 67% oxygen until the automatic righting reflex ceased. Animals were then transferred to a heat mat (Harvard Apparatus, UK) and connected to a nose cone in the supine position. The trachea was exposed by removing the skin above the throat and blunt dissection of the surrounding muscle. The trachea was raised slightly using forceps to lift it and two ligatures (2.0 suture silk) were loosely tied around it 1cm apart. An incision was made between the ligatures and two tracheal cartilage rings, and 5mm of a cannula (Portex nylon tubing, external diameter 2.1mm, internal diameter 1.5mm) of 5-6cm in length was inserted. The upper trachea was blocked and the cannula secured in place by tying the ligatures using a reef knot. The cannula was then connected to the anaesthetic system.

The animal was secured in place in the prone position using a stereotaxic frame (Medical Engineering Unit, University of Nottingham) and the head stabilised with ear bars. Temperature was maintained at 37±1°C using a heat mat and rectal probe (Harvard Apparatus, UK). An incision was made down the midline of the animals to expose the spinal column, and two further incisions were made either side of the column above the rib cage. The column was secured and raised slightly using a spinal clamp, and spinal processes above L4-7 regions were removed using fine-tipped rongeurs. The tip of the rongeurs were inserted between vertebrae to remove the bone above L4-5 regions and expose the spinal cord. Below the laminectomy, a second clamp was secured and the column was adjusted to ensure it was level and straight, and to prevent movement during the animal's breathing. The spinal cord dura was removed if necessary (present dura made the spinal cord appear dull) using fine forceps and physiological saline was applied to the spinal cord to prevent it from drying. The anaesthetic was then reduced and maintained at 1.5% throughout the procedure. The cord was kept wet with physiological saline.

2.2.7.4 Locating and Stimulating Wide-Dynamic Range Neurones

After a 15-20 min interval to allow for stabilisation of anaesthesia, the tungsten electrode was manually lowered onto the spinal cord lateral to the central vessel using a micromanipulator (SCAT-01 microdrive, Digitimer), until it touched the surface (the surface appeared slightly distorted), and then slowly inserted into the cord at 10μm increments. The electrode was lowered 500-1000μm from the surface, which corresponded to lamina V-IV, and WDR were located by gently tapping the ipsilateral hindpaw until distinguishable and uniform spikes were elicited.

Cells were selected if they had a graded response to mechanical stimulation (8-26g von Frey filaments, with an increased firing rate with higher weights) and Aβ, Aδ, C fibre and Post-Discharge (PD) responses from electrical stimulation. The following stimulation protocols were repeated until baseline responses were stable (three responses within

10% of each other).

2.2.7.5 Electrical Hindpaw Stimulation

Needle electrodes (26-gauge) were inserted into the animal's proximal metatarsal pads, which corresponds to the area innervated by the tibial nerve (Decosterd and Woolf 2000). Controlled electrical impulses were delivered to the rat hindpaw via these electrodes using an NL800A stimulator box. Stimulation was delivered as trains of 16 (0.5 Hz (NL304), 2-ms pulse width (NL401)) consecutive transcutaneous pulses. The intensity was controlled by a pulse generator (NL510) and a counter module (NL603) gated the signal upon completion.

C fibre threshold was determined by delivering a 0.5mA initial pulse and increasing in 0.1mA increments until Aβ, Aδ, and C fibre inputs were included (determined by firing latencies of 0-20ms, 20-90ms, 90-300ms respectively). Responses at 300-800ms post-stimulus were defined as PD. Experimental electrical stimuli (trains of 16 (0.5 Hz, 2-ms pulse width) consecutive transcutaneous pulses) were then applied at three times the C fibre threshold, and repeated every 15mins to monitor long-term drug effects.

2.3 In Vitro Procedures

In order to determine a more detailed understanding of the response of the vasculature, *in vitro* experiments were carried out using Human Brain Microvascular Endothelial Cells (HBMECs). Central Nervous System (CNS) endothelial cells differ from other non-neuronal endothelial cells (Kalucka et al. 2020), and so these cells were chosen over the more common Human Umbilical Vein Endothelial Cells (HUVECs). It is possible to purchase endothelial cells from spinal cord tissue, but these are not as readily available as HBMECs. Higher Passage (p) HBMECs (p27+) were a kind gift from Dr Paul Smith (University of Nottingham), and p1 HBMECs were purchased from ScienCell (ScienCell Research Laboratories, 1000, lot #20978). HBMECs were cultured at 37˚C in RPMI-1640 medium (Sigma, R0883) + 20% FBS, 2mM L-glutamine, 1mM Sodium Pyruvate, 1% MEM non-essential amino acids, 1% MEM vitamin, 1% penicillin/streptomycin. ScienCell HBMECs were cultured on fibronectin-coated (2µg/cm^2) flasks as recommended by the supplier. HUVEC (p5) cDNA was a kind gift from Dr Andy Benest. HUVEC (p5) was a kind gift from Dr Samuel Bestall.

I used Human Monocyte-like Cellss (THP-1s) to investigate endothelial cell 'activation' through THP-1 binding in a monocyte attachment assay (see 2.3.1). THP-1 (Sigma, 88081201) were cultured in suspension in RPMI-1640 + 10% FBS, 1% penicillin/streptomycin.

Stock concentration of TNFα (R&D Systems) was at 100µg/mL in sterile PBS, and Vascular Endothelial Growth Factor (VEGF)-A_{165}a (R&D Systems) at 10µg/mL in sterile PBS. See Section 4.2.9 for information on PTK787 used in cell studies.

2.3.1 The Monocyte Attachment Assay

When endothelial cells become activated by inflammatory mediators they can increase expression of adhesion molecules such as Vascular Cell Adhesion Molecule-1 (VCAM-1) and Intracellular Adhesion Molecule-1 (ICAM-1) (Liao 2013), leading to increased binding of circulating leukocytes as seen in some pain states (Montague-Cardoso et al. 2020; Newton et al. 2017; Zhang et al. 2007). I used this process in the monocyte attachment assay to try to tease out more specific mechanisms.

HBMECs were plated in flat clear bottom black 96 well microplates (Corning Incorporated, 3603) at 30,000 cells (counted with a haemocytometer) per well and either serum starved the same day or left to grow until confluent (2-3days) before serum starving. Cells were serum starved in 1% FBS overnight then pretreated with stimulators human recombinant TNFα or VEGF-A_{165}a (both R&D Systems) in RPMI-1640 + 1% FBS + 1% penicillin/streptomycin for 24 hours. Additionally, there were two control groups: a ″no HBMEC″ group where no HBMECs were seeded but THP-1s were added; and a ″no THP-1″ group where HBMECs were seeded but no THP-1s were added. If required, a blocking ICAM-1 antibody (100ng/mL, ThermoFisher, MA5407) or its concentration and species-matched IgG (100ng/mL, mouse IgG, Novus Biologicals, NBP1-97019) was added with TNFα or VEGF-A_{165}a treatment and again at the time of monocyte HBMEC co-culture. Alternatively, cells were pretreated with 100nM PTK787 for 20min then with recombinant human TNFα (20ng/mL) (R&D Systems) and PTK787 in RPMI-1640 + 1% FBS + 1% penicillin/streptomycin for 24 hours.

THP-1s were fluorescently tagged with 2.5μM Calcein Acetoxymethyl (Calcein-AM) (Sigma-Aldrich, 17783) for 1h at 37˚C, washed in warm PBS, and added to the HBMEC monolayer at 30,000 cells per well and incubated for 2h to allow attachment. Unattached THP-1s were washed off with PBS and gentle agitation (x3 washes) and cells fixed with 4% PFA. Calcein-AM fluorescence was measured on a fluorescence plate reader (VictorX4, Perkin-Elmer). Cells were washed until the level of fluorescence in the ″no HBMEC″ wells equalled that of the ″no THP-1″ wells. Alternatively, if wells were coated with fibronectin, the ″no HBMEC″ control was not included, and so wells were washed 4x and fluorescence was read.

Data shown are corrected for background values by subtraction of the mean fluorescence value of the ″no THP-1″ control group. Data are expressed as raw fluorescence or as a percentage of the maximal mean response.

2.3.2 Immunofluorescence

See Tables 2.1 and 2.2 for details on antibodies.

To investigate whether treatment had an effect on cell shrinkage, some plates were labelled with Hoechst and Phalloidin-conjugates to detect cell nuclei and actin filaments respectively. Wells were washed 3x 5 min in PBS + 0.2% Triton-X, then incubated for

1 h at room temperature with Phalloidin-Alexafluor 488 (Thermofisher, A12379) and Hoechst (Sigma) on a rocker. Wells were then washed 5x 5 min in PBS, then left in PBS and sealed with Parafilm™ wrapping film (Bemis™ HS234526B) until imaging.

Images were captured on Confocal and fluorescent intensity was measured using FIJI Image J software (National Institutes of Health, USA).

2.3.3 Western Blotting

Western blotting was used to look at protein expression from HBMECs with or without TNFα and VEGF-A_{165}a treatment. p31 HBMEC protein lysate was prepared from 80-90% confluent monolayers. Lysis buffer was made from RIPA lysis buffer (50 mM Tris-HCl, pH 8.0, with 150 mM sodium chloride, 1.0% Igepal CA-630 (NP-40), 0.5% sodium deoxycholate, and 0.1% sodium dodecyl sulfate, Sigma, R0278), Phenylmethylsulfonyl Fluoride (PMSF) protease inhibitor (1mM, Sigma, P7626), protease inhibitor cocktail (AEBSF at 104 mM, Aprotinin at 80 µM, Bestatin at 4 mM, E-64 at 1.4 mM, Leupeptin at 2 mM and Pepstatin A at 1.5 mM, Sigma, P8340), Na_3VO_4 (1mM), and NaF (10mM).

Cells were washed 3x with cold PBS, then ice cold lysis buffer was added to wells for 5min on ice to allow cells to lyse and dissociate. Using a cell scraper, cells were gathered to one side of the well and the lysate pipetted up and down to remove clumps. The lysate was collected and transferred to cold Eppendorf tubes then left on ice for 30min. Lysate was centrifuged at 13,000G for 15min at 4˚C, then the supernatant was transferred to cold Eppendorfs and stored at -80˚C until use. Protein quantification was performed using Bradford Reagent (Sigma, B6916) and read on a plate reader (VictorX4, Perkin-Elmer).

Sample buffer (4x, glycerol (40%), SDS (8%), Tris (200mM), mercaptoethanol (5%), bromothenol blue (0.06%), and deionised H_2O) was added to samples (15µg) were heated at 95˚C for 5min then centrifuged to ensure all liquid was at the bottom of the tube. Samples were separated by SDS-PAGE on a 12% gradient gel (Bio-Rad Mini PROTEAN® TGX Stain-Free™ (456-8043), 100V for 90 minutes) with a ladder reference (Bio-Rad, 1610393) in running buffer (Tris-glycine-SDS 10x, Sigma, T7777). Samples were transferred onto nitrocellulose membrane (Millipore, Boston, MA) by wet turbo transfer (Bio-Rad TransBlot Turbo, 25V for 7 minutes). Membranes were incubated in a 1% Bovine Serum Albumin (BSA) in Tris Buffered Saline-Tween (TBS-Tween) (0.05%) block solution for 1h at room temperature or 4˚C overnight, then overnight at 4˚C with primary antibodies (anti-VEGF-R2 and anti-ICAM-1, both see Table 2.1) in block with gentle agitation. Anti-β-actin antibody (0.5µg/ml) was used as a loading control. Secondary antibodies (IRDye® 680RD donkey anti-rabbit IgG, IRDye® 800CW donkey anti-mouse or IRDye® 800CW donkey anti-Goat IgG, all at 0.2µg/mL) were applied in block for 1h at room temperature then membranes were washed 3 x 5min in TBS-Tween. Membranes were visualised on LiCor Odyssey Fc.

2.3.4 RNA Isolation and cDNA Generation

HBMEC RNA was isolated from 80-90% confluent cultured p31 or p2 cells in clear, flat bottom 6-well plates (Corning® Costar®, CLS3516). Media was removed and cells were washed with PBS then 1mL TRI-Reagent (Sigma, T9424) was added per well. Cells were lysed by pipetting the solution up and down and the lysate was collected and incubated for 5 min at room temperature. 200µL chloroform (Sigma, C2432) was added, mixed thoroughly and incubated for 15 min at room temperature. The lysate was centrifuged at 12,000G for 15 min at 4˚C and the upper aqueous phase was transferred to a new tube. 500µL isopropranol (Fluka, 59304) was added, solution mixed thoroughly, and allowed to incubate for a further 10 min at room temperature. Tubes were then centrifuged at 12,000G for 10 min at 4˚C and supernatant discarded to leave a pellet. The pellet was washed using 1mL 75% ethanol then vortexed and centrifuged at 10,000G for 5 min at 4˚C. Supernatant was discarded again and the pellet dried, then dissolved in 20-25µL DEPC-treated water (Invitrogen, AM9915G) and incubated for 10 min at 55-60˚C. After this incubation, the amount of RNA present was quantified using a NanoDrop 2000c UV/IV Spectrophotometer (ThermoFisher Scientific, UK) and then stored at -80˚C until use.

DNA was removed using the RQ1 RNase-Free DNase kit (Promega, M610A). 1µg of RNA samples were incubated in DEPC-treated water (Invitrogen, AM9915G) with DNase (1U/1µg RNA) and DNase Reaction Buffer (400mM Tris-HCl (pH 8.0), 100mM $MgSO_4$ and 10mM $CaCl_2$, Promega, M198A) for 30 min at 37˚C. DNase Stop Solution (20mM EGTA, pH 8.0, Promega, M199A) was added and incubated at 65˚C for 10min. After DNase treatment, RNA was reverse transcribed into complimentary DNA (cDNA). Oligo-dT (500ng, Promega, C1101) and random primers (250ng, Promega, C1181) were added to samples and incubated at 95˚C for 10min then tubes were placed in ice cold water to prevent RNA from wrapping into 2˚ conformation. 0.5mM dNTPs (contains dATP, dGTP, dCTP, dTTP, New England Biolabs, N0447L), M-MLV Reverse Transcriptase (RT) (in 20mM Tris-HCl (pH 7.5), 200mM NaCl, 0.1mM EDTA, 1mM dTTP, 0.01% Nonidet® P-40 and 50% glycerol, Promega, M1701A) and M-MLV RT-buffer at 1X (50mM Tris-HCl (pH 8.3 at 25°C), 75mM KCl, 3mM $MgCl_2$, 10mM dTTP, Promega, M531A) were added to samples and incubated at 37˚C for 60 min, 42˚C for 30 min, then 70˚C for 10 min. cDNA was stored at -80˚C until use.

2.3.5 PCR

Conventional Polymerase Chain Reaction (PCR) was used to amplify cDNA. cDNA was amplified in Master Mix used at 1X (25 units/ml of Taq DNA polymerase (pH 8.5), 200µM dATP, 200µM dGTP, 200µM dCTP, 200µM dTTP, 1.5mM $MgCl_2$, Promega, M7501), 0.5µM forward and reverse oligonucleotide primers (as detailed in Table 5.3), and 1 or 2µL cDNA. PCR cycles followed the general protocol: Initial denaturation: 94˚C for 2min; Denaturation step: 94˚C for 30-60s; Annealing temperature for 30-60s; Extension step: 72˚C for 1min per 1000bp of PCR product; Final Extension: 72˚C for 5min. Bands

were visualised using loading dye at 1X (Bioline, BIO-37045) with HyperLadder™ 50bp (Bioline, BIO-33039) reference on 1.5% agarose gels (1.5% agarose (Bioline, BIO-41025) + 0.005% ethidium bromide in 0.5X Tris-acetate-EDTA buffer), which were imaged on Bio-Rad Gel Doc EZ and Image Lab™ Software.

2.3.6 Absorbance Assay

A simple absorbance assay was employed to measure the absorbance of PTK787 dissolved in PBS/or DMSO using a plate reader (VictorX4, Perkin-Elmer). See Section 4.2.11.

2.4 Statistical Analysis

Development of immunofluorescence analysis techniques will be described in Section 3. Data are presented as scatter plots with the mean ± Standard Deviation (SD) shown. Analysis of data was performed using GraphPad Prism (versions 7.01/7.05/8.4.3 for Windows, GraphPad Software, San Diego, California USA), and all tests performed are specified in relevant results.

3 | Optimisation of In Vivo Immunofluorescence Analyses

3.1 Introduction

During some pain states, the Blood Spinal Cord Barrier (BSCB) can become compromised. Acute and sustained increases in BSCB permeability and changes in Neurovascular Unit (NVU) protein expression has been detected in several models, including models of nerve injury and peripheral inflammation (Varatharaj and Galea 2016; Wu et al. 2016; Banks et al. 2015; Echeverry et al. 2011; Beggs et al. 2010; Argaw et al. 2009; Brooks et al. 2005; Huber et al. 2005; Huber et al. 2001). In general, barrier integrity can be measured through extravasation of endogenous (albumin, Immunoglobulin G, fibronectin) and exogenous (sodium fluorescein, horseradish peroxidase, Evans Blue) blood serum proteins into the spinal cord parenchyma. Alternatively, gliovascular alterations can be measured through changes in expression of important NVU proteins (claudin-1, occludin, Zona Occludens-1, Intracellular Adhesion Molecule-1 (ICAM-1), Glial Fibrillary Acidic Protein (GFAP)). For example, during astrocyte activation there is an increase in GFAP (Zamanian et al. 2012), and so an increase in GFAP fluorescence can give an indication of astrocyte activation. Simple detection techniques measure the global dorsal horn signal, but this can hide important and localised alterations that are happening at the vessels. Another way to investigate gliovascular alterations is by manually counting positive signals that associate with vessels, but this is labour intensive and can be subjective. In this chapter I will discuss the development of semi-automated, more rapid analysis techniques that focus on the gliovascular response (in particular the astrocyte-endothelial cell response, Figure 1.82) using tissue generated from pilot studies that employ different peripheral insults as pain models: Monosodium Iodoacetate (MIA) and λ-carrageenan.

MIA is used as a common animal model for osteoarthritis as it disrupts cellular glycolysis, leading to chondrocyte cell death when injected into the knee capsule (de Sousa Valente 2019). This causes rapid degeneration of the joint, which has similar joint alterations to those in clinical osteoarthritis (de Sousa Valente 2019; Fernihough et al. 2004). In the early phase (up to 7 days) MIA injection leads to joint swelling, and inflammation characterised by immune cell infiltration and increased production of pro-inflammatory mediators. There is progressive joint degeneration in the later stages, as demonstrated by loss of cartilage, formation of osteophytes (bony outgrowths), synovial thickening, and osteochondral angiogenesis (de Sousa Valente 2019). At a dose of 2mg, MIA injection led to an increase in Activating Transcription Factor-3 (ATF-3), which is a marker of neuronal injury, in Dorsal Root Ganglion (DRG) that innervate both the knee and the hindpaw beginning at 3-14 days post-injection (Thakur et al. 2012;

Ferreira-Gomes et al. 2012; Orita et al. 2011). The presence of ATF-3 suggests there is a neuropathic component in this model, however, only at a much higher dose (4.8mg) was there functional evidence of central sensitisation (Havelin et al. 2016). It is likely that the early stages of MIA-induced Osteoarthritis (OA) are mediated by inflammation, and the later stages by substantial structural alterations in the joint (and a possible neuropathic component) as a result of inflammation and chondrocyte cell death (de Sousa Valente 2019). In the human disease, inflammation plays an ongoing role (Chow and Chin 2020; Woodell-May and Sommerfeld 2020), with patients partially responding to anti-inflammatory drugs continuously (de Sousa Valente 2019). Reactive gliosis and spinal neuroinflammation has been previously demonstrated with the MIA model (Thakur et al. 2012; Orita et al. 2011). Thakur et al. (2012) showed spinal cord NVU alterations in this model through an increase in reactive microglia at 7 days, and so this chronic model was chosen to generate tissue in order to develop gliovascular-specific analysis techniques.

In terms of an acute insult, λ-carrageenan (hereby referred to as carrageenan) was chosen as it induces a rapid and robust inflammatory response through activation of immune cells, leading to the release pro-inflammatory molecules and significant pain behaviour (Chan et al. 2017; Sokolova et al. 2016; Radhakrishnan et al. 2003; Coulthard et al. 2003; Hargreaves et al. 1988). Previously, this model has demonstrated central NVU alterations measured through increased permeability of central vessels to exogenous substances and altered endothelial tight junction proteins (Schreiber et al. 2008; Hua et al. 2005; Huber et al. 2005; Huber et al. 2002; Huber et al. 2001). Due to its rapid effects, it was employed as an acute model for initial studies to generate tissue and develop analysis techniques before beginning longer-term models.

To determine whether analysis techniques were sensitive enough to detect alterations, they were validated against tissue from mice that underwent peripheral Complete Freund's Adjuvant (CFA)-induced inflammation and displayed gliovascular alterations measured by conventional manual counting of GFAP-positive vessel fragments (Beazley-Long et al. 2018b). Here, CFA caused a sustained peri-articular inflammatory response, and so is a model of chronic inflammation.

Hypothesis

Acute and chronic peripheral inflammation and chronic degenerative joint disease will result in spinal gliovascular alterations. Analysis techniques that specifically probe the NVU can detect these changes from the three different pain models.

Objectives

- Generate tissue from pilot studies using two pain models (acute carrageenan and chronic MIA) to develop gliovascular-specific immunofluorescence analysis techniques that can detect changes from the different models.

- Validate these analysis techniques using tissue that has previously shown gliovascular alterations.
- Determine the gliovascular response to acute and chronic peripheral inflammation, and to chronic degenerative joint disease.

3.2 Materials & Methods

3.2.1 Experimental Animals

All experiments and procedures were performed in accordance with the Animals (Scientific Procedures) Act (1986; 2012) and were authorised by the UK Home Office. Experiments were carried out on adult (≥200g) male Sprague Dawley (SpD) rats (Charles River, UK). The oestrus cycle in females causes hormone fluctuations that may interact with pain signalling and experimental outcomes (Becker et al. 2005a; Craft et al. 2004), and so male rats were used. Experiments involving transgenic mice (*vegfr2*$^{fl/fl}$ Tie2CreER^{T2}, see Beazley-Long et al. 2018b and Section 2.2.3.1) were carried out on both male and female adult mice.

Rats were group-housed (3-4 per cage) in conventional cages and mice were group-housed in individually ventilated cages (3-4 per cage). Animals were maintained in a 12 hour light/dark cycle at 22˚C and 55% humidity with access to food and water *ad libitum*. Animals were allocated to treatment groups by an independent investigator.

Pilot studies used samples sizes of 4-6 per group.

3.2.2 Induction of Peripheral Inflammation

3.2.2.1 Intraplantar Carrageenan

Male Sprague Dawley rats (≥200g) received an intraplantar injection of carrageenan (2% w/v, 100µL, n = 6) or saline (n = 2) into the left hindpaw under anaesthesia, as described in Section 2.2.2.4. Induction of inflammation was performed by Dr Emma Dayman.

Weight bearing asymmetry was recorded (detailed in Section 2.2.4.1) at baseline and 22 hours post-injection. Animals were housed in conventional cages (4 per cage) and were randomly divided into treatment groups by an independent investigator. 3 (n = 4) or 24 hours (n = 4) post-injection, animals were euthanised and spinal cords dissected and processed (sectioned at 40µm) for free-floating immunofluorescence as previously described (2.2.5).

3.2.2.2 Peri-articular CFA

Induction of inflammation, dissection, tissue processing and immunofluorescence were carried out by Dr Nick Beazley-Long.

Transgenic mice (*vegfr2*$^{fl/fl}$ Tie2CreER^{T2}, see (Beazley-Long et al. 2018b), n = 11) were used in this study. These mice have an endothelial cell Vascular Endothelial Growth Factor Receptor (VEGF-R) gene which can be knocked-out by tamoxifen injections. The mice used here were transgenic but did not receive tamoxifen, and so were uninduced and physiologically "wild-type". Uninduced male and female *vegfr2*$^{fl/fl}$ Tie2CreER^{T2} mice received a unilateral peri-articular injection of CFA (2mg/mL, 2 x 80µg CFA in 40µL mineral oil, n = 6) on both sides of the joint as described in Section 2.2.2.5. Shams were anaesthetised but received no injection (n = 5). Animals were randomly divided into treatment groups by an independent investigator, and housed in individually-ventilated cages (single-tier, 3-4 per cage) with other non-tamoxifen-dosed mice. 14 days after CFA-induction, animals were euthanised and spinal columns dissected and processed (sectioned at 20µm) for slide-mounted immunofluorescence as previously described Section 2.2.5. In the mouse, dissection, tissue processing (at 20µm thickness) and immunofluorescence were carried out by Dr Nick Beazley-Long.

3.2.3 Induction of Osteoarthritis

Under anaesthesia, male SpD rats (≥200g, n = 6) received an intra-articular injection of 50µL of 2 mg MIA (n = 4) or saline (n = 2). Animals were housed in conventional cages (3 per cage) and were randomly divided into treatment groups by an independent investigator. Induction of arthritis was performed by Dr James Burston.

Pain behaviour (weight bearing asymmetry and mechanical sensitivity using the up-down paradigm as described in Section 2.2.4) was recorded at baseline and 2, 5, and 7 days post-injection. 7 days post-injection, animals were euthanised and spinal cords dissected and processed (sectioned at 40µm) for free-floating immunofluorescence as previously described Section 2.2.5.

Study	Treatments	Number of Animals
Transgenic VEGF-R2 KO mice	Vehicle + Sham	5
	Vehicle + CFA	6
Peripheral Inflammation	Vehicle Control	2
	Carrageenan	6
Osteoarthritis	Vehicle Control	2
	MIA	4

Table 3.1: Details of animal numbers and treatment groups.

3.2.4 Pain Behaviour

Weight bearing and paw-withdrawal threshold were measured as detailed in Section 2.2.4. Weight bearing is displayed as the difference in weight borne between ipsilateral (left) and contralateral (right) hindpaws, and paw-withdrawal threshold was detected using the up-down paradigm (Chaplan et al. 1994).

3.2.5 Histology

Antibodies used are detailed in Table 3.2. Free-floating immunofluorescence was performed on rat tissue as described in Section 2.2.6 using 5% BSA + 10% FBS block in 0.3% Triton-X-100 in Phosphate Buffered Solution (PBS) for GFAP (1µg/mL), Cluster of Differentiation-31 (CD31) (2µg/mL) and concentration-matched Immunoglobulin G (IgG). Secondaries used were donkey anti-mouse Alexafluor-488 and donkey anti-goat Alexafluor-555, or donkey anti-goat Alexafluor-488 and donkey anti-rabbit Alexafluor-555, and Hoechst (all 1µg/mL). Sections were imaged on a confocal microscope (Leica TCS SPE, Leica Microsystems).

Target	Host	Supplier	Product Number	Working Concentration
CD31	Goat	R&D Systems	AF3628	2µg/mL
GFAP	Mouse	ThermoFisher	MS-1376-P	1µg/mL
GFAP	Rabbit	abcam	ab7260	1µg/ml
IgG	Mouse	Novus Biologicals	NBP1-97019	matched*
α-Mouse-488	Donkey	Invitrogen	A21202	1µg/ml
α-Goat-555	Donkey	Invitrogen	A21432	1µg/ml
α-Goat-488	Donkey	Invitrogen	A21202	1µg/ml
α-Rabbit-555	Donkey	Invitrogen	A31572	1µg/ml
Hoeschst-543334		Sigma	-	1µg/ml

GFAP: glial fibrillary acidic protein; **CD31**: cluster of differentiation 31; **IgG**: Immunoglobulin. *IgG concentration was matched to the relevant primary antibody concentration.

Table 3.2: Details of antibodies and probes

3.2.6 Immunofluorescence Analysis

Images were analysed using FIJI Image J software (National Institutes of Health, USA) with the additional BioVoxxel plugin (BioVoxxel, Germany). Analysis techniques were validated on mouse tissue that had previously been shown to have gliovascular alterations measured by a significant increase in the number of GFAP-positive vessel fragments (see Figure 3.1 for example (adapted from Beazley-Long et al. 2018b)). In Beazley-Long's study (2018b), the number of GFAP-associated vessel fragments (identified by CD31 signal) per animal were counted and expressed over the total sectional area per animal analysed to account for differences in the total area analysed.

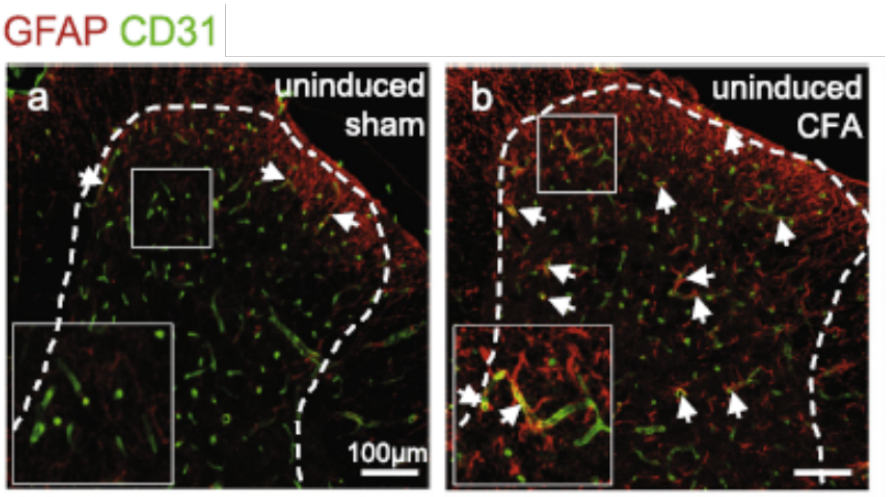


Figure 3.1: Representative images of GFAP-wrapped vessel fragments in the dorsal horn of the spinal cord in sham **(a)** and CFA **(b)** mice. The number of these GFAP-positive vessel fragments increased after peri-articular CFA. **Uninduced**: transgenic mice (*vegfr2*$^{fl/fl}$ Tie2CreER^{T2}) without tamoxifen-induced knockout and therefore physiologically "wild-type". Red: GFAP astrocyte marker; Green: CD31 vessel marker. Scale bar: 100µm. From Beazley-Long et al. (2018b).

3.2.6.1 Overlay Method: ROIs

Whole dorsal horn GFAP intensity was measured, but as the focus of this thesis is gliovascular alterations in response to peripheral inflammation, I used a vessel signal to measure vessel-associated GFAP intensity and study gliovascular-specific responses. In this thesis, a reliable vessel marker was difficult to establish in the rat. Commonly, Plant Lectin Isolectin B4 (IB4) or von Willebrand Factor (vWF) are used to identify vessels, but I found these inconsistent (data not shown). CD31 is an adhesion molecule present on endothelial cells and had been used in our lab previously to reliably identify vessels in the mouse, (Figure 3.10). It produced consistent results in rat tissue only when histology was performed via free-floating immunofluorescence (Figure 3.12). Subsequent studies (not in this chapter, in Chapter 4) utilised slide-mounted immunofluorescence to avoid damaging the contralateral spinal cord through identification marking, and CD31 became unreliable (data not shown). Laminin was used as an alternative marker but can have variable staining in the superficial laminae of the dorsal horn (discussed in Chapter 4). Rat Endothelial Cell Antigen-1 (RECA-1) was identified as an extremely reliable and consistent marker and was used for later studies (from Section 4.3.4).

For vessel-associated GFAP intensity to be measured, vessel signal was thresholded by eye to include only CD31-positive vessel-like structures and remove background signal. The threshold value was determined by trialling several threshold values on a random selection of vessel-marker images to produce the optimal value, and was then applied to all vessel images. After the vessel image was thresholded, it was analysed using Image J's "Analyze Particles" (particle size set to "5-infinity pixels"; circularity set to "0.00-1.00"). This produced Regions of Interest (ROIs) which corresponded to CD31-positive objects, and these were applied to GFAP signal in order for intensity to be measured (Figure 3.2). Each CD31-positive vessel-like structure (ROI) generated an area and mean

GFAP grey value, of which there were hundreds, and so the following formula was used to generate total fluorescence over total area for each image:

$$\frac{Sum\ of\ Total\ Fluorescence\ (= Individual\ ROI\ Area \times Mean\ Grey\ Value)}{Sum\ of\ All\ ROI\ Areas}$$

The intensity of the "no primary antibody" immunofluorescent controls were then subtracted from all experimental intensity values.

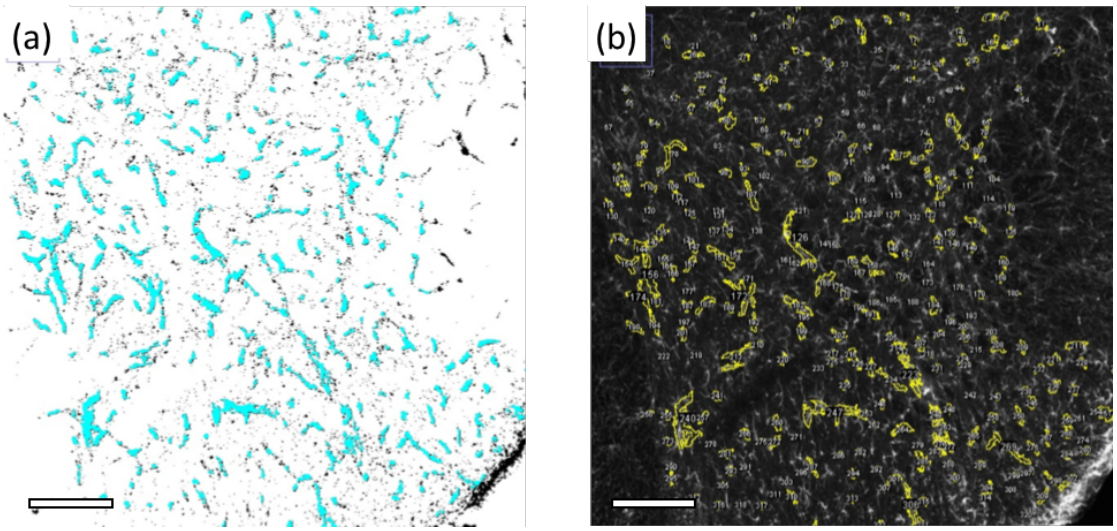


Figure 3.2: To allow for vessel-specific GFAP anaylsis and monitor gliovascular alterations after peripheral inflammation, the vessel signal (CD31, black) was thresholded to generate regions of interest (ROIs, size: 5-infinity pixels, blue, **a**). These ROIs (yellow) were applied to GFAP signal (white) and fluorescent intensity measured (**b**). Rat dorsal horn spinal cord tissue. Scale bar: 100µm.

3.2.6.2 Overlay Method: Selection

In later analyses (not in this chapter, from Section 4.3.4), it was noted that vessel lumina were included within the ROIs (see Figure 3.3). To exclude these, after the vessel image was thresholded and ROIs generated, a "selection" of these ROIs was made through Image J's "Create Selection" option to produce one combined ROI. This selection was then applied to GFAP signal and intensity measured, and thus one set of measurements for all vessels was generated (area, mean intensity, Integrated Density (IntDen) and Raw IntDen). To generate the mean intensity/fluorescence for each animal, data from each section were combined and the total fluorescence over total area was calculated using the following formula:

$$\frac{Total\ Area\ (= Sum\ of\ all\ areas)}{Total\ Fluorescence\ (= Sum\ of\ IntDen)}$$

The intensity of the "no primary antibody" immunofluorescent controls were then subtracted from all experimental intensity values. As with the ROI method, the overlay

method can give information on the area of vessel signal, allowing comparison between groups.

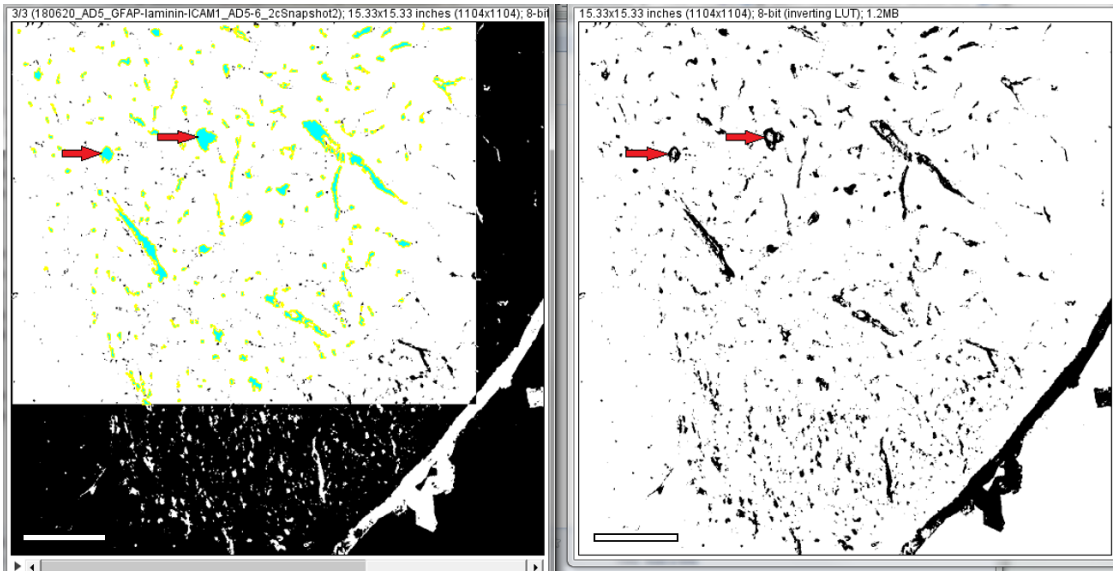


Figure 3.3: Vessel (CD31, black/white objects) lumina are included in the ROIs (yellow/blue, highlighted by arrows). Rat dorsal horn spinal cord tissue. Scale bar: 100µm.

3.2.6.3 Overlap Extraction Method

Astrocytes are part of the NVU and extend out away from Central Nervous System (CNS) vessels (see Figure 3.4), meaning that using the above analysis technique, astrocytes that are associated with vessels but not directly underneath the vessel mask are excluded from analyses. This means important changes that may be occurring within NVU components are being overlooked. In order to include these extending astrocytes, the Binary Feature Extraction (BFE) macro (BioVoxxel Toolbox, Jan Brocher) can be used to extract GFAP signal that overlaps with the vessel signal. Figure 3.5a & b shows the vessel mask over the top of the GFAP signal, demonstrating associated-GFAP structures that are excluded from the analysis. The BFE requires two images to be binary in order to extract overlapping features. The GFAP was manually thresholded to include GFAP-positive structures and exclude background signal. The threshold value was determined by measuring the intensity of some GFAP-positive structures and trialling several threshold values on a random selection of GFAP images to produce the optimal value to include relevant objects, and was then applied to all GFAP images. After thresholding, the following parameters were set within the BFE macro: "objects=[GFAP] selector=[vessel marker] object_overlap=0". As the object overlap is set to 0%, this means that any objects (GFAP) that overlap with the selector (vessel marker) will be extracted. The object overlap is the minimal overlap fraction of the selector area with the object area (in this order) and can be altered to change the conditions of which objects are extracted. For example, if it is set to 30%, only objects that the selector overlaps ≥30% with are extracted.

Figure 3.5c & d demonstrates how GFAP structures that are associated with vessels but

extend out are included when using the BFE macro. It is also possible to determine the response of astrocytes that are not associated with vessels by subtracting the vessel-associated fluorescence from total dorsal horn fluorescence. This macro can also give information on the number and total area of vessel-associated objects, and can be used to extract other vessel-associated objects (for example, ICAM-1 which can be expressed by the endothelium and by glial cells (Nordal and Wong 2004)).

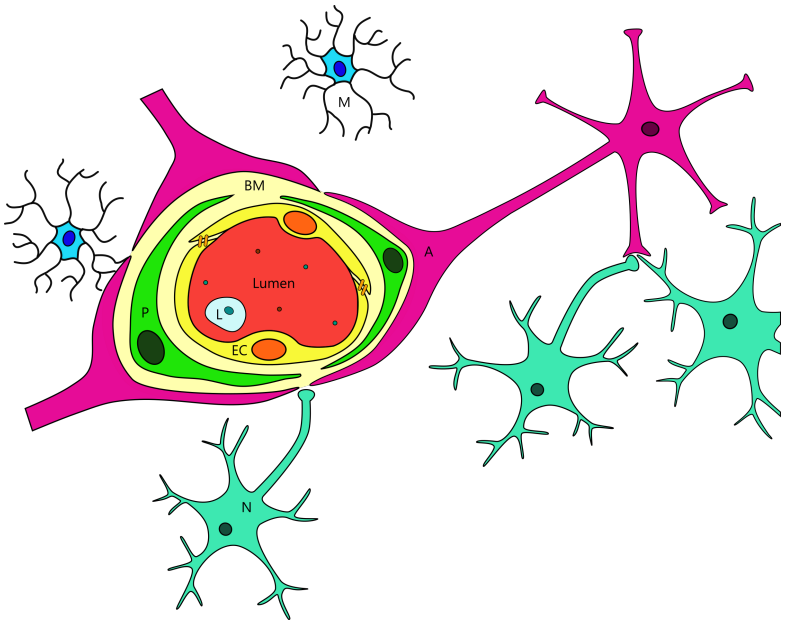


Figure 3.4: Astrocytes extend away from the Neurovascular Unit. **A**: Astrocyte; **BM**: Basement Membrane; **EC**: Endothelial Cell; **L**: Leukocyte; **M**: Microglia; **N** Neurone; **P**: Pericyte. Adapted from Beazley-Long et al. (2018a).

3.2.7 Statistical Analysis

Data are presented as scatter plots with the mean ± Standard Deviation (SD) shown. Analysis of data was performed using GraphPad Prism (versions 7.01/7.05 for Windows, GraphPad Software, San Diego, California USA), and all tests performed are specified in relevant results.

3.3 Results

3.3.1 Behavioural Data

A significant shift in weight bearing to the uninjured limb was observed at 22 hours post-carrageenan compared to baseline, and at 2-7 days post-MIA compared to saline-injected controls (Figure 3.6). In the MIA treated animals, mechanical withdrawal threshold also decreased in the ipsilateral hindpaw, that was significant at 7 days compared to saline injected control. There was also a trend of mechanical hypersensitivity in the contralateral hindpaw, which may be an indication of central sensitisation, however by the 7 day timepoint thresholds appeared to begin to renormalise. Thresholds also

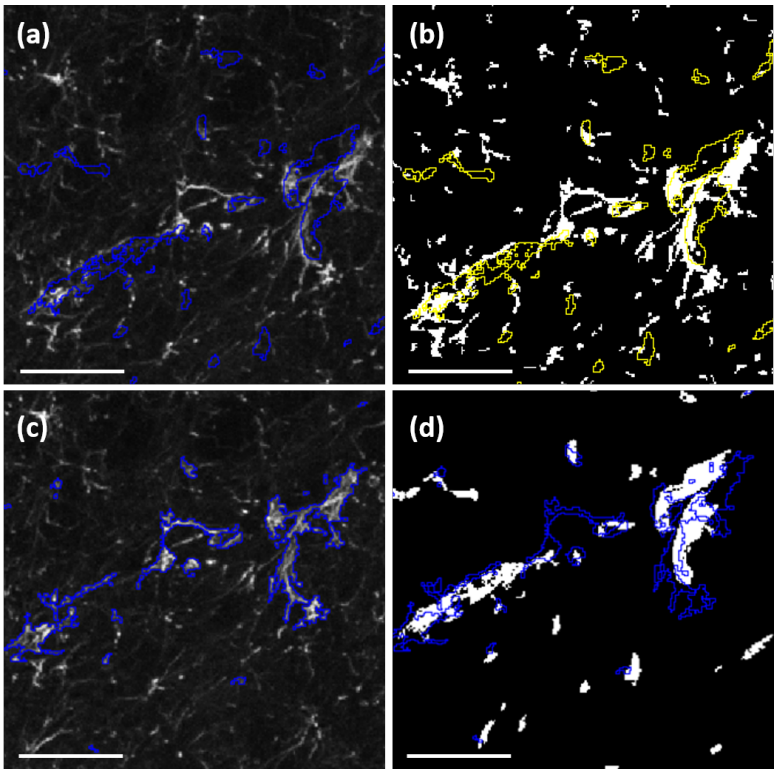


Figure 3.5: GFAP structures (white) that extend away from the vessel mask (blue/yellow) are not included in the overlay analysis **(a, b)**. Using the Binary Feature Extraction macro, GFAP structures (**c**, white) that are associated with vessels (**d**, white) are extracted to create a mask (blue) and are included in the overlap extraction analysis. Rat dorsal horn of the spinal cord. Scale bar: 50μm.

decreased in the control animals on the ipsilateral and contralateral side in the first 2 days, which may be due to injury caused by the injection itself (Figure 3.6c & d). CFA-treated mice showed a significant decrease in mechanical threshold throughout the duration of the study (see Figure 3.7, adapted from Beazley-Long et al. (2018b)).

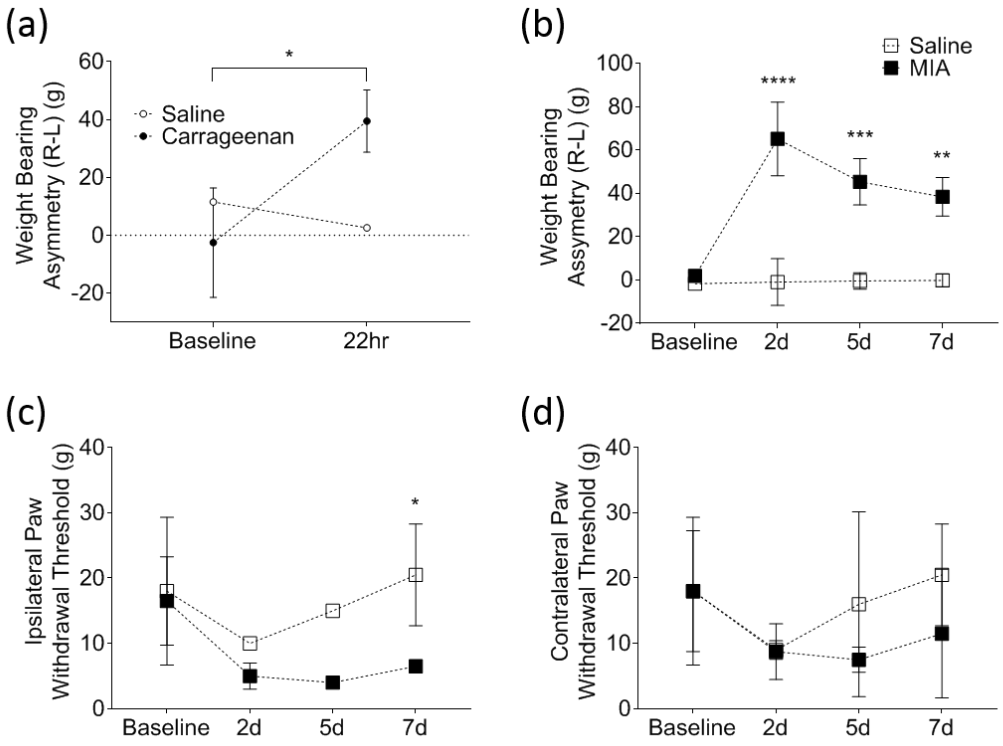


Figure 3.6: Nociceptive behaviour of carrageenan (**a**) and MIA (**b-d**) animals. **a**: Weight bearing asymmetry was significantly different 22 hours post-intraplantar carrageenan injection compared to baseline (Interaction: $p<0.05$; Row Factor: $p=0.06$; Column Factor: $p=0.18$). **b-d**: Weight bearing asymmetry was significantly different after intra-articular MIA throughout the study compared to intra-articular saline (**b**, Interaction: $p<0.01$; Row Factor: $p<0.01$; Column Factor: $p<0.01$). Mechanical threshold on the ipsilateral hindpaw in MIA animals was significantly different to saline at 7 days post-injection (**c**, Interaction: $p=0.11$; Row Factor: $p<0.05$; Column Factor: $p<0.05$), whereas threshold in the contralateral hindpaw was not significantly different for the duration of the study (**d**, Interaction: $p=0.65$; Row Factor: $p=0.25$; Column Factor: $p=0.30$). 2-way ANOVA with Sidak's multiple comparisons, compared to control. Mean ± SD. **a**: n = 1-3. **b**: n = 2-4 ****$p<0.0001$, ***$p<0.001$, ** $p<0.01$, * $p<0.05$.

3.3.2 Validation of Analysis Techniques

As analysis techniques shown in this chapter were new, they were validated against tissue that showed gliovascular alterations as measured by an increase in dorsal horn GFAP-positive vessel fragments (Figure 3.1 and Figure 3.8a) and GFAP signal (Figure 3.10 and Figure 3.8b) after peri-articular CFA (Beazley-Long et al. 2018b). The ROI and selection overlay analysis methods showed an increase in GFAP intensity at vessels (Figure 3.8c and 3.8d respectively). However, when using the overlap extraction method, no significant difference in GFAP intensity is detected (Figure 3.9a, ipsilateral $p=0.359$, contralateral $p=0.132$) but there is an increase in the area of vessel-associated GFAP

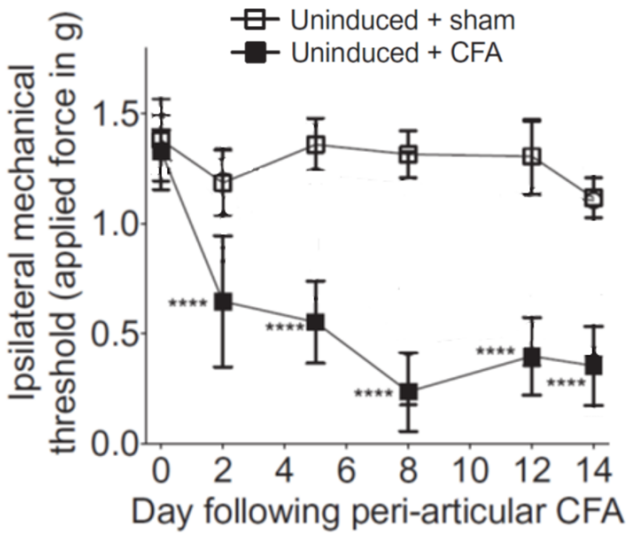


Figure 3.7: Peri-articular CFA causes a significant reduction in mechanical threshold in the ipsilateral hindpaw of uninduced mice (transgenic mice (*vegfr2*$^{fl/fl}$ Tie2CreER^{T2}) without tamoxifen-induced knockout and therefore physiologically "wild-type"). 2-way ANOVA with Dunnett's multiple comparisons, compared to respective baseline (day 0). Mean ± SD. n = 3-11. Combined data from male & female mice. ****p<0.0001. Adapted from Beazley-Long et al. (2018b).

signal (Figure 3.9b, ipsilateral p=0.078, contralateral p=0.026). This method also reveals there is a significant increase in GFAP intensity when not associated with vessels (Figure 3.9c, ipsilateral p<0.05, contralateral p=0.056).

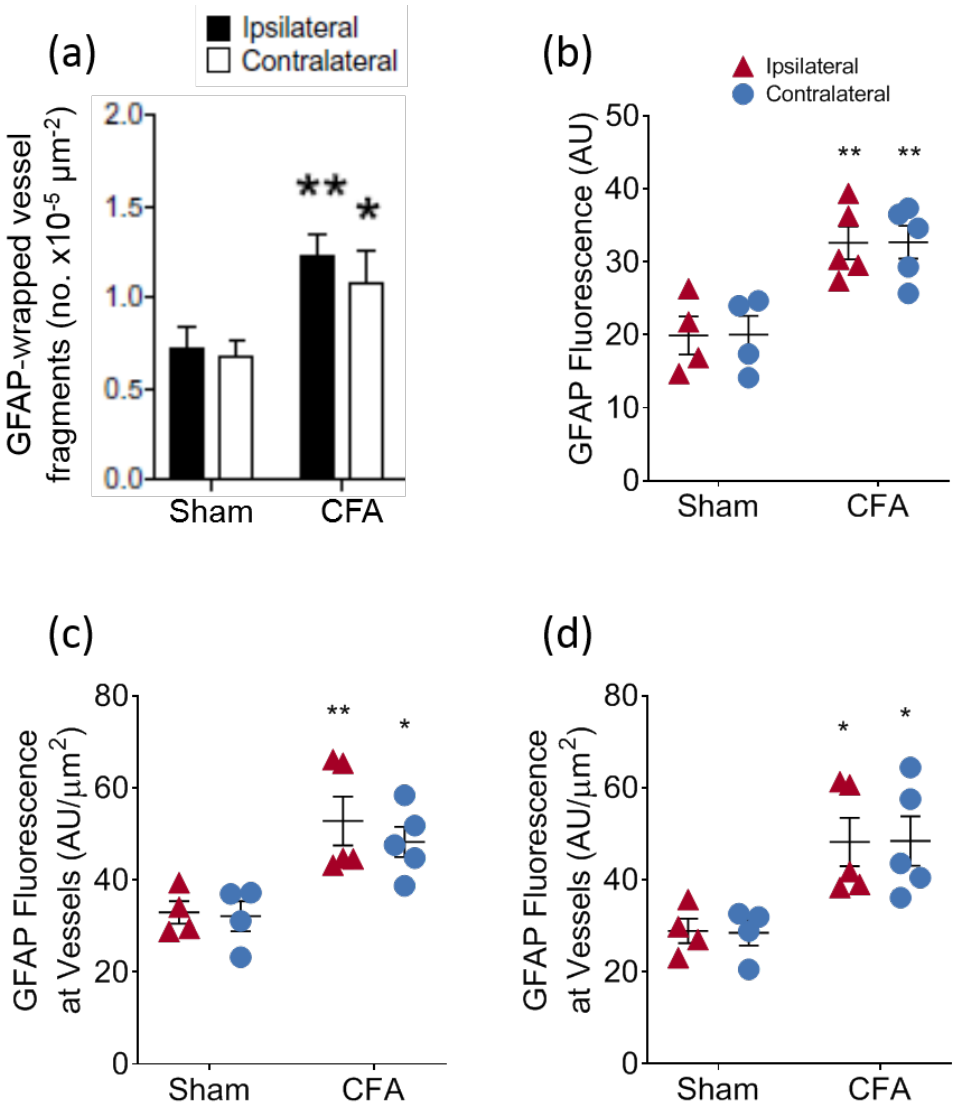


Figure 3.8: Validation of analysis techniques in the mouse CFA model. (a): Peri-articular CFA caused a significant increase in GFAP-wrapped vessel fragments compared to non-inflamed mice (Adapted from Beazley-Long et al. 2018b). (b): CFA led to a significant increase in whole dorsal horn GFAP intensity (Interaction: $p>0.99$; Row (treatment) Factor: $p<0.0001$; Column (ipsilateral-contralateral) Factor: $p=0.96$). This is matched using the vessel signal as an overlay using the earlier ROI method (c, Interaction: $p=0.65$; Row Factor: $p<0.001$; Column Factor: $p=0.51$) and the later selection method (d, Interaction: $p=0.94$; Row Factor: $p<0.001$; Column Factor: $p=0.98$). 2-way ANOVA with Sidak's multiple comparisons, CFA compared to non-inflamed. Mean ± SD. n = 4-5. ** $p<0.01$, * $p<0.05$.

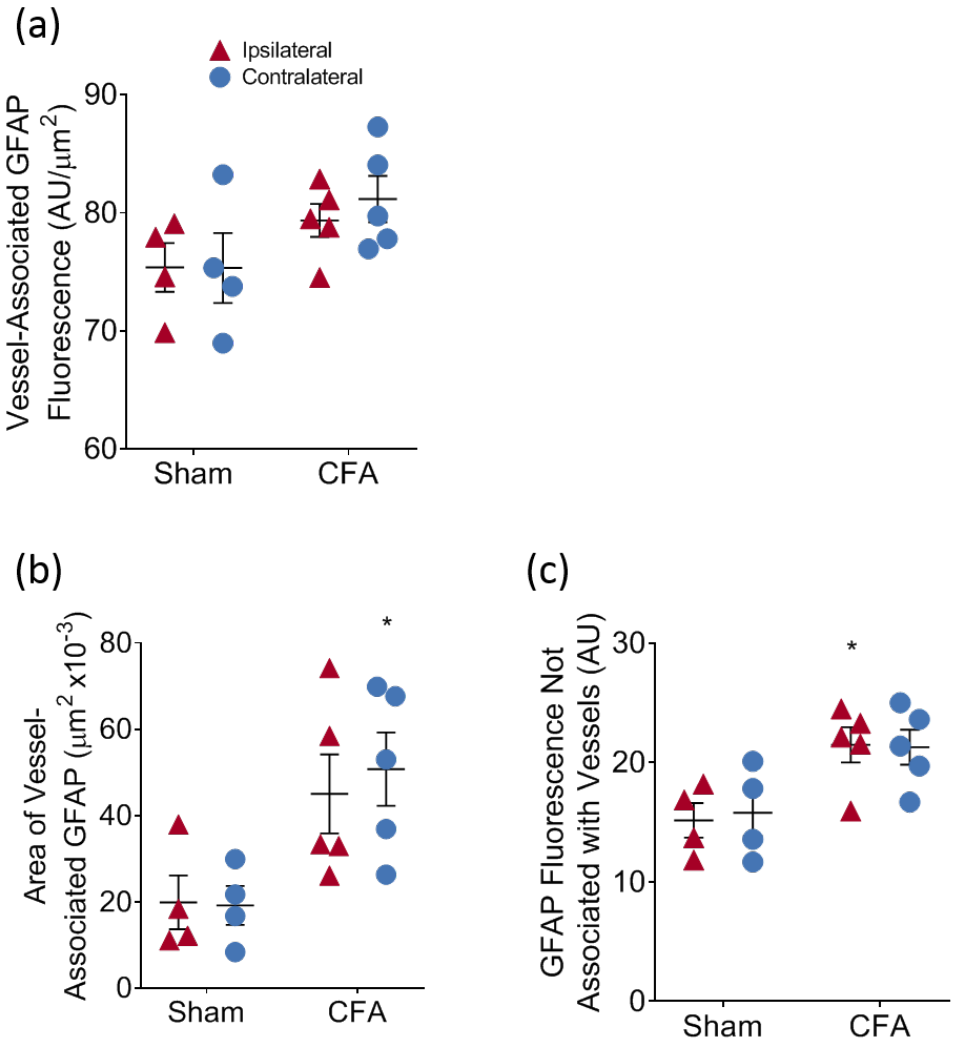


Figure 3.9: Validation of analysis techniques in the mouse CFA model. Using the overlap extraction method, no significant difference in GFAP intensity is detected (**a**, Interaction: p=0.66; Row (treatment) Factor: p<0.05; Column (ipsilateral-contralateral) Factor: p=0.68), but there is an increase in the area of vessel-associated GFAP signal (**b**, Interaction: p=0.69; Row Factor: p<0.01; Column Factor: p=0.75). This method also reveals there is a significant increase in GFAP intensity not associated with vessels (**c**, Interaction: p=0.80; Row Factor: p<0.01; Column Factor: p=0.89). 2-way ANOVA with Sidak's multiple comparisons. Mean ± SD. n = 4-5. * p<0.05.

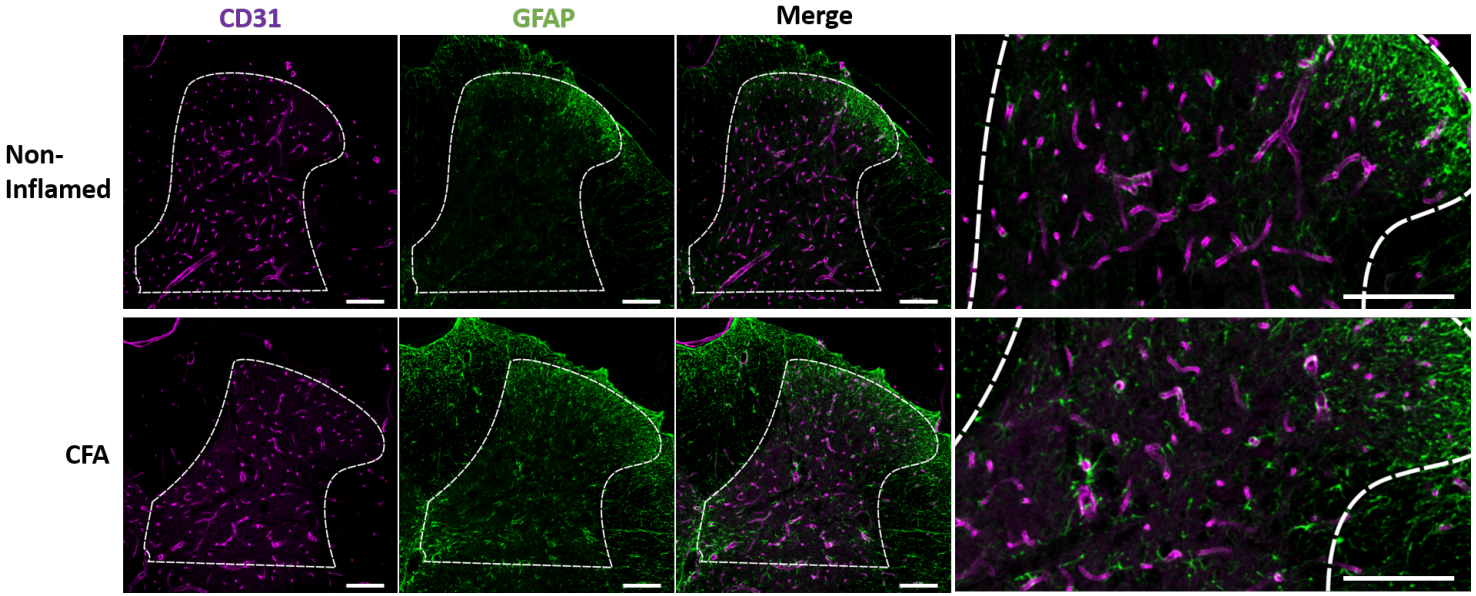


Figure 3.10: Representative images demonstrating increased GFAP in the dorsal horn of the mouse spinal cord after peri-articular CFA. Green: GFAP astrocyte marker; Magenta: CD31 vessel marker. Scale bar: 100μm.

3.3.3 Astrocyte Activation

It is assumed that an increase in GFAP fluorescence represents a degree of astrocyte activation. Under this assumption I measured global intensities of GFAP staining in the dorsal horn of the spinal cord (representative images in Figure 3.12) to test for general astrocytic activation after peripheral insults. No differences were observed in GFAP intensity in the dorsal horn between control and treatment animals (Figure 3.11a & b). Astrocytic endfeet wrap vessels, and reactive astrocytes can alter vessel permeability (Argaw et al. 2012; Argaw et al. 2009), therefore it is conceivable that GFAP is increased at the glial-vessel interface. For this reason, I measured GFAP intensity at CD31 positive vessels using the ROI overlay method as described in Section 3.2.6.1. No change in GFAP fluorescence at vessels was observed in these pilot studies (Figure 3.11c & d). This analysis technique can also be applied to microglial markers that are upregulated during microglial activation, such as Cluster of Differentiation-11b (CD11b) and Ionized Calcium Binding Adaptor Molecule-1 (IBA-1) (Ji et al. 2013), to investigate what is happening to these cells that are involved in the NVU.

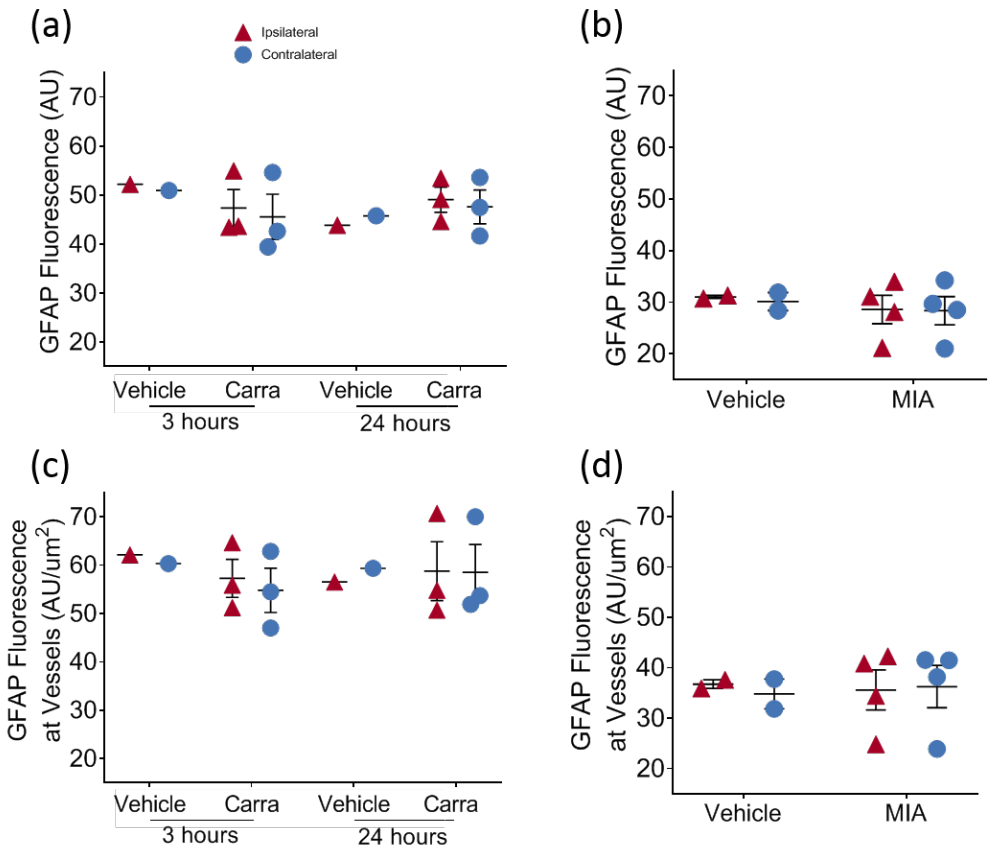


Figure 3.11: GFAP intensity in the dorsal horn of the spinal cord is not altered 3 or 24 hours after carrageenan (**a**, Interaction: p=0.99; Row Factor: p=0.71; Column Factor: p=0.86), nor 7 days after intra-articular MIA (**b**, Interaction: p=0.91; Row Factor: p=0.50; Column Factor: p=0.86). Vessel-specific GFAP is not altered either (carrageenan: **c** , Interaction: p=0.99; Row Factor: p=0.90; Column Factor: p=0.94. MIA: **d**, Interaction: p=0.77; Row Factor: p=0.97; Column Factor: p=0.89). Mean ± SD. n = 1-4.

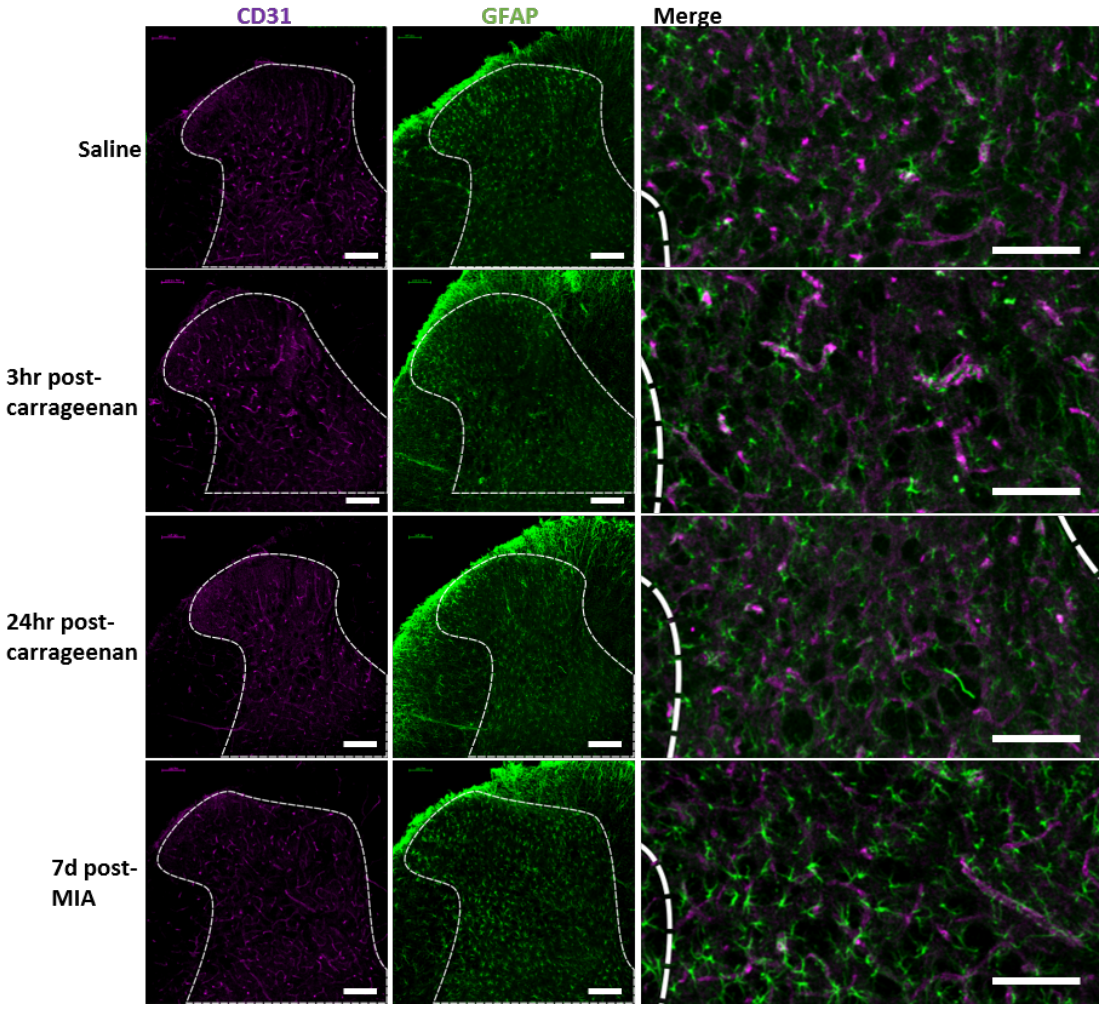


Figure 3.12: Representative images of GFAP and CD31 staining in the dorsal horn of the rat spinal cord. Green: GFAP astrocyte marker; Magenta: CD31 vessel marker. Scale bar: 100μm.

3.4 Discussion

I have developed and refined an analysis technique to study the glial-vessel relationship after nociceptive insults *in vivo*. This method allows location-specific investigation that may reveal changes in glial responses, which could be masked if only global signal was measured. To further this, GFAP and vessel signal in specific laminae can be investigated to tease out localised gliovascular effects, for example in superficial laminae (where there are many nociceptive inputs) compared to deeper laminae (where there is extensive spinal processing by interneurones and Wide Dynamic Range (WDR) neurones) (Todd 2010; Basbaum et al. 2009; D'Mello and Dickenson 2008; Millan 1999).

Vessel-specific analyses were validated against tissue from uninduced transgenic mice (i.e. physiologically "wild type" as the inducible endothelial cell VEGF-R knockout had not occurred) that received a peri-articular injection of CFA and showed an increase in GFAP-positive vessel fragments and dorsal horn GFAP signal (Figure 3.8a & b) (Beazley-Long et al. 2018b). All analysis techniques revealed an increase in GFAP signal, as measured by intensity and area of vessel-associated GFAP signal (Figures 3.8 and 3.9). The analysis techniques developed here are therefore sensitive enough to detect significant alterations in histology, and importantly are more rapid than conventional manual counting. They also allow for deeper analysis, for example segregating laminae, the area of intense vessel-associated GFAP signal (Figure 3.9b), and GFAP response when not associated with vessels (Figure 3.9c). Interestingly here, when the extraction overlap method was used in the mice, an increase in vessel-associated GFAP area in the ipsilateral dorsal horn was detected after CFA, but it was not significant (Figure 3.9b), whereas there was a significant increase in GFAP intensity with the ROI overlay method (Figure 3.9c & d), suggesting the majority of astrocytic response and subsequent increase in GFAP expression may be very focused at the vessels. These considerations are only possibly thanks to these analysis techniques.

There are several factors that must be taken into consideration when using these techniques however. Firstly, the vessel marker target may undergo changes itself. CD31 (or Platelet and Endothelial Cell Adhesion Molecule-1 (PECAM-1)), is an adhesion molecule and signalling receptor present on blood and vascular cells, such as platelets, leukocytes, and endothelial cells (Privratsky and Newman 2014; Lertkiatmongkol et al. 2016). CD31 is highly expressed at intercellular junctions, where it is involved in monocyte transmigration and structural integrity of endothelial cell junctions (Privratsky and Newman 2014; Lertkiatmongkol et al. 2016). It has been shown that alterations in CD31 expression directly affects vessel permeability and diapedesis of some leukocytes (Wimmer et al. 2019; Liu et al. 2012), and so it is conceivable that there will be a change in CD31 expression during nociception-induced barrier dysfunction. If a change in CD31 is associated with an increase in barrier permeability, then hypothetically astrocytic endfoot activation could also increase in these areas. There is the potential for this phenomenon to have an impact on the analysis technique outlined above, which high-

lights the importance of taking this into consideration when interpreting results. In subsequent studies, alternative vessel markers were used (laminin and RECA-1), and so the same alterations in these vessel markers need to be taken into consideration. Secondly, thresholding images excludes signal from analyses and so care is needed when setting threshold limits to include all relevant information. As mentioned, astrocytes that associate with vessels extend outwards, and using the overlay method, these astrocytes are excluded from analyses (see Section 3.2.6.3). These astrocytes can be included by using the Binary Feature Extraction macro from the BioVoxxel Toolbox and extracting the two overlapping binary signals (GFAP and the vessel marker). Both the vessel and GFAP and vessel signal need to be thresholded to produce binary images, but because the GFAP signal needs to be above a certain value to be included in the threshold, lower intensity GFAP objects are not included. This can therefore skew the results and mask any potential differences (see Figure 3.9a). By looking at the area of vessel-associated GFAP, a difference is demonstrated in inflamed animals compared to non-inflamed (Figure 3.9b), and so can help to overcome this issue. As demonstrated here, these results suggest there is increased activation of astrocytes (as measured by an increase in GFAP signal area) that are associated with vessels. All results generated from the overlay and extraction overlap methods should be taken into consideration together to draw conclusions.

In later analyses (from Section 4.3.4), it was noted that vessel lumina were included within the ROIs (see Figure 3.3), and so the analysis technique was adapted to exclude these holes. After the vessel-image was thresholded and regions of interests were generated using particle analysis, a "selection" of these ROIs was made using the ImageJ "Create Selection" option, which excluded holes. Including the lumina in analyses could mask any vessel-associated alterations as a large part of affected ROIs would be absent of glial and endothelial cells, thereby diluting the fluorescent signal. However, when validated against the mouse tissue, no signal was lost using the ROI overlay method (Figure 3.8c & d), suggesting this is not the reason for the lack of GFAP alterations.

In terms of experimental techniques, there may be issues in the control animals used here. Control animals in the MIA and carrageenan studies received an injection of saline, which can cause inflammation at the injection site (Jensen et al. 2008) and has the potential to increase swelling and hypersensitivity in the contralateral uninjured hindpaw (Levine et al. 1985; Denko and Petricevic 1978), possibly indicating spinal activation. This saline-induced inflammation could therefore mask effects of the experimental peripheral inflammation, and so to account for this an anaesthetic sham animal could be used. This control animal is placed under anaesthetic and receives the same preparation as the treatment animals, but does not receive an injection. This would ensure the control animals represents as physiologically 'normal' as possible, and any spinal alterations in the treatment animals are due to the inflammation alone. For these reasons, subsequent studies used anaesthetic sham control animals. This type of control (anaesthetic sham) was used in the mice, which supports the idea that the

saline-injected control may be masking effects in the rats. However, the difference in species (mice vs/ rat) and technique (CFA vs. MIA/carrageenan) may also explain why no glial changes were detected in the pilot studies here but were detected in the tissue from the previous study in our lab (Beazley-Long et al. 2018b). Additionally, the pilot studies here had a low sample size (n=1-4 per group), which may also mask any potential glial activation.

When these analysis techniques were applied to tissue from the MIA and carrageenan pilot studies, no changes in GFAP signal were observed for either pain model. As demonstrated, these analyses are able to detect changes in the gliovasculature and so the negative results here could be due to several factors. The timepoints investigated could be too early for astrocytic activation. Central microglial changes were observed at 7 days with 2mg MIA (Thakur et al. 2012), and whilst microglia were not probed in this study, there could be similar microglia activation here. Although, other studies did not detect microglial activation until 14-28 days post-MIA (Kawarai et al. 2018; Orita et al. 2011) so 7 days may still be too early. Generally, astrocyte activation follows microglial activation (Ji et al. 2019; Ji et al. 2013) so if probed later, astrogliosis might be observed. Similarly, with the carrageenan model, microglial, but not astrocytic, changes (as demonstrated by OX42, which targets CD11b, and GFAP immunoreactivity respectively) were observed at 5 days post-carrageenan (Schreiber et al. 2008), suggesting the 3 and 24 hour timepoint is too early to detect astrogliosis. However, there was an increase in Satellite Glial Cell GFAP in DRG as early as 3 and 6 hours post-carrageenan (Souza et al. 2013), meaning there may be peripheral glial alterations and implications on the Blood Nerve Barrier. For this reason, peripheral DRG were probed in subsequent studies. This highlights the importance of ensuring the correct timepoint is being investigated in order to be within the window of spinal activation.

In conclusion, I have developed several analysis techniques to investigate the responses of vessels and associated astrocytes to acute and chronic pain states *in vivo* that are more refined than measuring global dorsal horn intensities and more rapid than manual counting of positive vessel structures. In the next chapter, these techniques were applied to tissue collected from the intra-articular CFA model of monoarthritis as I hypothesised the activation state of the central vasculature and glial cells contribute to the development of chronic pain. I also targetted VEGF-R to test the hypothesis that Vascular Endothelial Growth Factor (VEGF)-A contributes to the development of referred pain behaviour and glial activation.

4 | VEGF-A and TNFα in the Development and Maintenance of Inflammatory Pain

4.1 Introduction

Rheumatoid Arthritis (RA) is an autoimmune condition that causes inflammation, pain and stiffness in joints. Patients are first offered conventional Disease Modifying Anti-Rheumatic Drugs (DMARDs) that attempt to manage the inflammation by suppressing the immune system (National Institute for Health and Care Excellence 2018), but this is not always enough to alleviate pain associated with the condition as patients can complain of pain during periods of low inflammation or in areas with no inflammation (referred or secondary pain) (Boyden et al. 2016). Determining why patients with little or no inflammation still experience pain is vital in developing treatments to manage and alleviate this. One line of reasoning is that there are central changes in nociceptive signalling at both spinal and supraspinal levels (Walsh and McWilliams 2014; Boyden et al. 2016), which may be attributed to activated glial cells/neuroinflammation (Flores Bjurström et al. 2020; Jung et al. 2020; Albrecht et al. 2018). The involvement of glia and neuroinflammation in chronic pain signalling in humans is still relatively unclear, but there is strong evidence for their role in animal models, including in models of inflammatory pain and arthritis (Ji et al. 2019; Ji et al. 2013; Milligan and Watkins 2009).

One pro-inflammatory molecule that has been implicated in chronic pain is Vascular Endothelial Growth Factor (VEGF)-A (Flores Bjurström et al. 2020; Llorián-Salvador and González-Rodríguez 2018; Beazley-Long et al. 2018b; Hulse et al. 2016; Hamilton et al. 2016; Hulse et al. 2014; De Bandt et al. 2003). VEGF is a subfamily of proteins, of which VEGF-A, and specifically its splice variant VEGF-A_{165}, has the most evidence for being involved in pain. The two VEGF-A_{165} variants, VEGF-A_{165}a and VEGF-A_{165}b, have seemingly opposite effects on pain, with VEGF-A_{xxx}a exacerbating neuropathic pain and VEGF-A_{xxx}b reversing/preventing neuropathic and inflammatory pain (Beazley-Long et al. 2018b; Hulse et al. 2016; Hulse et al. 2014).

VEGF-A and all its isoforms activate Vascular Endothelial Growth Factor Receptors (VEGF-Rs) 1 and 2, but VEGF-R2 appears to mediate many of its actions (Peach et al. 2018). VEGF-R1 shows decreased activity upon VEGF-A binding, and so is thought to be a decoy receptor and negative modulator of VEGF-R2 (Peach et al. 2018). By specifically blocking VEGF-R2 *in vivo*, nerve injury and inflammation-induced pain can be prevented (Beazley-Long et al. 2018b; Hulse et al. 2016; Hulse et al. 2014) and osteoarthritis progression is attenuated (Nagao et al. 2017). A previous study using a spontaneous polyarthritis transgenic mouse line (K/BxN) demonstrated blocking of VEGF-R1 but not VEGF-R2 attenuated disease progression (De Bandt et al. 2003). However, this model

did not look at the pain associated with arthritis, and it is known that disease progression and joint damage do not always correlate with pain (Walsh and McWilliams 2014). VEGF-R1's involvement in pain, however, is becoming more known. In a model of trigeminal pain, both VEGF-R1 and VEGF-R2 were involved in pain development, but the increased Blood Brain Barrier (BBB) permeability was attributed to VEGF-R1 only (Lee et al. 2019). Additionally, VEGF-R1 has been shown to be involved in both cancer and lower back pain signalling (Qiu et al. 2020; Selvaraj et al. 2015). Clearly VEGF-Rs are important in the generation of chronic pain, but perhaps more importantly and clinically relevant, it needs to be known whether they are involved in the *maintenance* of chronic secondary pain, and whether disruption of VEGF signalling can alleviate secondary inflammatory pain after it is already established.

In order to investigate VEGF-A signalling, VEGF-Rs can be pharmacologically inhibited. PTK787 (or Vatalanib) is a tyrosine kinase receptor inhibitor, with high affinity for VEGF-R2, but also inhibits VEGF-R2 and 3, and the related tyrosine kinases, c-Fms, c-Kit and Platelet Derived Growth Factor Receptor-β (PDGFR-β) at higher concentrations (Wood et al. 2000). It is a clinically approved drug that is being extensively researched as a chemotherapeutic for solid tumours owing to its inhibition of tumour angiogenesis (Wood et al. 2000). In the context of pain, PTK787 has previously demonstrated analgesic properties in inflammatory arthritis models when given at the time of inflammation (Beazley-Long et al. 2018b; Grosios et al. 2004). Importantly, it was systemic, but not local (intra-articular), PTK787 application that led to reduced inflammation-induced hypersensitivity (Beazley-Long et al. 2018b; Grosios et al. 2004). PTK787 can cross the BBB (Remko et al. 2011), so its analgesia properties may be evoked through actions on central Neurovascular Unit (NVU) cells (endothelial cells, glial cells, neurones) to prevent the development of chronic pain. As well as VEGF-Rs being present on spinal cord neurones, they are also present on primary afferents (Hamilton et al. 2016; Selvaraj et al. 2015; Hulse et al. 2014), and so its analgesic effect could also be due VEGF-R suppression in the peripheral nervous system.

Alterations in VEGF-A signalling have been demonstrated in several diseases, including both osteoarthritis and RA (Hamilton et al. 2016; Llorián-Salvador and González-Rodríguez 2018), but specific mechanisms of its contribution in the Central Nervous System (CNS) to the development and maintenance of chronic pain are still unclear. As well as effects in the periphery in arthritis (angiogenesis, swelling, synovial thickening, neurovascular invasion, inflammation and nociceptor stimulation (Hamilton et al. 2016; Llorián-Salvador and González-Rodríguez 2018)), it is involved in CNS signalling (increased BBB/Blood Spinal Cord Barrier (BSCB) permeability and experimental neurovascular angiogenesis (Argaw et al. 2012; Croll et al. 2004; Proescholdt et al. 1999; Dobrogowska et al. 1998)). An emerging hypothesis of VEGF-A's central contribution to chronic pain is that VEGF-A signalling in spinal endothelial cells can encourage endothelial 'activation' and downstream glial alterations. These could ultimately lead to neuronal sensitivity and increased pain signalling. Additionally, the reverse of this could

be true, with neurones activating astrocytes to release VEGF-A and increase BBB/BSCB permeability through signalling in endothelial cells (Li et al. 2014; Argaw et al. 2012; Argaw et al. 2009; Argaw et al. 2006). This could exacerbate neuroinflammation, glial activation and neuronal hyperexcitability through endothelial-released inflammatory factors and infiltrating blood-borne molecules and cells. This is supported by a study from our lab (Beazley-Long et al. 2018b) as blockade of VEGF-A signalling both systemically (with pharmacological VEGF-R inhibition) and specifically in endothelial cells (with inducible endothelial cell VEGF-R2 knockdown) in murine models of inflammatory monoarthritis prevented the development of secondary hyperalgesia.

In further support of endothelial cells having an important role in chronic pain signalling, patients with inflammatory diseases such as RA demonstrate endothelial dysfunction/activation and a higher risk of cardiovascular diseases (Steyers and Miller 2014). It is thought that endothelial cells may have been activated by elevated levels of circulating inflammatory mediators, such as VEGF-A and Tumour Necrosis Factor α (TNFα) (Totoson et al. 2016; Wei et al. 2015; Steyers and Miller 2014; Nakahara et al. 2003). As these molecules can also reach spinal endothelial cells, these may also become activated and trigger or exacerbate spinal neuroinflammation. Within the endothelial cell, there are several signalling cascades that lead to activation, classified by release of inflammatory molecules and increased barrier permeability (Varatharaj and Galea 2016; Radu et al. 2013). Zinc Finger E-Box Binding Homeobox-1 (ZEB-1) is a transcription factor that can initiate epithelial-mesenchymal transition in cells, which causes them to be more motile and invasive, and so has been extensively studied in the context of cancer (Salajegheh and Salajegheh 2016). Only recently has ZEB-1 been studied in the pain field. In neuropathic pain conditions there is an increase in ZEB-1 expression in the spinal cord and isolated microglia (Zhang et al. 2020; Shen et al. 2019; Yan et al. 2018a; Yan et al. 2018b), and we also found there was an increase in ZEB-1 expression in perivascular cells after peripheral Complete Freund's Adjuvant (CFA) in the mouse (Lopes and Beazley-Long, unpublished data). However, this increase was not in spinal endothelial cells (Lopes and Beazley-Long, unpublished data), meaning spinal endothelial cells may have a different ZEB-1 response to inflammation than non-spinal endothelial cells. This avenue requires more investigation, as there is little information on how endothelial cell ZEB-1 is altered in different species and models of pain.

The downstream effectors of activated neural endothelial cells could be astrocytes and microglia, thanks to their close proximity (Abbott et al. 2010). Activated astrocytes and microglia play key roles in pain regulation (Ji et al. 2019; Inoue and Tsuda 2018; Ji et al. 2013). Direct stimulation of spinal astrocytes through optogenetics can induce rapid pain sensitivity (Nam et al. 2016) and ablation of spinal microglia at early (2 weeks) and late (3 months) stages after nerve injury reversed hypersensitivity (Echeverry et al. 2017). These activated glial cells can increase neuronal sensitivity, decrease inhibitory interneurone function and contribute to neuroinflammation (Grace et al. 2014; Gosselin et al. 2010). Additionally, pain-induced BSCB opening can allow circulating im-

mune cells to infiltrate into the parenchyma, which can become activated or even differentiate into microglia, further sensitising neurones (Grace et al. 2014; Echeverry et al. 2011; Costigan et al. 2009a; Zhang et al. 2007).

In chronic pain, glial and endothelial activation, termed gliovascular alterations here, may include an increase in classic glial protein expression (Glial Fibrillary Acidic Protein (GFAP) in astrocytes (Ji et al. 2019; Eng and Ghirnikar 1994) and Cluster of Differentiation-11b (CD11b) in microglia (Ji et al. 2013; Sedgwick et al. 1998)), an increase in endothelial cell adhesion molecules (such as Intracellular Adhesion Molecule-1 (ICAM-1) (Beazley-Long et al. 2018b)) and infiltration of immune cells into the parenchyma (detected by Cluster of Differentiation-68 (CD68)-positive macrophages in the parenchyma (Jochmann et al. 2015)). Additionally, immune cell infiltration into the Dorsal Root Ganglion (DRG) has been observed in chronic inflammatory and neuropathic pain (Raoof et al. 2018). Disrupting VEGF-A signalling in prevented some gliovascular alterations that were induced by peripheral inflammation (Beazley-Long et al. 2018b), highlighting the importance of VEGF-R in chronic pain signalling. However, although no immune cell infiltration was detected in inflammatory pain, there was an increase in both spinal cord and DRG ICAM-1-positive vessels that was prevented by inhibiting VEGF-R2 (Beazley-Long et al. 2018b).

As well as interrupting VEGF-A signalling to alleviate pain, other inflammatory molecules can be targetted. TNFα is an inflammatory cytokine that is elevated in the plasma of arthritic rats and patients with RA (Wei et al. 2015; Totoson et al. 2016), and has been the main focus of RA treatment for the last two decades (Haraoui and Bykerk 2007). Etanercept (Enbrel®) is an approved anti-TNFα DMARD that competitively binds to TNFα preventing Tumour Necrosis Factor Receptor (TNFR) activation. It is given to many RA patients and has good efficacy in improving disease measures such as joint damage and quality of life (Haraoui and Bykerk 2007). However, even when the inflammation is well controlled with anti-TNFα drugs, many patients can still report pain (over 50% of patients in McWilliams and Walsh 2016). As well as a peripheral role in pain development, central TNFα is a major mediator in spinal neuroinflammation and is involved in chronic pain signalling in the spinal cord (Ji et al. 2018; Rustenhoven et al. 2017; Leung and Cahill 2010; Gosselin et al. 2010). It can enhance glutamate-induced excitatory currents in neurones (Kawasaki et al. 2008b) and induce glial activation (Koyama 2014). Additionally, TNFα can increase BBB permeability (Zhang et al. 2019; Daniels et al. 2014; Förster et al. 2008; Didier et al. 2003; Mark and Miller 1999) and lead to the release of further inflammatory molecules such as Interleukin (IL)-6, Interleukin-1β (IL-1β) and VEGF-A by glial cells and endothelial cells (Zhang et al. 2019; Lee et al. 2017; Varatharaj and Galea 2016; Ji et al. 2013). TNFα is clearly a key player in both peripheral and central pain signalling, but as many patients still report pain when peripheral inflammation is under control (McWilliams and Walsh 2016; Walsh and McWilliams 2014), it may be beneficial to supplement DMARD anti-inflammatory treatments, for example etanercept, with pharmaceuticals that specifically target mechanisms that lead to and/

or maintain chronic pain, such as VEGF-A signalling. It should be noted that whilst etanercept cannot cross the BBB, it can reach the luminal side of neural endothelial cells and may also have anti-inflammatory effects here as well as in the periphery.

The pain-induced gliovascular alterations mentioned here, for example increases in GFAP, CD11b and ICAM-1 signal in the spinal cord and DRG, can be prevented with VEGF-R inhibition (Beazley-Long et al. 2018b). However, this study looked at gliovascular alterations in the later stages of inflammation (days 8, 11, and 14), and as changes in central glial cells can be seen as early as 4 hours after peripheral inflammation (Raghavendra et al. 2004; Sun et al. 2007; Xu et al. 2014), to fully understand VEGF's role in the development of chronic pain it needs to be determined if disrupting signalling can prevent these very early changes. Additionally, prophylactic disruption of VEGF-A signalling may prevent secondary pain and associated gliovascular alterations (Beazley-Long et al. 2018b). For the patient, it is important to determine whether therapeutic inhibition of VEGF-A signalling can reverse established pain. This chapter aims to address these unknowns using intra-/peri-articular CFA as a model of inflammatory arthritis.

CFA is composed of heat-killed *Mycobacterium tuberculosis* suspended in mineral oil and activates Toll-Like Receptor (TLR)4 and TLR2 on macrophages and dendritic cells to initiate a robust inflammatory response (Faridgohar and Nikoueinejad 2017; Stils 2005; Billiau and Matthys 2001). CFA has been used extensively in pain research, and peri-/intra-articular injection can induce chronic monoarthritis that is localised to the joint, making it a useful model that can avoid systemic changes induced by other polyarthritic inflammatory models (Zhang and Ren 2011; Donaldson et al. 1993; Butler et al. 1992). However, CFA dose is an important consideration as different doses can lead to different phenotypes (Donaldson et al. 1993). Of course, this is true of many pharmacological interventions, but there is evidence that even very mild inflammation can cause central spinal neuroinflammation, which implies there will be measurable spinal glial activation in low and medium dose CFA models. For example, injection of saline can cause inflammation at the injection site (Jensen et al. 2008) and has the potential to increase swelling and hypersensitivity in the contralateral uninjured hindpaw (Levine et al. 1985; Denko and Petricevic 1978), which is suggestive of spinal activation. Less severe peripheral insults such as subcutaneous injection of λ-carrageenan have been shown to cause rapid central NVU alterations (Schreiber et al. 2008; Hua et al. 2005; Huber et al. 2005; Huber et al. 2002; Huber et al. 2001), again suggesting that peripheral inflammation will reliably cause measurable spinal neuroinflammation and gliovascular alterations. In support of this, low dose (50ug) intra-articular CFA caused astrocyte and microglial activation as early as 3 days post-injection (Sun et al. 2007; Sun et al. 2008).

In this chapter, I used the CFA model of inflammatory pain to investigate early (2 days) and later (10 days) gliovascular alterations, and disrupted VEGF-R2 and/or TNFα signalling to investigate their role on the development and maintenance of chronic pain

(and associated gliovascular alterations). This chapter aimed to address the unknowns highlighted in Section 1.4 and Figure 1.8 (in particular points 1, 2 and 4).

Hypothesis

Inhibition of VEGF-R2 function will result in altered inflammatory arthritis pain in rodents by blocking spinal and/or DRG gliovascular/neuroinflammatory interactions.

I tested this hypothesis experimentally by: confirming that CFA resulted in significant pain behaviour and gliovascular alterations; inhibiting VEGF-R2 and/or TNFα with pharmacological inhibitors both prophylactically and therapeutically for effects on pain behaviour and gliovascular alterations; and by comparing outcome measures with those from inducible VEGF-R2 endothelial cell knockout mice with hindpaw CFA inflammation. I used the histological analysis techniques developed in Chapter 3 (whole dorsal horn intensity, fluorescence at vessels, and fluorescence/area of vessel-associated objects, see Section 4.2.8) to detect gliovascular alterations in the dorsal horn of the spinal cord, and counted the number of infiltrating immune cells detected through CD68 immunofluorescence in the DRG.

Objectives

- To use PTK787 to block VEGF-R2 and investigate how VEGF-R2 contributes to the development and maintenance of secondary inflammatory pain and associated gliovascular changes.
- To investigate the synergistic effect of PTK787 and etanercept in the reversal of secondary pain and associated gliovascular changes.

4.2 Materials & Methods

4.2.1 Experimental Animals

All experiments and procedures were performed in accordance with the Animals (Scientific Procedures) Act (1986; 2012) and were authorised by the UK Home Office. Experiments were carried out on adult (≥175g) male Sprague Dawley (SpD) rats (Charles River, UK). The oestrus cycle in females causes hormone fluctuations that may interact with pain signalling and experimental outcomes (Becker et al. 2005a; Craft et al. 2004), and so male rats were used due to time constraints and because the work carried out in this thesis was early work within the gliovascular-pain field. Experiments involving transgenic mice (*vegfr2*$^{fl/fl}$ Tie2CreER^{T2} termed VEGF-R2^{ECKO}, see Beazley-Long et al. 2018b and Section 2.2.3.1) were carried out on both male and female adult mice.

Rats and mice were group-housed (3-4 per cage) in individually-ventilated cages. Animals were maintained in a 12 hour light/dark cycle at 22˚C and 55% humidity with access to food and water *ad libitum*.

A total of 89 rats and 22 mice were used in these studies (see Table 4.1). Sample size for mouse studies were calculated at n = 5/6 per group using previous data from our lab. Sample size for rat studies were calculated at n = 6 per group using previous data from our lab for the detection of gliovascular changes after intra-articular CFA in the rat using the following values:

Power = 0.8; Type 1 error rate = 5%; Group A mean = 4.705; Group B mean = 13.785; Standard Deviation (SD) = 5.531; Sampling Ratio = 1

`http://powerandsamplesize.com/Calculators/Compare-2-Means/2-Sample-Equality`

One rat (Study 3, CFA + PTK787 + etanercept) was removed from all analyses due to lack of CFA response (i.e. lack of swelling).

Study	Treatments	Number of Animals
1	Sham + Vehicle	6
	CFA + Vehicle	6
	CFA + PTK787	6
	CFA + Etanercept	6
2	Sham + Vehicle	5
	CFA + Vehicle	6
	CFA + PTK787	6
	CFA + d0 PTK787	6
	CFA + Etanercept	6
3	Sham + Vehicle	6
	CFA + Vehicle	6
	CFA + PTK787	6
	CFA + d0 PTK787	6
	CFA + Etanercept	6
	CFA + PTK787 + Etanercept	6*
4	Vehicle + Sham	5
	Vehicle + CFA	6
	Tamoxifen + Sham	5
	Tamoxifen + CFA	6

***** one animal was excluded from all analyses due to lack of CFA response

Table 4.1: Details of animal numbers and treatment groups.

4.2.2 Blinding

All treatment groups and experimental conditions were blinded. An independent investigator allocated animals to treatment groups using the standard = RAND() function in Microsoft Excel and shared the blinding code with a second independent investigator to help with drug dosing. At day 3 in Study 3 (prior to any drug dosing, except the

day 0 PTK787 group) an independent investigator unblinded the von Frey data and animals were assigned to therapeutic treatment groups ensuring there was an even spread across these groups.

Drugs were prepared by me but drawn up into syringes by an independent investigator so I was unaware of the drug being injected. For pain behaviour, an independent investigator randomly placed animals into the relevant behaviour boxes so I was unaware of which cage (or treatment group) animals were from. Tissue processing and immunofluorescence was also carried out on blinded sections, and animals and treatment groups were only unblinded after image analysis using the blinding code.

4.2.3 Experimental Design

- **Study 1.** Within/between subjects comparison of the effect of prophylactic pharmacological VEGF-R inhibition on acute peripheral CFA-induced inflammation and associated spinal gliovascular changes in rats.
- **Studies 2 & 3.** Within/between subjects comparison of the effect of prophylactic or therapeutic pharmacological VEGF-R and/or TNFα inhibition on peripheral CFA-induced inflammation and associated spinal gliovascular changes in rats.
- **Study 4.** Within/between subjects comparison of the effect of prophylactic endothelial cell-specific VEGF-R knockdown on peripheral CFA-induced spinal gliovascular changes in mice.

4.2.3.1 Study 1

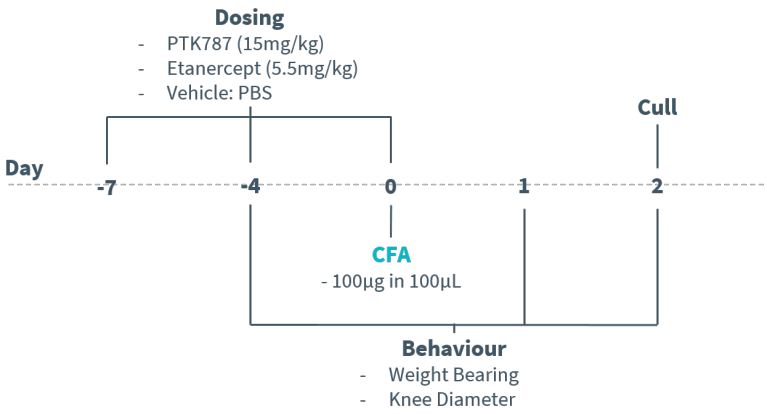


Figure 4.1: Timeline for prophylactic VEGF-R or TNFα inhibition (Study 1)

Animals were prophylactically dosed (Intraperitoneal (i.p.)) with the VEGF-R inhibitor, PTK787 (15mg/kg), or the anti-TNFα drug, Etanercept (5.5mg/kg), or vehicle (Phosphate Buffered Solution (PBS)) for one week prior to induction of inflammation with 100µg CFA in 100µL (see Figure 4.1). Weight bearing and knee diameter behaviour measurements were taken, and 2 days post-CFA, animals were culled and spinal cords and DRG taken for immunofluorescence analysis.

4.2.3.2 Study 2

Animals were dosed with vehicle (PBS, i.p.) for one week prior to inflammation from 100µg CFA in 50µL to allow animals to habituate to dosing. At the time of inflammation (day 0), one group received PTK787 as a positive control (Beazley-Long et al. 2018b), otherwise all treatment groups received PTK787, etanercept, or vehicle (PBS) after mechanical hypersensitivity was confirmed at 3 days (see Figure 4.2). All drugs were given at the same concentration as in Section 4.2.3.1. Weight bearing, mechanical hypersensitivity and knee diameter behaviour measurements were taken, and 10 days post-CFA, animals were culled and spinal cords and DRG taken for immunofluorescence analysis.

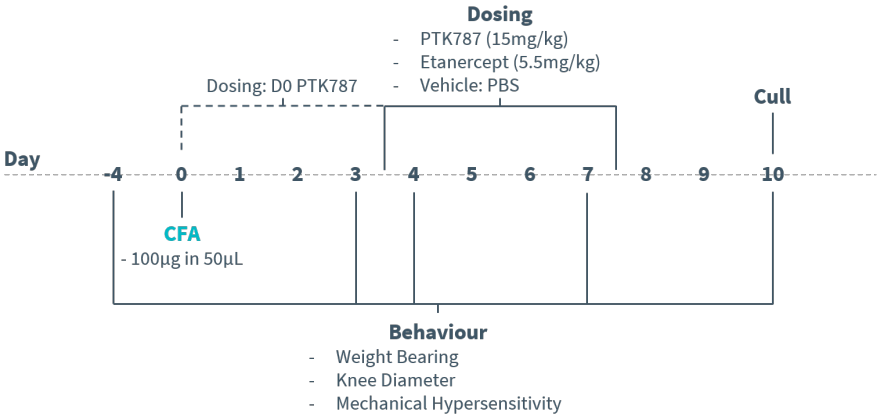


Figure 4.2: Timeline for therapeutic VEGF-R or TNFα inhibition (Study 2)

4.2.3.3 Study 3

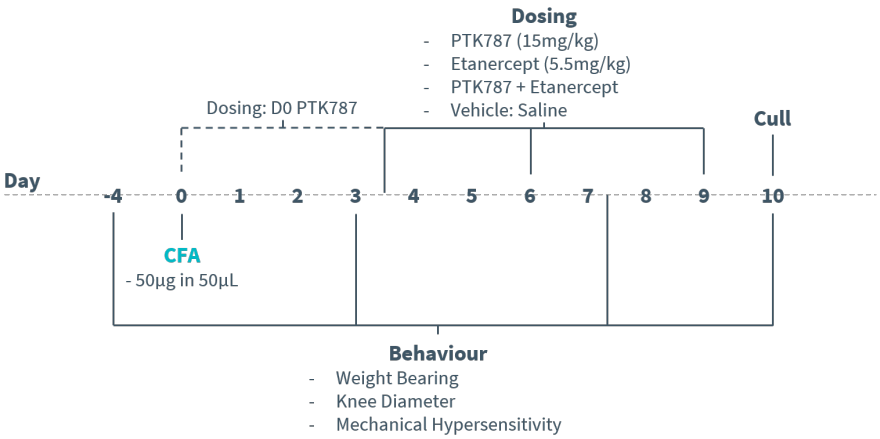


Figure 4.3: Timeline for therapeutic VEGF-R and/or TNFα inhibition (Study 3)

Animals were dosed with vehicle (sterile saline, i.p.) for one week prior to induction of inflammation with 50µg CFA in 50µL. At the time of inflammation (day 0), one group received PTK787 as a positive control (Beazley-Long et al. 2018b), otherwise all treatment groups received PTK787, etanercept, PTK787 + etanercept, or vehicle (saline) after mechanical hypersensitivity was confirmed at 3 days (see Figure 4.3). All drugs were given at the same concentration as in Section 4.2.3.1. Weight bearing, mechanical hypersen-

sitivity and knee diameter behaviour measurements were taken, and 10 days post-CFA, animals were culled and spinal cords and DRG taken for immunofluorescence analysis.

4.2.3.4 Study 4

To disrupt endothelial cell VEGF-A signalling, inducible endothelial *vegfr2* knockout mice (VEGF-R2^{ECKO}, see Section 4.2.6.2) received five daily doses of tamoxifen (1mg/100µL, i.p.) or vehicle (10% ethanol and 90% oil, volume/route matched) prior to induction of inflammation with commercial CFA (2 x 80µg CFA in 40µL). I carried out knock-out induction by tamoxifen injection; Dr Nick Bealkey-Long carried out induction of inflammation (see Section 4.2.4), behaviour, dissection, tissue processing and spinal cord immunofluorescence (Beazley-Long et al. 2018b). Mechanical hypersensitivity and knee diameter behaviour measurements were taken, and 14 days post-CFA, animals were culled and spinal cords and taken for immunofluorescence analysis.

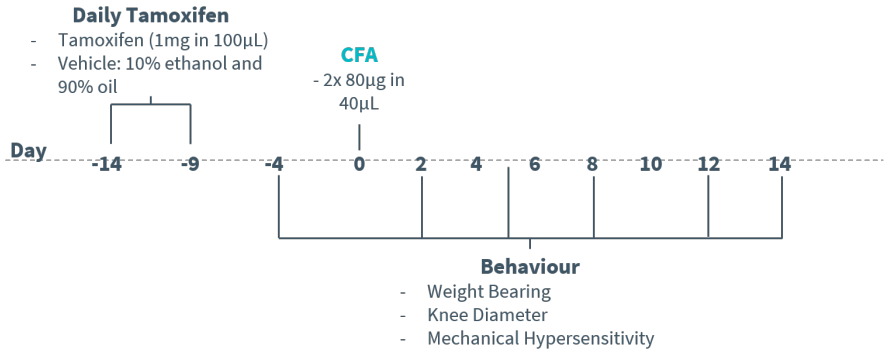


Figure 4.4: Timeline for genetic endothelial cell knockout in the mouse (Study 4).

4.2.4 Induction of Peripheral Inflammation

CFA (composed of heat-denatured *mycobacterium tuberculosis* suspended in mineral oil) was either purchased from Sigma-Aldrich (1mg/mL, F5881) or prepared by resuspending heat-denatured *mycobacterium tuberculosis* (UK Ministry of Agriculture Fisheries and Food, now known as DEFRA, UK) in mineral oil (2mg/mL), sonicated for 1 hr and and filtered (40µm pore size).

Male Wistar rats (≥175g, n = 72, see Table 4.1 for group-specific numbers) received an intra-articular injection of CFA (Study 1: commercial 100µg in 100µL (1mg/mL); Study 2: in-house 100µg in 50µL (2mg/mL); Study 3: commercial 50µg in 50µL (1mg/mL)) into the right knee under anaesthesia (2% isoflurane vaporized in 100% Oxygen), as described in Section 2.2.2.4. Shams (n = 17) were anaesthetised and shaved but received no injection.

Male and female transgenic mice (VEGF-R2^{ECKO} (see Beazley-Long et al. 2018b), n = 22, see Table 4.1) injected with tamoxifen or vehicle two-weeks prior received a unilateral peri-articular injection of CFA (2mg/mL, 2 x 80µg CFA in 40µL mineral oil) on both sides

of the joint under anaesthesia (2% isoflurane vaporized in 100% Oxygen) as described in Section 2.2.2.5. Shams were anaesthetised and shaved but received no injection. Animals were housed in individually-ventilated cages (single-tier, 3-4 per cage) with other tamoxifen-dosed mice to prevent tamoxifen cross-contamination through faeces and urine (Brake et al. 2004).

CFA vehicle was not injected into control animals because the oil and injection itself are sufficient to cause inflammation, therefore confounding the interpretation of results.

4.2.5 Pain Behaviour

All pain behaviour is detailed in Section 2.2.4. In study 1, weight bearing asymmetry and knee diameter (detailed in Sections 2.2.4.1 and 2.2.4.3) were measured at baseline and 2 days post-inflammation. It is not possible to record accurate mechanical thresholds using von Frey hairs at timepoints this early as animals put so little weight on the affected hindpaw, hairs can raise the paw and positive responses are difficult to discern. In studies 2 & 3, knee diameter, weight bearing and mechanical sensitivity (using the 50% threshold method detailed in Section 2.2.4.2) were recorded. In the mouse, knee diameter, weight bearing and mechanical sensitivity (50% threshold method) were recorded by Dr Nick Beazley-Long (published in Beazley-Long et al. 2018b).

Weight bearing data is displayed as percentage of weight borne on the ipsilateral side using the following formula:

$$\frac{Average\,Weight\,Borne\,on\,Ipsilateral}{Total\,Weight\,Borne\,on\,Both\,Limbs} \times 100$$

Mechanical threshold is displayed as 50% withdrawal response, determined by plotting the percentage of withdrawal responses against the log of the bending force to generate a stimulus-response curve (for example see Figure 4.5).

4.2.6 Inhibition of TNFα and VEGF-R2

4.2.6.1 Pharmacological VEGF-R2 and TNFα inhibition

PTK787 (AdooQ BioScience LLC, A10967 or Selleckchem, S1101) was prepared as described in Section 2.2.3.2. For Studies 1 & 2, PTK787 was dissolved in sterile PBS vehicle at 3.75mg/mL to give a final dose of 15mg/kg and required heating/vortexing/sonicating/filtering. 15mg/kg PTK787 has shown previously to prevent development of secondary pain (Beazley-Long et al. 2018b). An anti-TNFα drug, Etanercept (Enbrel®, Pfizer Limited, UK), used in the clinic to treat disorders such as RA was also tested at a dose of 5.5mg/kg diluted in sterile PBS to 1.375mg/mL. This dose has previously shown to alter secondary pain (Schaible et al. 2010; Boettger et al. 2008). For

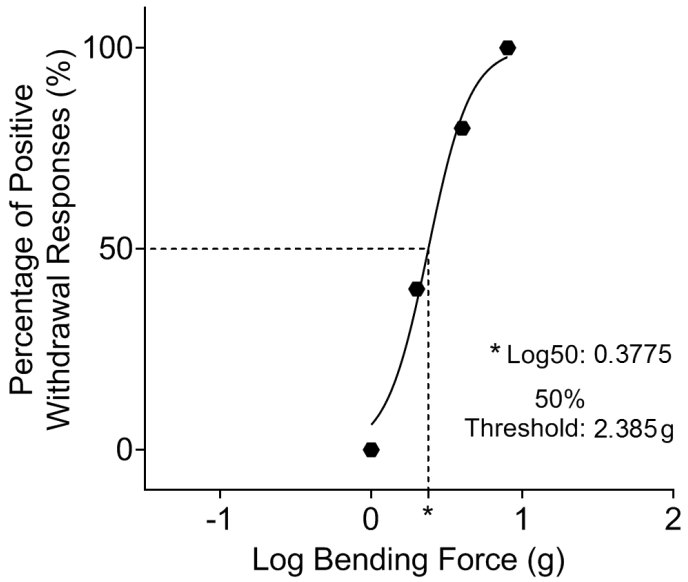


Figure 4.5: Example of a von Frey stimulus-response curve from which the 50% withdrawal response is determined. The percentage of positive withdrawal responses are plotted and a Sigmoidal dose-response (variable slope) curve is fitted to calculate the Log50 (*) and the 50% threshold.

Study 3, PTK787 and etanercept were made up in sterile saline vehicle, and no heating/vortexing/sonicating/filtering was needed to adequately dissolve PTK787. See Section 4.2.3 for dosing regimens.

4.2.6.2 Genetic VEGF-R2 Knockdown

Male and female inducible endothelial *vegfr2* knockout mice (Beazley-Long et al. 2018b), termed VEGF-R2^{ECKO}, were used (see Section 2.2.3.1 for information of mouse line production). Knockout of VEGF-R2 was induced by giving five daily doses of tamoxifen (1mg/100µL i.p.) or vehicle (volume/route-matched) to either Tie2CreER^{T2}-positive or Tie2CreER^{T2}-negative mice as a control for actions of tamoxifen prior to induction of inflammation.

Tamoxifen (Sigma, T5648) was dissolved in ethanol then diluted in autoclaved sunflower oil (vehicle: 10% ethanol and 90% oil) (Acharya et al. 2011).

4.2.7 Immunofluorescence

At the end of the studies (Mice: day 14; Study 1: day 2; Studies 2 and 3: day 10 post-CFA injection), animals were euthanised and spinal columns dissected and processed for slide-mounted immunofluorescence as previously described Section 2.2.5. For cryostat sectioning, the spinal cord was cut just above (for Study 1) or at (for Study 2 & 3 and the mice) the thickest part of the lumbar section and was sectioned (at 40µm) towards the head (rostrally) to allow study of Lumbar Section (L)5-3 and identification of

ipsilateral and contralateral sides of the cord once mounted. L5-3 correspond to the areas innervated by the foot and knee (Takahashi et al. 2002; Ivanavicius et al. 2004; Takahashi and Nakajima 1996; Takahashi et al. 1994; Bajrović and Sketelj 1998). For Study 1, ipsilateral L3 and L4 DRGs were sectioned at 20µm longitudinally in the orientation of the axon to obtain a cross-section of the DRG to investigate immune cell infiltration.

Slide-mounted immunofluorescence was performed as described in Section 2.2.6. Sections were washed in PBS + 0.2% Triton-X-100, and used 5% BSA + 10% Foetal Bovine Serum (FBS) in 0.2% Triton-X-100 in PBS as the block. Primary and secondary antibodies are detailed in Tables 4.2 and 4.3.

In the mouse, dissection, tissue processing (at 20µm thickness) and slide-mounted immunofluorescence were carried out by Dr Nick Beazley-Long.

Identifies	Antibody	Host	Supplier	Product Number	Working Concentration
Microglia	CD11b	Mouse	BIO-RAD	MCA275GA	2µg/ml
Vascular Endothelial Cells	CD31	Goat	R&D Systems	AF3628	2µg/ml
Monocytes/Macrophages	CD68	Rabbit	abcam	ab125212	1µg/ml
Astrocytes	GFAP	Goat	abcam	ab53554	1µg/ml
Astrocytes	GFAP	Rabbit	abcam	ab7260	1µg/ml
ICAM-1	ICAM-1	Mouse	abcam	ab171123	2µg/ml
Vascular Basement Membrane	Laminin	Rabbit	Novus Bio	NB300-144	2µg/ml
Vascular Endothelial Cells	RECA-1	Mouse	ThermoFisher	HIS52	1µg/ml
ZEB-1	ZEB-1	Rabbit	Santa Cruz	sc-515797	2µg/ml
-	IgG	Rabbit	LS Bio	LS-C109222	matched*
-	IgG	Mouse	Novus Biologicals	NBP1-97019	matched*

ICAM-1: intracellular adhesion molecule-1; **GFAP**: glial fibrillary acidic protein; **CD11b**: cluster of differentiation 11b; **CD31**: cluster of differentiation 31; **CD68**: cluster of differentiation 68; **IgG**: immunoglobulin; **RECA-1**: rat endothelial cell antigen-1; **ZEB-1**: Zinc finger E-box-binding homeobox-1. ***** IgG concentration was matched to the relevant primary antibody concentration.

Table 4.2: Details of primary antibodies

Target	Host	Fluorophore	Supplier	Product Number	Working Concentration
α-Goat	Chicken	AF® 488	Invitrogen	A21467	1µg/ml
α-Mouse	Donkey	AF® 488	Invitrogen	R37114	2 drops/1mL
α-Goat	Donkey	AF® 555	Invitrogen	A21432	1µg/ml
α-Mouse	Donkey	AF® 555	Invitrogen	A21202	1µg/ml
α-Rabbit	Donkey	AF® 555	Invitrogen	A31572	1µg/ml
α-Rabbit	Donkey	CF™ 633	Sigma	SAB4600132	1µg/ml
Hoeschst-543334		-	Sigma	-	1µg/ml

AF: Alexa Fluor®; **CF**: CruzFluor™

Table 4.3: Details of secondary antibodies

4.2.8 Immunofluorescence Analysis

Immunofluorescence analysis of histology was performed using techniques described in Chapter 3 using FIJI Image J software (National Institutes of Health, USA) with or

without the additional BioVoxxel plugin (BioVoxxel, Germany). The main analysis techniques were:

- Global dorsal horn fluorescence
- Fluorescence/area of vessel-associated objects using the overlap extraction method (Section 3.2.6.3)
  - This method uses the BioVoxxel FIJI plug-in to generate a Region of Interest (ROI) from overlapping binary vessel and GFAP signal. Overlap was set at 0%, meaning any objects (GFAP) that overlap with the selector (vessel marker) were extracted. This ROI can be used to determine GFAP intensity or the area of vessel-associated astrocytes, and includes astrocytes that extend away from the vessel, which are excluded with the overlay method. See Figure 4.6a & b for vessel-associated GFAP overlap signal (in blue) on top of GFAP (a) or vessel (b) signal.
- Fluorescence at vessels using the overlay method (Sections 3.2.6.1 and 3.2.6.2)
  - This method uses the binary vessel signal to generate a ROI that is applied to GFAP (astrocyte) signal to measure GFAP intensity directly at vessels. See Figure 4.6c & d for vessel signal (in blue and yellow respectively) on top of GFAP signal.

Analysis was semi-automated using custom FIJI macros which are listed in Section A.3. Additionally, the number of GFAP-associated vessel fragments (identified by either strings of flat endothelial nuclei or curved nuclei (Figure 4.7)) per animal were counted and expressed over the total sectional area per animal to account for differences in the total area analysed.

The number of CD68-positive cells (monocytes/macrophages) in DRG were counted and expressed over the total sectional area per animal. Cells were counted as positive if a punctate CD68 signal (<10µm) overlapped with the nuclear signal (Figure 4.8a & b, white arrows). Perivascular cells were defined as cells whose cytoplasm or nucleus overlapped with the Rat Endothelial Cell Antigen-1 (RECA-1) vessel signal (Figure 4.8c, yellow arrows).

Using the Rat Spinal Cord Atlas (Watson et al. 2009), approximate segments of the spinal cord were determined for stained sections based on dorsal horn morphology.

4.2.9 Cell Culture

Passage (p)1 Human Brain Microvascular Endothelial Cells (HBMECs) were purchased from ScienCell (ScienCell Research Laboratories, 1000, lot #20978). HBMECs were cultured on fibronectin-coated (2µg/cm^2) flasks at 37˚C in culture medium (see Section 2.3 for details). Free-floating Human Monocyte-like Cellss (THP-1s) (Sigma, 88081201) were cultured in culture medium (see Section 2.3 for details) at 37˚C.

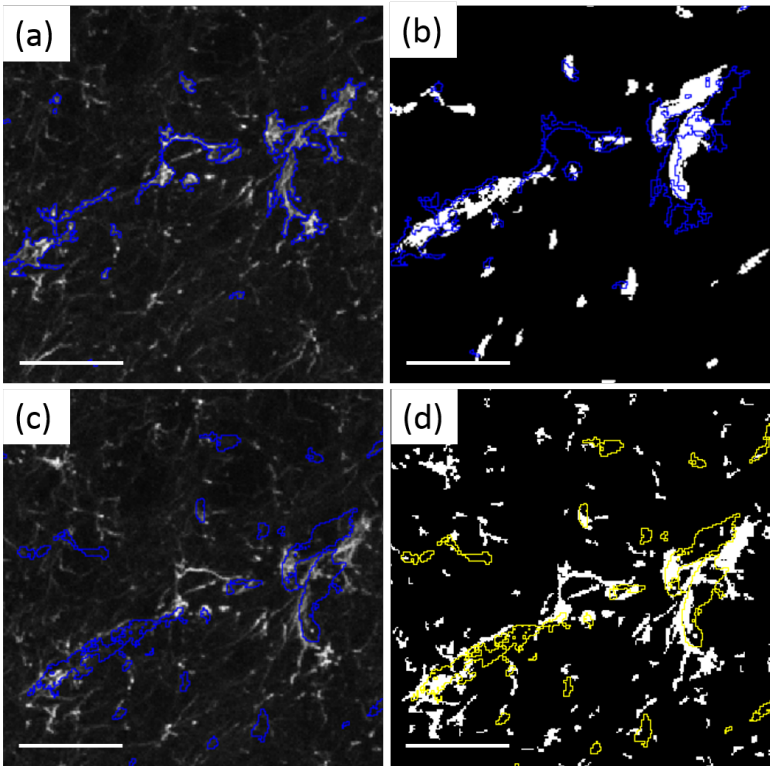


Figure 4.6: Representative images of regions of interest (ROIs) included in analyses in the overlap extraction method **(a & b)** vs the overlay ROI method **(c & d)**. GFAP structures that extend from the vessel signal (laminin) are included in the overlap method **(a & b)**, whereas they are excluded with the overlay ROI method **(c & d)**. **(a)** GFAP signal + overlap extraction in blue. **(b)** vessel threshold + overlap extraction in blue. **(c)** GFAP binary signal + vessel overlay in blue. **(d)** GFAP threshold + vessel overlay in yellow. Rat dorsal horn of the spinal cord. Scale bar: 50µm.

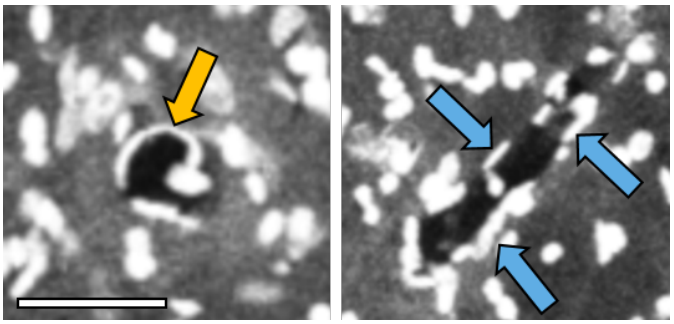


Figure 4.7: Endothelial cell nuclei identified by either curved nuclei (yellow arrow) or a string of flat nuclei (blue arrows). Hoechst nuclear marker in the rat dorsal horn spinal cord. Scale bar: 50μm.

Stock concentration of TNFα was at 100μg/mL in sterile PBS. There were three batches of PTK787 used here. 1: PTK787 (AdooQ BioScience LLC, A10967) from Studies 1 & 2 dissolved at 3.75mg/mL in PBS and diluted to 100μM in PBS; 2: PTK787 from Studies 1 & 2 (AdooQ BioScience LLC, A10967) dissolved at 3.75mg/mL in DMSO and diluted to 100μM in PBS; PTK787 from a previous experiment dissolved at 100μM in PBS. All batches of PTK787 were then diluted to 100nM in cell media.

4.2.10 The Monocyte Attachment Assay

Endothelial cells can become activated by inflammatory mediators, leading to release of VEGF-A and expression of adhesion molecules such as Vascular Cell Adhesion Molecule-1 (VCAM-1) and ICAM-1 (Zhang et al. 2019; Thichanpiang et al. 2014; Liao 2013). This can cause increase binding of monocytes, which can be modelled *in vitro* (Thichanpiang et al. 2014). I used this process in the monocyte attachment assay to test the activity of PTK787 in blocking VEGF-Rs.

The monocyte attachment assay is detailed in Section 2.3.1. Briefly, HBMECs were plated in fibronectin-coated 96 well plates and left to grow until confluent (2-3days) before serum starving in 1% FBS overnight. Cells were pretreated with 100nM PTK787 for 20min, then with recombinant human TNFα (20ng/mL) (R&D Systems) to induce adhesion molecule expression and PTK787 for 24 hours. THP-1s were fluorescently tagged with Calcein-AM (Sigma-Aldrich, 17783) and added to the HBMEC monolayer for attachment. Unattached monocytes were washed off and monolayers were fixed with 4% Paraformaldehyde (PFA). Calcein fluorescence was measured on a fluorescence plate reader (VictorX4, Perkin-Elmer). Data shown are corrected for background values by subtraction of the mean fluorescence value of the ”no THP-1” control group and are then expressed as a percentage of the maximal mean response (set at 100%) to account for variability in raw fluorescence.

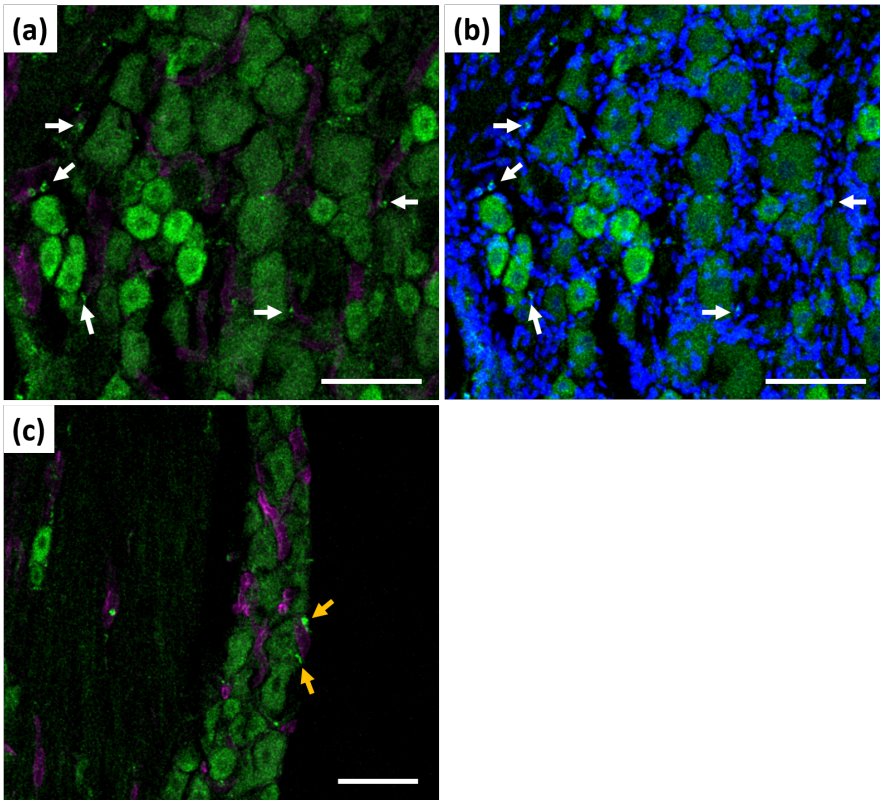


Figure 4.8: Criteria for counting CD68-positive cells in the rat DRG. Cells were counted as positive if the punctate CD68 signal (<10µm) overlapped with the nuclear signal (white arrows in **a** & **b**). Perivascular cells were defined as cells whose cytoplasm or nucleus overlapped with the RECA-1 vessel signal (yellow arrows in **c**) Green: CD68 marker; Magenta: RECA-1 vessel marker; Blue: Hoechst nuclear marker. Scale bar: 100µm.

4.2.11 Absorbance Assay

A simple absorbance assay was employed to test the PTK787 solution in PBS. PTK787 (AdooQ BioScience LLC, A10967) was dissolved in PBS pr DMSO at 3.75mg/mL. The absorbance of the PTK787 dissolved in PBS or DMSO, and PBS and DMSO blanks were read at three wavelengths (450nm, 490nm, 550nm) on a plate reader (VictorX4, Perkin-Elmer or CLARIOstar, BMG LABTECH).

4.2.12 Statistical Analysis

Data are presented as scatter plots with the mean ± SD shown. Analysis of data was performed using GraphPad Prism (versions 7.01/7.05/8.4.3 for Windows, GraphPad Software, San Diego, California USA), and all tests performed are specified in relevant results sections.

4.3 Results

4.3.1 Study 1: Prophylactic Inhibition of VEGF-Receptors and TNFα in Acute Inflammatory Arthritis

4.3.1.1 CFA Caused Significant Acute Pain Behaviour, which was Unaltered by Prophylactic PTK787 or Etanercept

In this study, rats received an intra-articular injection of a 100µg commercial CFA dose in 100µL volume. Intra-articular CFA caused a significant decrease in ipsilateral weight bearing and increase in ipsilateral knee diameter at 1 and 2 days ($p<0.0001$, Figure 4.9a & b respectively). There was no difference in weight bearing between CFA + vehicle and any treatment on either day, however, pretreatment with PTK787 caused significantly more swelling compared to pretreatment with vehicle on day 1 (CFA + PBS: 17.05±0.93mm; CFA + PTK787: 18.36±0.92mm, $p<0.05$, 2way ANOVA with Dunnett's multiple comparisons).

4.3.1.2 The Central Astrocytic Response to Acute Peripheral Inflammation and the Effect of VEGF-R or TNFα Inhibition

Using the rat spinal cord atlas (Watson et al. 2009), approximate spinal cord locations were determined. In Study 1, the area just above the thickest part of the lumbar section was sectioned to allow investigation of L5-3 segments, which correspond to the areas innervated by the foot and knee (Takahashi et al. 2002; Ivanavicius et al. 2004; Takahashi and Nakajima 1996; Takahashi et al. 1994; Bajrović and Sketelj 1998). Here, 95.83% of sections were in L3-5, with 40.28% of all sections in L3, 50% in L4 and 5.56% in L5 (Table 4.4).

To investigate the astroglial response to acute inflammation, global GFAP fluorescence

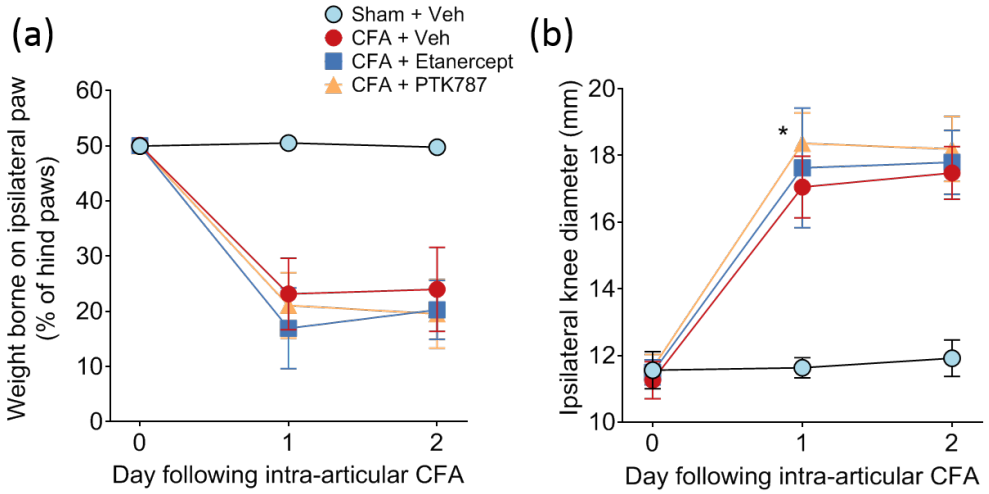


Figure 4.9: Weight bearing and knee diameter 2 days after intra-articular CFA. CFA caused a significant decrease in ipsilateral weight bearing compared to sham at days 1 and 2, that was not altered by pre-treatment (**a**, Interaction: $p<0.0001$; Row Factor: $p<0.0001$; Column Factor: $p<0.0001$). CFA also caused a significant increase in ipsilateral knee diameter compared to sham on both days (**b**, Interaction: $p<0.0001$; Row Factor: $p<0.0001$; Column Factor: $p<0.0001$), and pretreatment with PTK787 caused significantly more swelling compared to pretreatment with vehicle at day 1 (CFA + PBS: 17.05±0.93; CFA + PTK787: 18.36±0.92). *$p<0.05$, 2way ANOVA with Dunnett's multiple comparisons compared to CFA + vehicle. n = 6. Mean ± SD.

and the number of GFAP-positive vessels were measured in spinal cord sections at day 2 of inflammation. Global dorsal horn GFAP fluorescence was unaltered between treatment groups (Figure 4.10a, see Figure 4.11 for representative images) indicating that overall there was no global spinal dorsal horn astrocytic response in acute CFA arthritis.

Study		L2	L3	L4	L5
1	No.	3	29	36	4
	%	4.17	40.28	50.00	5.56
2	No.	0	6	38	7
	%	0.00	11.76	74.51	13.73
3	No.	0	9	38	7
	%	0.00	16.67	70.37	12.96

No.: Number of sections
%: Percentage of total sections

Table 4.4: Approximate spinal cord locations.

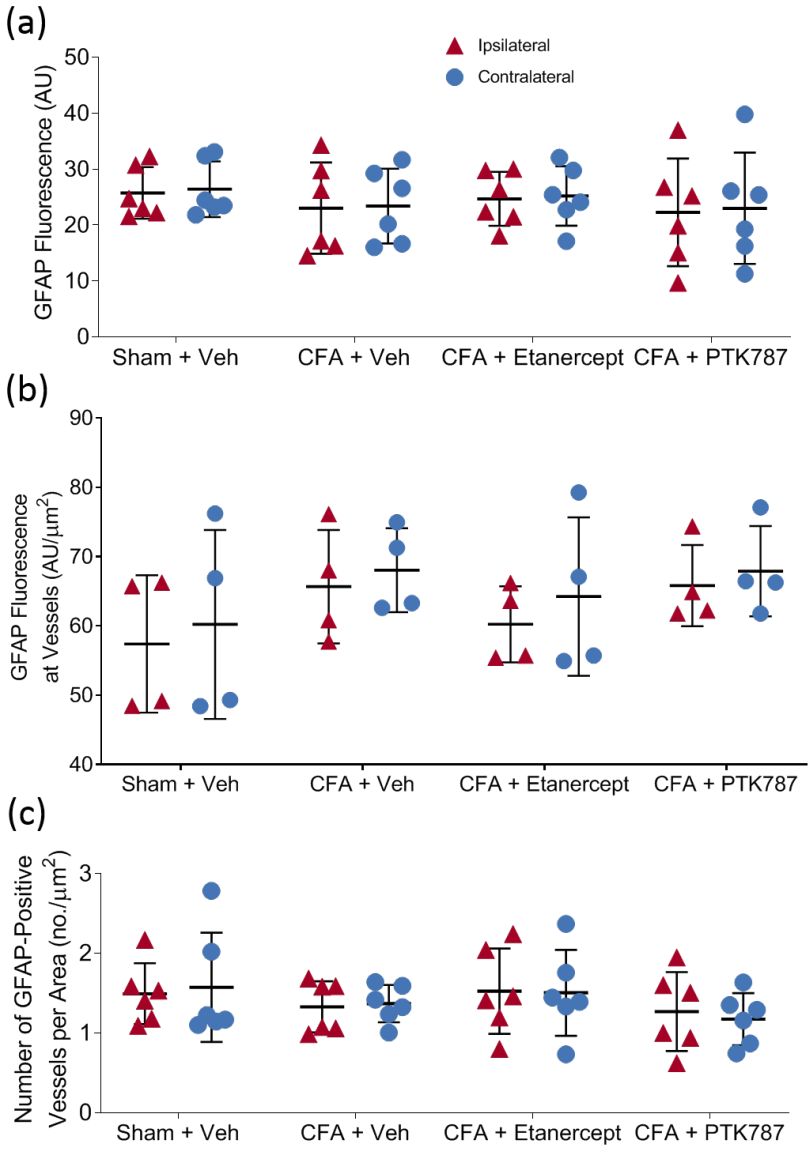


Figure 4.10: After 2 days, neither CFA nor drug pre-treatments had an effect on global dorsal horn (**a**, Interaction: p>0.99; Row Factor: p=0.62; Column Factor: p=0.78) or deeper laminae vessel-GFAP fluorescence (vessels identified by laminin, **b**, Interaction: p=0.99; Row Factor: p=0.61; Column Factor: p=0.43), or the number of GFAP-positive vessels (vessels/endothelial cells identified by curved or strings of flat nuclei, **c**, Interaction: p=0.97; Row Factor: p=0.31; Column Factor: p=0.99) in the dorsal horn of the spinal cord. 2way ANOVA. n = 4-6. Mean ± SD. Veh: Vehicle.

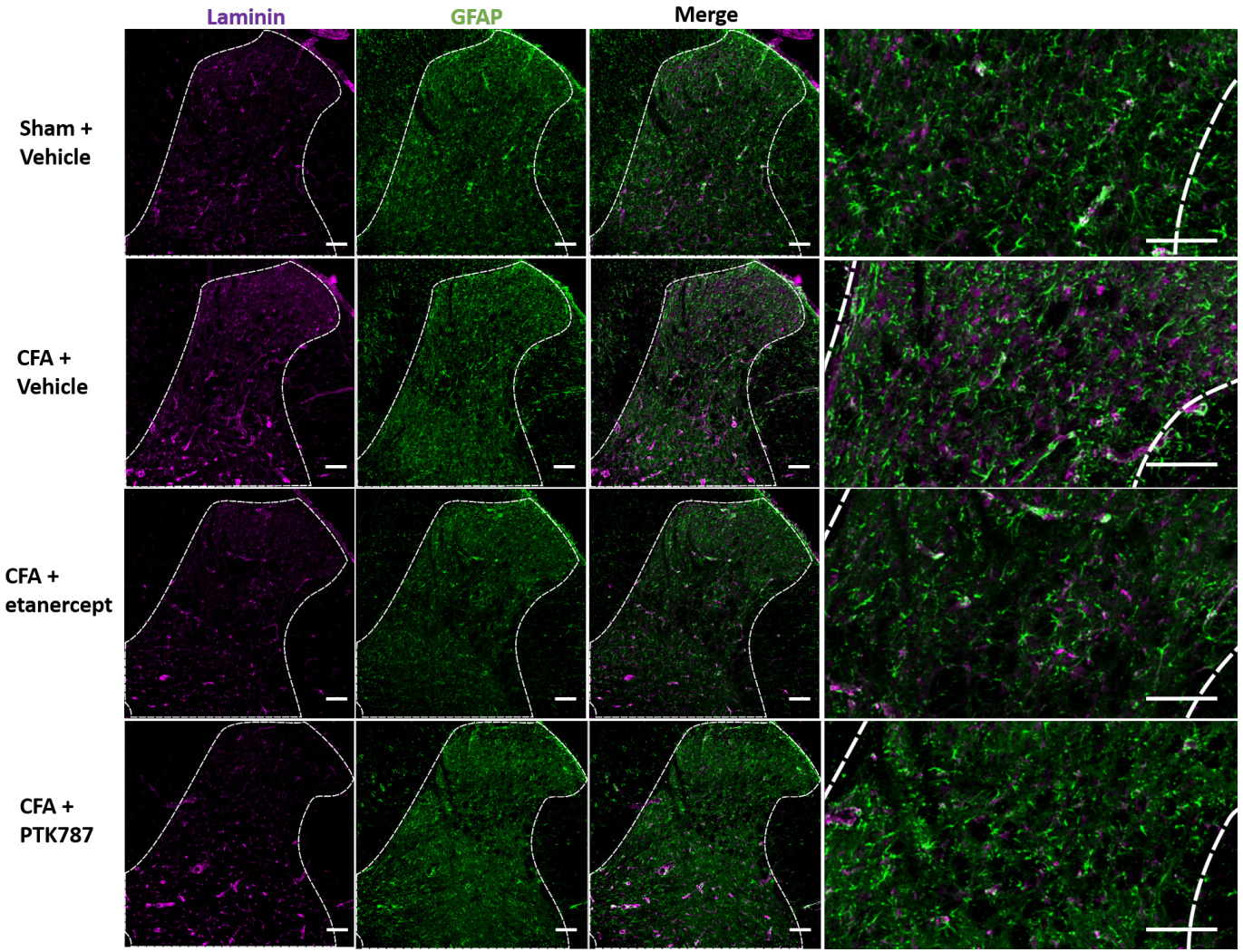


Figure 4.11: Representative images of GFAP immunofluorescence in the dorsal horn of the spinal cord 2 days after peripheral inflammation. Green: GFAP astrocyte marker; Magenta: CD31 vessel marker. Scale bar: 100μm.

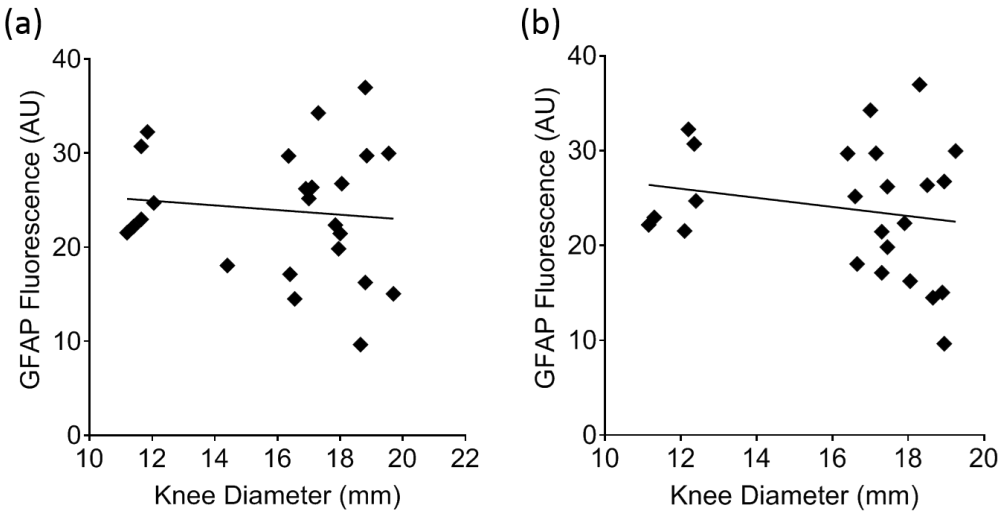


Figure 4.12: GFAP Intensity at day 2 was not correlated to ipsilateral knee diameter at day 1 (**a**, r = -0.1058, p = 0.6) or day 2 (**b**, r = -0.1930, p = 0.4). Pearson correlation test. Data combined from all groups. n = 24.

Global dorsal horn GFAP intensity at day 2 did not correlate with ipsilateral knee diameter at day 1 or day 2 (Figure 4.12a & b respectively).

As determining the neurovascular response to inflammation was the key aim of this project, a classical vessel marker (Cluster of Differentiation-31 (CD31)) was employed (as detailed in Section 3.2.6). However, the CD31 signal was unreliable in this tissue, demonstrating limited or no positive vessel signal (see Figure 4.13). This is possibly due to differences in immunofluorescence protocol between this study and in Chapter 3, namely the slide-mounted antibody incubations here as opposed to free-floating incubations in Chapter 3. Therefore, the number of GFAP-wrapped vessels were counted, identifying vessels by either strings of flat endothelial nuclei or curved nuclei (see Figure 4.7 for example). The numbers of GFAP-positive cells associated with vessels was unaltered by acute inflammation, and there was no effect of anti-VEGF-R or TNFα treatment (Figure 4.10c).

CD31 immunofluorescence was unsuccessful, and so spinal cord sections were investigated using an alternative vessel marker, laminin, in conjunction with GFAP. CD31 (also known as Platelet and Endothelial Cell Adhesion Molecule-1 (PECAM-1)) is an intracellular junction protein whereas laminins are extracellular matrix proteins that make up a large portion of the basal lamina of the basement membrane (Timpl et al. 1979). However, the laminin antibody showed non-specific signal in the superficial laminae (see Figure 4.17 for laminin images) and it was not possible to discern between vessels and other staining. Therefore, the superficial laminae were excluded from the analysis of GFAP fluorescence at laminin-positive vessel structures. Neither CFA nor the pharmacological treatments had any significant effect on GFAP fluorescence at laminin-positive vessel structures in the dorsal horn at 2 days (Figure 4.10b). This analysis is dependent on adequate laminin signal, which was not achieved in all sections, hence the lower

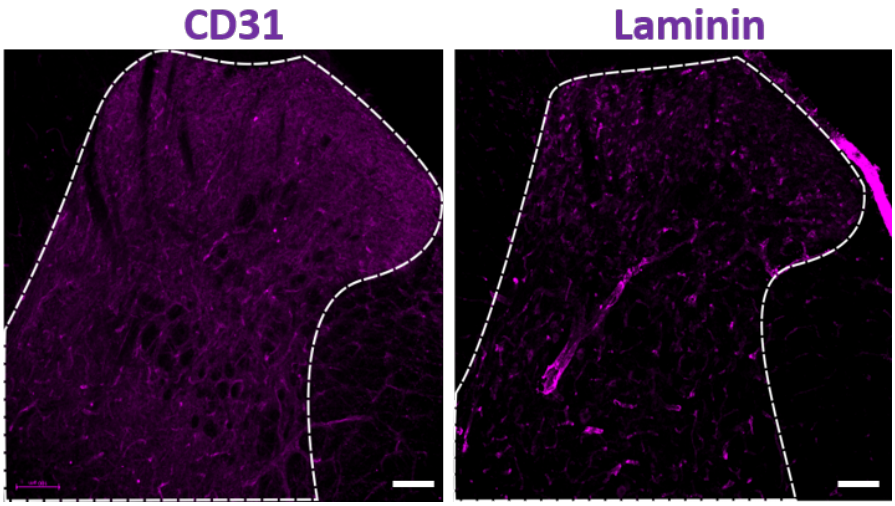


Figure 4.13: Sections from the same animal demonstrated limited CD31 (left image) vessel signal in the spinal cord dorsal horn compared to laminin (right). Scale bar: 100µm.

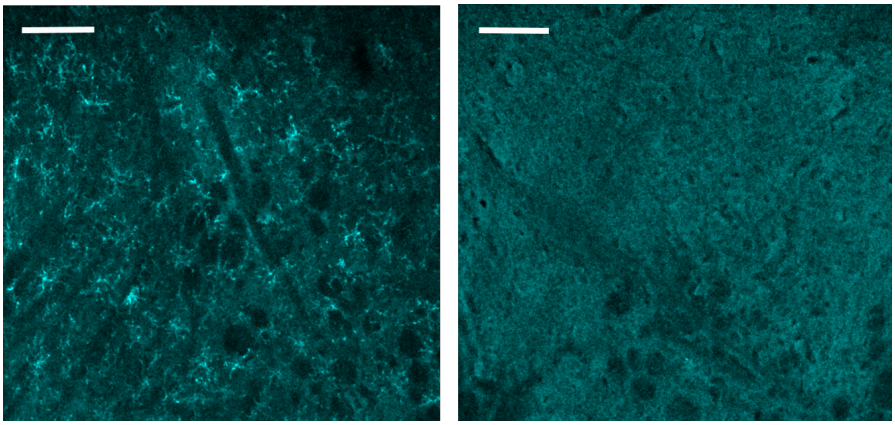
number included in analyses compared with the previous GFAP analyses.

4.3.1.3 The Central Endothelial and Microglial Response to Acute Inflammation and Effect of VEGF-R and TNFα Inhibition

To investigate the microglial and macrophage response to acute CFA, and determine whether pretreatment with PTK787 or Etanercept altered this response, spinal cord sections corresponding to L3-5 were probed for CD11b. CFA had no effect on global dorsal horn CD11b fluorescence at 2 days post-inflammation (Figure 4.14b). CD11b-positive microglial structures were however only visible in some sections and animals (see Figure 4.14a). 5.6% of sham and CFA + vehicle animals demonstrated CD11b-positive structures in the ipsilateral dorsal horn of the spinal cord in acute inflammation, whereas significantly more sections had positive structures in the CFA + PTK787 and CFA + etanercept animals compared to CFA + vehicle (both 33.3%, $p<0.0001$, Figure 4.15; see also Sections 4.3.2 and 4.3.4 for CD11b data in established inflammation). This trend was also true for the contralateral dorsal horns.

CD11b is a ligand for ICAM-1, which is expressed by endothelial cells and facilitates transmigration of leukocytes (Thompson and Matsushima 1992; Smith et al. 1989). Spinal cord sections were probed for ICAM-1 to investigate the endothelial response to acute CFA. Global ICAM-1 fluorescence was unchanged by CFA or drug treatment (Figure 4.16a, see Figure 4.17 for representative images). ICAM-1 fluorescence was also measured at vessel structures within the deeper laminae using laminin as a marker, but this was also unaltered by treatment (Figure 4.16b).

(a) Representative images of sections with and without microglial CD11b structures in the rat spinal cord dorsal horn. Scale bar: 100µm



(b) Spinal cord dorsal horn CD11b fluorescence 2 days after acute CFA-induced inflammation

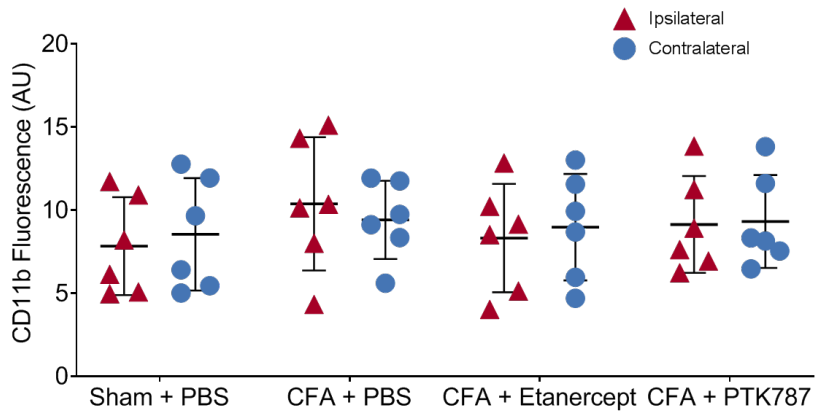


Figure 4.14: Acute CFA (2 days) had no effect on the presence of microglial CD11b structures or global dorsal horn CD11b fluorescence in the rat spinal cord, nor did drug pre-treatments (Interaction: p=0.91; Row Factor: p=0.58; Column Factor: p=0.87). 2way ANOVA. Scale bar: 100µm.

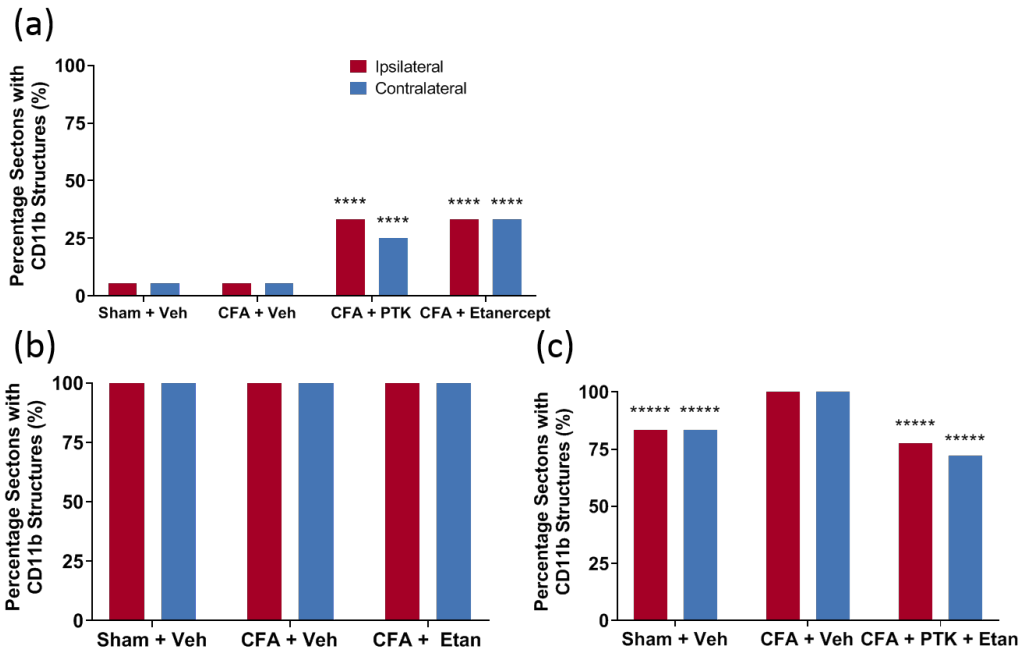


Figure 4.15: In Study 1 (**a**, 2 days post-CFA), CFA + PTK787/etanercept treatment caused a significant increase in the number of sections with CD11b-positive microglial structures (in both ipsilateral and contralateral dorsal horns), whereas CFA + vehicle did not compared to sham + vehicle. In Study 2 (**b**, 10 days post-CFA), all sections analysed showed CD11b-positive microglial structures. In Study 3 (**c**, 10 days after low dose CFA), CFA caused a significant increase in the proportion of sections with positive CD11b microglial structures (in both ipsilateral and contralateral dorsal horns), which was reduced by combined treatment with PTK787 + etanercept. Chi^2 contingency test. ****$p<0.0001$.

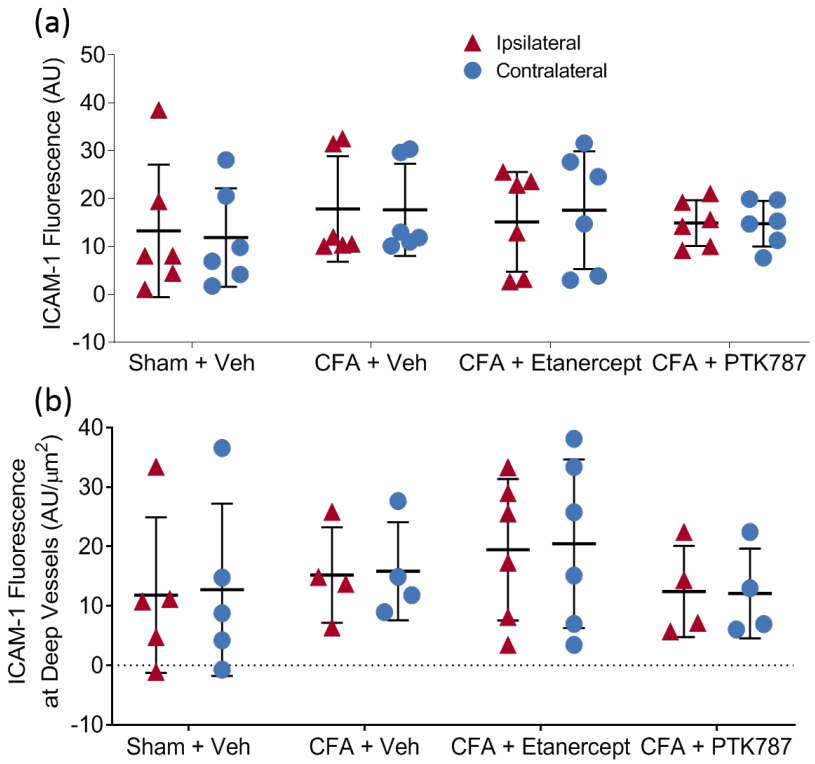


Figure 4.16: Neither acute CFA (2 days) nor drug pre-treatments had an effect on global dorsal horn (a, Interaction: p=0.97; Row Factor: p=0.67; Column Factor: p=0.99) or vessel-associated (b, Interaction: p>0.99; Row Factor: p=0.38; Column Factor: p=0.88) ICAM-1 fluorescence. 2way ANOVA. Scale bar: 100µm.

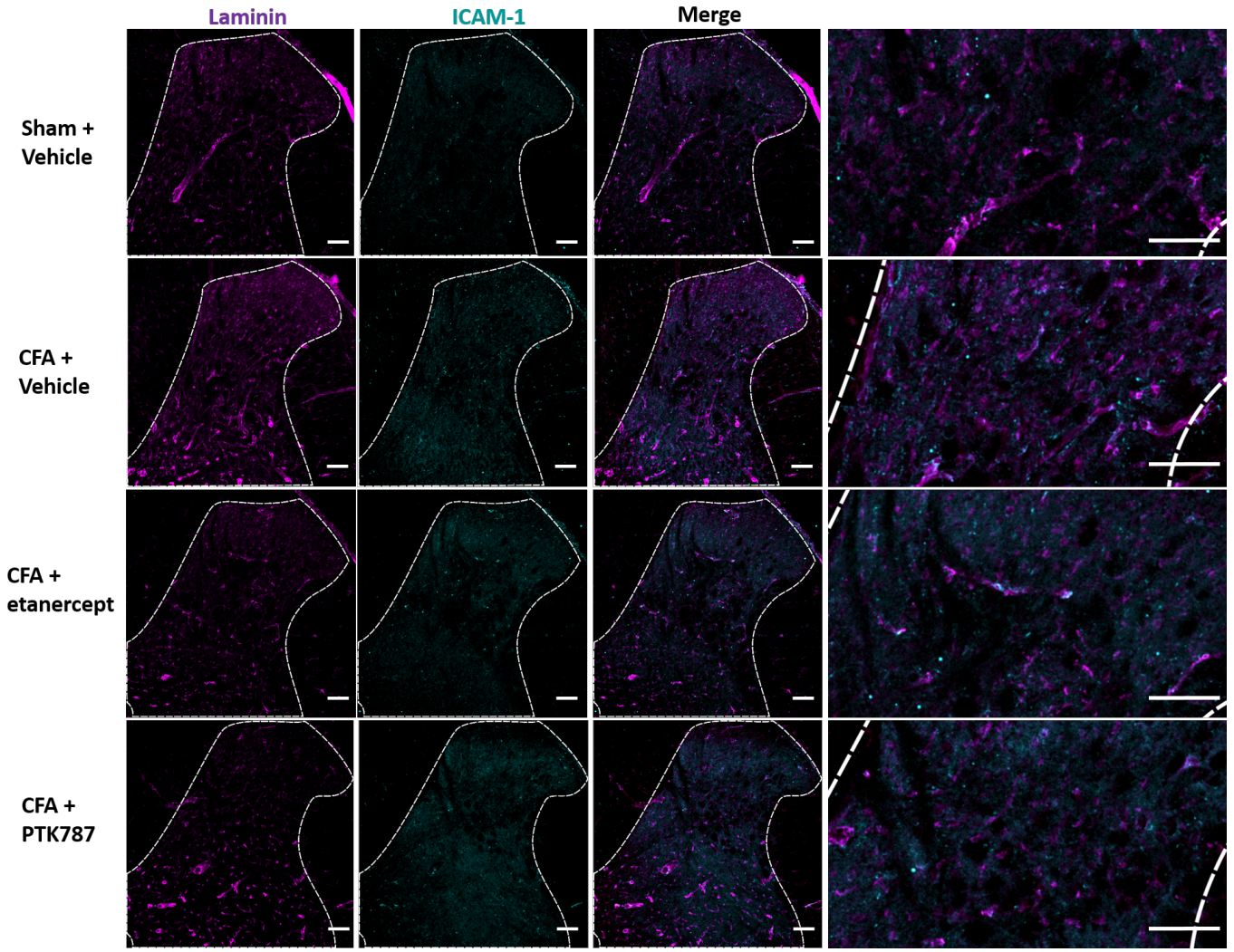


Figure 4.17: Representative images of ICAM-1 immunofluorescence in the dorsal horn of the spinal cord 2 days after peripheral inflammation. Cyan: ICAM-1 marker; Magenta: CD31 vessel marker. Scale bar: 100μm.

Although there is limited evidence for inflammation-induced angiogenesis in the spinal cord, PTK787 has anti-angiogenic properties and treatment can reduce the number of established microvessels due to disrupting endothelial cell signalling (Wood et al. 2000). The vessel markers used here allowed for simple investigation of blood vessel area, and so effects on vascular changes were investigated. There was no evidence of CFA-induced angiogenesis after 2 days, or of a reduction in vessel area after PTK787 in the deep dorsal horn (Figure 4.18) using laminin as a vessel marker.

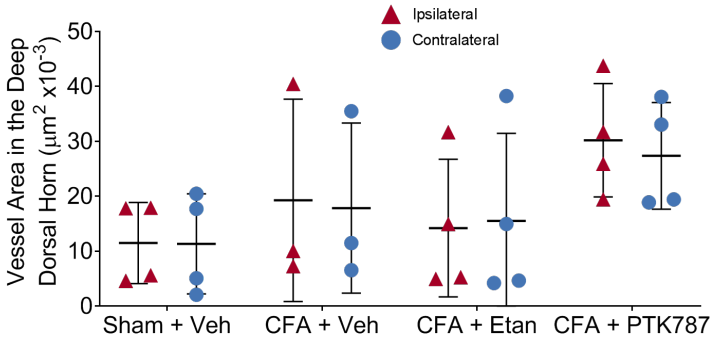


Figure 4.18: Deep vessel area in the dorsal horn of the spinal cord is not altered by CFA after 2 days nor drug pre-treatment (Interaction: p=0.99; Row Factor: p=0.06; Column Factor: p=0.87). 2-way ANOVA with Dunnett's multiple comparisons compared to CFA + vehicle. Mean ± SD. n = 3-6. Veh: Vehicle; Etan: Etanercept.

4.3.1.4 The Peripheral DRG Response to Acute Inflammation and Effect of VEGF-R and TNFα Inhibition

As there were no apparent central gliovascular alterations in response to acute CFA, the peripheral response was studied by investigating monocyte infiltration in DRGs. L3 and L4 DRGs were probed with CD68 (monocytes/macrophages) and RECA-1 (vessels) to investigate this. CD68-positive DRG neurones were apparent in the tissue, which were not visible in the control Immunoglobulin G (IgG) tissue (Figure 4.19). Two analyses were performed: CD68 intensity; and a manual count of small (<10µm) CD68-positive cells. In the interest of time, only Sham and CFA + vehicle groups were investigated.

CD68 fluorescence in Sham tissue was not significantly different to CFA + vehicle tissue, nor was it different between L3 and L4 (Figure 4.20a). Representative images for CD68 immunofluorescence in DRGs are shown in Figure 4.21. The number of small CD68-positive cells within the neuronal tissue were counted, and cells were differentiated between whether they were associated with vessels or not. Cells were counted as positive if the CD68 stain overlapped with the nuclear stain (see Figures 4.8a & b and 4.21 white arrows), and perivascular cells were defined as cells whose cytoplasm or nucleus overlapped with the RECA-1 vessel stain (Figure 4.8c and 4.21 yellow arrows). Neither the total number of CD68-positive cells nor perivascular CD68-positive cells were affected by CFA-induced inflammation (Figure 4.20b & c).

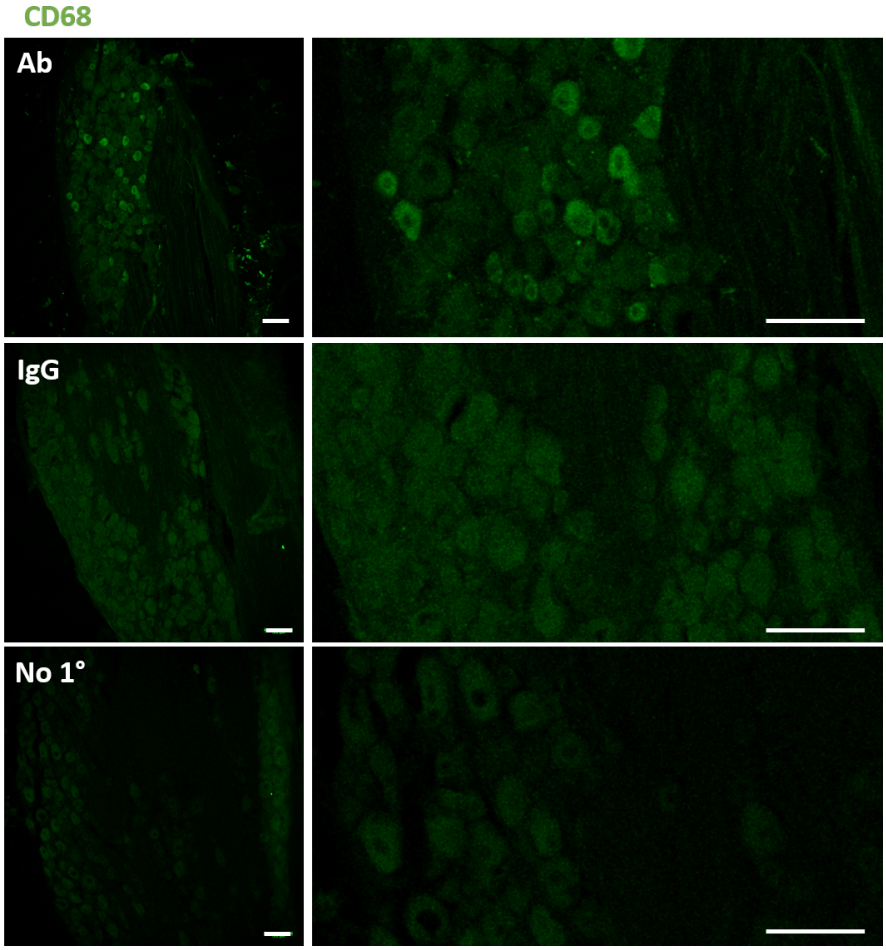


Figure 4.19: Representative images of CD68-positive DRG neurones in test and control antibody tissue. Green: CD68 marker. Ab: Antibody; IgG: Species-matched IgG control; No 1˚: No primary antibody control. Scale bar: 100µm

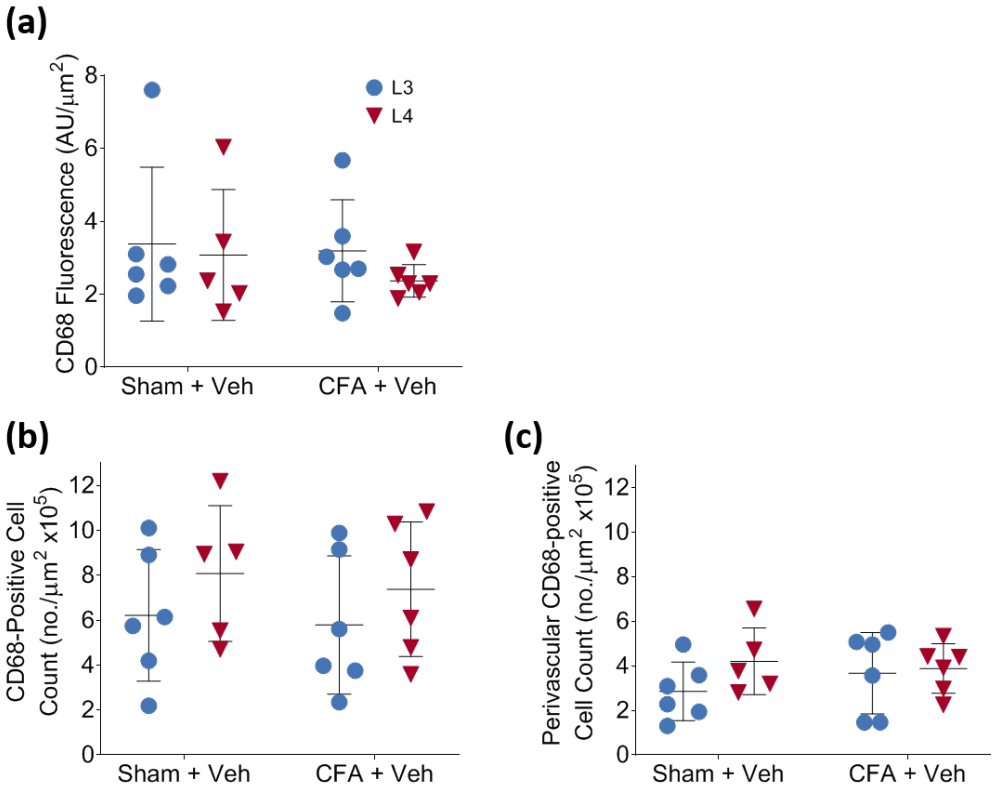


Figure 4.20: CD68 fluorescence **(a)** and the number of CD68-positive cells - total **(b)**, perivascular **(c)** were unchanged after acute peripheral CFA (2 days) and drug pre-treatment in L3 and L4 DRG. **a**: Interaction: p=0.69; Row Factor: p=0.50; Column Factor: p=0.40; **b**: Interaction: p=0.92; Row Factor: p=0.66; Column Factor: p=0.19; **c**: Interaction: p=0.36; Row Factor: p=0.70; Column Factor: p=0.22. 2way ANOVA. n = 5-6. Mean ± SD. Veh: vehicle

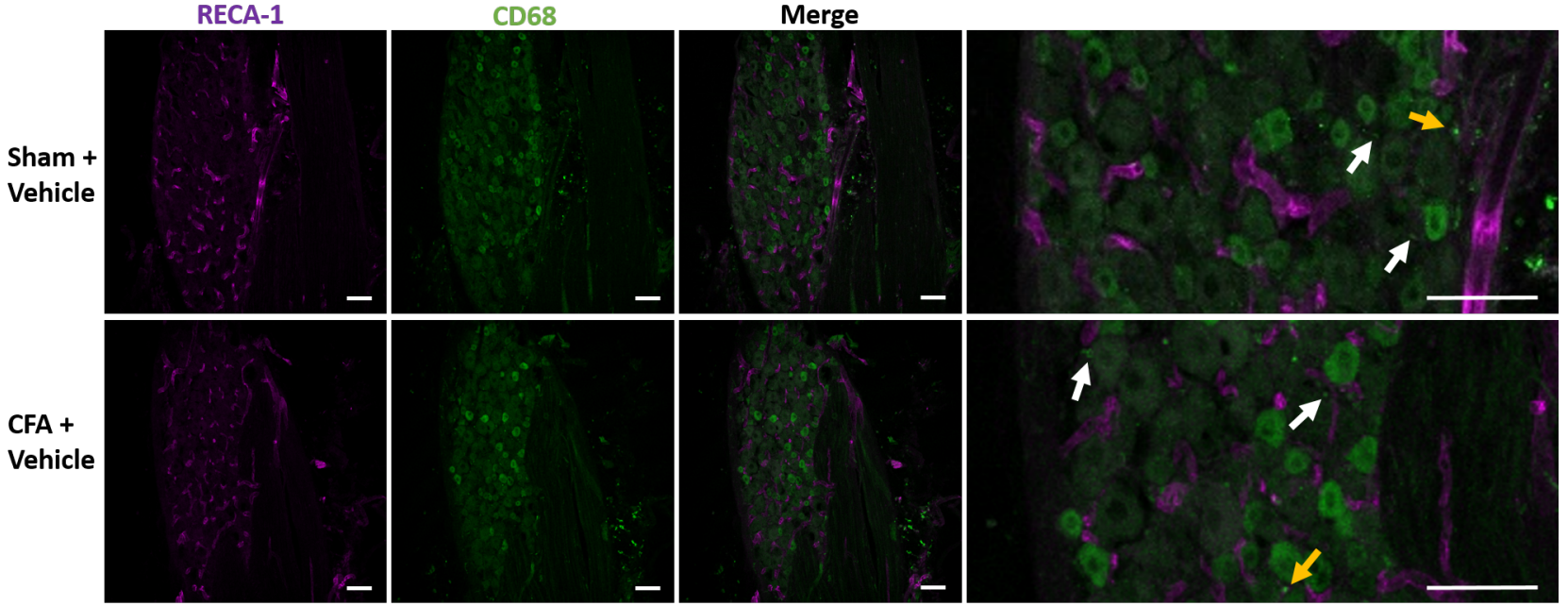


Figure 4.21: Representative images of CD68 immunofluorescence in the DRG after acute peripheral inflammation (2 days). Small (<10μm) CD68-positive cells within the neuronal tissue were counted (white arrows). Perivascular cells were defined as cells whose cytoplasm or nucleus overlapped with the RECA-1 vessel stain (yellow arrows). Green: CD68 marker; Magenta: RECA-1 vessel marker. Scale bar: 100μm.

4.3.2 Study 2: Therapeutic Inhibition of VEGF-Receptors and TNFα in Chronic Inflammatory Arthritis

4.3.2.1 CFA Caused Significant Pain Behaviour, which was Unaltered by Therapeutic PTK787 or Etanercept

In this study rats received an intra-articular injection of a 100µg in-house CFA dose in 50µL volume. Intra-articular CFA caused a significant reduction in ipsilateral paw withdrawal threshold ($p<0.01$), which was not changed by PTK787 treatment (Figure 4.22a). Treatment with etanercept appeared to prevented worsening of hypersensitivity after day 3 (Figure 4.22a), however, upon further investigation, no therapeutic treatment group significantly worsened after day 3 (Figure 4.23): as up to day 3 CFA + vehicle/D3 PTK787 /etanercept groups had all received the same treatment, these groups were expressed as change in 50% paw withdrawal threshold from day 3, and no group significantly worsened (Figure 4.23). Neither CFA nor treatment had an effect on contralateral paw withdrawal threshold (Figure 4.22b).

CFA caused a significant decrease in ipsilateral weight bearing compared to sham for the duration of the study ($p<0.05$), and animals that received PTK787 at the time of inflammation bore significantly less weight on their ipsilateral limb compared to CFA alone on day 3 (Figure 4.22c). CFA also caused a significant increase in ipsilateral knee diameter compared to sham until day 4 ($p<0.05$), and pretreatment with PTK787 (D0 PTK787) resulted in significantly less swelling compared to CFA + vehicle at day 3 (Figure 4.22d). Animals who received etanercept at day 3 appeared to have a less severe response to CFA in terms of paw withdrawal threshold, weight bearing and swelling throughout the duration of the study (Figure 4.22a, c & d respectively) but this was not significantly different from CFA + vehicle.

4.3.2.2 PTK787 May Have Been at the Incorrect Concentration

Von Frey withdrawal thresholds measured in the hind paw are an indication of hypersensitivity at a secondary site to the inflammation in the knee joint. PTK787 given at induction of inflammation (day 0) did not prevent the development of secondary pain, as was previously shown in our lab (Beazley-Long et al. 2018b). There was the potential that this could be attributed to the concentration of PTK787 as this had been difficult to dissolve in PBS. PTK787 in solution has a yellow colour so a simple assay measuring the absorbance of 3.75mg/mL PTK787 (AdooQ BioScience LLC, A10967) in PBS (the study vehicle) or DMSO (into which it dissolves into a solution much more easily) at three wavelengths (450nm, 490nm, 550nm) was used to give a crude estimate as relative concentration in PBS amd DMSO. Table 4.5 shows that the absorbance of PTK787 dissolved in PBS (from Studies 1 & 2) was no different to the PBS blank (containing no PTK787), whereas PTK787 in DMSO was different to the DMSO blank for every wavelength (450nm: 0.1117A vs 0.06133A, $p<0.0001$; 490nm: 0.08233A vs 0.05200A, $p<0.0001$; 550nm: 0.06000A vs 0.05100A, $p<0.0001$; 2way ANOVA with Sidak's multiple

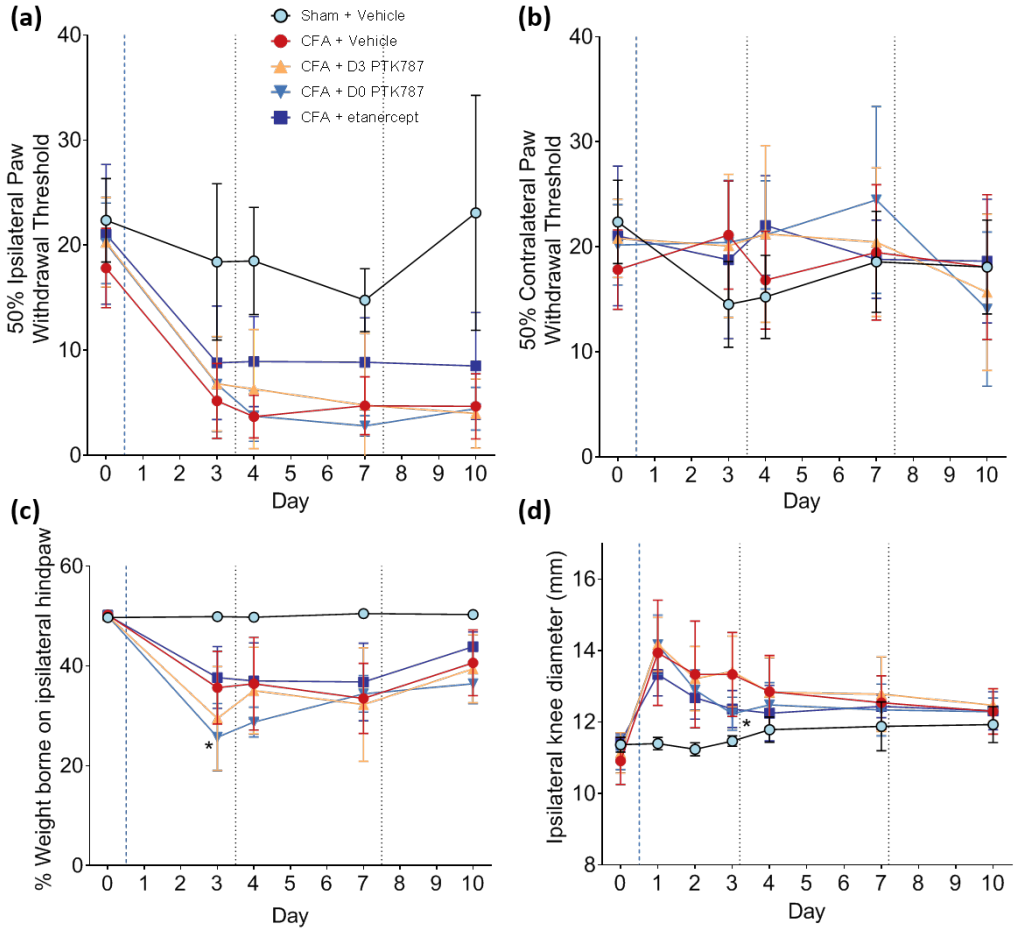


Figure 4.22: Intra-articular CFA caused a significant reduction in ipsilateral paw withdrawal threshold ($p<0.001$), which was not rescued or prevented with PTK787 treatment (**a**, Interaction: $p<0.001$; Row Factor: $p<0.0001$; Column Factor: $p<0.0001$). Treatment with etanercept appeared to prevent worsening of hypersensitivity after day 3 (**a**). Neither CFA nor treatment had an effect on contralateral paw withdrawal threshold (**b**, Interaction: $p=0.11$; Row Factor: $p<0.05$; Column Factor: $p=0.92$). CFA caused a significant decrease in ipsilateral weight bearing compared to sham for the duration of the study (**c**, Interaction: $p<0.0001$; Row Factor: $p<0.0001$; Column Factor: $p<0.0001$), and animals that went on to receive etanercept bore significantly less weight on their ipsilateral limb compared to CFA alone on day 3 (CFA + Vehicle: 35.65±7.28; CFA + etanercept: 37.67±6.19). CFA also caused a significant increase in ipsilateral knee diameter compared to sham until day 4 (**d**, Interaction: $p<0.0001$; Row Factor: $p<0.01$; Column Factor: $p<0.0001$), and pretreatment with PTK787 (day 0 PTK787) had significantly less swelling compared to CFA + vehicle at day 3 (**d**, CFA + Vehicle: 13.33±1.18; CFA + d0 PTK787: 12.23±0.46). *$p<0.05$ compared to CFA + vehicle, 2way ANOVA with Dunnett's multiple comparisons. n = 5-6. Mean ± SD. Dotted lines represent drug i.p. injections with the blue dashed line at day 0.5 representing D0 PTK787 only.

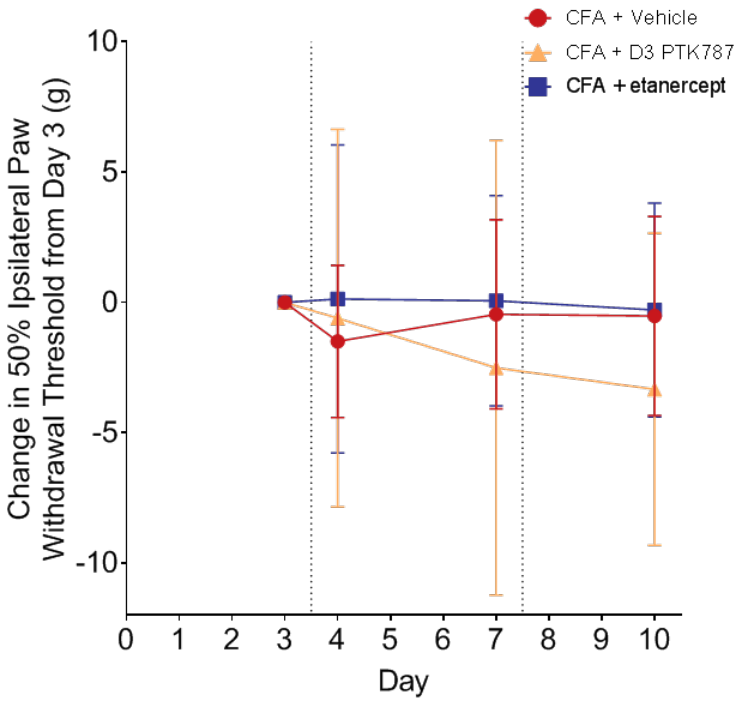


Figure 4.23: When expressed as change in mechanical threshold from day 3, no therapeutic treatment group significantly worsened (Interaction: p=0.75; Row Factor: p=0.53; Column Factor: p=0.78). 2way ANOVA. n = 6. Mean ± SD. Dotted lines represent drug i.p. injections.

comparisons).

	450nm (A)			490nm (A)			550nm (A)		
PTK787 in PBS	0.043	0.042	0.043	0.037	0.036	0.037	0.036	0.036	0.037
PBS Blank	0.042	0.042	0.044	0.038	0.037	0.037	0.037	0.036	0.036
Minus Blank		0.000			0.000			0.000	
PTK787 in DMSO	0.112	0.110	0.113	0.082	0.082	0.083	0.060	0.060	0.060
DMSO Blank	0.061	0.061	0.062	0.052	0.052	0.052	0.051	0.051	0.051
Minus Blank		0.051			0.030			0.009	

Table 4.5: The absorbance of 3.75mg/mL PTK787 in PBS is no different to the PBS blank (p>0.6), whereas 3.75mg/mL PTK787 in DMSO is different to the DMSO blank for every wavelength (p<0.0001, 2way ANOVA with Sidak's multiple comparisons).

The monocyte attachment assay was then employed to determine the activity of PTK787 (AdooQ BioScience LLC, A10967) used in Studies 1 & 2. The monocyte attachment assay uses binding of Human Monocyte-like Cellss (THP-1s) to Human Brain Microvascular Endothelial Cells (HBMECs) with pharmacological interventions to investigate attachment mechanisms. Treating HBMECs with TNFα caused a significant increase in binding of fluorescently tagged THP-1s compared to untreated HBMECs (Figure 4.24, group "-"). With the addition of 100μM of the experimental PTK787 used in these studies (group "1" in Figure 4.24), binding was reduced but not significantly (p=0.138), whereas 100μM PTK787 in Dimethyl Sulfoxide (DMSO) and a previous batch of PTK787 in PBS were significantly different to TNFα alone (p<0.001). It was for these reasons that a PTK787 was dissolved in an alternative vehicle (in saline rather than PBS) for use in

subsequent studies (Study 3).

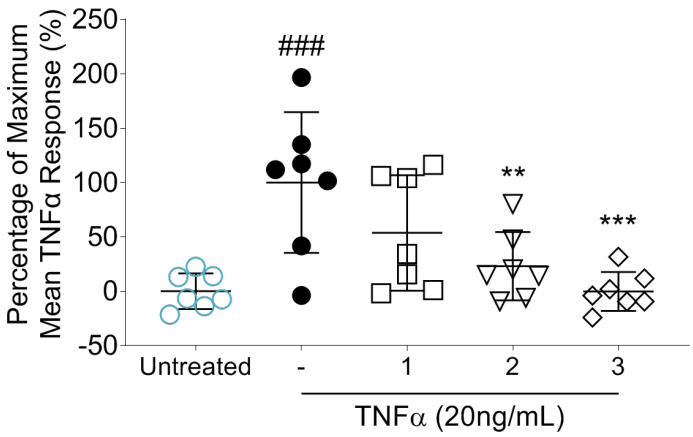


Figure 4.24: Using the monocyte attachment assay the activity of PTK787 was investigated. Human brain microvascular cells were plated on a 96-well plate and treated with 20ng/mL TNFα, with or without the addition of three batches of 100μM PTK787 (1: PTK787 used in Studies 1 & 2; 2: PTK787 in DMSO; 3: previous batch of PTK787 in PBS). Fluorescently tagged human monocyte-like cells (THP-1s) were added to the wells and binding was assessed by measuring the fluorescence. The PTK787 used in Studies 1 & 2 (group 1) did not significantly prevent the TNFα-induced increase in binding ($p=0.138$), whereas PTK787 in DMSO (2) and a previous batch of PTK787 (3) did. Data is displayed as percentage of the maximum mean TNFα response. 2-way ANOVA with Sidak's multiple comparisons performed on raw data. ###$p<0.001$ compared to untreated; ***$p<0.001$, **$p<0.01$ compared to TNFα only. n = 1 plate.

4.3.3 The Central Astrocytic Response to Peripheral Inflammation and the Effect of TNFα Inhibition

In the interest of time and as treatment with etanercept initially appeared to prevent worsening of paw withdrawal threshold after day 3 (Figure 4.3.2.1, although this was found not to be exclusive to etanercept in Figure 4.23), only this group, along with Sham + vehicle and CFA + vehicle, were investigated for histology. Due to the long length of time from tissue dissection and processing to histology caused by animal licence issues, the quality of the tissue and resulting immunofluorescence was poor in some sections leading to a reduction in numbers during analysis.

Using the rat spinal cord atlas (Watson et al. 2009), approximate spinal cord segments were determined. In Study 2, the thickest part of the lumbar section was sectioned to allow investigation of L5-3 segments, which correspond to the areas innervated by the foot and knee (Takahashi et al. 2002; Ivanavicius et al. 2004; Takahashi and Nakajima 1996; Takahashi et al. 1994; Bajrović and Sketelj 1998). Here, 100% of sections were in L3-5, with 11.76% of all sections in L3, 74.51% in L4 and 13.73% in L5 (Table 4.4).

Sections were investigated for GFAP in the spinal cord and revealed a significant increase in fluorescence after CFA compared to Sham + vehicle (Figure 4.25a). Treatment with etanercept did not reduce this CFA-induced increase in GFAP (Figure 4.25a). As the gliovasculature is of interest, GFAP signal at vessels was investigated, but only the

deep gliovasculature could be analysed due to non-specific laminin signal in the superficial dorsal horn. At vessel structures there was a similar trend of increased GFAP fluorescence after CFA, but it was not significant (Figure 4.25b). Astrocytes extend away from vessels, and so measuring the fluorescence or area of vessel-associated GFAP structures includes these (see Sections 4.2.8 and 4.6 for further explanation). The intensity and area of vessel-associated GFAP structures were both increased after CFA compared to sham + vehicle, with area being significantly increased, and treatment with etanercept did not significantly reduce this (Figure 4.25c & d respectively). Images of vessel-associated GFAP structures are shown in Figure 4.26.

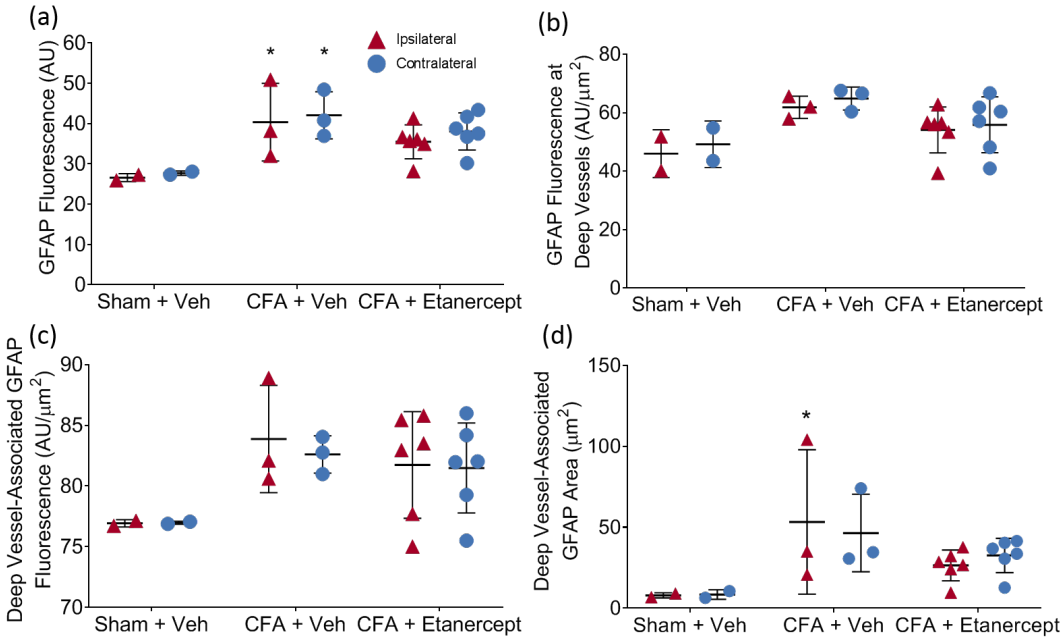


Figure 4.25: Global GFAP signal in the dorsal horn 10 days after peripheral CFA is significantly increased compared to sham, and etanercept treatment had no effect on this (**a**: Interaction: p=0.97; Row Factor: p<0.01; Column Factor: p=0.48). This trend is mirrored when deep vessels were investigated, with GFAP fluorescence at these vessels using the ROI overlay method (**b**: Interaction: p=0.98; Row Factor: p<0.05; Column Factor: p=0.48) and at GFAP structures associated using the overlap extraction method (**c**: Interaction: p=0.95; Row Factor: p<0.05; Column Factor: p=0.78). However, this is not significant, most likely due to low numbers through tissue loss. Similarly, there is an increase in vessel-associated GFAP area with CFA but etanercept has no significant effect on this (**d**: Interaction: p=0.80; Row Factor: p<0.05; Column Factor: p=0.99). 2-way ANOVA with Sidak's multiple comparisons compared to CFA + vehicle or sham + vehicle. Mean ± SD. n = 2-6. * p<0.05 compared to CFA + vehicle. Veh: Vehicle.

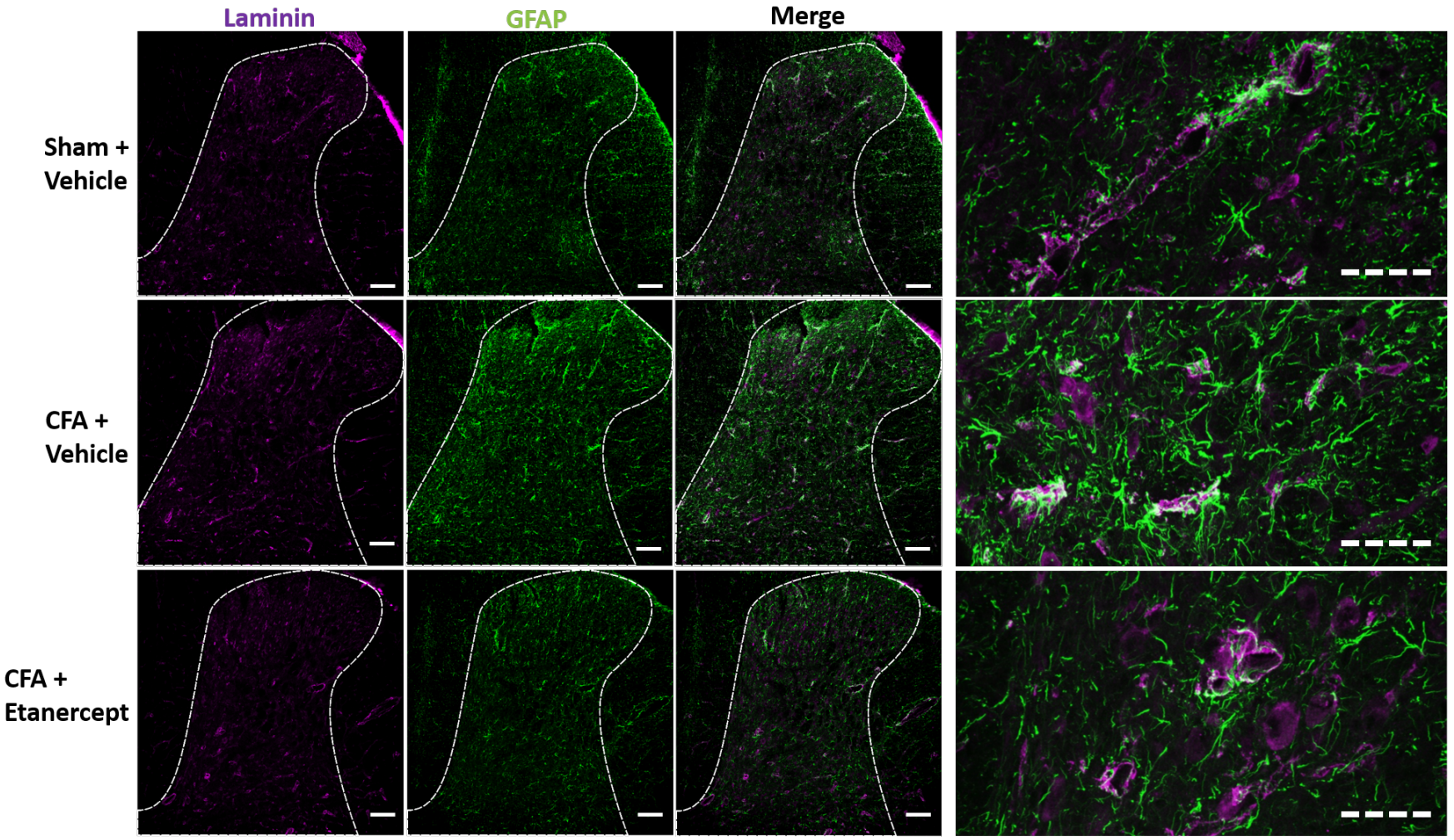


Figure 4.26: Representative images of GFAP signal in the dorsal horn of the spinal cord 10 days after peripheral inflammation. Green: GFAP astrocyte marker; Magenta: Laminin vessel marker. Solid scale bar: 100μm; Dashed scale bar: 50μm.

When the global dorsal horn GFAP response was investigated further, GFAP intensity at day 10 was correlated to ipsilateral knee diameter at day 1 and day 2 but not day 3 (Figure 4.27a, b & c respectively).

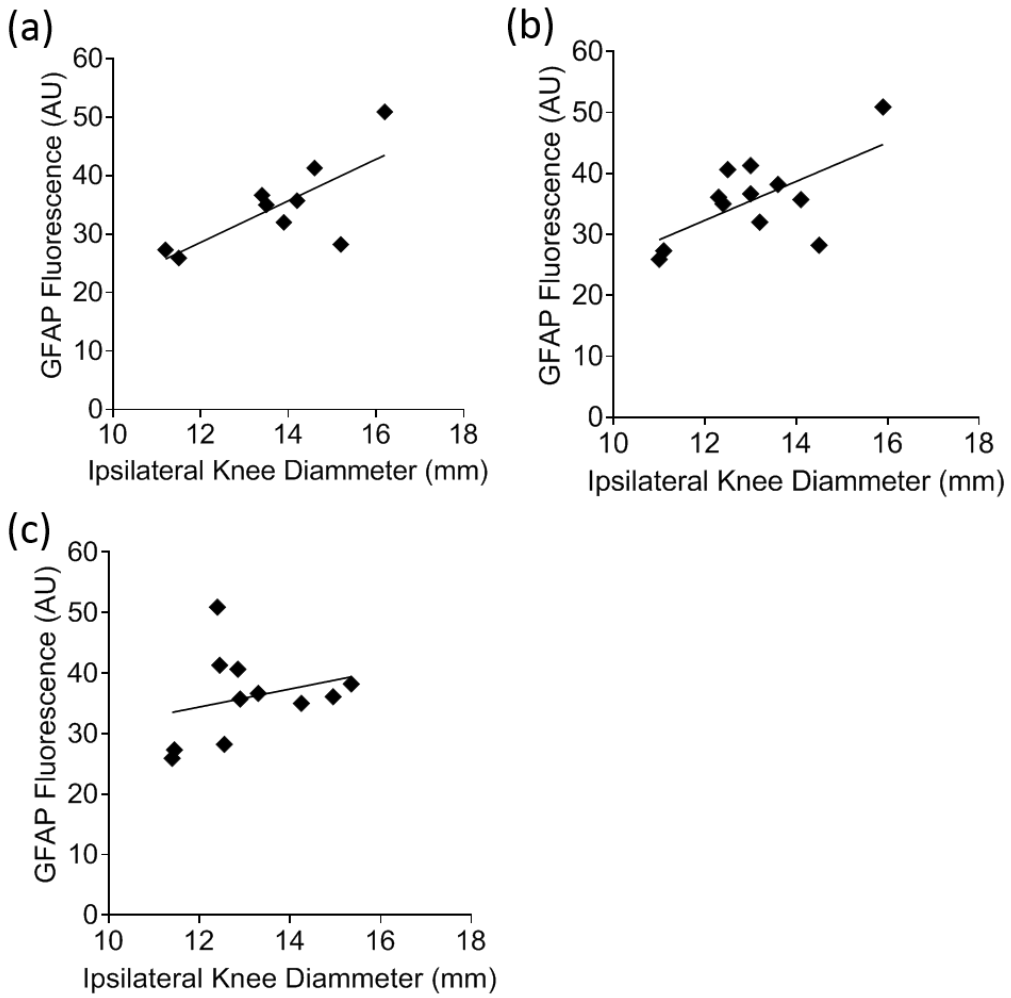


Figure 4.27: GFAP intensity at day 10 was correlated to with ipsilateral knee diameter at day 1 (a, r = 0.7295, p<0.05) and day 2 (b, r = 0.6338, p<0.05) but not day 3 (c, r = 0.2679, p = 0.43) after peripheral CFA. Pearson correlation test. Data combined from groups: Sham + vehicle; CFA + vehicle; CFA + day 3 PTK787. day 1 n = 9, day 2 n = 12, day 3 n = 11.

4.3.3.1 The Central Endothelial and Microglial Response to Chronic Inflammation and the Effect of TNFα Inhibition

Neither global CD11b signal nor ICAM-1 in the dorsal horn after peripheral CFA were significantly altered with CFA or treatment (Figure 4.28a & b respectively). CD11b-positive microglial structures in the spinal cord dorsal horn were visible in all sections analysed (Figure 4.15). Images of CD11b-structures and ICAM-1 signal are shown in Figures 4.29 and 4.30 respectively.

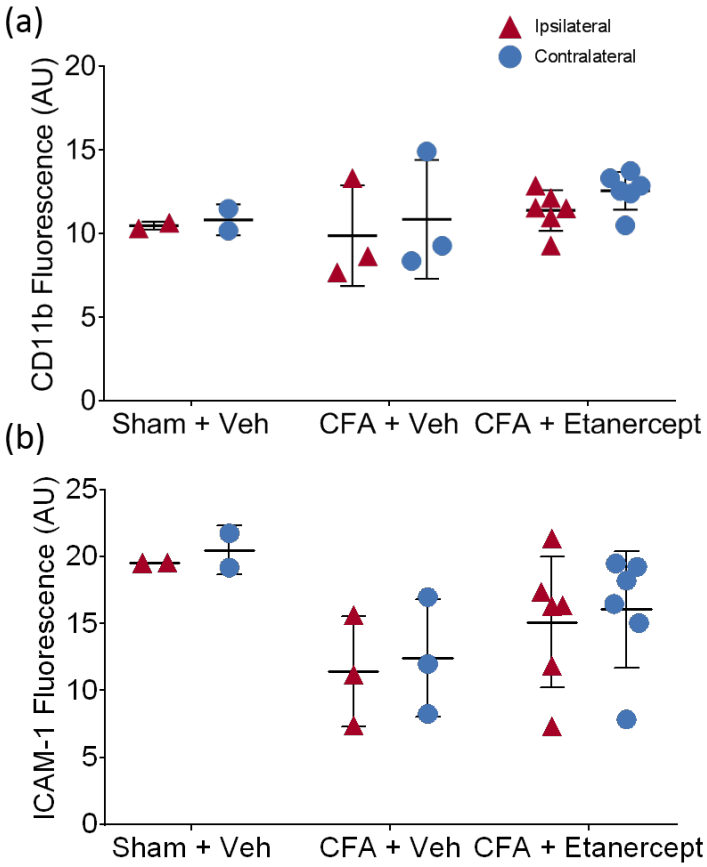


Figure 4.28: Global CD11b signal in the dorsal horn 10 days after peripheral CFA is not significantly altered compared to sham (**a**: Interaction: p=0.93; Row Factor: p=0.21; Column Factor: p=0.37), nor is global dorsal horn ICAM-1 (**b**: Interaction: p>0.99; Row Factor: p<0.05; Column Factor: p=0.64). Treatment with etanercept also had no effect on either CD11b or ICAM-1 signal. 2-way ANOVA with Dunnett's multiple comparisons compared to CFA + vehicle or sham + vehicle. Mean ± SD. n = 2-6. Veh: Vehicle.

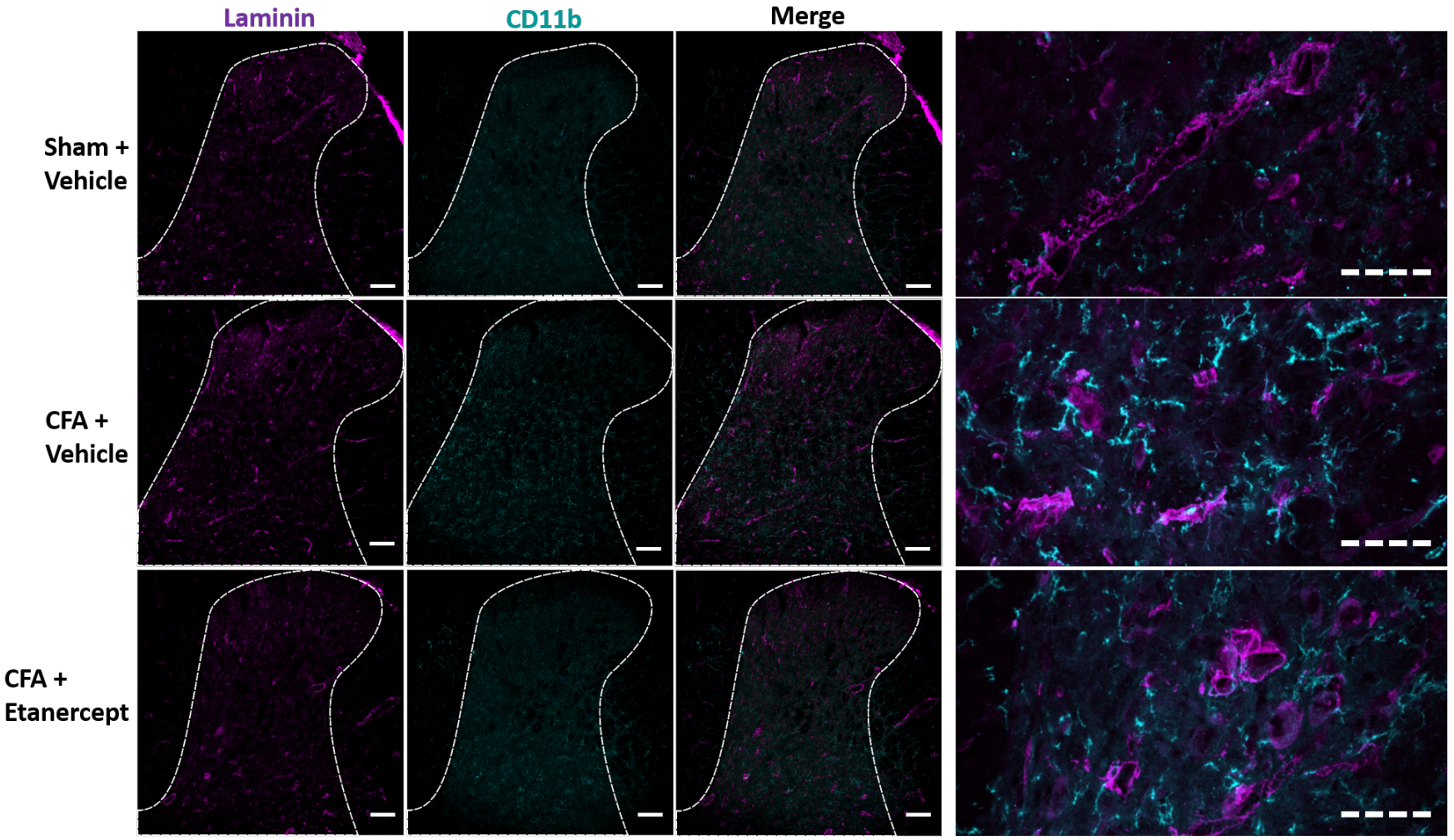


Figure 4.29: Representative images of CD11b signal in the dorsal horn of the spinal cord 10 days after peripheral inflammation. Cyan: CD11b microglia marker; Magenta: CD31 vessel marker. Solid scale bar: 100μm; Dashed scale bar: 50μm.

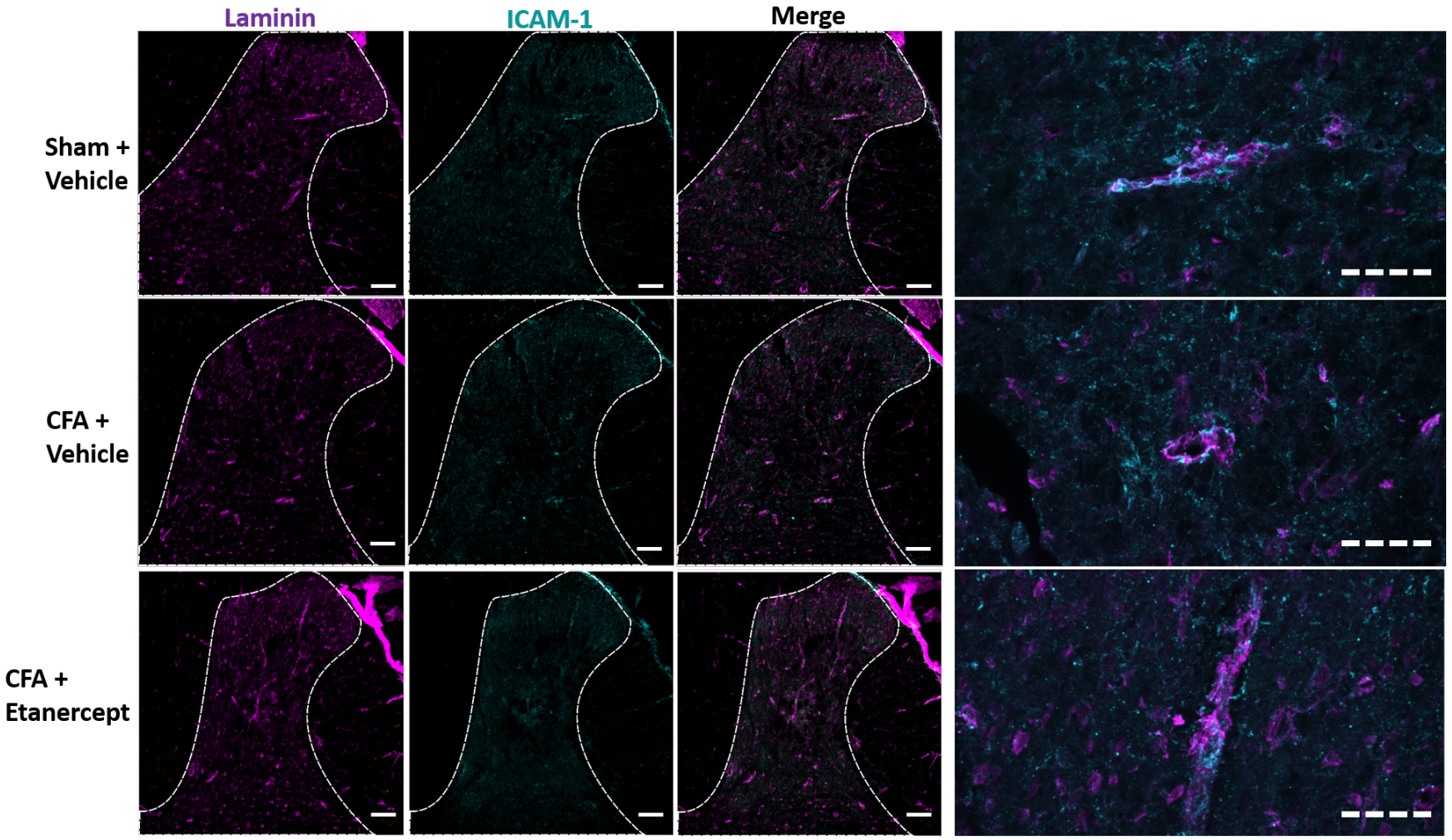


Figure 4.30: Representative images of ICAM-1 signal in the dorsal horn of the spinal cord 10 days after peripheral inflammation. Cyan: ICAM-1 marker; Magenta: CD31 vessel marker. Solid scale bar: 100μm; Dashed scale bar: 50μm.

Vessel area was investigated again 10 days after CFA-induced inflammation. Deep vessel area in the dorsal horn of the spinal cord was not altered with CFA or anti-TNFα treatment (Figure 4.31).

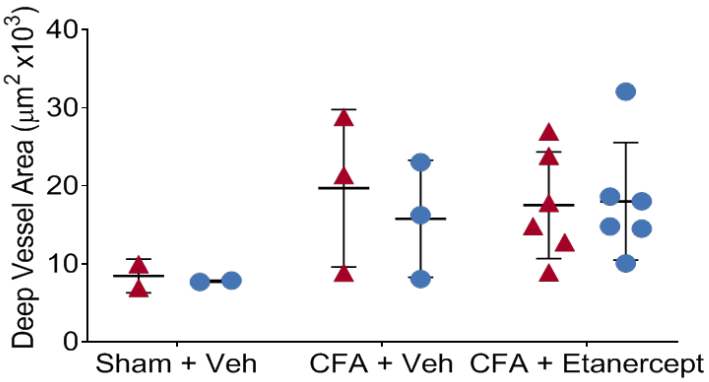


Figure 4.31: Deep vessel area in the dorsal horn of the spinal cord is not altered 10 days after CFA or by etanercept treatment (Interaction: p=0.90; Row Factor: p=0.09; Column Factor: p=0.62). 2-way ANOVA. Mean ± SD. n = 2-6. Veh: Vehicle.

4.3.4 Study 3: Refined Arthritis Model and Inhibition of VEGF-Receptors and/or TNFα in Chronic Inflammatory Arthritis

4.3.4.1 Low Dose CFA Caused Significant Pain Behaviour, which was Partially Reversed by a Combination of PTK787 and Etanercept Therapeutic Treatment

In this study rats received an intra-articular injection of a lower 50µg commercial CFA dose in 50µl volume. One animal from the CFA + PTK787 + etanercept group was excluded from all analyses due to a lack of swelling after CFA injection, which was attributed to poor intra-articular injection technique. Intra-articular CFA caused a significant reduction in ipsilateral paw withdrawal threshold ($p<0.01$), which was not reversed by PTK787 treatment (Figure 4.32a). There was no change in the withdrawal thresholds in the CFA + PTK787 + etanercept group between days 7 and 10, whereas the other CFA groups all continued to show decreases in withdrawal thresholds (Figure 4.32a). When expressed as the change in paw withdrawal threshold from day 3 (when treatment began), the CFA + PTK787 + etanercept group was significantly different to CFA + Vehicle, on day 10 (Figure 4.33). Neither CFA nor treatment had a significant effect on contralateral paw withdrawal threshold (Figure 4.32b).

CFA caused a significant decrease in ipsilateral weight bearing compared to sham for the duration of the study in all groups ($p<0.0001$). Animals that received a combination of PTK787 and etanercept bore slightly but not significantly less weight on their ipsilateral limb compared to other CFA animals on days 3 to 10 (Figure 4.32c). CFA also caused a significant increase in ipsilateral knee diameter in all groups compared to sham until day 4 ($p<0.0001$), and this was not altered by drug treatment (Figure 4.32d).

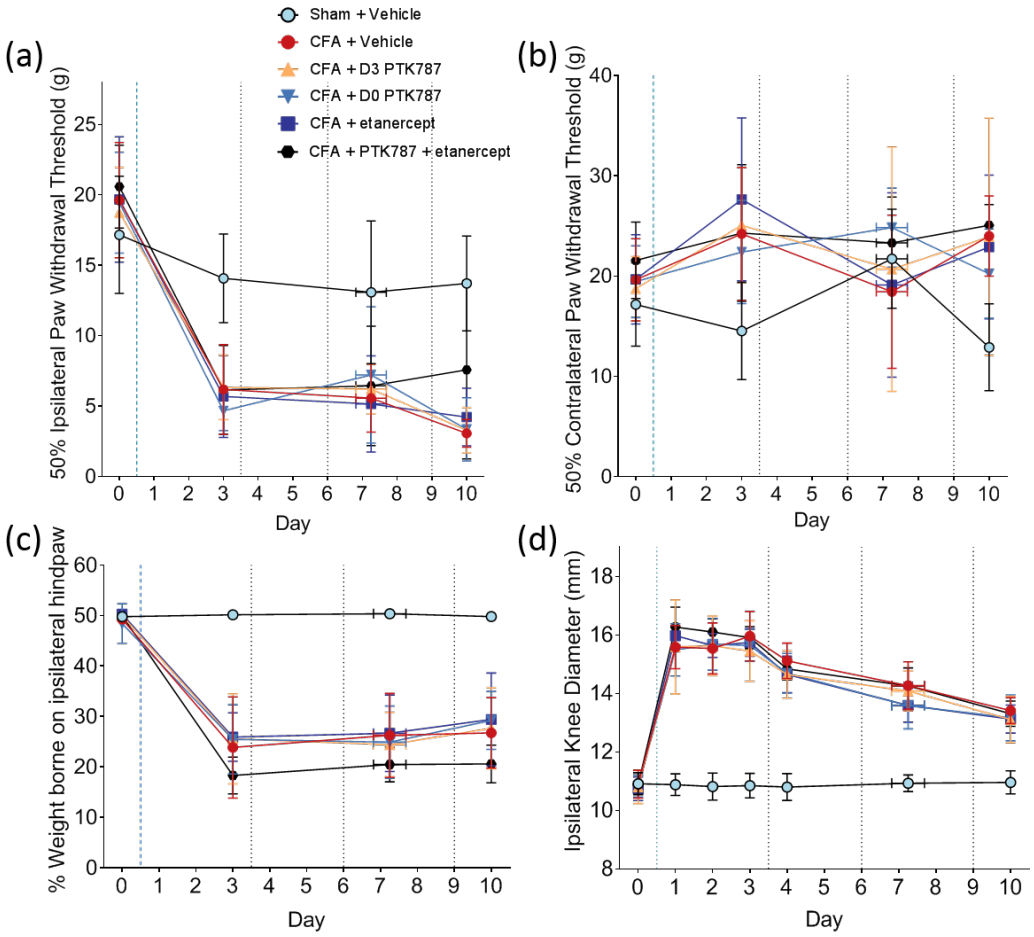


Figure 4.32: Low Dose (50µg) intra-articular CFA caused a significant reduction in ipsilateral paw withdrawal threshold (**a**: Interaction: p<0.0001; Row Factor: p<0.0001; Column Factor: p<0.01), which was not rescued after PTK787 treatment. However, by day 10 mechanical threshold was returning to baseline after treatment with PTK787 + etanercept **(a)**. Neither CFA nor treatment had an effect on contralateral paw withdrawal threshold (**b**: Interaction: p=0.15; Row Factor: p=0.09; Column Factor: p<0.05). CFA caused a significant decrease in ipsilateral weight bearing compared to sham for the duration of the study, and animals that went on to receive PTK787 + etanercept bore slightly less weight on their ipsilateral limb compared to CFA alone on day 3-10, but not significantly (**c**: Interaction: p<0.0001; Row Factor: p<0.0001; Column Factor: p<0.0001). CFA also caused a significant increase in ipsilateral knee diameter compared to sham throughout the duration of the study, which was not altered by treatment (**d**: Interaction: p<0.0001; Row Factor: p<0.0001; Column Factor: p<0.01). 2way ANOVA with Dunnett's multiple comparisons compared to sham + vehicle or CFA + vehicle. n = 5-6. Mean ± SD. Dotted lines represent drug i.p. injections with the blue dashed line at day 0.5 representing D0 PTK787 only.

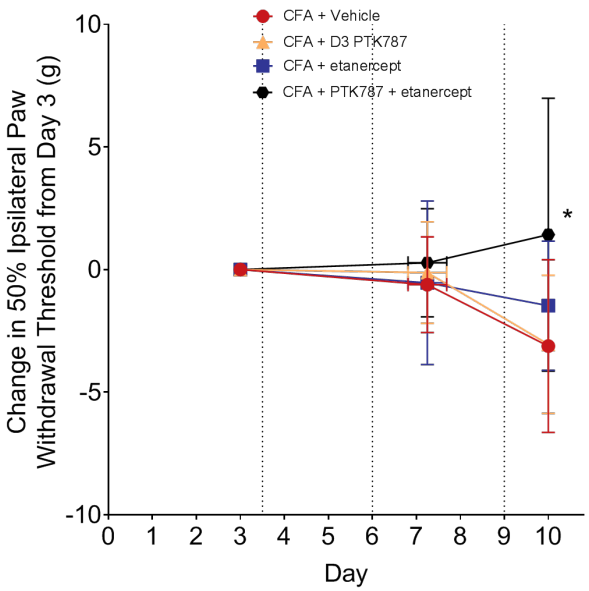


Figure 4.33: Animals that received a combination of low dose (50µg) CFA + PTK787 + etanercept at day 3 showed a significantly greater change in paw withdrawal threshold (towards baseline) on day 10. Interaction: p=0.31; Row Factor: p=0.08; Column Factor: p=0.31. *p<0.05 compared to CFA + vehicle, 2way ANOVA with Dunnett's multiple comparisons. n = 6. Mean ± SD. Dotted lines represent drug i.p. injections.

4.3.4.2 The Central Astrocytic Response to Chronic Peripheral Inflammation and the Effect of Inhibition and VEGF-R and TNFα

In the interest of time, only the Sham + Vehicle, CFA + Vehicle, and CFA + PTK787 + etanercept groups were examined histologically. CFA + PTK787 + etanercept was chosen due to the small effect on mechanical threshold (see Section 4.3.4.1 and Figure 4.33).

To investigate the astroglial response to acute inflammation, GFAP fluorescence was measured in spinal cord segments corresponding to L3-5. Using the rat spinal cord atlas (Watson et al. 2009), 100% of sections were in L3-5, with 16.67% of all sections in L3, 70.37% in L4 and 12.96% in L5 (Table 4.4).

In contrast to the literature and Study 2, global dorsal horn GFAP fluorescence was unaltered by low dose (50µg) CFA (Figure 4.34a). PTK787 and etanercept treatment also had no impact on GFAP intensity (Figure 4.34a). For representative images of GFAP signal in the dorsal horn, see Figure 4.35. Global dorsal horn GFAP intensity at day 10 was plotted against ipsilateral knee diameter at days 1 2 or 3, but these measures were not correlated (Figures 4.36a, b & c respectively).

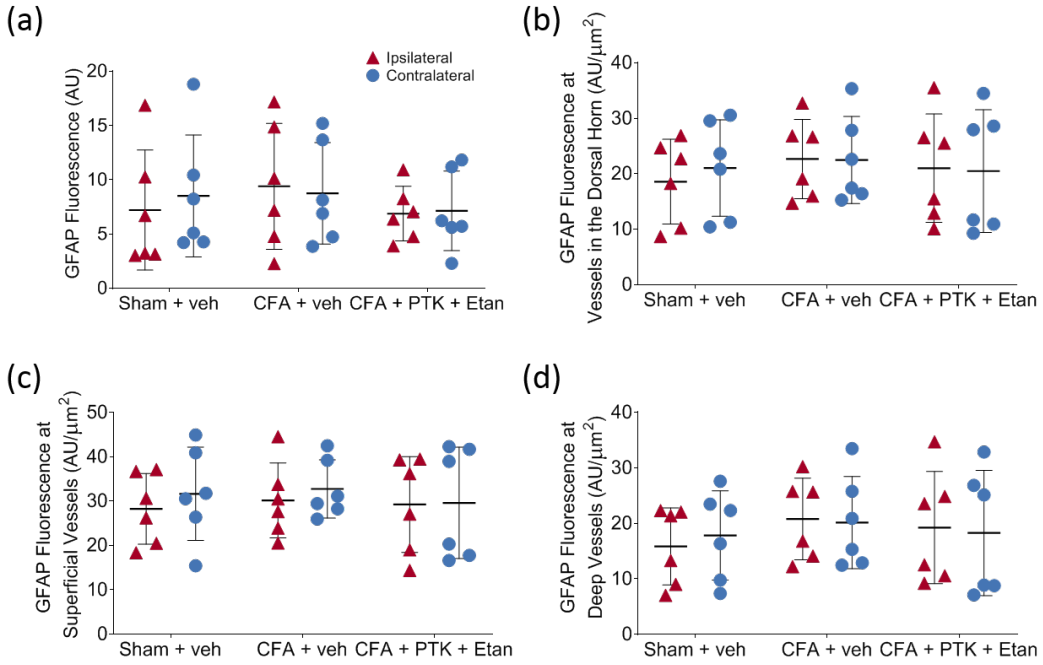


Figure 4.34: Neither global GFAP **(a)** nor GFAP signal at vessels (global **(b)**, superficial laminae **(c)**, deep laminae **(d)**) were altered 10 days after low dose CFA. Treatment with PTK787 and etanercept also had no effect. **a**: Interaction: p=0.88, Row Factor, p=0.57, Column Factor: p=0.85; **b**: Interaction: p=0.90, Row Factor, p=0.74, Column Factor: p=0.84; **c**: Interaction: p=0.92, Row Factor, p=0.87, Column Factor: p=0.52; **d**: Interaction: p=0.90, Row Factor, p=0.60, Column Factor: p=0.97. 2way ANOVA. n = 6. Mean ± SD. Veh: Vehicle; PTK: PTK787; Etan: Etanercept.

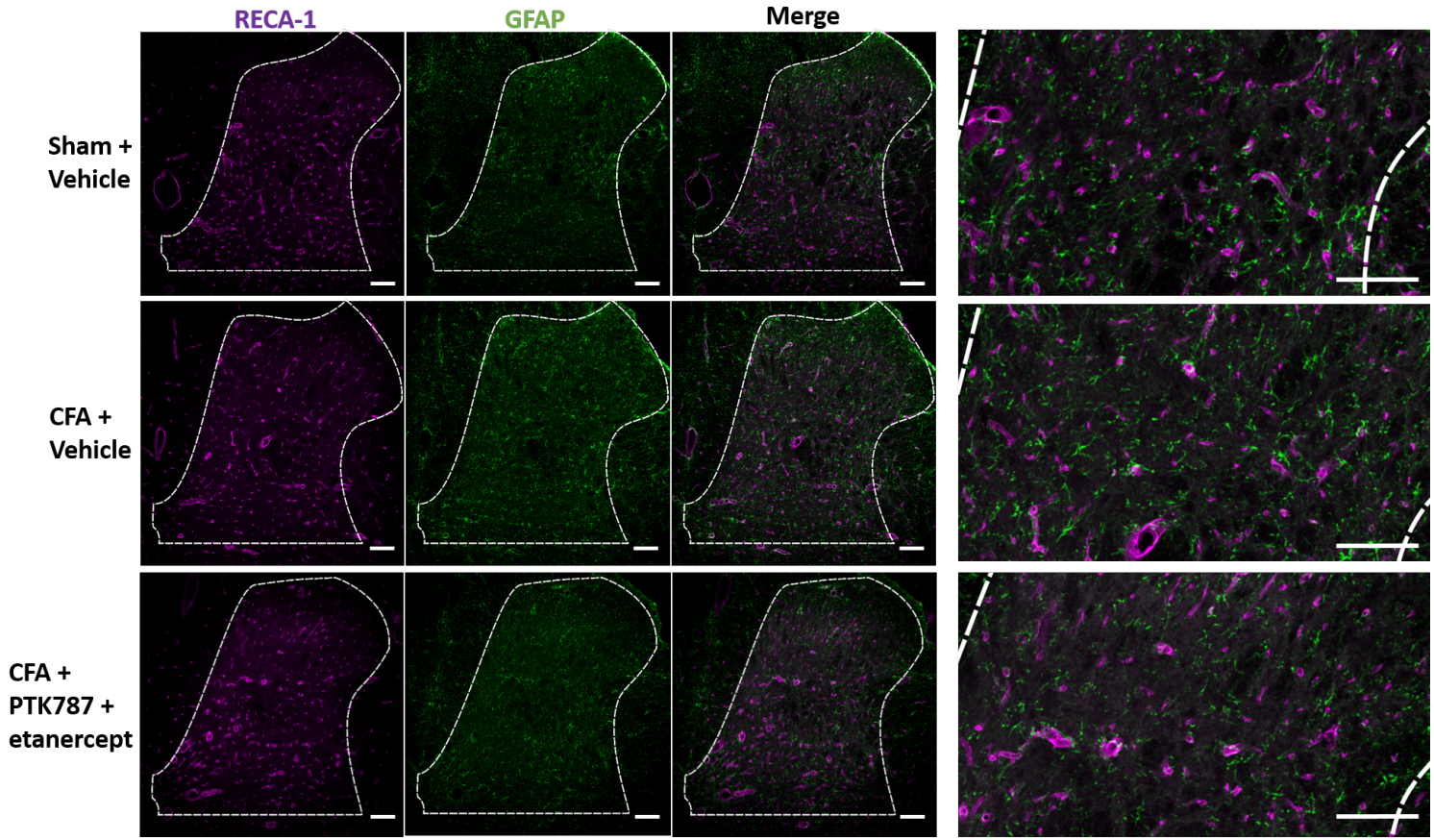


Figure 4.35: Representative images of GFAP signal in the dorsal horn of the spinal cord 10 days after low dose CFA-induced peripheral inflammation. Green: GFAP astrocyte marker; Magenta: RECA-1 vessel marker. Scale bar: 100µm.

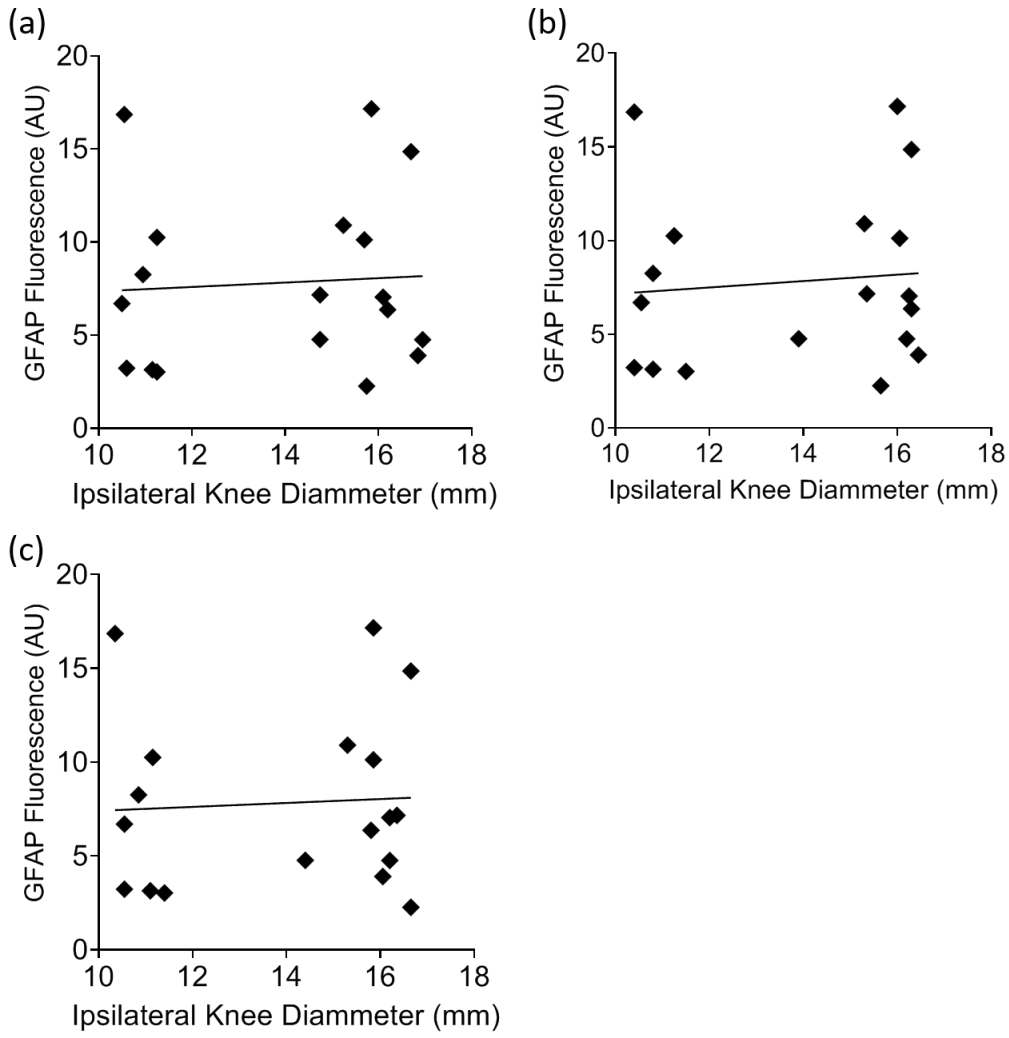


Figure 4.36: GFAP intensity 10 days after low dose CFA (50µg) was not correlated to ipsilateral knee diameter at day 1 (a, r = 0.06502, p = 0.8), day 2 (b, r = 0.09348, p = 0.7) or day 3 (c, r = 0.05819, p = 0.8). Pearson correlation test. Data combined from groups: Sham + vehicle; CFA + vehicle; CFA + PTK787 + etanercept. n = 18.

As before, the neurovascular response to inflammation was investigated but the new vessel marker, RECA-1 was used instead as this did not give the non-specific signal in superficial laminae seen with laminin (see Figure 4.13 right image). Neither CFA nor treatment with PTK787 + etanercept had a significant effect on GFAP fluorescence at vessel structures at 10 days (Figure 4.34b). The RECA-1 marker allows segregation of the superficial and deeper laminae of the dorsal horn (Figure 4.37), but no difference in GFAP signal at vessel structures was detected (Figures 4.34c & d).

Higher powered analysis of GFAP signal in the superficial (Figure 4.38a) and deep dorsal horn (Figure 4.38c) again showed no difference between treatment types, nor at superficial or deep vessels (Figure 4.38b & d). For representative images see Figures 4.39 and 4.40.

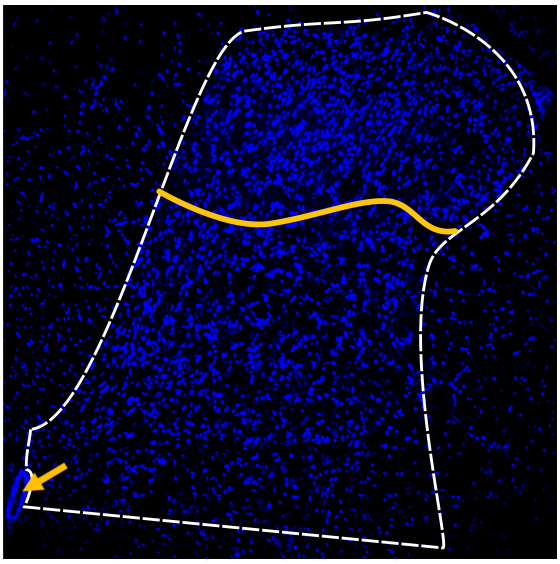


Figure 4.37: Representative image of superficial vs deep laminae segregation (at yellow line) in the dorsal horn of the spinal cord using the nuclear signal from Hoechst (blue). Yellow arrow: Central canal.

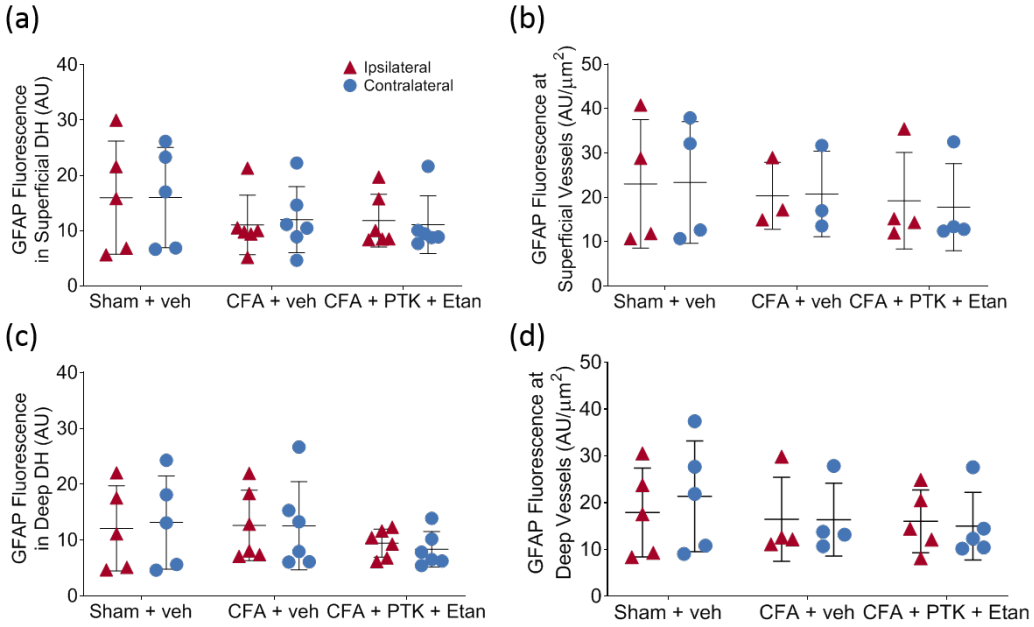


Figure 4.38: Higher power analysis of GFAP signal in the dorsal horn of the spinal cord 10 days low dose (50µg) CFA revealed no difference in GFAP signal in the superficial (**a**: Interaction: p=0.95; Row Factor: p=0.24; Column Factor: p=0.97) or deep (**c**: Interaction: p=0.93; Row Factor: p=0.28; Column Factor: p=0.99) dorsal horn, or at superficial (**b**: Interaction: p=0.98; Row Factor: p=0.72; Column Factor: p=0.96) and deep (**d**: Interaction: p=0.84; Row Factor: p=0.56; Column Factor: p=0.82). Treatment with PTK787 and etanercept also had no effect. 2way ANOVA. n = 3-6. Mean ± SD. DH: Dorsal horn; Veh: Vehicle; PTK: PTK787; Etan: Etanercept.

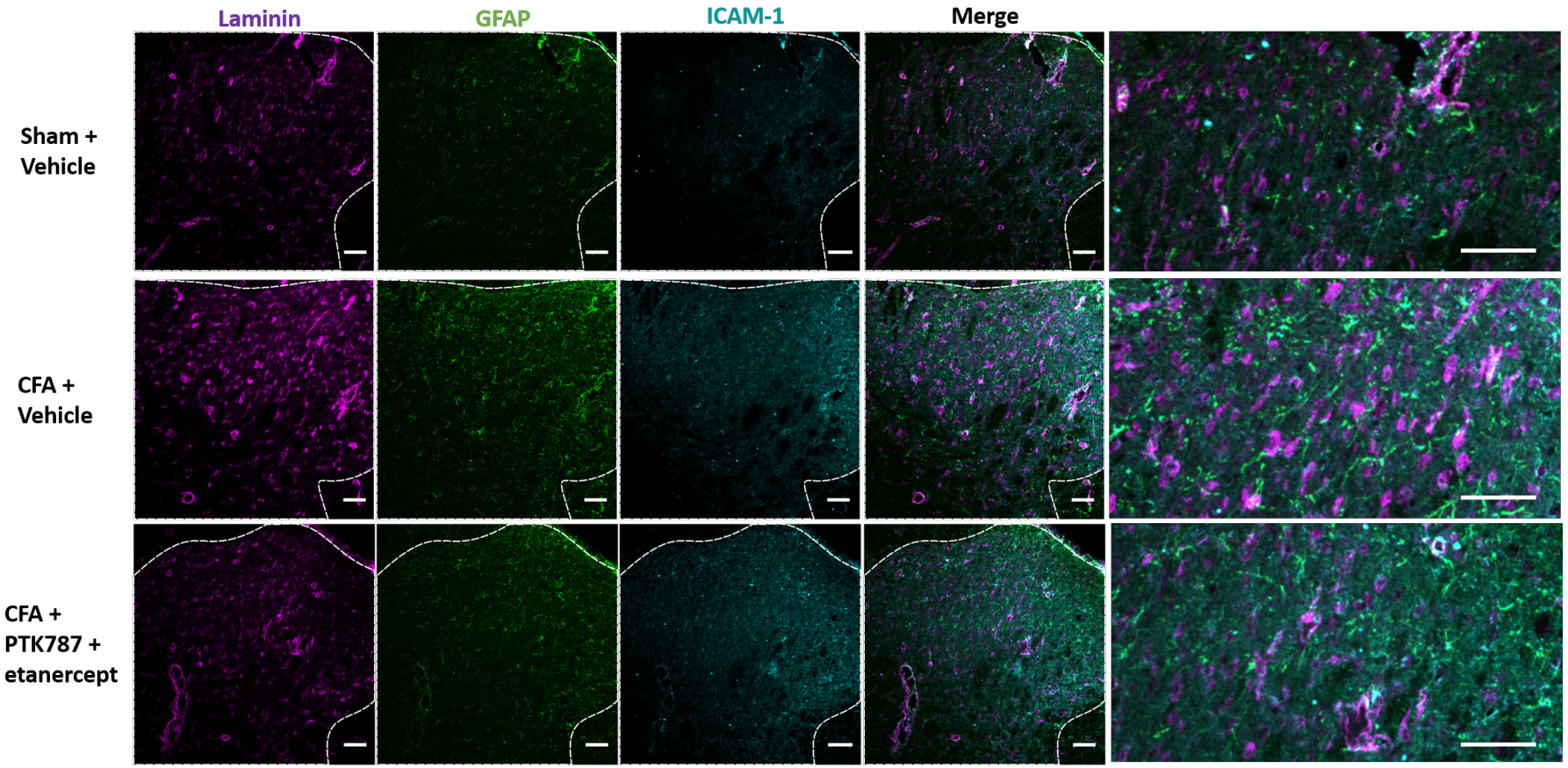


Figure 4.39: Representative images of GFAP and ICAM-1 signal in the superficial dorsal horn 10 days after low dose peripheral inflammation. Green: GFAP astrocyte marker; Cyan: ICAM-1 marker; Magenta: Laminin vessel marker. Scale bar: 50μm.

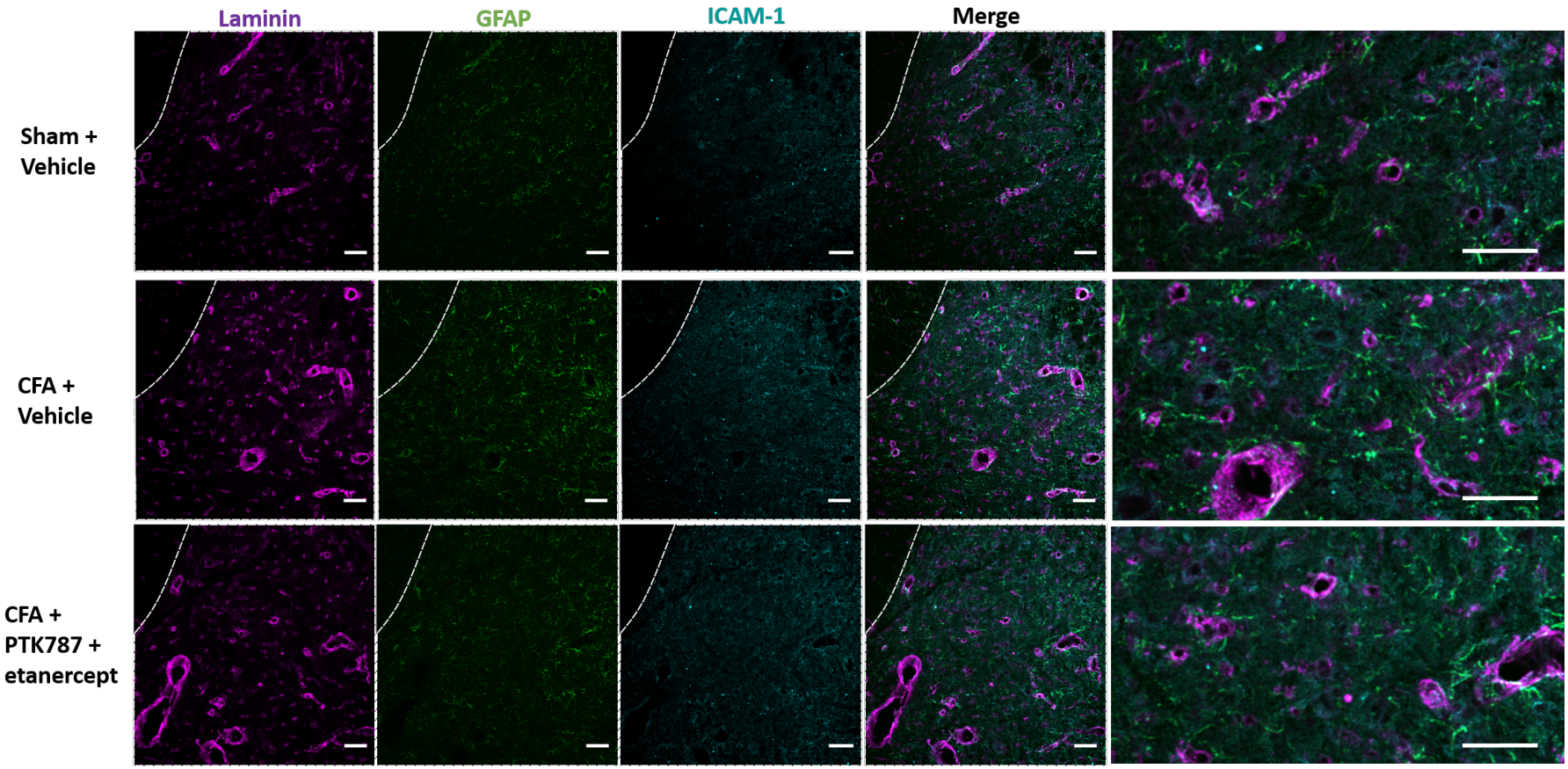


Figure 4.40: Representative images of GFAP and ICAM-1 signal in the deep dorsal horn after peripheral inflammation (50µg CFA). Green: GFAP astrocyte marker; Cyan: ICAM-1 marker; Magenta: Laminin vessel marker. Scale bar: 50µm.

As noted in Chapter 3, astrocytes extend out from vessels, demonstrated in Figure 4.6. By using the extraction overlap analysis technique (see Section 4.2.8), these structures are included in analyses, whereas they are excluded in previous analyses when investigating GFAP at vessels. Analysing GFAP signal using this overlap technique detected no difference in fluorescence or area of vessel-associated GFAP structures (Figure 4.41a & b respectively).

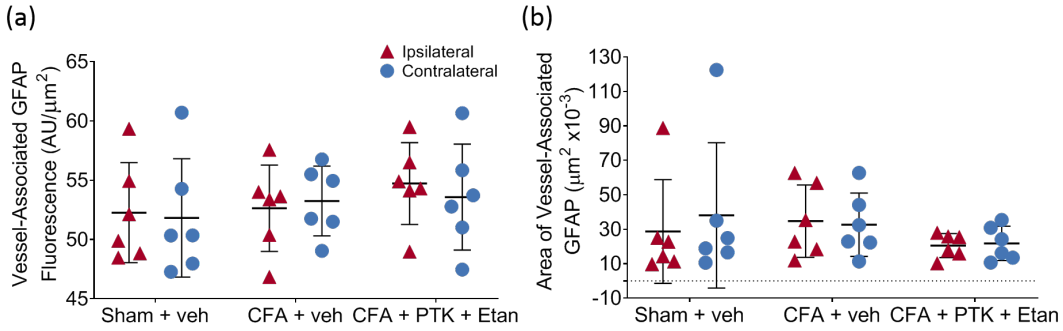


Figure 4.41: Vessel-associated GFAP intensity in the dorsal horn of the spinal cord did not change with low dose (50µg) CFA **(a)**, nor did the area of vessel-associated GFAP **(b)**. Treatment with PTK787 and etanercept also had no effect. 2way ANOVA with Dunnett's multiple comparisons compared to sham + vehicle or CFA + vehicle. n = 6. Mean ± SD. Veh: Vehicle; PTK: PTK787; Etan: Etanercept.

4.3.4.3 The Central Endothelial and Microglial Response to Chronic Inflammation and the Effect of VEGF-R combined with TNFα Inhibition

CD11b was investigated to determine the microglial response to CFA and whether PTK787 and etanercept worked in tandem to affect microglial activation. However, there was no change in CD11b signal after peripheral inflammation (Figures 4.43 & 4.42). As seen before, there were CD11b-positive structures, but these were not specific to one treatment group (Figure 4.15). CD11b-positive structures were found in significantly more spinal cord sections from CFA + vehicle animals than sham + vehicle or CFA + PTK787 + etanercept animals (in both ipsilateral and contralateral dorsal horns, Figure 4.15).

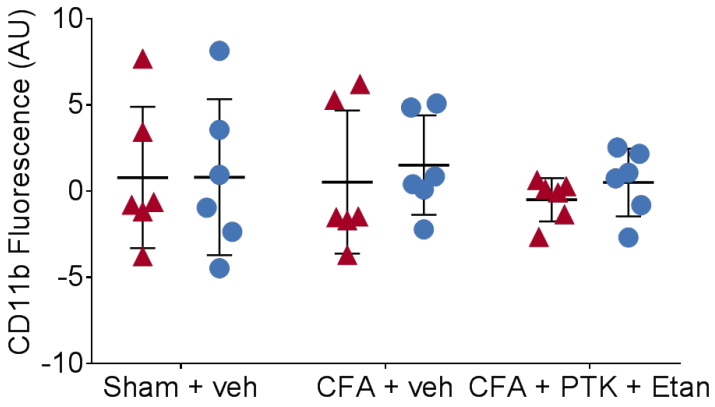


Figure 4.42: CD11b signal in the dorsal horn of the spinal cord was not altered by low dose CFA at day 10 nor by PTK787 and etanercept treatment. Interaction: p=0.92; Row Factor: p=0.74; Column Factor: p=0.56. 2way ANOVA. n = 6. Mean ± SD. DH: Dorsal horn; Veh: Vehicle; PTK: PTK787; Etan: Etanercept.

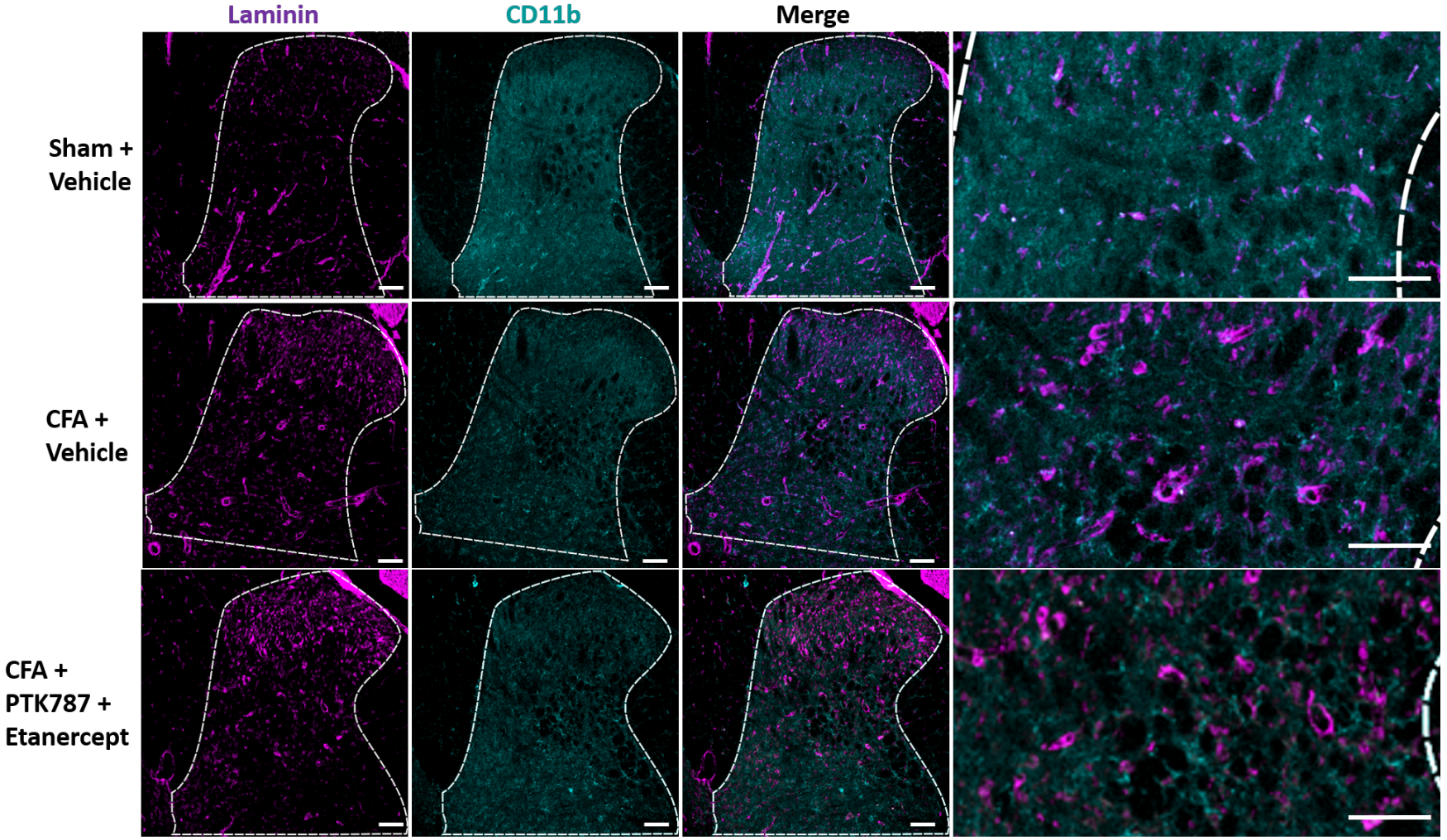


Figure 4.43: Representative images of CD11b signal in the dorsal horn of the spinal cord 10 days after low dose (50μg) CFA-induced peripheral inflammation. Cyan: CD11b microglia marker; Magenta: Laminin vessel marker. Scale bar: 100μm.

High power analysis of ICAM-1 signal in the dorsal horn of the spinal cord (Figures 4.40 and 4.39) revealed no difference in the superficial or deep dorsal horn (Figure 4.44a & c respectively), or at superficial and deep vessels (Figure 4.44b & d respectively).

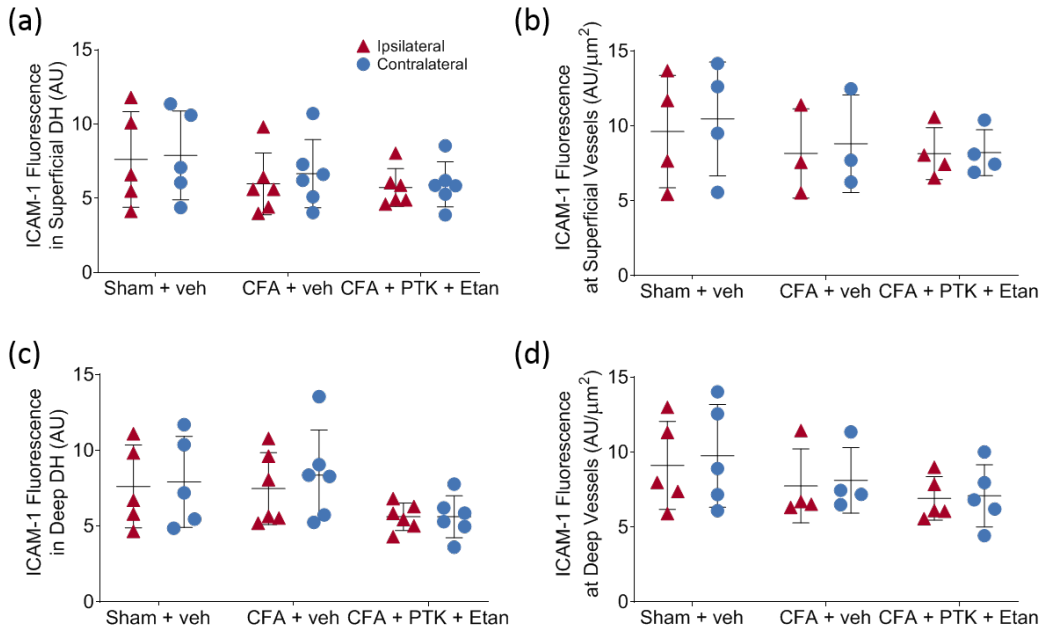


Figure 4.44: High power analysis of ICAM signal in the dorsal horn of the spinal cord revealed no difference in the superficial (**a**: Interaction: p=0.96; Row Factor: p=0.15; Column Factor: p=0.62) or deep (**c**: Interaction: p=0.89; Row Factor: p<0.05; Column Factor: p=0.62) dorsal horn, or at superficial (**b**: Interaction: p=0.96; Row Factor: p=0.43; Column Factor: p=0.69) and deep (**d**: Interaction: p=0.98; Row Factor: p=0.12; Column Factor: p=0.69). Treatment with PTK787 and etanercept also had no effect. 2way ANOVA with Sidak's multiple comparisons compared to CFA + Vehicle. n = 3-6. Mean ± SD. DH: Dorsal horn; Veh: Vehicle; PTK: PTK787; Etan: Etanercept.

As mentioned previously, vessel area was investigated after peripheral CFA-induced inflammation and PTK787 treatment. There was no evidence of either CFA-induced angiogenesis or a reduction in vessel area after PTK787 in the global dorsal horn (Figure 4.45a) or in superficial and deep areas using RECA-1 as a vessel marker (Figure 4.45b & c respectively). When using laminin as a vessel marker at higher magnification, there was also no evidence of a change in vessel area in the superficial or deep dorsal horn after either CFA or PTK787 treatment (Figure 4.45d & e respectively). Laminin gives a larger value for vessel area in the superficial dorsal horn than RECA-1 (Figure 4.45d vs. b), possibly due to the higher magnification identifying more laminin-positive structures (see Figure 4.44 for examples).

ZEB-1 is a transcription factor that can trigger epithelial-mesenchymal transition in cells, which causes them to be more motile and invasive. In neuropathic pain conditions there is an increase in ZEB-1 in spinal cord tissue and glial cells (Zhang et al. 2020; Shen et al. 2019; Yan et al. 2018a; Yan et al. 2018b) and in our lab we found there was an increase in ZEB-1 expression in spinal cord perivascular cells after 14 days of CFA-induced inflammation in the mouse, but it was not altered in endothelial cells

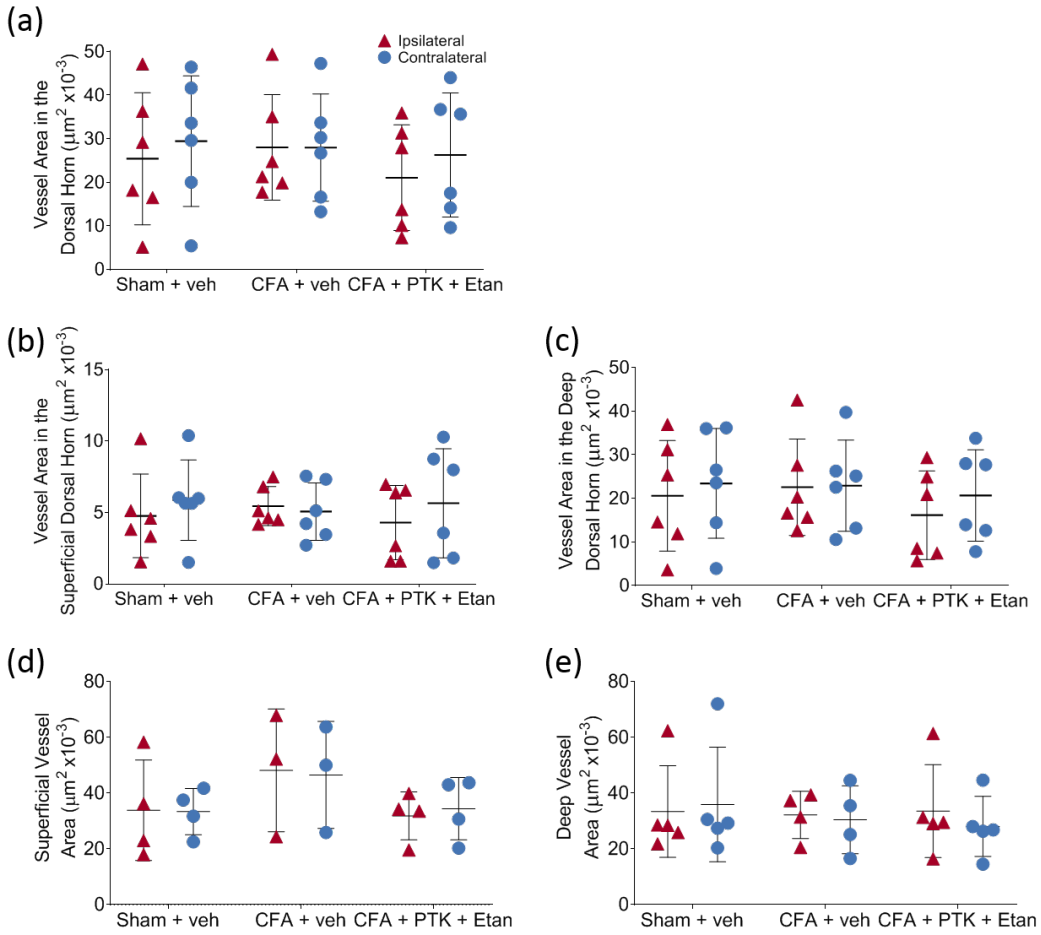


Figure 4.45: Vessel area in the dorsal horn of the spinal cord was not altered 10 days after low dose CFA or PTK787 and etanercept treatment ((a): global dorsal horn; (b & d): superficial dorsal horn; (c & e): deep dorsal horn). a, b & c: RECA-1 vessel marker; d & e: Laminin vessel marker. a: Interaction: p=0.88, Row Factor, p=0.70, Column Factor: p=0.50; b: Interaction: p=0.70, Row Factor, p=0.85, Column Factor: p=0.45; c: Interaction: p=0.90, Row Factor, p=0.61, Column Factor: p=0.50; d: Interaction: p=0.96, Row Factor, p=0.17, Column Factor: p=0.98; e: Interaction: p=0.82, Row Factor, p=0.76, Column Factor: p=0.93. 2way ANOVA. n = 6. Mean ± SD. DH: Dorsal horn; Veh: Vehicle; PTK: PTK787; Etan: Etanercept.

(Lopes and Beazley-Long, unpublished data). For this reason ZEB-1 immunofluorescence was probed in the rat. Here, CFA had no impact on global dorsal horn ZEB-1 fluorescence (Figure 4.46a) or at vessels (Figure 4.46b, see Figure 4.47 for representative images). There was also no change in ZEB-1 signal in vessel-associated nuclei (Figure 4.46c). The area of vessel-associated ZEB-1 nuclear signal was also not altered by CFA (Figure 4.48).

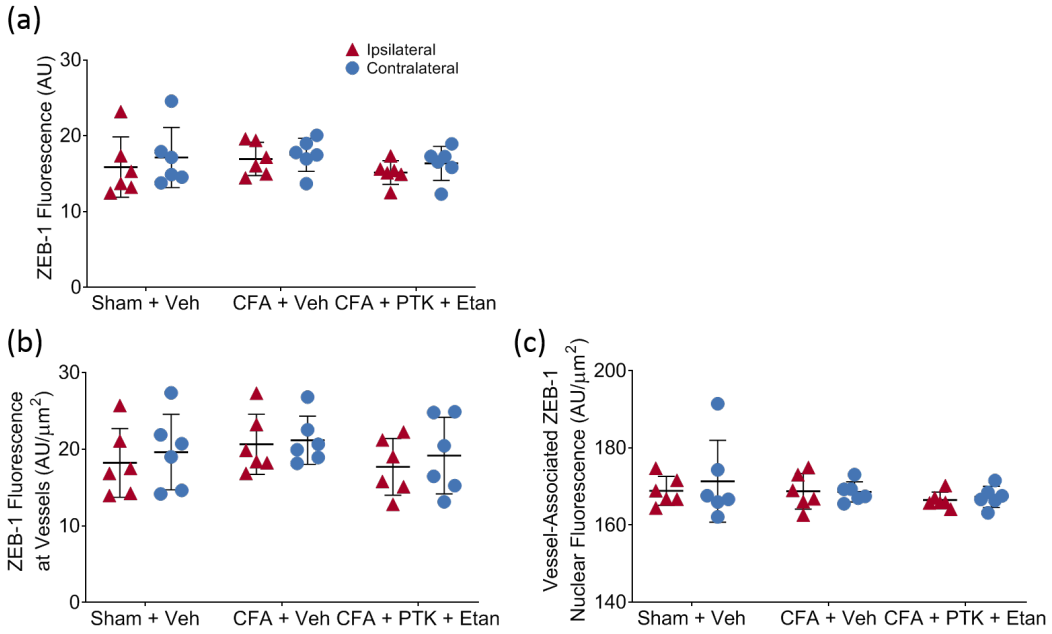


Figure 4.46: Global dorsal horn intensity of ZEB-1 signal in the dorsal horn of the spinal cord is not altered 10 days after low dose CFA (**a**, Interaction: p=0.94; Row Factor: p=0.46; Column Factor: p=0.30). ZEB-1 signal is also not altered at vessel structures when using the overlay ROI method (**b**, Interaction: p=0.96; Row Factor: p=0.33; Column Factor: p=0.43), nor is vessel-associated nuclear-ZEB-1 signal using the extraction method (**c**, Interaction: p=0.83; Row Factor: p=0.34; Column Factor: p=0.55). Treatment with PTK787 and etanercept also had no effect. 2way ANOVA. n = 6. Mean ± SD. DH: Dorsal horn; Veh: Vehicle; PTK: PTK787; Etan: Etanercept.

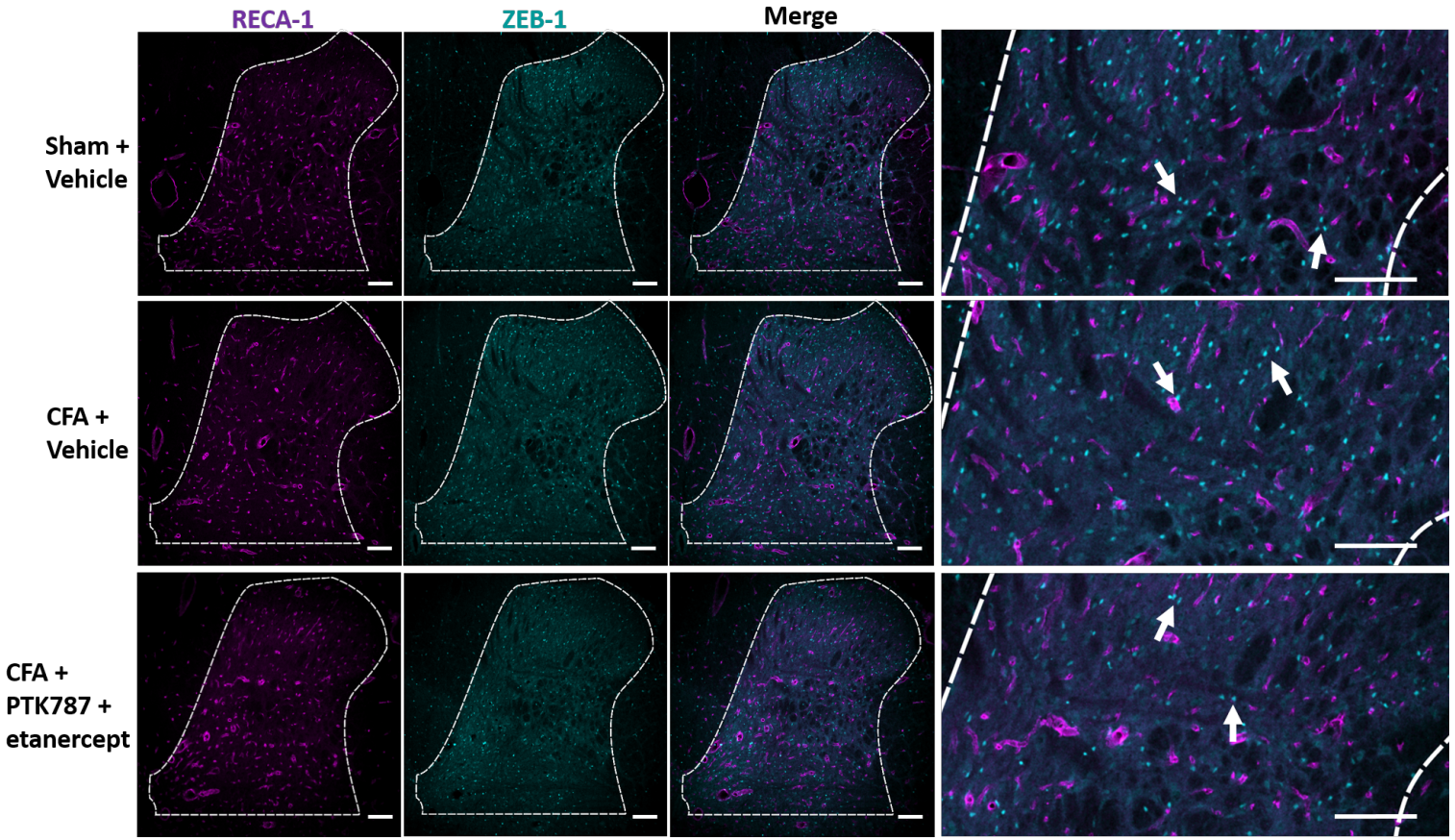


Figure 4.47: Representative images of ZEB-1 signal (white arrows) in the dorsal horn of the spinal cord after peripheral inflammation (50µg CFA). Cyan: ZEB-1 transcription factor marker in nuclei (white arrows); Magenta: RECA-1 vessel marker. Scale bar: 100µm.

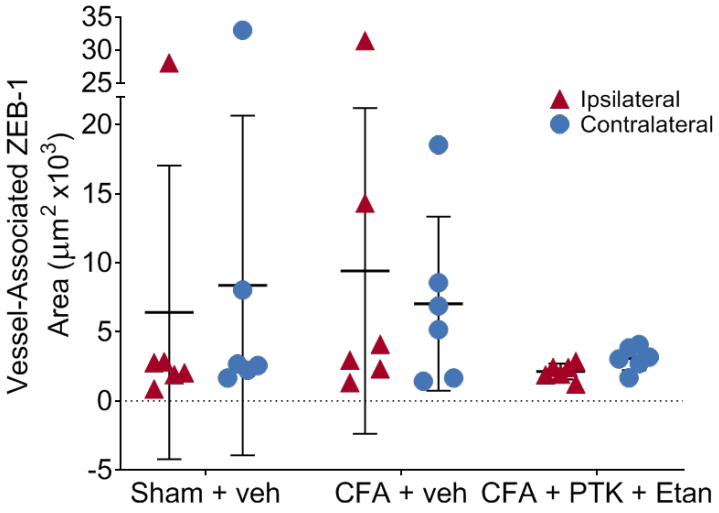


Figure 4.48: Area of nuclear-ZEB-1 signal in the dorsal horn of the spinal cord is not altered 10 days after low dose CFA. Interaction: p=0.81; Row Factor: p=0.24; Column Factor: p=0.95. 2way ANOVA. n = 6. Mean ± SD. Veh: Vehicle; PTK: PTK787; Etan: Etanercept.

4.3.5 Differences Between CFA Regimens

There were differences in the CFA doses and regimes used between each study due to animal welfare and Home Office issues. Knee diameter, weight bearing and von Frey data were compared across the studies (Figure 4.49). Data from CFA + day 3 treatment animals (CFA + PTK787 and/or etanercept) within the commercial 50µg CFA and in-house 100µg CFA groups were combined as they all received the same treatment up to day 3, this was not possible with the commercial 100µg CFA as all animals received pre-dosing of different treatments. Commercial CFA at 100µg led to significantly larger knee diameters within the first 2 days than both the in-house 100µg CFA and the commercial 50µg CFA (Figure 4.49a). Commercial CFA at 50µg caused significantly larger knee diameters than in-house CFA at 100µg throughout the duration of the study (Figure 4.49a). Additionally, on days 3 and 10, the commercial 50µg CFA caused animals to bear significantly less weight on the ipsilateral hindpaw (Figure 4.49b). There was no difference in von Frey mechanical data between commercial 50µg and in-house 100µg (Figure 4.49c).

The significant increase in GFAP signalling seen in the dorsal horn of the spinal cord in Study 2 using the high dose of in-house CFA (100µg in 50µL) was lost in Study 3 with the lower dose of CFA (50µg in 50µL, see Figures 4.50 and 4.51). This is surprising considering that when comparing the CFA + vehicle groups only, the commercial 50µg CFA had significantly higher knee diameters than the in-house CFA for the duration of the study (Figure 4.49a). Additionally, despite the commercial 50µg CFA causing significantly more swelling than the in-house 100µg CFA, GFAP intensity at day 10 was only correlated with early knee diameter in the in-house 100µg CFA but not with the 50µg CFA (Figures 4.27 and 4.36 respectively).

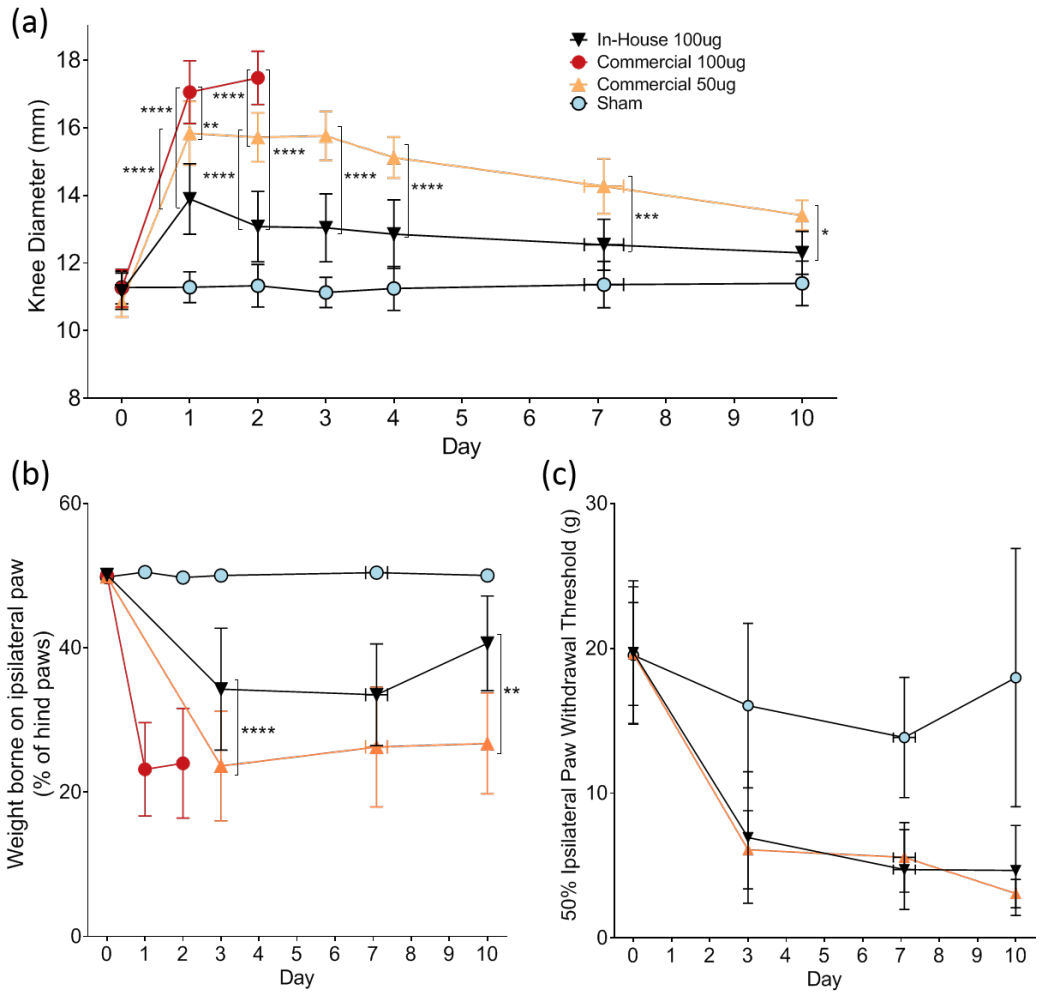


Figure 4.49: Commercial 100µg CFA caused significantly more swelling than in-house 100µg CFA and commercial 50µg in the first 2 days, and commercial 50µg CFA caused more swelling than in-house throughout the study **(a)**. Commercial 50µg CFA caused animals to bear significantly less weight on the ipsilateral hindpaw than in-house 100µg CFA on days 3 and 10 **(b)**. There was no difference in von Frey data throughout the study between in-house CFA and commercial 50µg CFA **(c)**. ****p<0.0001, ***p<0.001, **p<0.01, *p<0.05. Data from CFA + day 3 treatment groups (CFA + PTK787 and/or etanercept) are pooled within in-house 100µg and commercial 50µg CFA up to day 3. In-house 100µg CFA n = 6-18, Commercial 100µg CFA n = 6, Commercial 50µg CFA n = 6-23. Sham n = 11-17. Mean ± SD. 2way ANOVA with Sidak's or Tukey's multiple comparisons. Sham + vehicle data was not included in analyses.

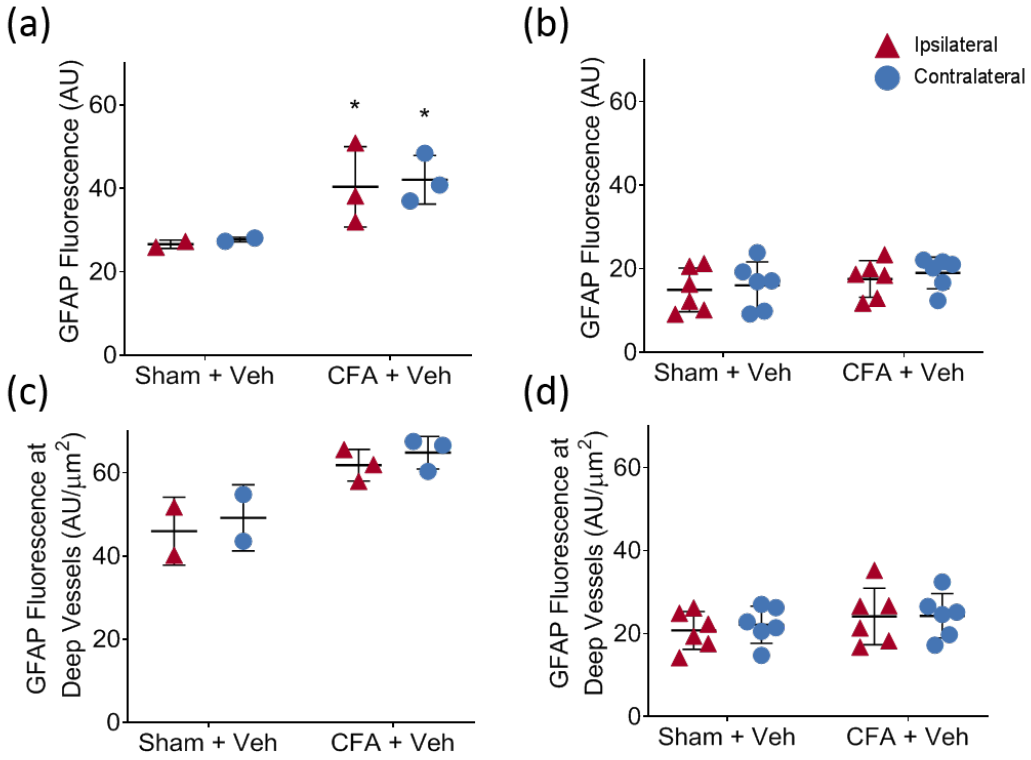


Figure 4.50: There was significantly higher GFAP intensity in the dorsal horn with CFA compared to Sham **(a)** and more GFAP at vessels (although not significant) **(c)** using the high dose of CFA (100µg in 50µL), but this difference is lost with the lower dose CFA (50µg in 50µL) **(b & d)**. 2 way ANOVA with Dunnett's multiple comparisons compared to sham + vehicle. n = 2-6. Mean ± SD. Veh: Vehicle.

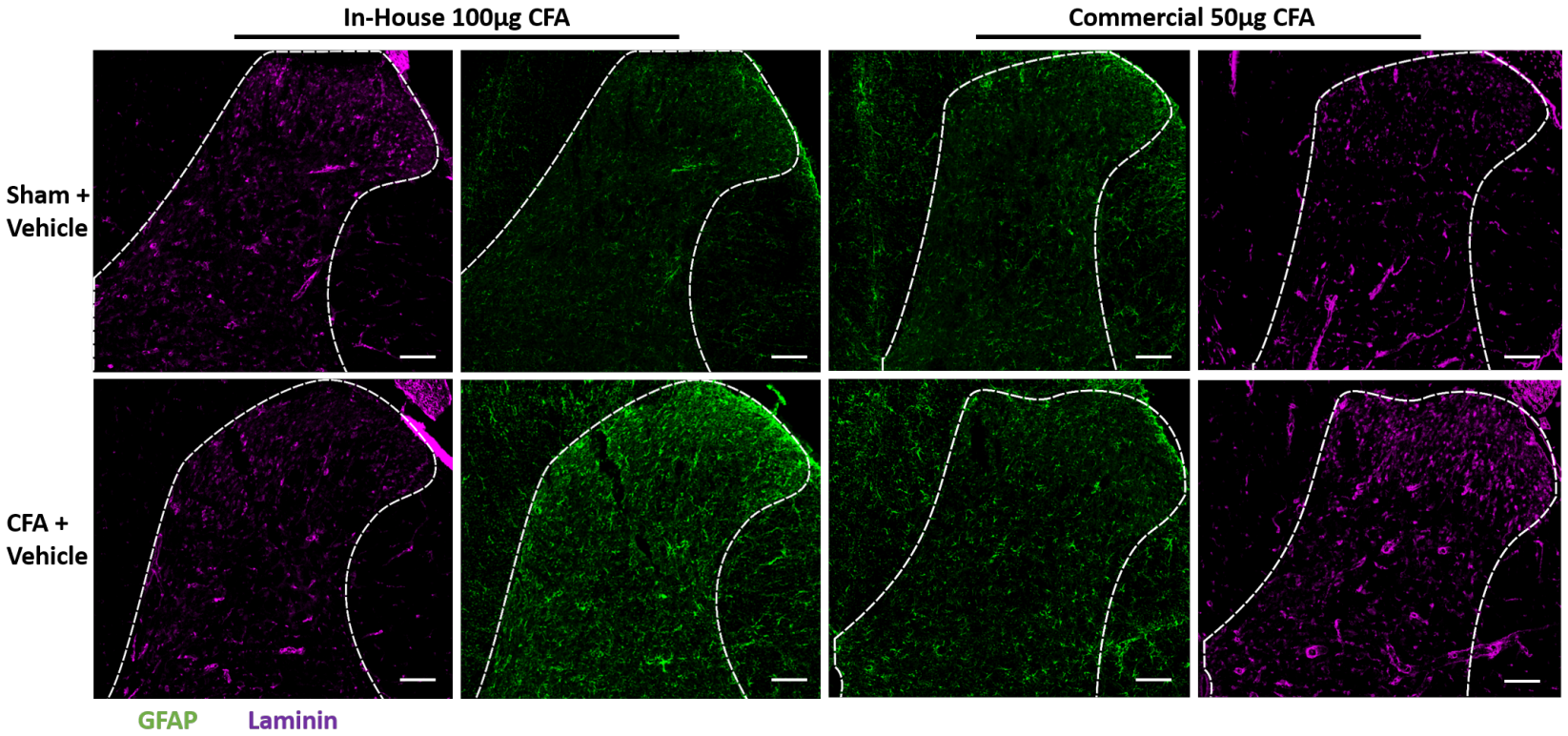


Figure 4.51: The increase in GFAP intensity in the dorsal horn with the higher dose CFA (100µg in 50µL) compared to Sham was lost with the lower dose CFA (50µg in 50µL). Green: GFAP astrocyte marker; Magenta: Laminin vessel marker. Scale bar: 100µm.

4.3.6 The Central Gliovascular Alterations in Response to CFA were Prevented in VEGF-R2 KO Mice

VEGF-R2 is expressed on neurones and some glial cells as well as endothelial cells (Hulse et al. 2014; Wuestefeld et al. 2012; Brockington et al. 2006), and PTK787 can also act on other cells and tyrosine kinase receptors, for example PDGFR-β on pericytes (Wood et al. 2000). To determine the specific contribution of endothelial cell VEGF-R2 to the development of secondary pain, we used an endothelial cell-specific VEGF-R knockout mouse line (VEGF-R2^{ECKO}). These mice demonstrated a reduction in pain behaviour from CFA-induced inflammation (Figure 4.52, adapted from Beazley-Long et al. (2018b)). Using the advanced analysis techniques developed in this thesis, I re-analysed the tissue from these animals using vessel-associated signal, and detected an increase in GFAP in the global dorsal horn and at vessels after peri-articular CFA in uninduced mice (i.e. mice in which endothelial cell VEGF-R2 had not been knocked out, controls; Section 3.3.2 and Figures 4.53a & b and 4.54 here). Interestingly, when endothelial cell VEGF-R is knocked out, there is an increase in basal GFAP signal in the dorsal horn before inflammation is induced (Beazley-Long et al. 2018b). When re-analysed, I found the same increase in basal GFAP, in terms of the intensity of GFAP in the global dorsal horn and at vessels (Figure 4.53a & b respectively), and in the intensity and area of vessel-associated GFAP signal (Figure 4.53c & d respectively, see Sections 4.2.8 and 4.6 for distinction between analyses). After CFA-induced inflammation, there is no further increase in astrocyte activation in these knockout mice (Figure 4.53). As both male and female mice were used and there are known differences in microglial contributions to chronic pain development between sexes (Raoof et al. 2018; Rosen et al. 2017; Mapplebeck et al. 2016), the ipsilateral astrocytic response was separated by sex (Figure 4.55). Due to low numbers, the data was not analysed, but there were no obvious differences in the astrocytic response between sexes (Figure 4.55).

As before, the analyses used here allowed for estimates of vessel area after CFA and endothelial VEGF-R2 knockout. Neither VEGF-R2 knockout in endothelial cells nor CFA had an impact on vessel area in the dorsal horn of the spinal cord (Figure 4.53e).

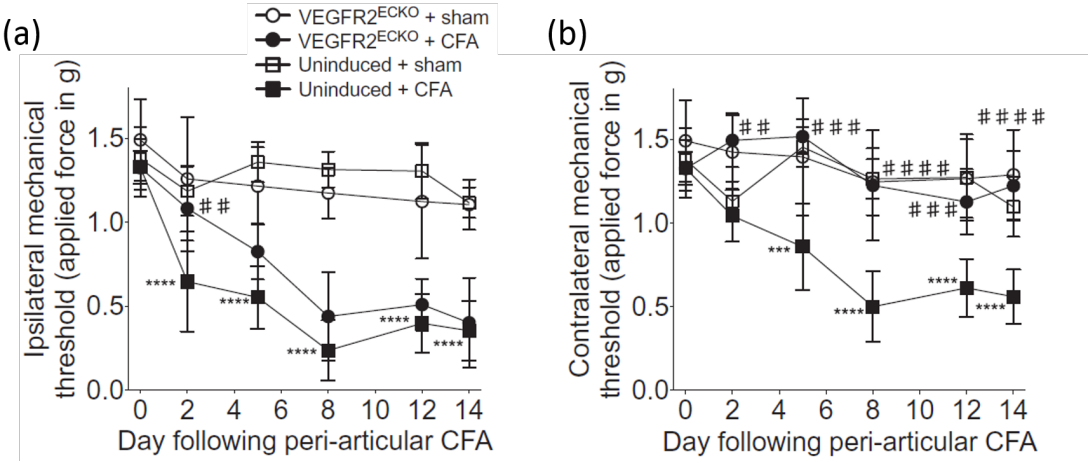


Figure 4.52: Endothelial cell VEGF-R2 knockout significantly delayed CFA-induced reduction in paw withdrawal threshold in the ipsilateral hindpaw **(a)** and prevented the reduction in the contralateral hindpaw **(b)**. 2-way ANOVA with Dunnett's multiple comparisons. *compared to respective baseline (day 0): ****p<0.0001, ***p<0.001, **p<0.01, *p<0.05. #compared to respective control at given timepoint: ##p<0.01, ###p<0.001, ####p<0.0001. Mean ± SD. n = 3-11. VEGFR2^{ECKO}: vascular endothelial growth factor endothelial cell knockout. Adapted from Beazley-Long et al. (2018b).

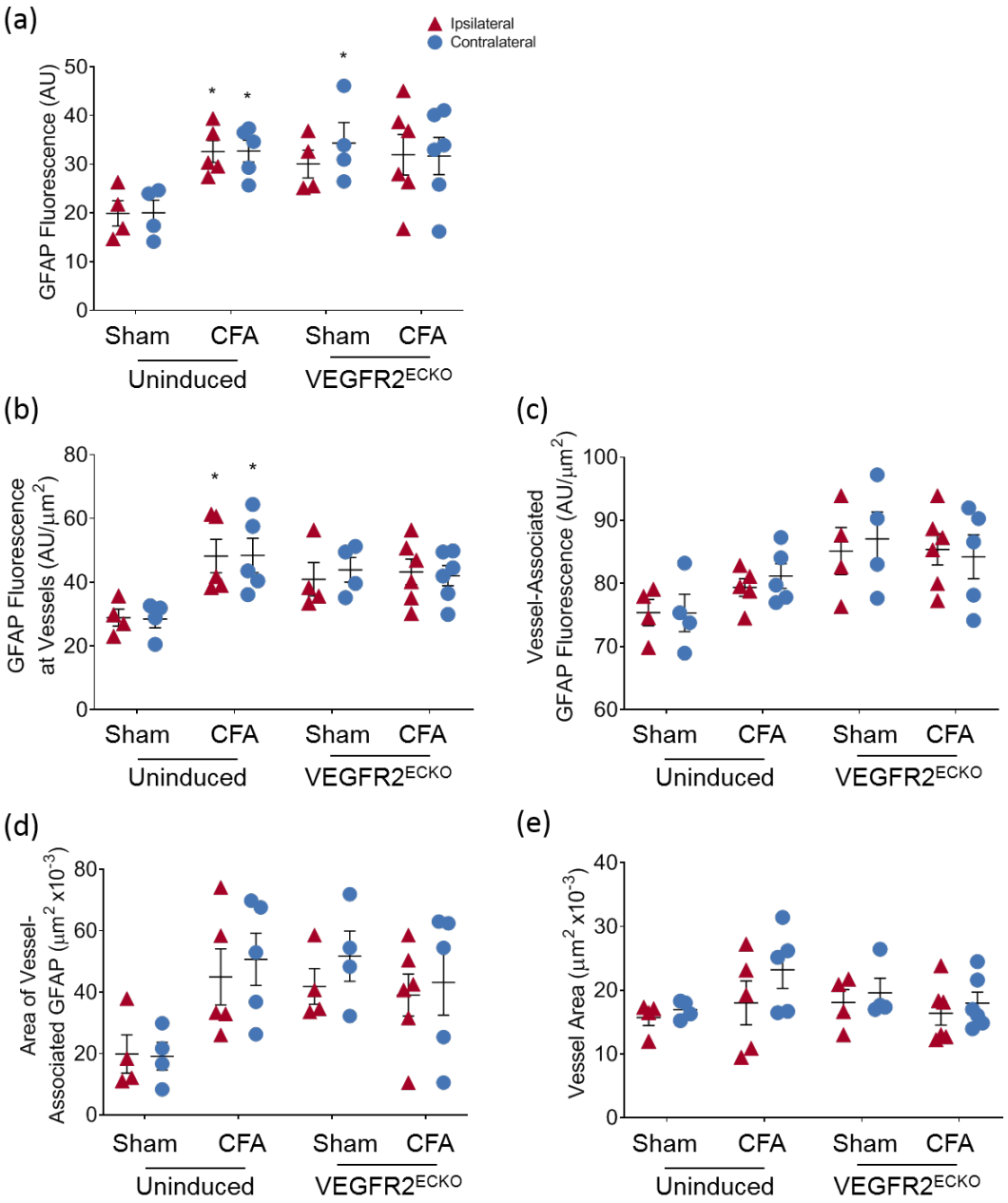


Figure 4.53: Global GFAP signal in the dorsal horn after peripheral CFA is significantly increased in uninduced mice compared to sham **(a)**. When induced and endothelial cell VEGF-R2 is knocked out, there is an increase in GFAP signal even before CFA **(a)**. This trend is mirrored in GFAP signal at vessels **(b)** and area of vessel-associated GFAP signal **(d)**. There is no difference between uninduced sham and CFA animals in vessel-associated GFAP fluorescence **(c)**, but there is a slight increase in intensity with of KO animals. There is no clear difference in vessel area with CFA or VEGF-R2 KO **(e)**. **a**: Interaction: p=0.91, Row Factor, p<0.01, Column Factor: p=0.66; **b**: Interaction: p=0.97, Row Factor, p<0.01, Column Factor: p=0.90; **c**: Interaction: p=0.93, Row Factor, p<0.01, Column Factor: p=0.76; **d**: Interaction: p=0.94, Row Factor, p<0.01, Column Factor: p=0.42; **e**: Interaction: p=0.79, Row Factor, p=0.27, Column Factor: p=0.15. 2-way ANOVA with Sidak's multiple comparisons compared to uninduced vehicle. Mean ± SD. n = 2-6. **p<0.01, *p<0.05. Uninduced: "wild type"; VEGFR2^{ECKO}: vascular endothelial growth factor endothelial cell knockout. Tissue processing and immunofluorescence performed by Dr Nick Beazley-Long (published in Beazley-Long et al. 2018b) and reanalysed by me.

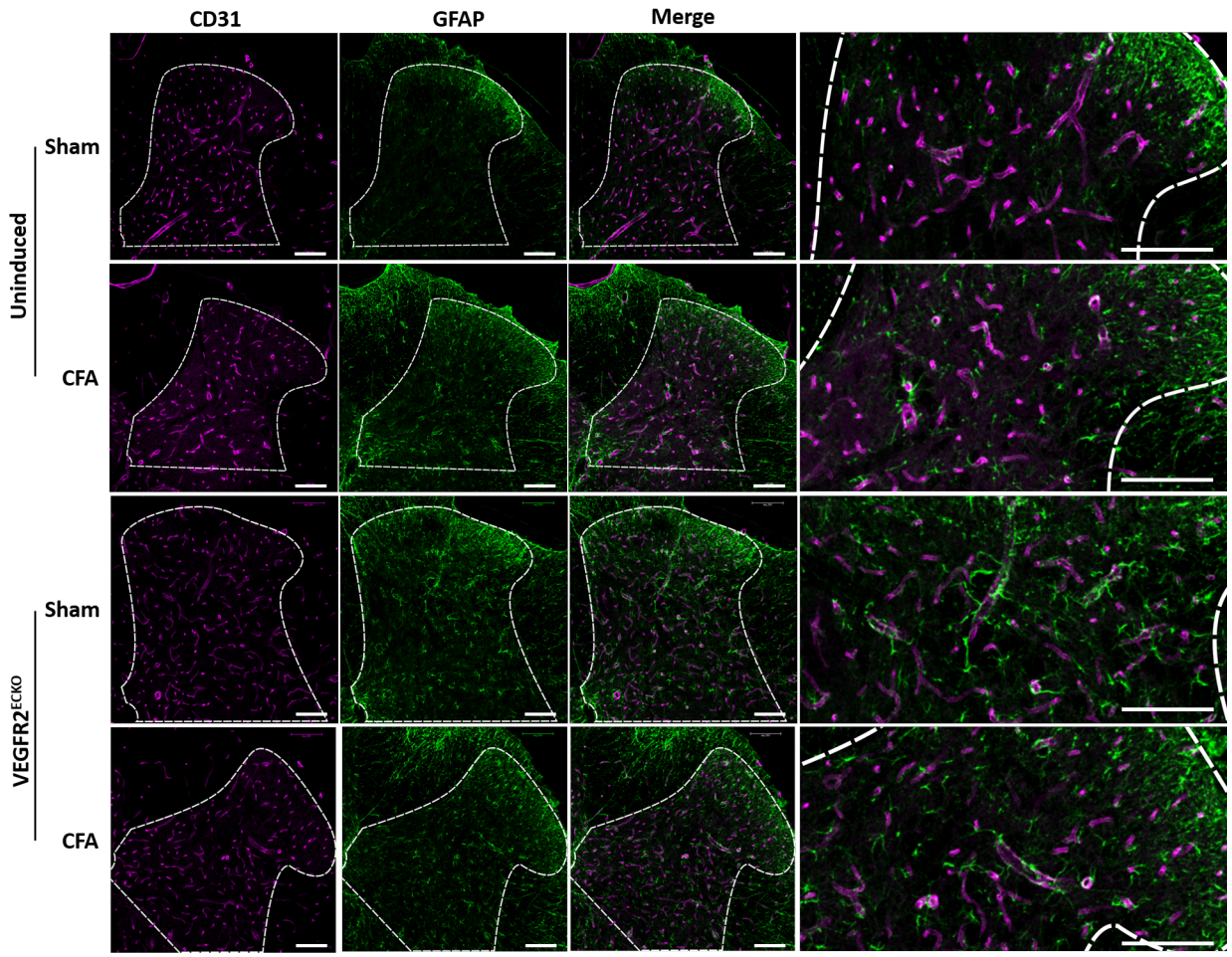


Figure 4.54: Representative images of GFAP signal in the mouse spinal cord dorsal horn after peripheral inflammation. Green: GFAP astrocyte marker; Magenta: CD31 vessel marker. Uninduced: ″wild type″; VEGFR2^{ECKO}: vascular endothelial growth factor endothelial cell knockout. Scale bar: 100µm. Tissue processing and immunofluorescence performed by Dr Nick Beazley-Long (published in Beazley-Long et al. 2018b).

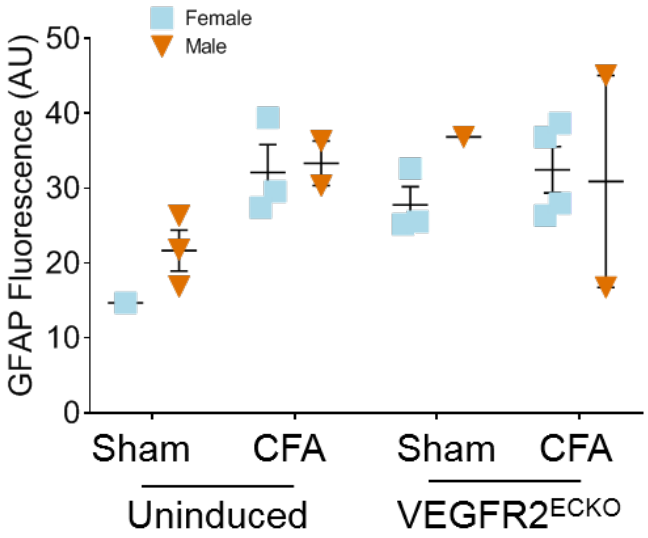


Figure 4.55: Sex differences in global dorsal horn GFAP signal after peri-articular CFA in the mouse. Uninduced: "wild type"; VEGFR2^{ECKO}: vascular endothelial growth factor endothelial cell knockout. Tissue processing and immunofluorescence performed by Dr Nick Beazley-Long (published in Beazley-Long et al. 2018b).

4.4 Discussion

These studies were designed to address the hypothesis that inhibition of VEGF-R2 function will result in altered inflammatory arthritis pain in rodents by blocking spinal and/or DRG gliovascular/neuroinflammatory interactions. This built on previous work in the lab in which VEGF-R2 endothelial cell specific knockout, and more than one VEGF-R blocker had reduced inflammatory pain in mice (Beazley-Long et al. 2018b).

In these studies, CFA induced a robust inflammatory response and caused significant pain behaviour, however this was only accompanied by glial alterations when using a high dose (100µg) of CFA made in-house after 10 days. The VEGF-R2 inhibitor, PTK787, and the anti-TNFα drug, etanercept, had no impact on pain behaviour or swelling when given alone, but therapeutic dosing of the two together resulted in a small reversal of hypersensitivity (Figure 4.33). A summary of the main experimental findings can be found in Table 4.6.

4.4.1 The Effect of VEGF-R2 and/or TNFα Inhibition on Pain

Previously in our lab, systemic PTK787 dosing at the time of induction of inflammation prevented the development of secondary pain in both ipsilateral and contralateral hindpaws (Beazley-Long et al. 2018b). In Study 2, the PTK787 prophylactic positive control was ineffective (Figure 4.22) as the PTK787 was a lower concentration than needed due to solubility problems, and had no functional effect against VEGF-R2 (as shown in the monocyte adherence assay, Figure 4.24). Study 1 used the same PTK787 vehicle as Study 2, and so it was assumed that the PTK787 used here was also inactive. However,

although the PTK787 results in Studies 1 & 2 are not reliable, conclusions can still be drawn from spinal cord histology (see below).

Study 3 used a different vehicle with no solubility issues. Additionally, the drug dosing regimen was modified so pain behaviour was measured the day immediately after dosing and received three doses by the end of the study. Here, PTK787 also had no impact on chronic pain development or maintenance (Figure 4.32). This lack of effect is in direct contradiction to previous results from our lab (Beazley-Long et al. 2018b) and in mice (Figure 4.52) where secondary pain development is prevented by VEGF-R2 inhibition. The half-life of PTK787 (with oral administration) is approximately 4-6h (Wood et al. 2000), therefore the PTK787 concentration achieved with this dosing regimen used may not be sufficient to prevent or reverse chronic pain. Additionally, previous studies have used higher doses of PTK787 (Hulse et al. 2016; Hulse et al. 2014; Schoenberger et al. 2004; Grosios et al. 2004; Wood et al. 2000), with one study determining an effective dose range above 45mg/kg daily (albeit via oral administration) (Wood et al. 2000; Schoenberger et al. 2004; Grosios et al. 2004), and so perhaps a higher dose would be effective at preventing pain.

Although completed in the same laboratory and conditions as the study by Beazley-Long and colleagues (2018b) where PTK787 prevented secondary pain development, PTK787 had no impact on pain here (Figure 4.32). One notable difference between the two studies is the sex of the investigators: the behavioural investigations carried out by Beazley-Long et al. (2018b) were done by a male investigator whereas I am female. Stress-induced pain inhibition has been demonstrated in rodents when pain behaviour is carried out by male investigators (Sorge et al. 2014), however, if this is the reason for the reduction in pain seen in Beazley-Long et al. (2018b), then analgesia should be seen across all experimental groups, including the CFA + vehicle group, and not just the treatment groups.

It could be that here, PTK787 was not successfully inhibiting VEGF-R2 due to a suboptimal dosing regimen or concentration (discussed above). PTK787 can access neural endothelial cells through the vasculature and as it can cross the BBB/BSCB (Remko et al. 2011), it should also be able to penetrate neural tissue. To investigate whether PTK787 was successfully inhibiting VEGF-R2, probing for phosophylated-VEGF-R2 could therefore be carried out on spinal cord tissue. Binding of VEGF-A to VEGF-R2 causes the receptor to autophosphorylate (resulting in phospho-VEGF-R2), initiating signalling cascades (Peach et al. 2018), and PTK787 disrupts this autophosphorylation (Wood et al. 2000). Therefore, probing of phospho-VEGF-R2 should give an idea of whether this process has been targeted (for example in Li et al. 2020). However, due to time and COVID19 restraints, this was not possible.

PTK787 pretreatment caused significantly more swelling in CFA animals compared to those receiving vehicle (Figure 4.9b). In our lab we found CFA-induced joint damage to be significantly worse in the endothelial cell-specific VEGF-R knockout mice (VEGF-

R2^{ECKO}) than in the wild-type controls (Sohail and Beazley-Long, unpublished data). However, upon investigation there was no difference in joint damage between treatment groups (Sohail, unpublished data). Therefore this effect is likely to be a false positive and due to the natural variation in CFA response.

As well as investigating the role of VEGF-A and its receptor, VEGF-R2, TNFα was also studied. Etanercept is an anti-TNFα drug approved for the treatment of RA (Haraoui and Bykerk 2007). Here, etanercept failed to have a significant impact on either weight bearing or swelling when given prophylactically (Figure 4.9). There was an apparent mild effect on mechanical sensitivity, weight bearing, swelling and hypersensitivity when given therapeutically in Study 2 but not in Study 3 (Figures 4.22 and 4.32 respectively). However, when investigated further, the extent of the swelling, weight bearing and von Frey data for the CFA + etanercept animals were all less pronounced than the CFA + vehicle animals, although not significantly (Figure 4.22), before they received any treatment at day 3. These animals had received the same treatments up to this point as other CFA animals (except the d0 PTK787 animals), meaning the etanercept's apparent effect on pain may be unrelated to the treatment and could be due to the normal variation in house-made CFA's response. Additionally, neither the mechanical thresholds for the etanercept, PTK787 or vehicle groups worsened from day 3 when expressed as change in 50% paw withdrawal threshold from day 3 (Figure 4.23), supporting the idea that etanercept had no real impact on hypersensitivity in this model.

In Study 2, all animals were randomly allocated into treatment groups before the study began, which serendipitously grouped in all the animals with a less severe response in the CFA + etanercept group. To avoid this, when the Study 3 was conducted, day 3 hypersensitivity data was independently unblinded and animals were assigned to treatment groups ensuring there was an even spread across these groups, rather than randomly assigning animals to treatment groups before the beginning of the study.

Etanercept has previously shown to reduce mechanical hypersensitivity in neuropathic pain when given prophylactically, but only sometimes when given therapeutically (Marchand et al. 2009; Schäfers et al. 2003; Sommer et al. 2001). In experimental arthritis, etanercept is generally effective, despite varying doses. For example, in Collagen-Induced Arthritis (CIA), therapeutic etanercept reduced arthritis score and inflammation when given at 5mg/kg either every other day or once a week (Gözel et al. 2018; Lon et al. 2011). In Antigen-Induced Arthritis (AIA) rats, a similar dose of 5.5mg/kg etanercept every 3-4 days reduced thermal and mechanical hypersensitivity, and moderately reduced swelling but did not fully resolve histological inflammation (Schaible et al. 2010; Boettger et al. 2008). In CFA-induced arthritis, therapeutic dosing of etanercept at a lower dose of 0.3-0.5mg/kg every other day was able to decrease swelling and thermal and mechanical hypersensitivity (Elsheemy et al. 2019; Inglis et al. 2005). Etanercept was expected to have an impact on both swelling and pain behaviour in these studies as the dosing regimens were comparable (5.5mg/kg, every 3-4 days). Etanercept has good penetration into arthritic tissue, with higher expose in arthritic tissue than in

non-inflamed tissue (Chen et al. 2015), so etanercept should be reaching the site of inflammation. However, etanercept's half-life in rats is 1.2–1.9 days (Lon et al. 2011), and so perhaps the concentration reached in these studies with dosing every 3-4 days was not enough to counteract severe inflammation induced by inter-articular CFA. Therefore if repeated, the dosing frequency could be increased. Alternatively, if the studies were allowed to continue past 2/10 days post-inflammation, effects of etanercept may emerge as many of the studies discussed above looked over a longer time-period of dosing (2 weeks).

When etanercept was given in combination with PTK787, hypersensitivity was significantly reversed by day 10 (when expressed as the change from day 3, Figure 4.33). This suggests that whilst PTK787 and etanercept could not alleviate secondary pain in isolation, they were able to work in tandem to partially reverse hypersensitivity. As discussed in Chapter 5, TNFα and VEGF-A are both increased in pain states, and are therefore interlinked in inflammation and pain development. In fact, TNFα can drive VEGF-A expression and splicing into VEGF-A$_{xxx}$a isoforms (Nowak et al. 2008). Through the blood, PTK787 and etanercept can reach neurovascular endothelial cells, and can both prevent "activation" of these cells by disrupting TNFα and VEGF-A signalling. Whilst PTK787 can cross the BBB, etanercept cannot, and so perhaps it is through their action on endothelial cells (and tissues in the periphery) combined with VEGF-R2 inhibition in the CNS that can overcome spinal hyperactivity and lead to analgesia. As no glial alterations were detected using immunofluorescence in Study 3, combined PTK787 + etanercept therapy had no window to reverse glial activation. Therefore, they are likely to be working in the periphery. Therapeutic etanercept was shown to reduce joint damage as well as VEGF and VEGF-R expression (unspecified as to which VEGF splicing and receptor variant) in CIA joints (Gözel et al. 2018), highlighting their combined role in joint inflammation and damage. However, no differences in swelling were identified here with this combined treatment (Figure 4.32), and when joint damage was assessed by a colleague (Sohail, unpublished data), there was no difference compared to CFA + vehicle. This suggests PTK787 + etanercept could be having an effect on peripheral nerves (or at the NVU) rather than directly reducing inflammation or joint damage. VEGF-Rs are present on neurones (both primary afferents and in the spinal cord) (Hamilton et al. 2016; Selvaraj et al. 2015; Hulse et al. 2014; Schaible 2014), making this a possibility. Future investigations into DRG and the Blood Nerve Barrier (BNB) could shed light on their combined action.

4.4.2 Spinal Gliovascular Alterations after CFA

The other aim of this study was to determine whether peripheral inflammation also causes acute gliovascular alterations within the spinal cord, and whether targeting VEGF-R2 could prevent these alterations. In the acute prophylactic study (Study 1) and the refined therapeutic study (Study 3), there were no central gliovascular alterations, as measured by increases in GFAP, CD11b, and ICAM-1 fluorescence, and number of

GFAP-positive vessels at days 2 and 3 respectively. However, Study 2 demonstrated an increase in GFAP signal intensity in the dorsal horn of the spinal cord at day 10 (Figure 4.25). The degree of GFAP intensity at day 10 was correlated with the ipsilateral knee diameter in the early phases (days 1 and 2) of CFA-induced inflammation (Figure 4.27a & b respectively). This suggests that spinal astrocyte changes are dependent on the initial response to injury. The lack of GFAP changes in the spinal cord in Study 3 are therefore surprising, especially since the lower CFA insult (50µg) caused significantly more swelling throughout the duration of the study (Figure 4.49a). Previously, this dose of intra-articular commercial CFA has caused astrocyte activation after 3 days when injected into the knee (Sun et al. 2008; Sun et al. 2007). This evidence suggests that 2 days post-intra-articular CFA is too early to detect astrocyte changes, but astrocyte activation was expected at day 10. In the mouse, increases in GFAP in the dorsal horn and at/associated with vessels are evident at 14 days after CFA (Figure 4.53), confirming that the analysis techniques used here are able to detect astrocytic alterations. Interestingly, knocking out endothelial VEGF-R2 increases basal GFAP signal in the dorsal horn before inflammation is induced, but peripheral inflammation does not increase GFAP further. This increase could be due to VEGF-R2^{ECKO} mice having aberrant microvessel morphology (Ved et al. 2018) causing ischaemia and astrocyte activation (see below).

Microglial activation generally occurs before astrocyte activation, with studies demonstrating microglial activation within the first 24 hours post-inflammation (Xu et al. 2014; Sun et al. 2007; Raghavendra et al. 2004). These microglial alterations can last for 11 days post-CFA (Beazley-Long et al. 2018b). Therefore, microglial activation was also expected at days 2 and 10 in these studies, but this was not observed the global intensity was measured (Figures 4.14b, 4.28 and 4.42). This could be due to a suboptimal analysis technique in detecting CD11b fluorescence. When plotted as the percentage of sections that demonstrated CD11b-positive structures (Figure 4.15), there was an increase in sections with CD11b-positive structures 10 days after CFA, which was reduced with combined PTK787 + etanercept treatment in Study 3 (Figure 4.15c). However, this was not seen in Study 2 (see limitations below). When comparing across studies, more sections showed CD11b-positive structures at 10 days than 2 days post-CFA. This is surprising as I would expect the sham animals to have a similar level. It could be that animals from Studies 2 & 3 had 2 weeks of injections (1 week of vehicle injections for habituation and 1 week of treatments), whereas those in Study 1 had only 1 week of injections. Repeated hindpaw saline injections have been demonstrated to cause increased swelling and hypersensitivity in the contralateral uninjured hindpaw (Levine et al. 1985; Denko and Petricevic 1978), which is suggestive of spinal activation. However, Intraperitoneal injections map to a different area of the spinal cord (thoracic 13/L1, (Takahashi et al. 2002)) whereas the majority of sections analysed in all studies were L3-5. The other difference between Study 1 and Studies 2 & 3 are that animals in Study 1 did not have mechanical sensitivity recorded and so did not receive repeated mechanical stimulation, but this is unlikely to be the reason for the disparity. Therefore

it is difficult to draw conclusions from these comparisons.

Norden and colleagues (2016) demonstrated glial activation and cytokine release preceded increases in microglial Ionized Calcium Binding Adaptor Molecule-1 (IBA-1) and astrocytic GFAP expression after peripheral inflammation, and so although expected glial activation was not detected here through immunofluorescence (except astrocyte activation in Study 2), it could still be occurring. Additionally, astrocytes and microglia undergo morphological changes (for example hypertrophy) when activated (Li et al. 2019; Ji et al. 2013; Tsuda et al. 2013; Ransohoff and Brown 2012) that may not be reflected through measuring intensity of immunofluorescence, and so in the future this could be investigated.

It should be noted that there are sex differences in microglial response to chronic pain (Mapplebeck et al. 2016). This will discussed below (Section 4.4.4.3).

Although not seen here, increases in the adhesion molecule, ICAM-1, have been demonstrated in brain regions from 3h post-peripheral inflammation (Huber et al. 2005), and in the spinal cord at days 8 and 11 (Beazley-Long et al. 2018b). The lack of ICAM-1 changes in these studies (and the surprising reduction in ICAM-1 intensity after CFA in Study 2, Figure 4.28) could be due to the analysis technique chosen. A manual count of ICAM-1-positive structures may be more appropriate (as was performed in Beazley-Long et al. 2018b). However, due to time constraints this was not carried out.

It is also possible that changes are occurring in regions other than those investigated here. Every effort is made during tissue processing to ensure the same spinal cord regions are probed, and here spinal cords were cut just below (Studies 2 & 3) or at (Study 1) the thickest part of the lumbar enlargement and sliced up the cord on a cryostat. The rationale for this was that in Studies 2 & 3, secondary pain from the foot was being measured and so the area of the spinal cord that corresponded to the foot (predominantly L4 and L5 (Takahashi et al. 2002; Takahashi and Nakajima 1996; Takahashi et al. 1994; Bajrović and Sketelj 1998)) was investigated. In Study 1, primary pain was investigated so the area of the spinal cord innervated by the knee was probed (L3 and L4, (Ivanavicius et al. 2004; Takahashi et al. 2002)). Using the rat spinal cord atlas (Watson et al. 2009), locations were estimated. 100% of spinal cord sections in Studies 2 & 3 and 96% in Study 1 were from L3-5 in the spinal cord (Table 4.4). However, it was difficult to accurately identify sections due to the difference in structures identified here and in the atlas, and so these should be used as an approximation only. As the majority of sections are in L3 & L4 in Study 1 and L4 in Studies 2 & 3, it is unlikely that areas with potential gliovascular changes are being excluded in analyses. In the future, other areas could be sectioned and probed, for example more from L3, to determine the response higher in the cord.

There is limited evidence for inflammation-induced angiogenesis (although there is some evidence for adult neurovascular angiogenesis in Multiple Sclerosis (MS) and motorneurone disease (Yamadera et al. 2015; Lengfeld et al. 2014; Kirk and Karlik 2003)),

but PTK787 has anti-angiogenic properties and treatment can reduce the number of established microvessels due to disrupting endothelial cell signalling (Wood et al. 2000). The vessel markers used in here allowed for simple investigation of blood vessel area, and so this was investigated. No changes in dorsal horn vessel area were detected, except in Study 2 where there was an increase with CFA (Figure 4.31). However, this may be due to the low numbers of sections in the Sham group. This is a fairly rudimentary measure of blood vessel density and was a retrospective measure. There are more sophisticated image capture and analysis techniques available, for example by acquiring 3D images and performing density and network analyses, but due to time, and a lack of evidence to support CFA or PTK787-induced changes in vessel density, these were not pursued.

Although not detected here, knocking out VEGF-R2 in endothelial cells in mice (VEGF-R2^{ECKO} mice) caused aberrant spinal cord microvasculature morphology, with decreased microvessel diameter and volume compared to control mice (Ved et al. 2018). VEGF-R2^{ECKO} mice also had an increase in the number of smaller microvessels. Ved and colleagues (2018) used 3D capture and Imaris software to quantify microvessel integrity, allowing fine investigation of both small (<8μm) and larger (8–12μm) microvessels. This supports the idea that the measurements used here (estimating vessel area from whole dorsal horn sections) are not sensitive enough to detect differences in vessel integrity. The functional consequences of smaller microvessels are ischaemia and may possibly have implications on nutrient and cell delivery. This could explain the increase in basal GFAP signal in the dorsal horn in these mice (Figure 4.53) as ischaemia can lead to astrocyte activation (Zamanian et al. 2012).

As discussed above, ZEB-1 is a transcription factor that causes endothelial cells to be more motile and invasive (Salajegheh and Salajegheh 2016). In neuropathic pain conditions there is an increase in ZEB-1 expression in the spinal cord and isolated microglia (Zhang et al. 2020; Shen et al. 2019; Yan et al. 2018a; Yan et al. 2018b), and we previously found there was an increase in ZEB-1 expression in perivascular cells after peripheral CFA in the mouse (Lopes and Beazley-Long, unpublished data). However, this increase was not in spinal endothelial cells (Lopes and Beazley-Long, unpublished data), meaning spinal endothelial cells may have a different ZEB-1 response to inflammation compared to non-spinal endothelial cells. Here, no change in global or perivascular ZEB-1 intensity in the spinal cord dorsal horn was detected, but this could be due to the lower dose CFA not initiating gliovascular alterations in the spinal cord. At a higher dose of CFA, a global and perivascular ZEB-1 increase is expected with no change in endothelial cells, in line with Lopes and Beazley-Long's finding above (unpublished data). This avenue requires more investigation, especially in light of the emerging role of spinal endothelial cells and the BSCB in chronic pain.

As there was a lack of central gliovascular alterations after CFA, the peripheral DRGs were investigated. Immune cell infiltration into the DRG plays an important role in chronic pain maintenance and development (Yu et al. 2020; Raoof et al. 2018). Due

to time limitations, only Study 1 L3 and L4 DRGs from sham and CFA + vehicle groups were investigated using CD68 as a marker. Here, no infiltrating macrophages were detected after 2 days of CFA inflammation DRG (Figure 4.20). Infiltrating macrophages have previously been demonstrated in inflammatory arthritis at 3 and 7 days post-induction, which could be attenuated by TNFα inhibition (Schaible et al. 2010; Segond von Banchet et al. 2009; Inglis et al. 2005), although none were detected at 8 days post-arthritis in our lab (Beazley-Long et al. 2018b). The adhesion molecules ICAM-1 and VCAM-1 were increased in DRG at 8/11 days and 3 days post-arthritis respectively (Beazley-Long et al. 2018b; Segond von Banchet et al. 2009). 2 days may be too early to detect infiltrating macrophages here, but mirroring these investigations in Studies 2 & 3 may have identified DRG changes at later timepoints, however, due to time and COVID19 constraints these investigations were not possible.

4.4.3 Differences in CFA Regimens

CFA was chosen to induce inflammatory monoarthritis as it a well-established model that induces a long-lasting and robust response (Donaldson et al. 1993; Butler et al. 1992). CFA is composed of heat-denatured *mycobacterium tuberculosis* suspended in mineral oil, which allows a sustained antigen release and causes an innate immune response (Billiau and Matthys 2001). Intra-articular CFA injection causes a localised and rapid inflammatory response that leads to swelling and a reduction in affected hindpaw use, which peaks after 48-72hr and begins to return to normal over 10 days (Beazley-Long et al. 2018b; Donaldson et al. 1993). At higher doses (above 150µg), there can be a second inflammatory phase that can also spread to contralateral joints (polyarthritis) (Cook and Moore 2006; Chillingworth and Donaldson 2003; Donaldson et al. 1993).

In these three studies, three different variations of the rat CFA inflammatory model were used. A summary of the differences in experimental outcomes between the three CFA regimens can be found in Table 4.7. Study 2 was performed first using 50µL of house-made CFA at 2mg/mL to give a final dose of 100µg, which gives a robust inflammatory response and has been used previously in our lab (Beazley-Long et al. 2018b). There are several welfare checks made on the animals over the course of the study to monitor the health and well-being of the animals, and to ensure severity limits are not reached by following humane endpoints. By 2 days post-injection, some of the animals in Study 2 were nearing the humane endpoints as described in the relevant Home Office Licence version, which highlighted lack of limb use for 48hr but not explicitly up to 72hr. After discussion with the Biomedical Support Unit (BSU) staff and the Project Licence holder, the decision was made to cull the affected animals and pause the study (the study was performed in two batches: some animals in the first batch were affected and so the second batch was postponed). A commercial CFA was sourced on the advice of the BSU staff as it was felt this would reduce any future variation in CFA response and the likelihood of endpoints being reached. In order to also complete Study 2 and

begin the second batch of animals, an amendment to the Licence was submitted to the Home Office to explicitly state reduced limb use up to 72hr. Whilst this amendment was going through, a short-term (2 day) study (Study 1) was carried out to investigate early gliovascular changes after inflammatory pain and the contribution of VEGF-Rs to the development of secondary pain using the commercial CFA. Commercial CFA is only available at a stock concentration of 1mg/mL, which is half the in-house CFA stock (2mg /mL), meaning a volume of 100µL needed to be injected to give the same dose of 100µg as the in-house CFA. 100µL is the maximum allowed volume for intra-articular injection in the rat. The larger volume caused significant swelling (Figure 4.9), which, when investigated, was significantly higher than the in-house 100µg CFA (Figure 4.49a). There was further concern that in longer studies animals that received 100µL of the commercial CFA might reach humane endpoints at 72hr as stipulated in the amended Licence, and so the decision was reluctantly made to reduce the volume and dose to 50µL and 50µg respectively for Study 3. However, upon comparison, the commercial CFA at half the dose still caused significantly larger knee diameters than the in-house CFA for the duration of the study (Figure 4.49a). Weight bearing data for these commercial CFA animals is also significantly different to the in-house animals (Figure 4.49b). This is somewhat surprising as the gliovascular alterations due to CFA seen with GFAP signal in the dorsal horn of the spinal cord in Study 2 (using 100µg in-house CFA) were not seen in Study 3 (50µg commercial CFA) (Figure 4.50, see below for discussion).

The in-house CFA was made from suspending heat-denatured *mycobacterium tuberculosis* (UK Ministry of Agriculture Fisheries and Food, now known as DEFRA, UK) in mineral oil. The commercial CFA is suspended in 85% paraffin oil (synonymous with mineral oil (Speight 2011)) and 15% mannide monooleate. Mannide monooleate is a lipophilic surfactant used as an emulsifying agent to aid the suspension of adjuvants in oil. Mannide monooleate can induce an immune reaction (Berlin and Wyman 1971; Berlin 1962) and enhance the immune response when in an emulsion (Van Doorn et al. 2016; Billiau and Matthys 2001). Commercial CFA may therefore be more immunopotent than the in-house CFA due to the presence of this surfactant, which would explain the significantly larger knee diameters seen in these animals (Figure 4.49a). However, if the commercial CFA is more immunopotent than the in-house CFA but fails to lead to spinal glial activation when the in-house did, this suggests that spinal activation with a low dose of CFA is not dependent on the peripheral immune reaction to the injury. It is likely that the reduction in the amount of CFA means the threshold for glial activation in the spinal cord is not being reached, despite there being significant swelling in the periphery.

Here, only indirect measures of arthritis (joint diameter and nociceptive threshold) were recorded. Joint circumference correlates closely with the histological state of the joint (Donaldson et al. 1993), but evaluation of joint destruction through scoring is able to accurately determine the extent of damage. This was very recently performed by a colleague, and there was no difference between CFA + treatment groups within studies

in terms of cartilage damage, synovial inflammation, pannus infiltration or fibrovascular tissue (Sohail, unpublished data). When comparing across CFA doses (between the in-house high dose and the commercial low dose) there were also no detectable differences in joint damage (Sohail, unpublished data). This is interesting considering the commercial low dose led to significantly larger knee diameters than the higher dose in-house CFA. It could be that the histological scoring technique used here reached a ceiling and was therefore unable to detect a more severe phenotype in the commercial low dose. Alternatively, the increase in knee diameter with the low dose may be due to oedema that does not lead to worsening joint damage/does not correlate with joint histological score. In support of this, when investigated further, cartilage damage score was positively correlated to knee diameter at day 10 with the high dose in-house CFA ($r = 0.9272$, $p < 0.01$), whereas it was not with the low dose commercial CFA ($r = -0.6453$, $p = 0.1664$, Figure 4.56).

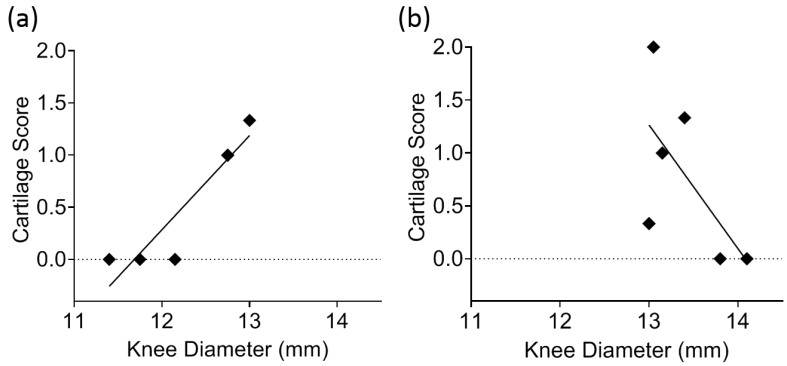


Figure 4.56: cartilage damage score was positively correlated to knee diameter at day 10 with the high dose in-house CFA (**a**, $r = 0.9272$, $p < 0.01$), whereas it was not with the low dose commercial CFA (**b**, $r = -0.6453$, $p = 0.1664$). Pearson R correlation test. Joint preparation, histology and cartilage scoring was performed by Roheena Sohail (unpublished).

What this data does highlight is that reducing the dose to 50µg from 100µg had no impact on the extent of joint damage (or pain), but prevented glial activation in the spinal cord. Therefore, in terms of animal welfare there was no difference between doses, and lowering the dose actually prevented outcome measures, meaning the model had been over-refined and was no longer useful for these investigations.

4.4.4 Limitations

4.4.4.1 Low Group Numbers

There are limitations in drawing conclusions from histology data in Study 2 due to the low number in groups. Licence issues we faced during Study 2 meant there was a long length of time between beginning Study 2 and processing the tissue for histology (over 1 year). This meant that some of the tissue resulted in poor histology quality, giving low numbers for the gliovascular investigations in the sham and CFA + vehicle groups. Therefore these results are less reliable and the conclusions reached about

these gliovascular alterations are less robust than higher powered studies. However, because spinal gliovascular alterations, namely increases in GFAP signal, are expected and well-known to occur after inflammation (Ji et al. 2019), I am confident the significant increase in GFAP seen here (Figure 4.25) is representative of what is going on. I am less confident about the CD11b results indicating that 100% of sham animals had CD11b-positive structures, and that there was no change after CFA (Figure 4.15), as this is contrary to what is in the literature (Ji et al. 2013). Furthermore, in Study 3, there is an increase in the number of sections with positive CD11b structures with CFA (which is reduced by treatment with PTK787 + etanercept, Figure 4.15), suggesting this should be mirrored in Study 2. It is therefore difficult to draw reliable conclusions from CD11b data from Study 2. Additionally, as discussed above, limited conclusions can be drawn from PTK787 results from Studies 1 & 2 due to issues with solubility.

4.4.4.2 Using GFAP as an Astrocytic Marker

Whilst GFAP remains a common marker for astrocytic labelling, it has limitations. GFAP does not label all astrocytic branches and processes (Ji et al. 2013), and not all astrocytes actually express GFAP (Cahoy et al. 2008). Therefore, GFAP labelling underrepresents the size and number of astrocytes, but considering astrocytes are heterogeneous with a varied gene expression during reactive astrogliosis (Zamanian et al. 2012), multiple markers would be needed to investigate the whole astrocytic response, for example Aquaporin-4 (AQP4), Lipocalin-2 (LCN2) and Serine Protease Inhibitor A3N (SerpinA3N) (Liddelow et al. 2017; Zamanian et al. 2012), which is beyond the scope of this thesis. Nevertheless, astrocytic expression of GFAP remains important in the context of pain as it has repeatedly been found to be increased in painful conditions (Ji et al. 2019), making it a reliable and comparable marker. Additionally, mice that lack the *Gfap* gene had a shorter duration of pain than their wild type counterparts (Kim et al. 2009).

4.4.4.3 Sex-Differences

Here, only male rats were used in all *in vivo* studies, but there have been notable sex-differences in pain research, particularly in some of the glial responses to pain (Chen et al. 2018a; Taves et al. 2015). The microglial response to chronic pain is well-known to be different between sexes (Mapplebeck et al. 2016), with microglial inhibitors being effective at reducing pain in inflammatory and neuropathic models in male mice, but not in female mice (Chen et al. 2018a; Taves et al. 2015; Sorge et al. 2015). T-cell involvement appears to be more important than microglial activation in female mice (Raoof et al. 2018; Rosen et al. 2017). Future studies should mirror these investigations in female rats, especially those regarding microglial activation and immune cell infiltration. In the mice, both female and male mice were investigated, and no differences in global dorsal horn astrocyte activation were detected, suggesting astrocytes are important in pain development in both sexes.

These sex differences are also apparent in painful conditions in humans. For example, Monocyte Chemoattractant Protein 1 (MCP1) and IL-8 were elevated in Cerebrospinal Fluid (CSF), indicating neuroinflammation, and MCP1 levels were positively correlated across CSF, serum and synovial fluid in female but not male patients with Osteoarthritis (OA) (Kosek et al. 2018). Additionally, female patients have a worse RA disease progression than males (Vollenhoven 2009).

Male rats were used in all these studies due to time constraints and because work carried out was early work within the gliovascular-pain field. Additionally, the oestrus cycle in females causes hormone fluctuations that may interact with pain signalling and experimental outcomes (Becker et al. 2005a; Craft et al. 2004). Once the roles of neural endothelial cells and VEGF-A/VEGF-R2 (and TNFα) in the contribution of chronic pain development/maintenance are more well-established, work should be repeated in female rats, especially considering chronic pain is more prevalent in women than men (Rosen et al. 2017).

4.4.5 Conclusion

In conclusion, gliovascular changes were only detected in the later stages (10 days) after high dose CFA, which were correlated with knee diameter in the early stages. Low dose CFA did not cause any detectable gliovascular alterations, despite causing significant increases in knee diameter. This highlights the importance of ensuring that animal models are not over-refined to the point where research and study outcome measures (gliovascular alterations here) are lost. Neither therapeutic nor prophylactic dosing of the VEGF-R2 blocker, PTK787, and/ or etanercept had any impact on gliovascular alterations, but a combination of both partially reversed secondary pain 10 days after CFA. This suggests that both TNFα and VEGF-A are important factors in the maintenance of secondary pain, and as both are approved clinical pharmaceuticals, their synergistic effect is an attractive drug research avenue. VEGF-R blockade with PTK787 and TNFα inhibition with etanercept could be working together through suppression of endothelial cell activation to reduce downstream glial and neuronal activation and secondary pain. PTK787 could also be inhibiting VEGF-A signalling in neurones and glial cells whilst etanercept works in the periphery to inhibit TNFα. In order to test these hypotheses, *in vitro* techniques could probe the endothelial-glial relationship in response to inflammatory mediators that are known to increase in inflammatory pain. To study neuronal VEGF-A signalling, models using a neuronal VEGF-R2 knockdown mouse line or electrophysiology could be used. Although not demonstrated in isolation here, VEGF-A is clearly an important mediator in the development and maintenance of chronic pain, and further work is required to fully understand its role.

Study	Species	CFA Dose (Study Length)	Commercial or In-House	Treatments	CFA-Induced Gliovascular Alterations? Spinal cord Astrocytes (GFAP)	Microglia (CD11b)	ICAM-1	DRG Infiltrating Monocytes (CD68)	Drug Treatment Effect on Pain Behaviour? Mechanical Threshold	Weight Bearing	Knee Diameter
1	Rat	100µg in 100µL (2 days)	Commercial	Prophylactic Vehicle/PTK/ Etan	× 4.10	× 4.14b	× 4.16	× 4.20	× -	× 4.9a	× 4.9b
2	Rat	100µg in 50µL (10 days)	In-house	Therapeutic Vehicle/PTK/ Etan	✓ 4.25	× 4.28a	× 4.28b	-	× 4.22a & b	× 4.22c	× 4.22d
3	Rat	50µg in 50µL (10 days)	Commercial	Therapeutic Vehicle/PTK &/or Etan	× 4.34, 4.38 & 4.41	× 4.42	× 4.44	-	✓PTK&Etan 4.32a&4.33	× 4.32c	× 4.32d
4	Mouse	2x 80µg in 40µL (14 days)	In-house	Prophylactic R2 KO	✓ 4.53	✓ 1	✓ 1	× 1	✓R2 KO 4.53	✓ 1	× 1

CD11b: Cluster of differentiation 11b; **CD68**: Cluster of differentiation 68; **CFA**: Complete Freund's adjuvant; **DRG**: Dorsal root ganglion; **Etan**: Etanercept; **GFAP**: Glial fibrillary acidic protein; **ICAM-1**: Intracellular adhesion molecule 1; **PTK**: PTK787; **R2 KO**: Endothelial cell vascular endothelial growth factor receptor 2 knockout. 4.x: Figure reference; 1, Beazley-Long et al. 2018b. ✓detected; × not detected; - not investigated.

Table 4.6: Summary of *in vivo* experimental findings.

Study	CFA Dose (Study Length)	Pain Behaviour				Spinal Cord Astrocyte Activation?	
		Mechanical Threshold Decrease	Weight Bearing Asymmetry	Knee Diameter Increase	Knee Diameter Correlated to Cartilage Score	Increase in GFAP	Correlated to Knee Diameter
1	Commercial 100µg in 100µL (2 days)	-	++ 4.49	+++	- 4.10	×	-
2	In-House 100µg in 50µL (10 days)	+	++ 4.49	++	✓at day 10 4.56a	✓ 4.50	✓at 1&2 days 4.27
3	Commercial 50µg in 50µL (10 days)	+	+ 4.49	+	× 4.56b	× 4.50	× 4.36

CFA: Complete Freund's adjuvant; **GFAP**: Glial fibrillary acidic protein. 4.x: Figure reference. + refers to the degree of change from control, with + being the smallest change and +++ being the largest. ✓detected; × not detected; - not investigated.

Table 4.7: Summary of effect of CFA dose on experimental outcomes.

5 | In Vitro Models of Endothelial Cell Activation Using VEGF-A and TNFα

5.1 Introduction

The previous chapter dealt with gliovascular responses to peripheral inflammation and used pharmacological interventions to investigate receptor contributions in the whole animal. In order to determine and pinpoint specific mechanisms, functional assays need to be employed. There are several *in vivo* techniques that allow functional measurements using transgenic mice. For example, inducible knockout mice can be used to study specific receptor or cell contributions to chronic pain development, such as with the inducible endothelial *vegfr2* knockout mice used in this thesis and in Beazley-Long and colleagues (2018b). Alternatively, reporter "knock-in" mice can be used to investigate several functions of cell and receptor activity when combined with *in vivo* imaging (Li et al. 2018a; Li et al. 2018b; Maggi et al. 2004). However, these *in vivo* techniques can be costly and complex, whereas *in vitro* models are generally cheaper and simpler whilst allowing specific mechanistic investigation in controlled environments. An *in vitro* approach was taken using functional assays to study the gliovascular interactions seen in *in vivo* systems.

Brain and spinal cord endothelial cells form the walls of blood vessels and are the first line of defence in the Neurovascular Unit (NVU), so their proper functioning has an impact on barrier efficacy. By measuring expression of tight junction proteins and adhesion molecules after insults, barrier health can be inferred, for example expression of occludin, Zona Occludens-1 (ZO-1) and claudin-5 can be detected through Western Blotting or immunohistochemistry (Varatharaj and Galea 2016; Wu et al. 2016; Lim et al. 2014; Echeverry et al. 2011; Huber et al. 2002; Huber et al. 2001). These can be measured in the whole organism, but as mentioned above, *in vitro* models allow isolated investigation and specific mechanisms to be probed. There are sophisticated Blood Brain Barrier (BBB) and Blood Spinal Cord Barrier (BSCB) models that incorporate endothelial cells and several other cells in the NVU (Stone et al. 2019; Herland et al. 2016; Martínez-Estrada et al. 2003), but at the most basic level, monolayers of brain or spinal cord endothelial cells can be targeted to study endothelial cells in isolation. By stimulating endothelial cells with known chronic pain-associated inflammatory molecules, endothelial cell-specific responses can be measured through protein and gene expression, and functional mechanisms can be studied, for example measuring monocyte binding to endothelial cells (Beazley-Long et al. 2018b; Thichanpiang et al. 2014). As endothelial cells are key components of the NVU, and have been shown to directly impact chronic pain development and associated glial alterations (Beazley-Long et al. 2018b), these cells were first chosen to establish *in vitro* assays for mechanistic

studies, with the aim of moving to co-cultures once optimised.

Changes in tight junction expression (as a result of pain or injury) can lead to increased permeability to blood-borne cells and molecules, altering the neural microenvironment and potentially leading to neural and glial activation (Zhao et al. 2015b). There is some evidence for immune cell infiltration into the spinal cord and Dorsal Root Ganglion (DRG) after insults. For example, in neuropathic pain, infiltrating macrophages in the DRG and spinal dorsal horn can contribute to both the initiation and the maintenance of chronic pain (Yu et al. 2020; Peng et al. 2016). Additionally, some studies have demonstrated that bone marrow-derived macrophages/monocytes can migrate into spinal cord parenchyma and differentiate into microglia and play a role in chronic pain development after nerve injury (Echeverry et al. 2011; Zhang et al. 2007), although this is not always detected (Guimarães et al. 2019; Tashima et al. 2016). Peripherally circulating leukocytes are able to cross the BBB and BSCB through (transceullular) or between (paracellular) endothelial cells (Wittchen 2009). Ligands expressed on leukocytes interact with selectins on endothelial cells, which increase exposure of leukocytes to endothelial chemokines. These chemokines can activate leukocyte integrins to cause a conformational change and increase leukocyte binding (Lawson and Wolf 2009). Leukocytes then migrate along and firmly attach to the endothelium through binding to adhesion molecules, for example Intracellular Adhesion Molecule-1 (ICAM-1), which initiates either transcellular or paracellular migration (Reglero-Real et al. 2012; Lawson and Wolf 2009). The adhesion molecules, ICAM-1 and Vascular Cell Adhesion Molecule-1 (VCAM-1) are constitutively expressed in low levels on the endothelial cell surface, and are upregulated during inflammation (Reglero-Real et al. 2012; Wong and Dorovini-Zis 1995; Dustin et al. 1986). By modelling monocyte attachment and transmigration in 'activated' endothelial cell cultures, specific mechanisms can be investigated. The monocyte attachment assay is a simple technique that allows probing of these mechanisms (Beazley-Long et al. 2018b; Thichanpiang et al. 2014), and was employed here.

Two key inflammatory mediators were chosen to study brain microvascular endothelial-specific responses: Tumour Necrosis Factor α (TNFα) and Vascular Endothelial Growth Factor (VEGF)-A. TNFα is an inflammatory cytokine that acts on the Tumour Necrosis Factor Receptor (TNFR) and can enhance glutamate-induced excitatory currents in neurones (Kawasaki et al. 2008b). As well as neuronal actions, TNFα can also induce glial activation (Koyama 2014), and act on endothelial cells to cause reduced expression of tight junctions and increased permeability to blood-borne cells and molecules (Zhang et al. 2019; Daniels et al. 2014; Förster et al. 2008; Didier et al. 2003; Mark and Miller 1999). TNFα is released by cells within the NVU such as astrocytes, microglia, and pericytes during neuroinflammation, and has been implicated in chronic pain (Ji et al. 2018; Rustenhoven et al. 2017; Leung and Cahill 2010). TNFα can induce the release of further inflammatory molecules such as Interleukin (IL)-6, Interleukin-1β (IL-1β) and VEGF-A by glial cells and endothelial cells (Zhang et al. 2019; Lee et al. 2017; Varatharaj

and Galea 2016; Ji et al. 2013), meaning endothelial cells themselves can contribute to neuroinflammation and central sensitisation seen in chronic pain. Similar to, and related to, TNFα (Nakahara et al. 2003), VEGF-A is a key mediator in chronic pain and its signalling has been implicated in the development of chronic secondary pain (Llorián-Salvador and González-Rodríguez 2018; Beazley-Long et al. 2018b; Hulse et al. 2016; Hamilton et al. 2016; Hulse et al. 2014; De Bandt et al. 2003). VEGF-A splice variants are upregulated in peripheral nerves, DRGs and the spinal cord in chronic pain and neuroinflammation (Lee et al. 2019; Kiguchi et al. 2014; Argaw et al. 2012; Lin et al. 2010; Kirk and Karlik 2003), and can be released by astrocytes, immune cells and endothelial cells (Lee et al. 2019; Kiguchi et al. 2014; Argaw et al. 2012). VEGF-A, and specifically the splice variant VEGF-A_{165}a, causes BBB permeability and angiogenesis through its activation of Vascular Endothelial Growth Factor Receptor (VEGF-R)2 on endothelial cells (Peach et al. 2018; Argaw et al. 2012; Holmes et al. 2007; Croll et al. 2004; Proescholdt et al. 1999; Dobrogowska et al. 1998). VEGF-A increases permeability of vessels and endothelial cells by down-regulating tight junction proteins such as VE-cadherin, claudin-5 and occludin, and enhances immune cell trafficking into the Central Nervous System (CNS) through increased expression of adhesion molecules (Argaw et al. 2012; Argaw et al. 2009; Gavard and Gutkind 2006; Heil et al. 2000; Proescholdt et al. 1999; Lu et al. 1999). VEGF-A can also activate Signal Transducer and Activator of Transcription-3 (STAT3) and other inflammatory pathways, leading to further VEGF-A release and the release of other pro-inflammatory molecules such as IL-6 (Gao et al. 2017; Bartoli et al. 2003).

As well as being increased within the neural parenchyma, both TNFα and VEGF-A are elevated in the plasma of arthritic rats and patients with Rheumatoid Arthritis (RA) (Totoson et al. 2016; Wei et al. 2015; Nakahara et al. 2003), so are therefore important mediators in pain and endothelial health. If circulating TNFα and VEGF-A are increased, they will have direct access to CNS endothelial cells, meaning endothelial cells can be exposed to TNFα and VEGF-A on both the luminal (blood) and abluminal (neural) side. Therefore, as well as increasing permeability in the microvessels and allowing infiltration of blood-borne cells and molecules to the parenchyma, TNFα and VEGF-A have the ability to "activate" endothelial cells (also termed "endothelial dysfunction") to release signalling molecules that may go on to activate both neurones and glial cells. This endothelial activation/dysfunction could contribute to, and perhaps even help to initiate, spinal activation and central sensitisation seen in chronic pain. In support of this, patients with RA show signs of and markers for endothelial dysfunction, such as increased endothelial cell expression of cellular adhesion molecules and inflammatory molecules (Yang et al. 2016; Chimenti et al. 2015). Additionally, elevated levels of cytokines (including TNFα) have even been found in the serum of pre-symptomatic RA patients (Kokkonen et al. 2010).

Endothelial cells clearly play a key role in RA and chronic pain, and this is supported by a study from our lab demonstrating how endothelial signalling contributes to chronic

pain development and associated glial activation (Beazley-Long et al. 2018b). I theorised that their contribution is through endothelial activation resulting in downstream glial alterations that ultimately contribute to neuronal sensitisation and increased pain signalling. Although the endothelial response to inflammatory mediators has been well investigated, the endothelial response and its downstream effects on glial (and neuronal) activity within the context of pain has not been clearly defined. Namely, it is not known whether endothelial alterations and activation precede neuronal and glial activation or are a result of neuroinflammation and gliosis. It is therefore important to study the endothelial response to certain inflammatory molecules known to be increased in RA and neuroinflammation in order to begin to answer these questions. As mentioned above, *in vitro* models allow for finer investigation of cell-specific responses, but it is important to choose the correct model and assay. As endothelial cells from distinct organs differ (Kalucka et al. 2020), using neural-specific endothelial cells is key when modelling the neurovasculature. Immortalised cells can differ significantly from their primary counterparts, for example immortalised brain endothelial cells exhibit lower Transendothelial Electrical Resistance (TEER) (a measure of ionic permeability) than primary brain endothelial cells (Weksler et al. 2005), and may actually be misindentified as a result (Alston-Roberts et al. 2010). Low passage primary cells are gold standard when studying cell responses as cell phenotype may change in higher passages (Kapałczyńska et al. 2018; Nestor et al. 2015). For these reasons, Human Brain Microvascular Endothelial Cells (HBMECs) were sourced; HBMECs were used rather than spinal cord endothelial cells due to the limited availability of the latter. Spinal cord endothelial cells have a comparable phenotype to brain endothelial cells, but are more permeable, perhaps due to their lower expression of some tight junction proteins (for example, ZO-1, occludin, β-catenin and VE-cadherin) (Watson et al. 2013; Ge and Pachter 2006).

The *in vitro* models used here investigated endothelial-specific responses to inflammatory mediators, such as VEGF-A and TNFα, with the aim of developing these assays into co-cultures with astrocytes and/or neurones in the future. This chapter aimed to address the unknowns highlighted in Section 1.4 and Figure 1.8 (in particular points 1, 3 and 4).

Hypothesis

Application of TNFα and VEGF-A will increase monocyte-like cell binding to HBMECs, whilst reducing tight junction protein expression and increasing expression of adhesion molecules in HBMECs.

Objectives

- To investigate the effects of TNFα and VEGF-A on Human Monocyte-like Cells (THP-1) binding to endothelial cells.

- To measure endothelial expression of key junction and adhesion proteins (Cluster of Differentiation-31 (CD31), claudin-5, ZO-1, ICAM-1 and VCAM-1) in response to TNFα and VEGF-A exposure.

5.2 Materials & Methods

5.2.1 Cell Culture

Higher Passage (p)27+ HBMECs were a kind gift from Dr Paul Smith (University of Nottingham). p1 HBMECs were purchased from ScienCell (ScienCell Research Laboratories, 1000, lot #20978). HBMECs were cultured at 37˚C in culture medium (see Section 2.3 for details). ScienCell HBMECs were cultured on fibronectin-coated (2µg/cm^2, Sigma-Aldrich, F1141) flasks according to ScienCell's recommended culture conditions, whereas higher passage HBMECs were not. Human Umbilical Vein Endothelial Cell (HUVEC) (p5) cDNA was a kind gift from Dr Andy Benest. HUVEC protein (p5) was a kind gift from Dr Samuel Bestall.

Free-floating THP-1s (Sigma, 88081201) were cultured in culture medium (see Section 2.3 for details) at 37˚C.

Stock concentration of TNFα (R&D Systems) was at 100µg/mL in sterile Phosphate Buffered Solution (PBS), and VEGF-A_{165}a (R&D Systems) at 10µg/mL in sterile PBS.

Cells were counted using a haemocytometer.

5.2.2 The Monocyte Attachment Assay

When endothelial cells become activated by inflammatory mediators they can increase binding of circulating leukocytes, which can be modelled *in vitro* (Thichanpiang et al. 2014). I used this process in the monocyte attachment assay to try to investigate mechanisms in the neural endothelial response during inflammation.

The monocyte attachment assay is detailed in Section 2.3.1. Briefly, HBMECs were plated in 96 well plates either with (low passage ScienCell HBMECs according to ScienCell's recommended culturing conditions) or without (higher passage HBMECs) fibronectin coating (2µg/cm^2). Additionally, there were two control groups: a "no HBMEC" group where no HBMECs were seeded but THP-1s were added; and a "no THP-1" group where HBMECs were seeded but no THP-1s were added. The "no HBMEC" group was used to control for THP-1 binding to plates and the "no THP-1" group was used to control for background fluorescence. Higher passage HBMECs were serum starved the same day as seeding whereas ScienCell HBMECs were left to grow for 2-3 days until confluence to increase cell coverage before serum starving (see Figure 5.5). Cells were serum starved in 1% Foetal Bovine Serum (FBS) overnight then pretreated with recombinant human TNFα (0, 0.2, 2, or 20ng/mL) or VEGF-A_{165}a (0, 1, 10, 40, or 100ng/mL) in for 24 hours.

If required, a blocking ICAM-1 antibody (100ng/mL, ThermoFisher, MA5407) or its concentration and species-matched Immunoglobulin G (IgG) (100ng/mL, mouse IgG, Novus Biologicals, NBP1-97019) was added with TNFα or VEGF-A_{165}a treatment and again at the time of monocyte HBMEC co-culture. THP-1s were fluorescently tagged with 2.5μM Calcein-AM (Sigma-Aldrich, 17783) and added to the HBMEC monolayer for attachment. If blocking ICAM-1 antibody treatment was required, this was added again with the monocytes. Unattached monocytes were washed off with and monolayers were fixed with 4% Paraformaldehyde (PFA). Calcein fluorescence was measured on a fluorescence plate reader (VictorX4, Perkin-Elmer or CLARIOstar, BMG LABTECH). Some THP-1s stuck to the empty wells, so to ensure only the fluorescence of THP-1s adhering to HBMECs were measured, HBMECs were washed until the level of fluorescence in the "no HBMEC" wells equalled that of the "no THP-1" wells (i.e. all non-HBMEC adhering THP-1s were washed off). Alternatively, if wells were coated with fibronectin, the "no HBMEC" control was not included as the monocytes adhere to the coating (see Figure 5.1), and so wells were washed 4x and fluorescence was read. The level of HBMEC confluency was investigated to ensure that increased THP-1s binding from TNFα or VEGF-A treatment was not due to cell shrinkage and increased fibronectin exposure (i.e. that a change in THP-1 binding was due to HBMEC adherence and not due to adherence to fibronectin).

Data shown are corrected for background values by subtraction of the mean fluorescence value of the "no THP-1" control group. Data are either expressed as the raw fluorescence values, or the mean fluorescence value of the untreated group (without TNFα or VEGF-A_{165}a stimulation) is also subtracted and expressed as a percentage of the maximal mean response (set at 100%) to account for variability in raw fluorescence.

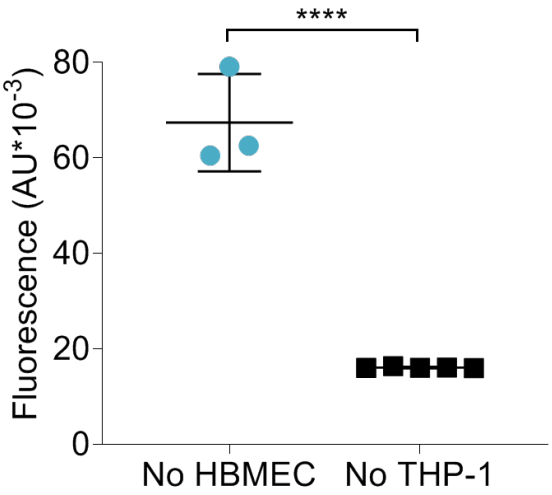


Figure 5.1: THP-1s adhere to the fibronectin coating in the "No HBMEC" control group, making the fluorescence in this group significantly higher than the "No THP-1" control group. ****p<0.0001, Unpaired t test. n = 1 plate.

5.2.3 Immunofluorescence

To investigate whether treatment had an effect on HBMEC shrinkage, some plates were labelled with Hoechst and Phalloidin-conjugates to detect cell nuclei and actin filaments respectively, as described in Section 2.3.2. See Tables 5.1 and 5.2 for detailed information on antibodies.

Images were captured on a confocal microscope (Leica TCS SPE, Leica Microsystems), fluorescence intensity and cell coverage were measured using FIJI Image J software (National Institutes of Health, USA, see Section 5.2.6). Cell coverage was determined by manually thresholding the Phalloidin image to create a binary image. This allowed the percentage of area of Phalloidin signal to be calculated. A semi-automated Image J macro was developed for this analysis (see Appendix A.3.7).

Identifies	Antibody	Host	Supplier	Product Number	Working Concentration
ICAM-1	ICAM-1	Mouse	ThermoFisher	MA5407	2µg/ml (WB) 100ng/ml (MA)
-	IgG	Mouse	Novus Biologicals	NBP1-97019	100ng/mL
VEGF-R2	VEGF-R2	Rabbit	Cell Signalling Technology	2479	1:200
Actin Filaments	β-actin	Goat	Santa Cruz	sc1615	0.5µg/ml

ICAM-1: intracellular adhesion molecule-1; **IgG**: Immunoglobulin; **MA**: Monocyte Attachment; **VEGF-R2**: vascular endothelial growth factor receptor 2; **WB**: Western Blot.

Table 5.1: Details of primary antibodies

Target	Host	Fluorophore	Supplier	Product Number	Working Concentration
α-Goat	Donkey	IRDye® 680CW	LI-COR	926-68074	0.2µg/ml
α-Mouse	Donkey	IRDye® 800CW	LI-COR	926-32212	0.2µg/ml
α-Rabbit	Donkey	IRDye® 680RD	LI-COR	926-68073	0.2µg/ml
F-Actin	Phalloidin-conjugate	AF® 488	ThermoFisher	A12379	1:500
Hoeschst-543334		-	Sigma	-	1µg/ml

AF: Alexa Fluor®

Table 5.2: Details of secondary antibodies

5.2.4 Western Blotting

Western blotting was used to investigate p31 HBMECs protein expression with or without TNFα and VEGF-A_{165}a treatment from 80-90% confluent monolayers. Full methods are described in Section 2.3.3. Primary antibodies used were anti-ICAM-1 (2µg/mL) and anti-VEGF-R2 (1:200), with anti-β-actin antibody (0.5µg/ml) used as a loading control. Secondary antibodies were IRDye® 680RD donkey anti-rabbit IgG, IRDye® 800CW donkey anti-mouse or IRDye® 800CW donkey anti-Goat IgG, all at 0.2µg/mL. Details of antibodies are in Tables 5.1 and 5.2.

5.2.5 cDNA Generation and Amplification

HBMEC RNA was isolated from 80-90% confluent cultured p31 or p2 cells in clear, flat bottom 6-well plates (Corning® Costar®, CLS3516) and cDNA generated as described in Sections 2.3.4 and 2.3.5.

Conventional Polymerase Chain Reaction (PCR) was used to amplify cDNA as detailed in Section2.3.5. See Table 5.3 for information on primers. PCR cycles followed the general protocol: Initial denaturation: 94˚C for 2min; Denaturation step: 94˚C for 30-60s; Annealing temperature for 30-60s; Extension step: 72˚C for 1min per 1000bp of PCR product; Final Extension: 72˚C for 5 min. Bands were visualised on 1.5% agarose gels and imaged on Bio-Rad Gel Doc EZ and Image Lab™ Software.

Gene	Forward/ Reverse	Sequence	Product Size (bp)
CD31	F	ATTGCAGTGGTTATCATCGGAGTG	141
	R	CTCGTTGTTGGAGTTCAGAAGTGG	
Claudin-5	F	CTGTTTCCATAGGCAGAGCG	302
	R	AAGCAGATTCTTAGCCTTCC	
GAPDH	F	CAACTACATGGTTTACATGTTC	260
	R	GTGTCTCCTTCTTTGACACT	
ICAM-1	F	GGCCTCAGTCAGTGTGA	217
	R	AACCCCATTCAGCGTCA	
IL10R	F	CTCCATCTCCAACTGTAGCCAGAC	301
	R	GGCAATCTCATACTCTCGGAAGTG	
IL1R1	F	ACACATGGTATAGATGCAGC	300
	R	TTCCAAGACCTCAGGCAAGA	
IL6R	F	CATTGCCATTGTTCTGAGGTTC	251
	R	AGTAGTCTGTATTGCTGATGTC	
STAT3	F	GGAGGAGTTGCAGCAAAAAG	322
	R	TGTGTTTGTGCCCAGAATGT	
VCAM-1	F	ATGACATGCTTGAGCCAGG	302
	R	AAGCAGATTCTTAGCCTTCC	
ZO-1	F	TGGAGCTGCGCTTACCAC	339
	R	AGCCAATACCAACAGTCCCG	

CD31: cluster of differentiation 31; **GAPDH**: Glyceraldehyde 3-phosphate dehydrogenase; **ICAM-1**: intracellular adhesion molecule-1; **IL10R**: Interleukin 10 receptor; **IL1R1**: Interleukin 1 receptor 1; **IL6R**: Interleukin 6 receptor; **STAT3**: signal transducer and activator of transcription 3; **VCAM-1**: vascular cell adhesion molecule-1; **ZO-1**: zona-occludens-1.

Table 5.3: Sequence of PCR Primers

5.2.6 Statistical Analysis

Data are presented as scatter plots with the mean ± Standard Deviation (SD) shown. Analysis of data was performed using GraphPad Prism (versions 7.01/7.05/8.4.3 for Windows, GraphPad Software, San Diego, California USA), and all tests performed are specified in relevant results.

5.3 Results

5.3.1 The Monocyte Attachment Assay Can Be a Useful Tool to Study Functional Endothelial Responses to Inflammatory Molecules

TNFα is upregulated during acute and chronic pain states (Ji et al. 2013), and acts on endothelial cells to increase permeability and adhesion molecule expression (Mark and Miller 1999; O'Carroll et al. 2015). I therefore tested TNFα's ability to elevate monocyte adherence to HBMECs. There was a concentration-dependent increase in THP-1 attachment to late passage (p34) HBMECs (Figure 5.2). In p25 and p28 HBMECs, TNFα caused a significant increase in THP-1 binding, but this was not concentration-dependent (Figure5.3a & c respectively). VEGF-A_{165}a at 10ng/mL failed to enhance adhesion (Figure 5.2), contrary to previous results obtained in the laboratory (with these cells at p20-24) and others (Beazley-Long et al. 2018b; Avraham et al. 2003).

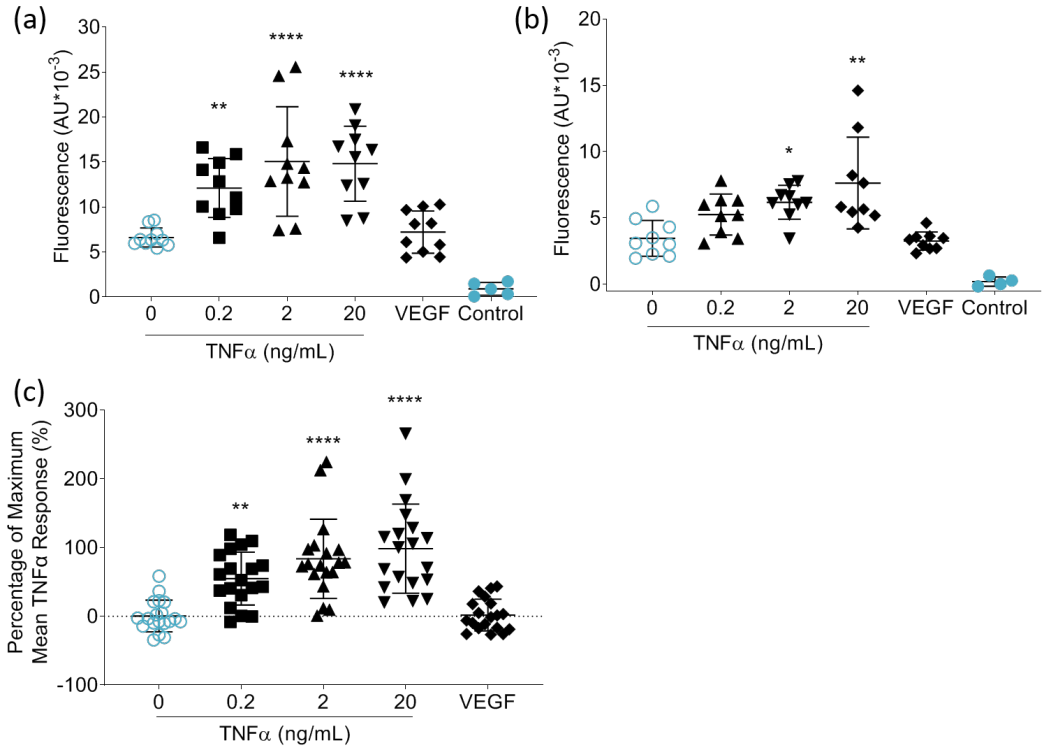


Figure 5.2: TNFα treatment caused significant concentration-dependent THP-1 binding in p34 (**a**) and p37 (**b**) HBMECs. (**c**): Data collated and normalised to maximum mean TNFα response. VEGF: VEGF-A_{165}a, 10ng/mL. 1way ANOVA with Dunnett's multiple comparisons. *p<0.05, **p<0.01, ****p<0.0001 compared to untreated (0ng/mL). (a & b): n = 1 plate; (c): n = 2 plates.

The monocyte attachment assay can be manipulated to study up- or down-stream signalling of endothelial-monocyte binding. As ICAM-1 is involved in TNFα-induced monocyte attachment and transcytosis (Yang et al. 2005), I hypothesised monocyte attachment may be prevented by blocking ICAM-1's function with an antibody directed at the adhesion molecule. At 20ng/mL, TNFα caused a significant increase in monocyte binding to p25 HBMECs (Figure 5.3a & b). Pre-treatment with an ICAM-1 blocking antibody

was not sufficient to block this significant increase in monocyte binding (Figure 5.3a & b). When repeated on p28 HBMECs, 2ng/mL TNFα caused a significant increase in monocyte binding (Figure 5.3c & d). When ICAM-1 antibody was added at the time of monocyte seeding as well as pre-treatment, this significant 2ng/mL TNFα-induced increase in binding to HBMECs was prevented (Figure 5.3c & d). However, fluorescence in anti-ICAM-1-treated wells was not significantly different to the IgG wells, suggesting that adhesion molecules other than ICAM-1 are likely to be involved in monocyte binding in these HBMECs. Note the difference in raw fluorescence between the two experiments (Figure 5.3a & c), which is why data is normalised and displayed as a percentage of the maximum mean TNFα response (Figure 5.3b & d). Representative images of monocyte-like THP-1 attachment to HBMECs are in Figure 5.3e.

The data presented here showed reduced responses of HBMECs to stimulation: previous work in the laboratory demonstrated more robust and magnified responses to TNFα, VEGF-A_{165}a, and the ICAM-1 blocking antibody (Beazley-Long et al. 2018b). HBMECs used here were at p25-37, and previous work in the laboratory used them at <p24. As cells are known to change phenotype in culture (Kapałczyńska et al. 2018; Nestor et al. 2015), commercially available primary (p1) HBMECs were purchased from ScienCell (ScienCell Research Institutes, 1000) and the monocyte attachment assays were repeated.

TNFα induced an increase in monocyte binding to p4 ScienCell HBMECs, which was significant at 20ng/mL (Figure 5.4a & b). 10ng/mL VEGF-A_{165}a also caused a significant increase in THP-1 binding (Figure 5.4c). These HBMECs are recommended to be cultured on fibronectin-coated plates (whereas the higher passage HBMECs are not) and THP-1s appeared to adhere to the fibronectin coating in the "no HBMEC" control wells, as demonstrated by significantly higher fluorescence in the "no HBMEC" group than the "no THP-1" group (Figure 5.4d). To rule out whether the increase in monocyte binding with TNFα was due to TNFα-induced HBMEC shrinkage and increased contact of THP-1s to fibronectin, the level of HBMEC coverage was investigated. HBMECs were labelled with Hoechst and Phalloidin-488 (a filamentous actin marker), and cell coverage was analysed from three random fields of view in three wells from each treatment. Treatment had no effect on cell coverage (Figure 5.5a), but there were gaps in the monolayer (Figure 5.5b), and so in subsequent studies to increase cell coverage, cells were left to grow until confluent after seeding (2-3 days).

Due to the THP-1s binding to the fibronectin coating, the "no HBMEC" control group was excluded and wells were washed 4x before fluorescence was read. This was fewer washes than was previously needed with the high passage HBMECs when comparing the "no THP-1" group to the "no HBMEC" group. This is attributed to higher HBMEC coverage as they were allowed to grow to confluence before the assay began, therefore minimising the availability of THP-1s to bind to the plate. One plate was imaged to ensure THP-1s that could bind to the plate were washed off with 4 washes. Figure 5.6 demonstrates how THP-1s bound to HBMECs (white arrows) and not to gaps (yellow

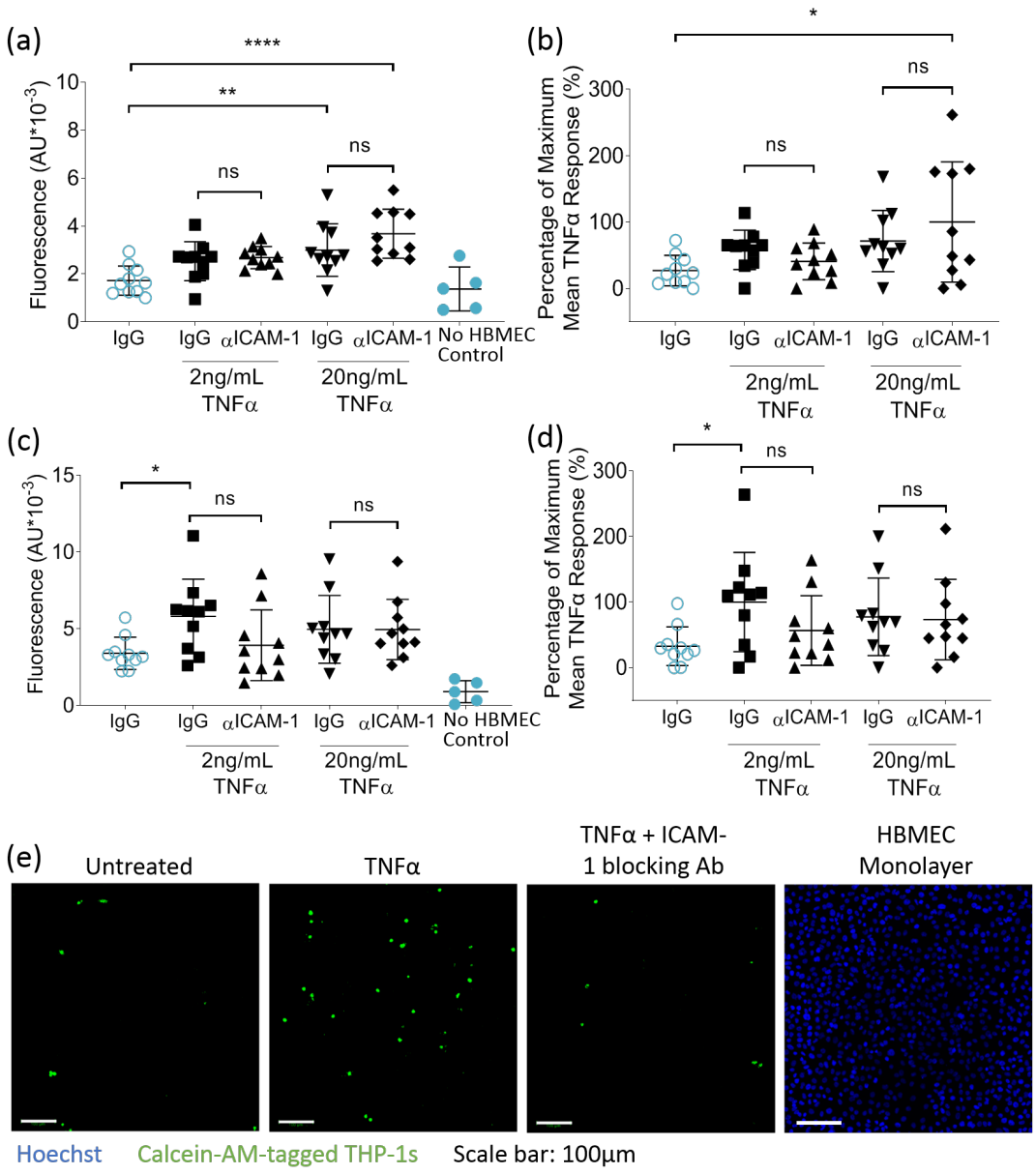


Figure 5.3: **a & b**: 20ng/mL TNFα significantly increased THP-1 binding to p25 HBMECs. Addition of ICAM-1 blocking antibody during TNFα pretreatment only did not block this TNFα-induced binding. **c & d**: 2ng/mL TNFα caused significantly more THP-1 binding to p28 HBMECs. Addition of ICAM-1 blocking antibody at both TNFα pretreatment and monocyte seeding prevented this significant increase in binding. However, fluorescence in anti-ICAM-1-treated wells was not significantly different to the IgG wells, suggesting that adhesion molecules other than ICAM-1 are likely to be involved here. IgG: Concentration and species-matched IgG was used as a control for the ICAM-1 antibody. One-way ANOVA with Sidak's or Dunnett's multiple comparisons. *p<0.05, **p<0.01, ****p<0.0001 compared to untreated (IgG). **e**: Representative immunofluorescence images demonstrating reduced TNFα induced monocyte binding after ICAM-1 blocking antibody. TNFα: 2ng/mL. Green: Calcein-AM-tagged THP-1s; Blue: Hoechst nuclear marker; Ab: Antibody. Scale bar: 100μm. (a & b): n = 1 plate; (c & d): n = 1 plate.

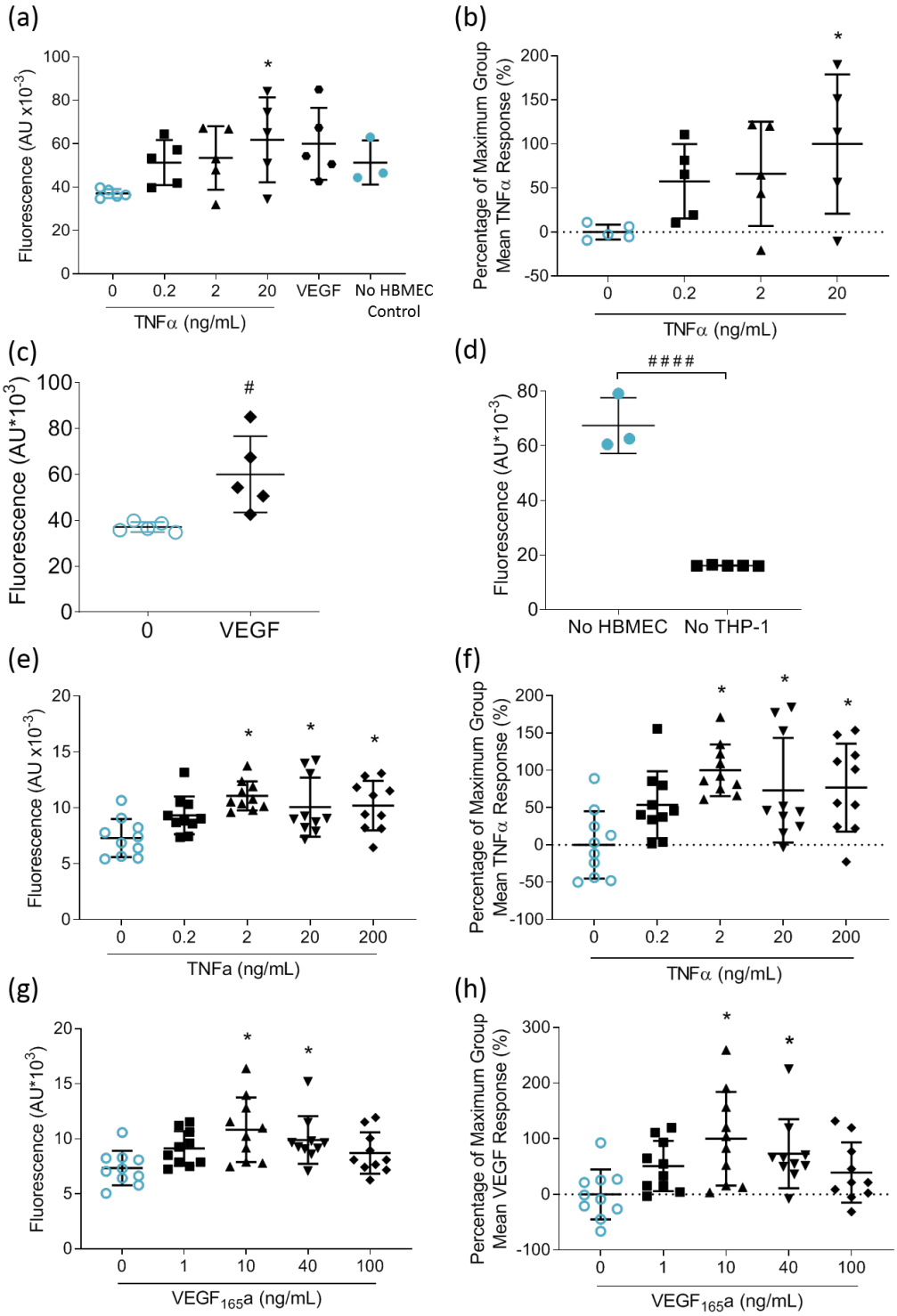
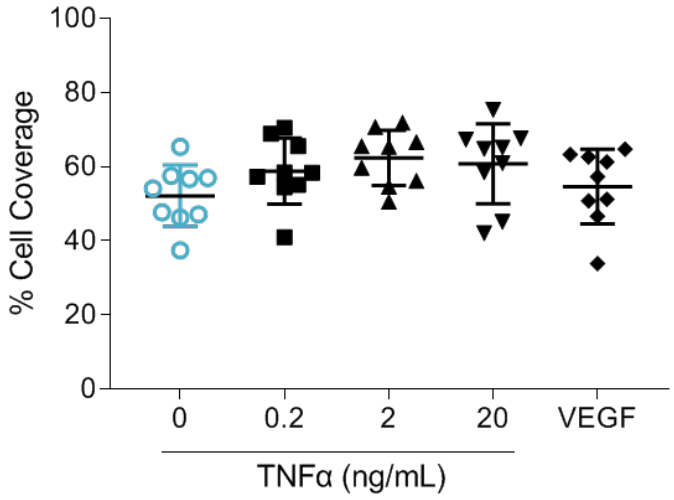


Figure 5.4: Monocyte fluorescence after TNFα or VEGF-A_{165}a treatment on ScienCell HBMECs. (**a-d**): 6-8hr after seeding, p4 HBMECs were serum starved. 20ng/mL TNFα significantly increased THP-1 binding to p4 HBMECs. 10ng/mL VEGF-A_{165}a also caused a significant increase in THP-1 binding (**c**). However, THP-1s appeared to bind to the fibronectin coating in the "no HBMEC" control wells as demonstrated by significantly higher fluorescence in the "no HBMEC" group than the "no THP-1" group (**d**). **VEGF**: VEGF-A_{165}a, 10ng/mL. (**e-h**): After seeding, p6 HBMECs were left to grow to confluence (2-3d) before serum starving. THP-1 binding to p6 ScienCell HBMECs is significantly increased when stimulated with TNFα (**e & f**) or VEGF-A_{165}a (**g & h**). *p<0.05 compared to 0ng/mL TNFα or 0ng/mL VEGF-A_{165}a, 1way ANOVA with Dunnett's or Sidak's multiple comparisons. #P<0.05, ####p<0.0001, unpaired t test. (a-d): n = 1 plate; (e-f): n = 1 plate.

(a) Analysis of cell coverage after treatment.



(b) Immunofluorescence of HBMEC coverage.

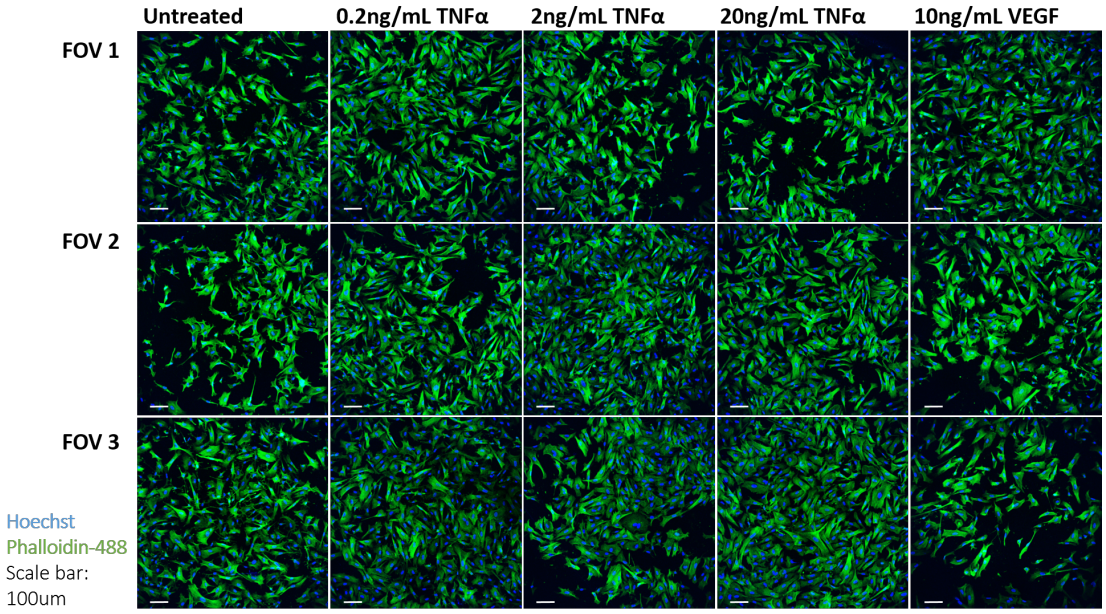


Figure 5.5: HBMEC (p4) coverage is not dependent on treatment. 1way ANOVA with Sidak's multiple comparisons. FOV: field of view. Blue: Hoechst nuclear marker; Green: Phalloidin-488 actin marker. VEGF: VEGF-A_{165}a. Scale bar: 100µm. n = 3 wells/treatment.

stars) in the monolayer (and therefore to fibronectin).

The monocyte attachment assay was repeated in HBMECs that were allowed to grow to confluence over 2-3 days, and both TNFα (Figure 5.4e & f) and VEGF-A_{165}a (Figure 5.4g & h) caused a significant increase in monocyte binding to p6 HBMECs.

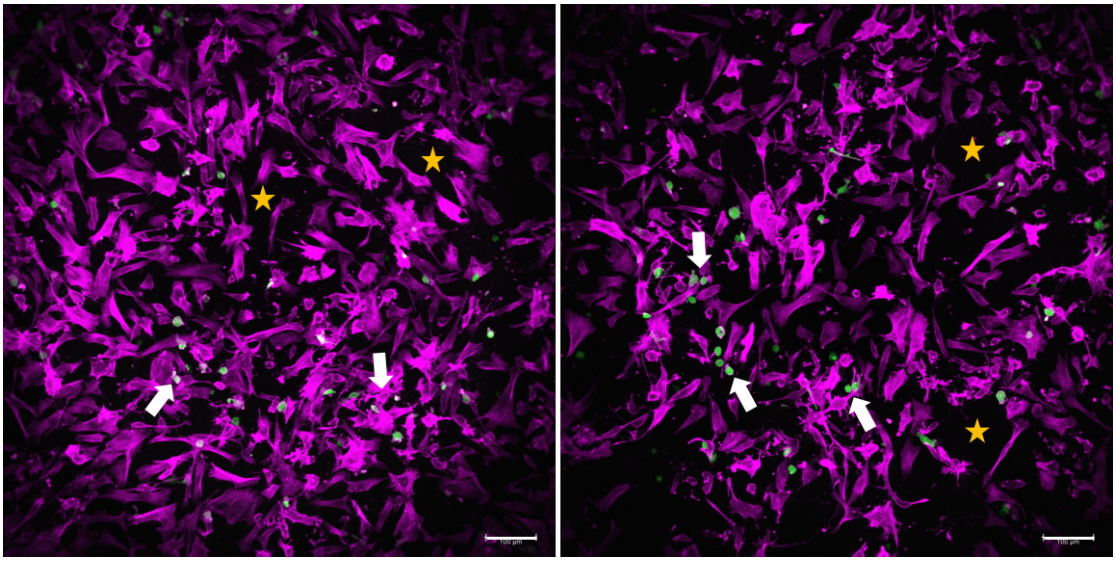


Figure 5.6: Representative images demonstrating THP-1 (green) binding to HBMECs (magenta), demonstrated by white arrows, rather than to gaps in the monolayer (yellow stars), after TNFα or VEGF-A_{165}a treatment. Magenta: Phalloidin-555 actin marker; Green: Calcein-AM-tagged THP-1s. Scale bar: 100μm.

As described above, an ICAM-1 blocking antibody was introduced at the time of TNFα or VEGF-A_{165}a treatment and again at THP-1 incubation. TNFα at 20ng/mL had previously induced a significant increase in monocyte binding (Figure 5.4a & d), as did 10ng/mL VEGF-A_{165}a (Figure 5.4f) and so these concentrations were chosen. In p6 and p8 HBMECs, TNFα significantly increased THP-1 binding (Figure 5.7a & b respectively), however here, VEGF-A_{165}a did not reliably increase binding. This suggests the ScienCell HBMECs lose their ability to respond to VEGF-A_{165}a around p6. Blocking ICAM-1 did not reduce the significant increase in TNFα-induced binding (Figure 5.7). As there is variability in the raw fluorescence between experiments (Figure 5.7a & b), data were also normalised and displayed as the percentage of the maximum group mean (Figure 5.7c).

To confirm an endothelial phenotype of the HBMECs, I probed expression of typical endothelial cell markers in both the high passage (at p25/31) and the ScienCell (p2) HBMECs.

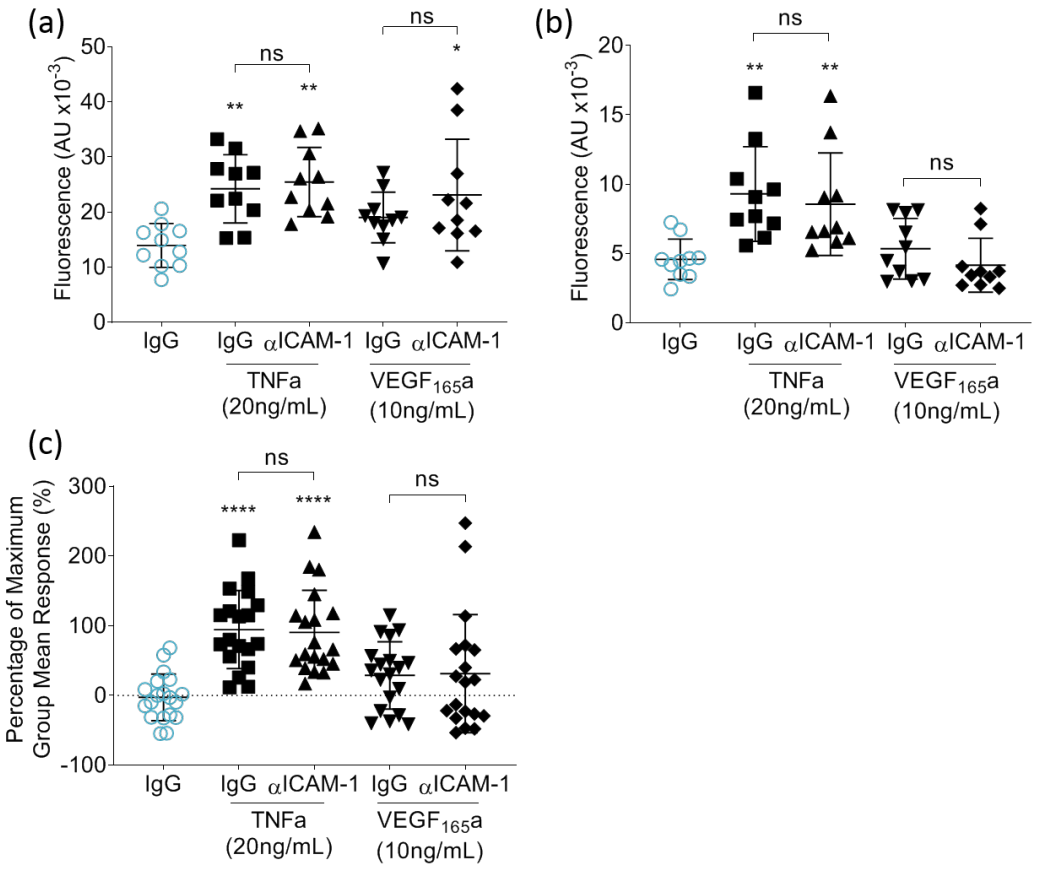


Figure 5.7: Monocyte fluorescence after TNFα or VEGF-A$_{165}$a treatment with an ICAM-1 blocking antibody or an IgG control on p6 (a) and p8 (b). Data are normalised in (c). TNFα significantly increased THP-1 binding to HBMECs, but blocking ICAM-1 could not prevent this. VEGF-A$_{165}$a did not increase THP-1 binding. 1way ANOVA with Sidak's or Dunnett's multiple comparisons. **p<0.01, ***p<0.001, ****p<0.0001. (a&b): n = 1 plate; (c): n = 2 plates.

5.3.2 Commercially Available HBMECs Do not Express Typical Endothelial Markers

I performed western blot and PCR to confirm the presence or absence of the typical endothelial cell products, VEGF-R2, CD31, claudin-5, ZO-1, ICAM-1 and VCAM-1. VEGF-R2 and ICAM-1 could not be detected in the high passage (p25-32) HBMECs (Figure 5.8), even when cells were treated with TNFα or VEGF-A_{165}a. These same HBMECs at a lower passage (p20-24) used previously in our lab and HUVECs expressed both constitutively. The bands at ~50kDa & ~120kDa on the VEGF-R2 blot (Figure 5.8 top) are likely to be from VEGF-R2 degradation.

Additionally, claudin-5, ICAM-1 or VCAM-1 Messenger Ribonucleic Acid (mRNA) could not be detected in p31 HBMECs using conventional PCR (Figure 5.9). The lack of ICAM-1 mRNA expression would explain the lack of a significant blocking effect with the ICAM-1 antibody on TNFα-induced THP-1 binding (Figure 5.3c & d). Due to COVID19 constraints, further endothelial cell markers could not be investigated in the higher passage HBMECs.

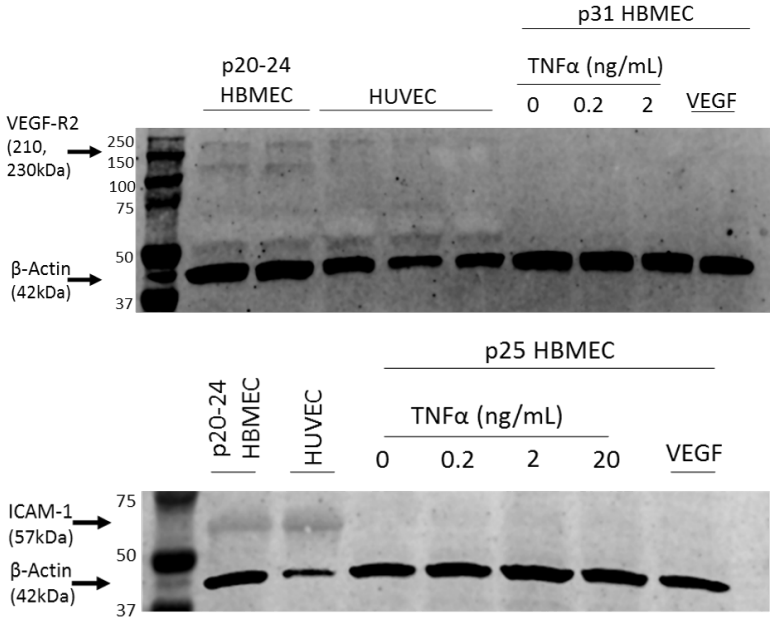


Figure 5.8: Western blot of human brain microvascular endothelial cells (HBMECs) after TNFα or VEGF-A_{165}a treatment. High passage (p31) HBMECs did not express the classic endothelial cell markers VEGF-R2 (top) or ICAM-1 (bottom), even when treated with TNFα or VEGF-A. Lower passage HBMECs (p20-24) from our lab and HUVECs expressed both constitutively. The bands at ~50kDa & ~120kDa on the VEGF-R2 blot are likely to be from VEGF-R2 degradation. VEGF-R2: Vascular endothelial growth factor receptor-2; β-Actin: Loading control. HUVEC: Human umbilical vein endothelial cells. VEGF: VEGF-A_{165}a 10ng/mL. 15µg protein. n = 1 plate.

At p2, ScienCell HBMECs were probed for the endothelial markers through conventional PCR. As demonstrated in Figure 5.10, CD31 was not detected in the ScienCell HBMECs despite being characterised as CD31-positive by the supplier. Claudin-5 and ZO-1 were not detected, but after re-probing new cDNA, ZO-1 was faintly detected in some untreated and TNFα-treated wells (Figure 5.10 bottom). Expression of ICAM-1

and VCAM-1 could be induced with 20ng/mL TNFα, but not with 10ng/mL VEGF-A_{165}a (Figure 5.10 top).

Expression of several receptors for pro- and anti-inflammatory molecules were also probed with the aim of stimulating HBMECs with their respective ligands or disrupting their binding in future monocyte attachment assays. p2 HBMECs constitutively expressed STAT3, Interleukin-1 Receptor-1 (IL1R1) and very low levels of Interleukin-6 Receptor (IL6R) (Figure 5.10 bottom). Interleukin-10 Receptor (IL10R) was not detected in HBMECs. cDNA from HUVECs was used as a positive control, which expressed all markers except VCAM-1 and STAT3.

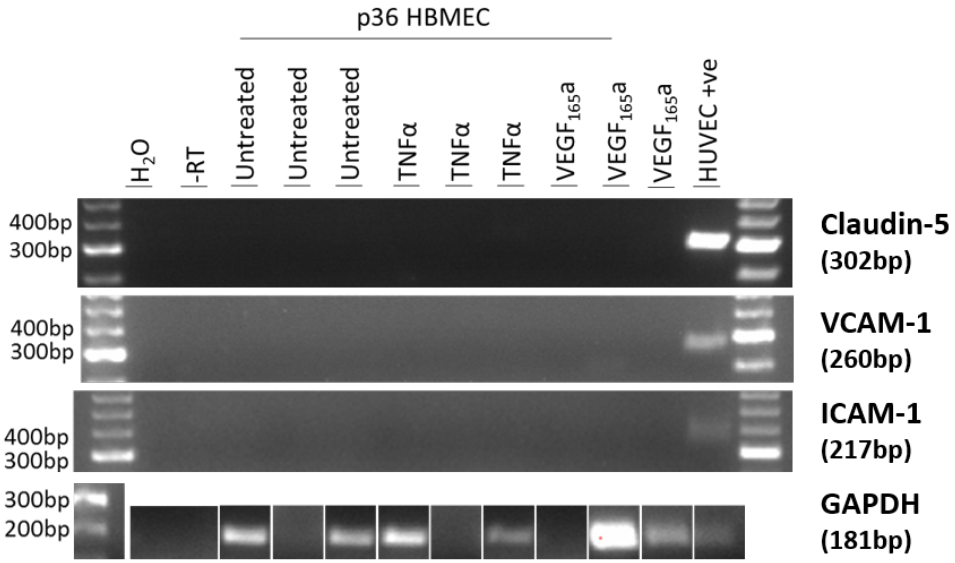


Figure 5.9: Conventional PCR of human brain microvascular endothelial cells (HBMECs) after TNFα or VEGF-A_{165}a treatment. High passage (p36) HBMECs did not express the classic endothelial cell markers VCAM-1, Claudin-5 and ICAM-1. P5 HUVECs expressed all genes constitutively. H_2O: water negative control; -RT: minus reverse transcriptase negative control; HUVEC+ve: Human umbilical vein endothelial cell positive control; VCAM-1: Vascular cell adhesion molecule-1; ICAM-1: Intracellular adhesion molecule-1. GAPDH: Glyceraldehyde 3-phosphate dehydrogenase housekeeping gene control. 50ng cDNA, TNFα: 20ng/mL; VEGF-A_{165}a: 10ng/mL. n = 1 plate.

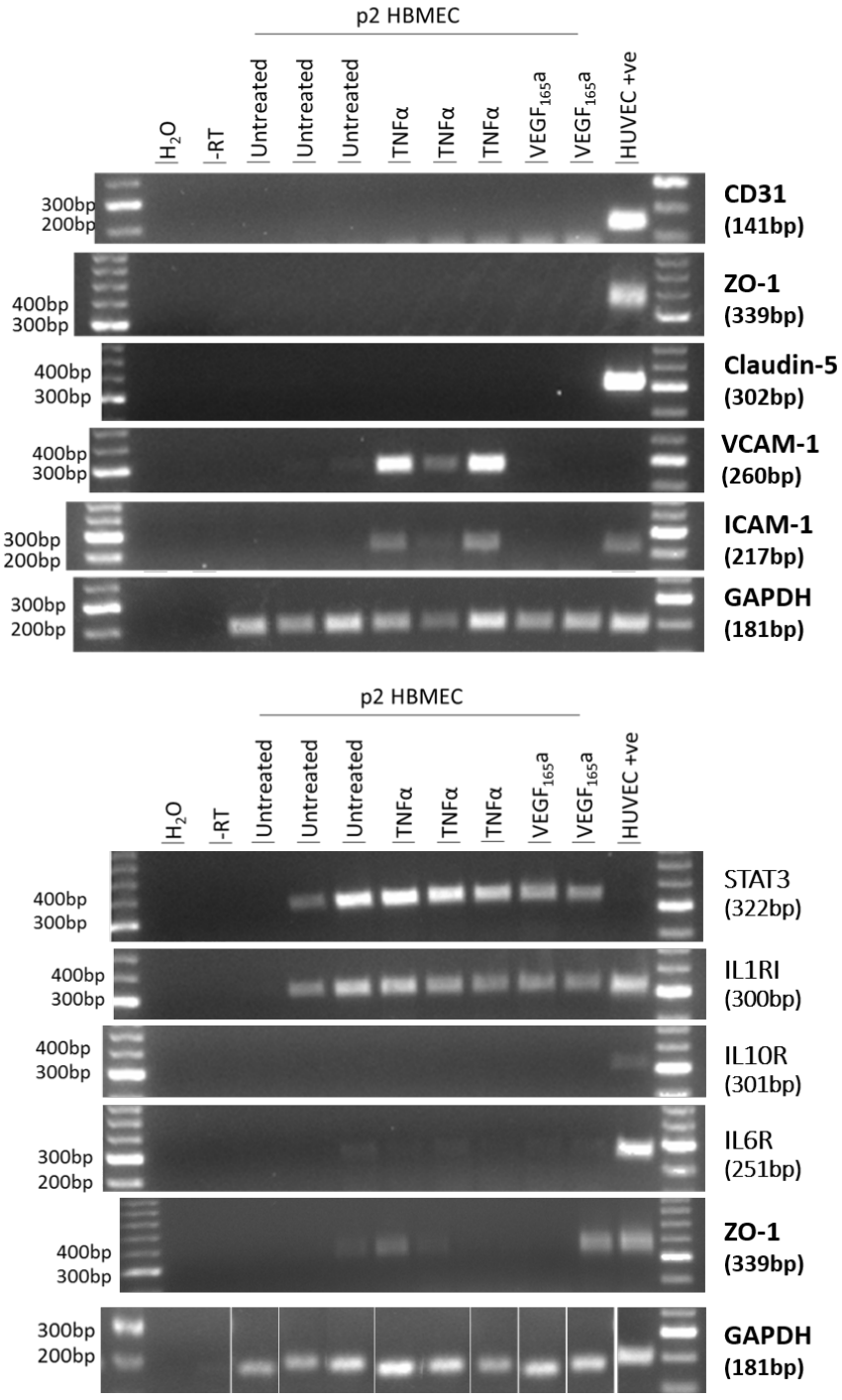


Figure 5.10: Conventional PCR of human brain microvascular endothelial cells (HBMECs) after TNFα or VEGF-A_{165}a treatment. Low passage (p2) ScienCell HBMECs did not express the classic endothelial cell markers CD31, ZO-1 or Claudin-5, but TNFα induced expression of VCAM-1 and ICAM-1. However, upon re-probing, HBMECs had low expression of ZO-1. These HBMECs did also not express IL10R, but did constitutively express IL1RI and STAT3, and had low expression of IL6R. HUVECs expressed all genes constitutively, except for VCAM-1 and STAT3. H_2O: water negative control; -RT: minus reverse transcriptase negative control; HUVEC+ve: Human umbilical vein endothelial cell positive control; CD31: Cluster of differentiation 31; GAPDH: Glyceraldehyde 3-phosphate dehydrogenase housekeeping gene control; ICAM-1: Intracellular adhesion molecule-1; IL1RI: Interleukin-1 Receptor I; IL10R: Interleukin-10 Receptor; IL6R: Interleukin-6 Receptor; VCAM-1: Vascular cell adhesion molecule-1; ZO-1: Zona occludens-1. 50ng cDNA, TNFα: 20ng/mL; VEGF-A_{165}a: 10ng/mL. n = 1 plate.

5.4 Discussion

In this chapter, the monocyte attachment assay was employed as an *in vitro* technique to model the neural endothelium under inflammatory conditions. The monocyte attachment assay has been demonstrated to be a useful tool in probing specific binding mechanisms in epithelial and endothelial cells (Beazley-Long et al. 2018b; Thichanpiang et al. 2014). However, here the responses were diminished, with fewer THP-1s binding to endothelial cells and a lack of response to VEGF-A (Section 5.3.1). Two batches of HBMECs were used (low p2-8 HBMECs and high p25-37), both at varying passages, and their characteristics appeared to change depending on their passage. A summary of all experiments and findings grouped by passage is detailed in Tables 5.4 and 5.5.

TNFα-induced adherence is common at all passages and does not seem to be lost, whereas the ability to respond to VEGF-A_{165}a was lost early on, at around passage 6 (Figures 5.4g & h and 5.7a) and between passage 24 and 31 (passage 20-24 demonstrated VEGF-A_{165}a-induced THP-1 binding (Beazley-Long et al. 2018b); whereas passage 31 did not, Figure 5.2). VEGF-R2 expression was lost in the same time period with the higher HBMECs (passage 24-31, Figure 5.8), but unfortunately, due to COVID19 restraints, VEGF-R2 expression could not be probed in the early passage (p2) HBMECs. Presumably these p2 HBMECs would express this receptor as there was an increase in VEGF-A_{165}a-induced binding, but if probed at p6, expression may have been lost. The lack of VEGF-A_{165}a response could also be due to alterations in the co-receptor, Neuropilin-1 (NRP1). NRP1 enhances VEGF-R2 signalling (Peach et al. 2018), and is required for VEGF-A_{165}a-induced permeability (Becker et al. 2005b; Soker et al. 1998). Deletion of brain endothelial NRP1 reduced leakage of fluorescently-labelled albumin and immune cell infiltration in Experimental Autoimmune Encephalomyelitis (EAE) (Wang et al. 2016), highlighting its key role in inflammatory-induced endothelial permeability.

There was a lack of effect of anti-ICAM-1 blocking on monocyte binding to HBMECs in all passages used here. ICAM-1 was not detected in the higher passage HBMECs with PCR or Western Blot (Figures 5.9 and 5.8), which could explain the lack of significant effect in blocking ICAM-1 activity. p20-24 HBMECs previously responded to anti-ICAM-1 blockade (Beazley-Long et al. 2018b), and so this function must have been lost between p24 and p28. Disrupting ICAM-1 activity in the low passage ScienCell HBMECs did not prevent the increase in TNFα-induced THP-1 binding (Figure 5.7), despite these cells expressing ICAM-1 after TNFα application (Figure 5.10). There are several other adhesion molecules involved in monocyte binding, for example VCAM-1 and CD31/Platelet and Endothelial Cell Adhesion Molecule-1 (PECAM-1), which could be mediating the process here (Wong et al. 1999; Wong and Dorovini-Zis 1995). VCAM-1 is upregulated in response to inflammatory mediators (Wong et al. 1999; Wong and Dorovini-Zis 1995), and has previously been found to increase in spinal cord endothelial cells after peripheral Complete Freund's Adjuvant (CFA)-induced inflammation (Donaldson and Wise-

man 2000). VCAM-1 may be a suitable target in the low passage (p2) as TNFα induced VCAM-1 expression (Figure 5.10), and ideally, this assay would have been repeated using a VCAM-1-blocking antibody but due to time and COVID19 restraints, this was not possible. However, VCAM-1 is unlikely to be regulating binding in the high passage HBMECs (p25-36) as it could not be detected, even after TNFα stimulation (Figure 5.9). PECAM-1/CD31 could be mediating the process in the higher passage HBMECs, but it is unlikely to be involved in the low passage HBMECs as this was also not detected after TNFα stimulation. ICAM-1 disruption, either through knock-down or antibody blockade, was shown to impair migration even though adhesion was unaffected (Wittchen 2009). Therefore, even though blocking ICAM-1 did not significantly prevent THP-1 binding here, it may have prevented migration and diapedesis across the endothelium. In order to test this, cell migration assays using transwell inserts could be used, but due to time restraints this was not pursued.

Typical endothelial cell markers were probed in both batches of HBMECs, and claudin-5 could not be detected in either (Figures 5.9 and 5.10). The low passage (p2) HBMECs also did not constitutively express CD31 (Figure 5.10), despite being verified by the supplier as CD31-positive. ZO-1 could only be weakly detected in the p2 HBMECs (Figure 5.10). CD31, claudin-5 and ZO-1 are adhesion molecules and tight junction proteins, and so it is conceivable that levels will be low and therefore not detectable if HBMECs are not confluent and forming tight junctions. Indeed, the level of endothelial cell confluency is correlated with CD31, claudin-5 and ZO-1 expression (Osada et al. 2011; Raychaudhury et al. 2001; Li and Poznansky 1990). However, when extracting protein or RNA, both high and the low passage HBMECs were left to grow until cells were 80-90% confluent, meaning the vast majority of cells had formed connections with other cells. Therefore, these HBMECs were not regarded as being of reliable endothelial cell phenotypes, and further studies with these cells, for example TEER measurements and co-culturing with astrocytes, pericytes and/or neurones were not pursued.

It should be noted that no information was provided on the donor of the two batches of HBMECs, such as age, sex or health. This means the two cell lines (and future HBMECs) could be from very different donors with different genetics, and could potentially come from contrasting microenvironments.

HBMECs change characteristics and phenotypes depending on what passage they are, restricting which experiments they can be used for. This change is clear from the mechanistic studies and expression profiles listed in this chapter (summarised in Tables 5.4 and 5.4). This phenomenon of cells changing in culture and in different conditions is well known. Culturing endothelial cells in different medium can affect cell quality, viability and phenotype (Leopold et al. 2019), and 2D vs. 3D culture conditions also have an impact on cell characteristics and functions (Kapałczyńska et al. 2018). The culture-induced change in characteristics can be rapid, with one study demonstrating gene expression changes and cell adaption within one week in culture (Nestor et al. 2015). HBMECs were purchased from ScienCell at p1 and were ready for passage after

10 days and for RNA extraction after a further 6 days (at p2). The study by Nestor and colleagues (2015) supports that this was enough time for the HBMECs to change and adapt to culture, especially if the culture medium was not optimal for HBMEC culture (Leopold et al. 2019).

It could be that HBMEC in *isolation* in culture are easily altered by their conditions, and co-culturing with other NVU cells may support HBMEC viability and prevent phenotype changes (Stone et al. 2019; Daniels et al. 2013). As neural endothelial cells are not in isolation in the neurovasculature, they are in constant communication with other cells of the NVU. Co-culturing brain endothelial cells with other NVU cells decreases their permeability and strengthens their inflammatory response compared to culturing them alone (Stone et al. 2019; Herland et al. 2016; Daniels et al. 2013; Wilhelm et al. 2011). However, the TEER values obtained from co-cultures are still below physiological values (Destefano et al. 2018). Additionally, these more complex BBB and BSCB models can be expensive and more labour-intensive (Stone et al. 2019), highlighting the importance of establishing a reliable endothelial cell model before embarking on more complex co-cultures. Further studies involving co-culture with astrocytes and their media was one of the future aims of optimising HBMEC culture here in order to study endothelial-astrocyte interactions, but due to time restrains and the lack of a suitable endothelial cell line, these studies were not pursued.

Whilst HUVECs may be more reliable cells for culture as they retain their phenotype with several passages (up to p6-10 (Medina-Leyte et al. 2020; Bouïs et al. 2001)) and high commercial availability, HBMECs appear to be easily influenced by culture conditions. HBMEC lose CD31 expression by p2 (Figure 5.10) and VEGF-A_{165}a activation by p6 (Figure 5.7), and therefore should avoid being passaged. Immediate primary HBMEC isolation and use in experiments is not viable due to their cost and slow growing nature. Rat brain endothelial cells could be used, especially as they can be co-cultured with sister NVU cells. Watson et al. (2013) developed a method for co-culturing rat brain and spinal cord endothelial cells with glial cells that resulted in high yields and maintained neural endothelial cell properties when used at very low passage (p1). Although cells were still in culture for 3 weeks, which can be enough time for cell characteristics to change (Nestor et al. 2015), this may be the most viable primary cell *in vitro* technique to model the BBB/BSCB.

Alternatives to using brain endothelial cells may include using other endothelial cells such as HUVECs to model certain functions. However, endothelial cells from different organs differ significantly, especially brain endothelial cells thanks to their specialised junctions (Kalucka et al. 2020; Abbott et al. 2010). HUVECs are therefore not suitable in modelling the BBB or BSCB. Immortalised cells such as the hCMEC/D3 (Weksler et al. 2005) can be used, and whilst they maintain several barrier properties (Daniels et al. 2013), these cells have lower TEER measurements than primary brain endothelial cells (Weksler et al. 2005). Additionally, there are issues with ensuring that immortalised cell lines remain uncontaminated and correctly identified (Alston-Roberts et al. 2010).

THP-1 cells are an immortalised monocyte-like cell line derived from the blood of a child with acute monocytic leukaemia (Tsuchiya et al. 1980). Whilst these cells maintain monocytic characteristics for a long period of time in culture (Tsuchiya et al. 1980), it is important to note that there are limitations with this cell line. For example, THP-1 cells have a less pronounced response to Lipopolysaccharide (LPS) stimulation than primary monocytes due to their lower expression of CD14 (Bosshart and Heinzelmann 2016). THP-1s used here were p20-30 and so the reduced responses seen here compared to previously in our lab (Beazley-Long et al. 2018b) may be because they were used at a later passage. However, these cells have been shown to maintain their monocyte-like properties for up to 14months in culture (Tsuchiya et al. 1980). A review by Chanput and colleagues (2014) stated that THP-1s "can be cultured in vitro up to passage 25 (approx. 3 months) without changes of cell sensitivity and activity." However, studies to support this statement could not be found. These cells should ideally be authenticated using karyotyping or isozyme analysis, but these cells are not identified as being mislabelled or cross-contaminated by the ICLAC Register of Misidentified Cell Lines (Capes-Davis et al. 2010).

In conclusion, whilst glial/brain endothelial cell co-cultures may have the potential to better model the BBB/BSCB and study NVU cell interactions, the results presented here demonstrate that some endothelial cell-specific responses and mechanisms can be studied in isolation with HBMECs alone. For example, the monocyte attachment assay was able to successfully detect increased TNFα-induced THP-1 binding and can be manipulated to investigate binding mechanisms. There are, however, a number of gaps due to COVID19 restraints, for example the involvement of VCAM-1 in monocyte binding or whether p2 HBMECs express VEGF-R2 or higher passage HBMECs express CD31 or ZO-1. These results also highlight the difficulties in culturing primary HBMECs due to their changing phenotype whilst in culture, and the importance of recognising which assays are appropriate depending on HBMEC passage number.

Passage	TNFα Adherence	VEGF-A_{165}a Adherence	Anti-ICAM-1 Blockade	VEGFR2 Expression	Constitutive ICAM-1 Expression	Induced ICAM-1 Expression	Induced VCAM-1 Expression	Endothelial Marker Expression
P2	-	-	-	-	×	✓	✓	ZO-1 only 5.10
P4	✓ 5.4a & b	✓ 5.4c	-	-	-	-	-	-
P6	✓ 5.4e & f, 5.7a	✓ 5.4g & h × 5.7a	× 5.7a	-	-	-	-	-
P8	✓ 5.7b	× 5.7b	× 5.7b	-	-	-	-	-
P20-24	✓ 1	✓ 1	✓ 1	✓ 5.8	✓ 5.8	-	-	vWF, Occludin 1
P25-28	✓ 5.3	-	× 5.3c & d	- -	× 5.8	× 5.8	-	-
P31-37	✓ 5.2	× 5.2	-	× 5.8	× 5.9	× 5.9	× 5.9	None detected 5.9

ICAM-1: Intracellular adhesion molecule-1; **P**: Passage; **VCAM-1**: Vascular cell adhesion molecule-1; **VEGF**: Vascular endothelial growth factor; **VEGFR2**: Vascular endothelial growth factor receptor 2; **vWF**: von Willebrand Factor; **ZO-1**: Zona occludens-1. 5.x: Figure reference; 1, Beazley-Long et al. 2018b. ✓detected; × not detected; - not investigated.

Table 5.4: Summary of HBMEC experimental responses

Passage	CD31 Expression	ZO-1 Expression	Claudin-5 Expression	VEGFR2 Expression	Constitutive ICAM-1 Expression	Induced ICAM-1 Expression	Induced VCAM-1 Expression	Other
P2	× 5.10	✓ 5.10	× 5.10	- 5.10	× 5.10	✓ 5.10	✓ 5.10	STAT3, IL1RI, IL6R 5.10
P20-24	-	-	-	✓ 5.8	✓ 5.8	-	-	vWF, Occludin-1 1
P25-28	-	-	-	-	× 5.8	× 5.8	-	-
P31-37	-	-	× 5.9	× 5.8	× 5.9	× 5.9	× 5.9	-

ICAM-1: Intracellular adhesion molecule-1; **IL1RI**: Interleukin 1 Receptor I; **IL6R**: Interleukin 6 Receptor; **P**: Passage; **STAT3**: Signal Transducer and Activator of Transcription-3; **VCAM-1**: Vascular cell adhesion molecule-1; **VEGFR2**: Vascular endothelial growth factor receptor 2; **vWF**: von Willebrand Factor. 5.x: Figure reference; 1, Beazley-Long et al. 2018b. ✓detected; × not detected; - not investigated.

Table 5.5: Summary of HBMEC expression of endothelial cell markers.

6 | Spinal Electrophysiology as a Model of Neuroinflammation Using TNFα

6.1 Introduction

The previous chapters dealt with the gliovascular responses to peripheral inflammation, and whilst these effects are important, pain signalling and central sensitisation are dependent on neuronal signalling to higher centres in the Central Nervous System (CNS). Therefore, investigating the effect of these gliovascular alterations on dorsal horn pain signalling is necessary.

Peripheral Complete Freund's Adjuvant (CFA)-induced inflammation leads to glial activation (and neuroinflammation) in the spinal cord (Beazley-Long et al. 2018b; Xu et al. 2014; Ji et al. 2013; Sun et al. 2007; Sun et al. 2008; Raghavendra et al. 2004), which can in turn contribute to central sensitisation and chronic pain signalling (Ji et al. 2019; Ji et al. 2018; Ji et al. 2016). Animals with CFA-induced monoarthritis were found to have increased baseline activity of spinal cord Wide Dynamic Range (WDR) neurones and nociceptive-like responses to innocuous stimulation (Naeini et al. 2005). WDR neurones are often used in spinal electrophysiology to study pain signalling due to the range of inputs they receive and their key role in spinal pain processing. WDR neurones reside predominantly in lamina V and receive direct input from Aβ and Aδ fibres, and indirect input from C fibres, and so respond to the full range of stimuli (from innocuous to noxious) (Basbaum et al. 2009; D'Mello and Dickenson 2008; Millan 1999). They form part of the ascending nociceptive pathways, which project to supra-spinal centres in the brain to process nociceptive signalling and generate pain perception. WDR neurones can increase their firing intensity in response to successive low frequency (<5Hz) and high intensity (3 times C fibre activation threshold) C fibre stimuli in a process termed Wind-Up (WU) (D'Mello and Dickenson 2008; Ji et al. 2003).

Neuroinflammation occurs as a result of peripheral insults and glial activation, and can enhance spinal cord excitability through the release of pro-inflammatory mediators, such as Tumour Necrosis Factor α (TNFα) (Ji et al. 2018; Ellis and Bennett 2013; Hwang et al. 2008; DeLeo and Yezierski 2001). TNFα is an inflammatory cytokine that is released by cells within the Neurovascular Unit (NVU) such as astrocytes, microglia, and pericytes and acts on the Tumour Necrosis Factor Receptor (TNFR). TNFRs are expressed on dorsal horn neurons, astrocytes, microglia, and endothelial cells (Kanda et al. 2017). TNFα has been demonstrated to be a key molecule in chronic pain signalling (Ji et al. 2018; Rustenhoven et al. 2017; Leung and Cahill 2010), through enhancing glutamate-induced excitatory currents in neurones (Kawasaki et al. 2008b) and increasing WDR neurone firing in response to nociceptive stimuli (Cuellar et al. 2004; Onda

et al. 2002; Reeve et al. 2000). It was for this reason that TNFα was chosen as proof of concept that single unit spinal electrophysiology can be used to study downstream effects of glial-derived neuroinflammation on neuronal pain signalling (as in Reeve et al. 2000), with the aim of investigating other pro-inflammatory molecules involved in neuroinflammation (including modulating Vascular Endothelial Growth Factor (VEGF)-A and Vascular Endothelial Growth Factor Receptor (VEGF-R)2 signalling) in the future.

Similar to TNFα, VEGF-A has been implicated as a key molecule in central (and peripheral) pain signalling (Llorián-Salvador and González-Rodríguez 2018; Beazley-Long et al. 2018b; Hulse et al. 2016; Hamilton et al. 2016; Hulse et al. 2014; De Bandt et al. 2003). VEGF-A, and specifically its splice variant $VEGF_{165}a$, can cause increased sensitivity of primary afferent neurones in the periphery (Hulse et al. 2014). Enhancing $VEGF\text{-}A_{xxx}a$ (where xxx refers to the number of amino acids in the mature protein sequence) in the spinal cord was shown to increase pain sensitivity, whereas blocking VEGF-A signalling and enhancing the anti-angiogenic $VEGF\text{-}A_{xxx}b$ in the spinal cord led to increased and heat mechanical thresholds (Hulse et al. 2016). These experiments were carried out in naive and nerve injury rodents, but studying the effect of inflammatory monoarthritis and modulating central VEGF-A signalling has not been carried out. Mirroring these types of experiments in CFA-induced peripheral inflammation are needed to understand VEGF-A's role in chronic pain signalling, especially considering blocking of VEGF-A signalling systemically and in endothelial cells can prevent development of secondary pain (and associated glial activation) (Beazley-Long et al. 2018b).

This chapter aimed to address the unknowns highlighted in Section 1.4 and Figure 1.84.

Hypothesis

Intrathecal application of TNFα will increase spinal excitability and cause increased WDR neuronal firing to noxious stimuli.

Objectives

- To demonstrate how spinal electrophysiology can be used as a technique to study downstream effects of neuroinflammation and gliosis on neuronal signalling.
- To use TNFα to sensitise WDR neurones and record their responses to noxious stimuli.

6.2 Materials & Methods

6.2.1 Experimental Animals

All experiments and procedures were performed in accordance with the Animals (Scientific Procedures) Act (1986; 2012) and were authorised by the UK Home Office. Animals were habituated by myself prior to any surgical procedures being carried out.

Experiments were carried out on adult (≥175g, n = 8) male Sprague Dawley (SpD) rats (Charles River, UK). The oestrus cycle in females causes hormone fluctuations that may interact with pain signalling and experimental outcomes (Becker et al. 2005a; Craft et al. 2004), and so male rats were used due to time constraints.

Rats were group-housed in conventional cages (3 per cage) and maintained in a 12 hour light/dark cycle at 22˚C and 55% humidity with access to food and water *ad libitum*.

Sample size for these pilot studies were calculated (n = 10) using previous data from our lab. Animals were allocated to treatment groups by an independent investigator. However, drug treatment was not blinded as drugs needed to be made up on the day and no-one else was available to assist with blinding for this.

6.2.2 Drugs

Rat recombinant TNFα (carrier-free; 10µg; 510-RT-010/CF; R&D systems) was diluted in vehicle (0.1% Bovine Serum Albumin (BSA) (A2153-10G, Sigma) in Phosphate Buffered Solution (PBS)). Rats received the following cumulative intrathecal doses, based on Reeve et al. (2000): 5pg/50uL (100pg/mL); 50pg/50uL (1ng/mL); 500pg/50uL (10ng/mL); 5ng/50uL (100ng/mL).

6.2.3 In Vivo Spinal Electrophysiology

Full details on materials and methods are described in Section 2.2.7. Male SpD rats (≥175g, n = 8: TNFα n = 6; vehicle n = 2) were prepared for *in vivo* spinal electrophysiology as detailed in Section 2.2.7.3 (see Figure 6.1 for an overview of the animal setup for spinal electrophysiology). Briefly, animals were anaesthetised with 3% isoflurane (Abbott Laboratories, Kent, UK) vaporised in 33% nitrous oxide and 67% oxygen until the automatic righting reflex ceased. Nitrous oxide was used in addition to isoflurane as it can counteract some of isoflurane's cardiodepressive effects (Constantinides and Murphy 2016). Animals were then transferred to a heat mat (Harvard Apparatus, UK) and connected to a nose cone in the supine position. A tracheotomy was performed, and 5mm of a cannula (Portex nylon tubing, external diameter 2.1mm, internal diameter 1.5mm) of 5-6cm in length was inserted and connected to the anaesthetic system. The animal was secured in place in the prone position using a stereotaxic frame (Medical Engineering Unit, University of Nottingham) and a laminectomy was performed to expose spinal Lumbar Section (L)4-5 regions (see Section 2.2.7.3). The anaesthetic was then reduced and maintained at 1.5% throughout the procedure. The cord was kept wet with physiological saline.

After a 15-20 min interval to allow for stabilisation of anaesthesia, the recording electrode was manually lowered onto the spinal cord lateral to the central vessel using a micromanipulator (SCAT-01 microdrive, Digitimer), then slowly inserted into the cord at

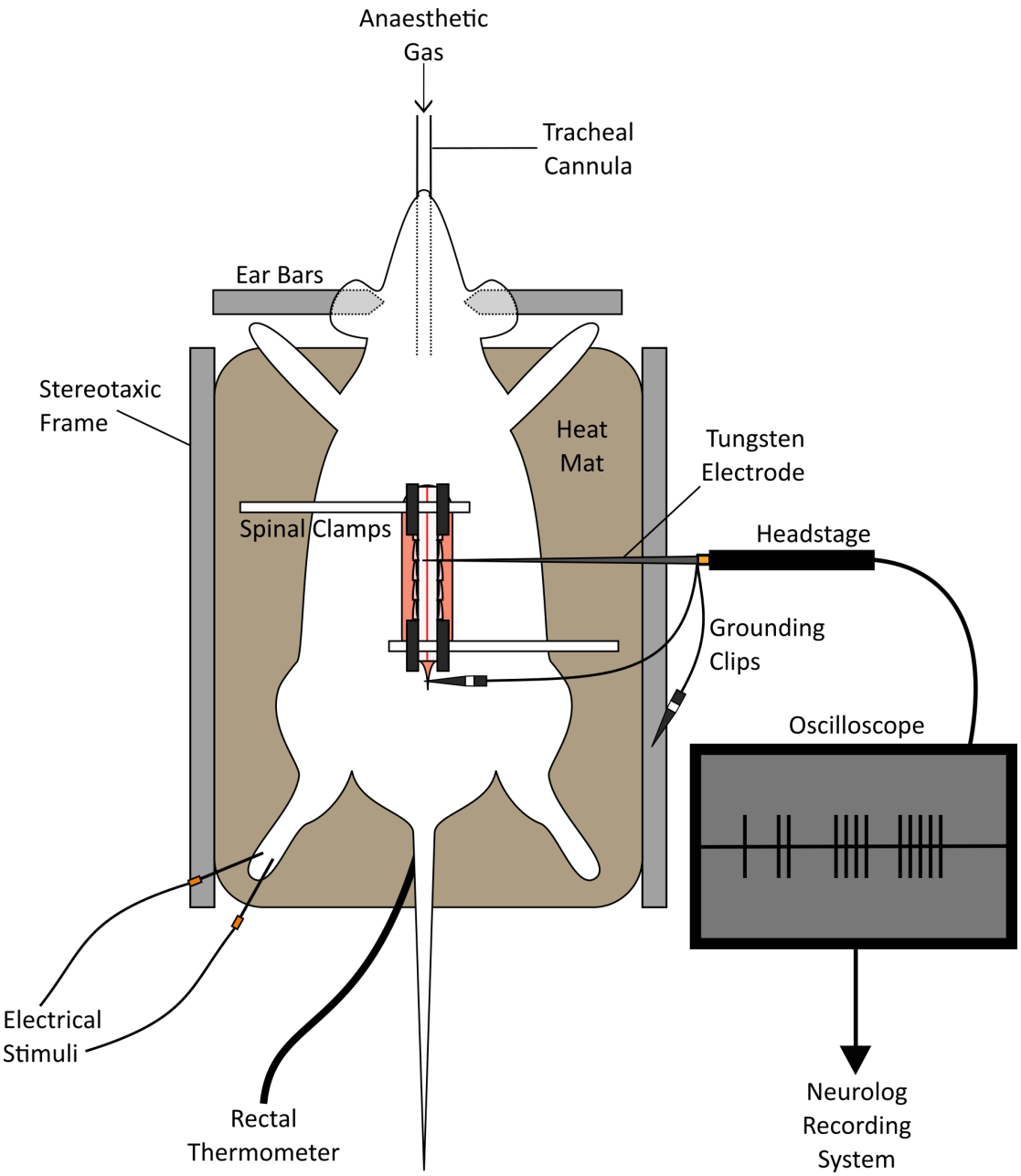


Figure 6.1: Setup of electrophysiology studies. Rats were secured in place using a stereotaxic frame and maintained under anaesthetised with 1.5% isoflurane in 33% nitrous oxide and 67% oxygen delivered via a tracheal cannula. A laminectomy exposed spinal regions L4-5 and the spine was clamped in place. The tungsten recording electrode was inserted into the spinal cord and mounted via a headstage and grounded to the rat and stereotaxic frame. The headstage connected to an oscilloscope to allow visualisation of neuronal responses and on to a Neurolog recording system. Electrical stimulation was delivered to the ipsilateral hindpaw. A heat mat and rectal thermometer maintained the temperature at 37˚C.

10µm increments (detailed in Section 2.2.7.4). The electrode was lowered 500-1000µm from the surface, which corresponded to lamina V-IV, and WDR were located by gently tapping the ipsilateral hindpaw until distinguishable and uniform spikes were elicited.

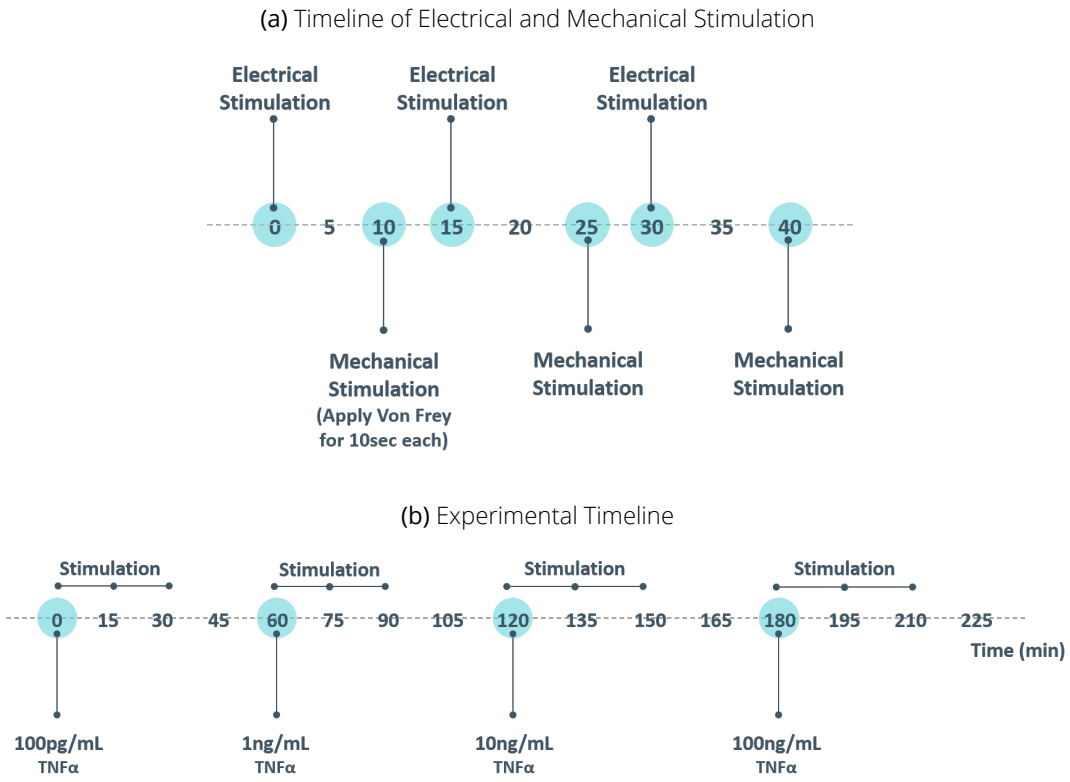


Figure 6.2: Experimental timeline of electrophysiology studies. **(a)** Electrical stimulation was followed by mechanical stimulation after 10 min, and then electrical stimulation again after 5 min. **(b)** Drugs were given at 0 min, followed by 3 sets of stimulations every 15 min, and then an increased dose after 60 min.

Once a cell was located, it was characterised as a WDR neurone if it had a graded response to mechanical stimulation (8-26g von Frey filaments, with an increased firing rate with higher weights) and Aβ, Aδ, C fibre and Post-Discharge (PD) responses from electrical stimulation. Electrical stimulation was delivered as trains of 16 consecutive transcutaneous impulses (0.5 Hz, 2-ms pulse width, three times C fibre threshold) at the centre of the ipsilateral hindpaw. Trains were recorded every 15 min (electrical stimulation followed by mechanical 10 min after, then electrical after 5 min and so on, see Figure 6.2a). These stimulation protocols were repeated until there were three consistent responses (within 10% of each other). The average of these three responses was recorded as the baseline response. If consistent responses could not be achieved or a cell could not be located, the recording electrode was removed and reinserted to search for another WDR neurone. Depth, C fibre threshold and C fibre latency measurements of WDR neurones were recorded (see Table 6.1). C fibre threshold was determined by delivering a 0.5mA initial pulse and increasing in 0.1mA increments until Aβ, Aδ, and C fibre inputs were included (determined by firing latencies of 0-20ms, 20-90ms, 90-300ms respectively (Urch and Dickenson 2003)).

50uL TNFα (in 0.1%BSA in PBS vehicle) was given via intrathecal application to the spinal cord using a Hamilton Syringe (Hamilton Company, NV, USA) at 0 min and three sets of stimulations were recorded, then a higher dose was given 60 min after the first dose to generate a cumulative concentration:response, where possible (see Figure 6.2b). Some animals received three doses, whilst some only received one dose due to time limitations of performing the procedures. Vehicle animals received one intrathecal application of 0.1%BSA in PBS and were followed for 30-40 min.

6.2.4 Data Analysis

Data are expressed as the percentage of the baseline response (determined as the average of three responses to electrical stimulation within 10% of each other). Area under the curve data were calculated from the means of fibre-specific responses. Data are presented as the mean ± Standard Deviation (SD). Analysis of data was performed using GraphPad Prism 7.05/8.4.3, and all tests performed will be specified in relevant results.

6.3 Results

6.3.1 Characteristics of WDR Neurones

Depth, C fibre latencies, and C fibre thresholds of WDR neurones were recorded and are listed in Table 6.1. There were no statistical differences between groups for depth, threshold for C fibre stimulation or latency of firing (1way ANOVA with Tukey's multiple comparisons).

Group	Depth (μm)	Threshold (mA)	Latency (ms)	n
Vehicle	765±106.1	1.35±0.35	213±69.3	2
5pg/50μL	910	1.7	106	1
50pg/50μL	802.5±142.2	1.85±0.73	173.5±50.4	4
500pg/50μL	756.7±133.2	1.93±0.87	155.3±42.8	3
5ng/50μL	700±116.9	2.13±0.9	160±41.4	4

Table 6.1: There were no statistical differences between groups for depth, threshold for C fibre stimulation or latency of firing (1way ANOVA with Tukey's multiple comparisons). n = number of neurones.

6.3.2 Intrathecal TNFα has No Effect on Spinal WDR Firing

To determine whether TNFα had an effect on spinal excitability, I recorded WDR neuronal responses to varying doses of intrathecal rat recombinant TNFα (n = 6 rats) or vehicle (0.1%BSA in PBS, n = 2 rats) at an average depth of 772.5±13μm from the surface of the dorsal horn of the spinal cord.

Data are displayed as percentage of baseline response (%). Vehicle had no impact on

WDR firing (Figure 6.3a). Addition of intrathecal TNFα also had no discernable effect on WDR firing (Figure 6.3b). This lack of effect on firing rate is apparent when data was separated into fibre types (Figure 6.4) and calculating the area under the curve for each dose (Figure 6.5).

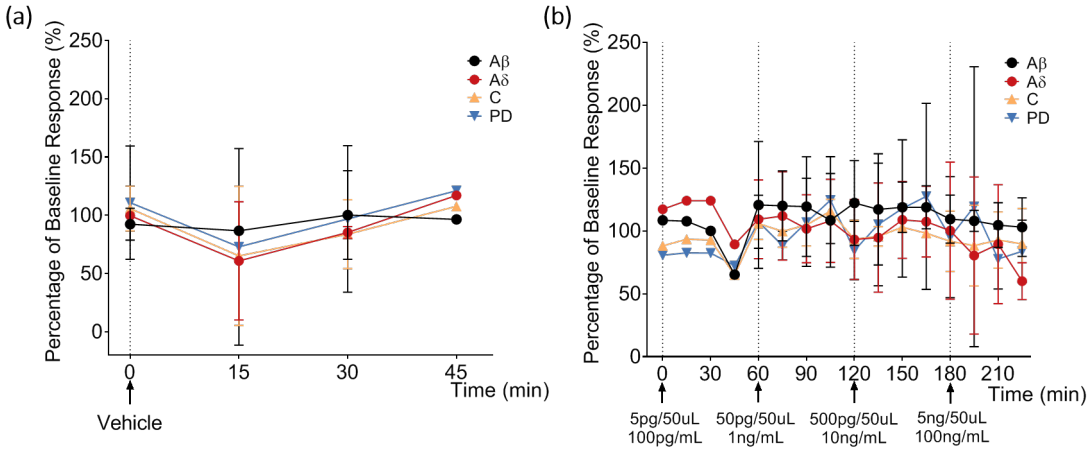


Figure 6.3: Spinal electrophysiology responses to electrical stimulation and vehicle (a Depth = 765±106.1µm, C fibre threshold = 1.35±0.35, C fibre latency = 213±69.3ms) or TNFα (b Depth = 775±147.6µm, C fibre threshold = 1.97±0.74, C fibre latency = 50.29±162.3ms). Neither vehicle nor TNFα application had an effect on WDR neurone firing. n = 1-4. Aβ: Aβ fibres; Aδ: Aδ fibres; C: C fibres; PD: Post Discharge; VF: von Frey hairs.

6.4 Discussion

The purpose of this chapter was to demonstrate skills in a powerful technique to measure the downstream effects of neuroinflammation and gliovascular alterations in chronic pain on spinal excitability. However, here intrathecal application of rat recombinant TNFα had no measurable impact on spinal WDR excitability.

The lack of TNFα-induced hyperexcitability on A and C fibres could be due to the drug not penetrating the spinal cord and reaching WDR neurones. The question is whether intrathecally applied drugs can reach the WDR neurone that is being recorded, and whether the drug is having an effect on the area [depth] of the spinal cord that is being recorded. It is generally accepted that drugs penetrate the spinal cord after intrathecal application (Cridland et al. 1987), but the length of time for drugs to penetrate the spinal cord differs depending on size and lipid solubility of the drug (McQuay et al. 1989). Using a Multi Electrode Array (MEA) that records from different depths of the dorsal horn simultaneously showed there was a significant lag in drug action and differing fibre responses between superficial and deep areas of the dorsal horn with intrathecal/topical application of morphine (Greenspon et al. 2019; Greenspon 2018). Here, Greenspon and colleagues detected a significant drug effect on C fibre responses starting at 15 minutes in the superficial dorsal horn, but not until the 85 minute timepoint in the deep dorsal horn (Greenspon et al. 2019; Greenspon 2018). This temporal effect of drug action in the deep dorsal horn was evident with responses of all fibres

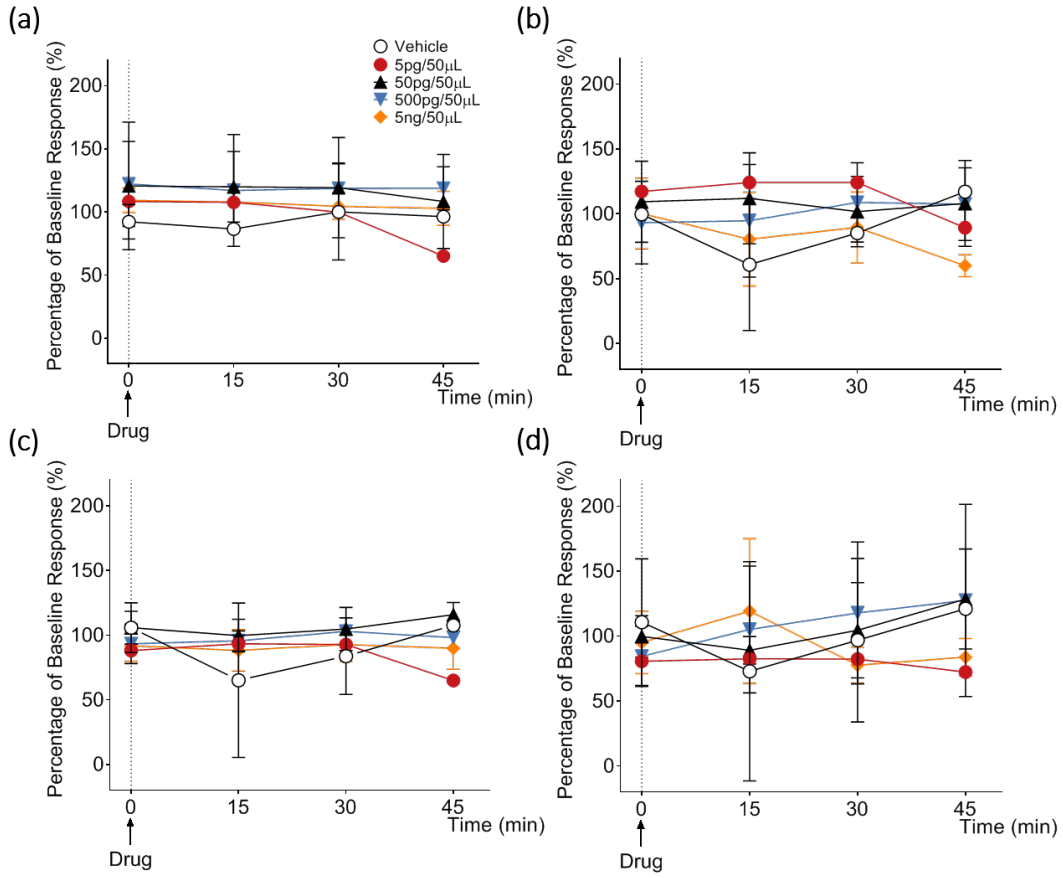


Figure 6.4: There was no statistical difference between fibre-specific responses to intrathecal TNFα or vehicle. (a): Aβ fibres; (b): Aδ fibres; (c): C fibres; (d): post-discharge. Depth = 772.5±131.1µm, C fibre threshold = 1.81±0.7mA, C fibre latency = 175±55.16ms. Mixed-effects analysis, n = 4-16.

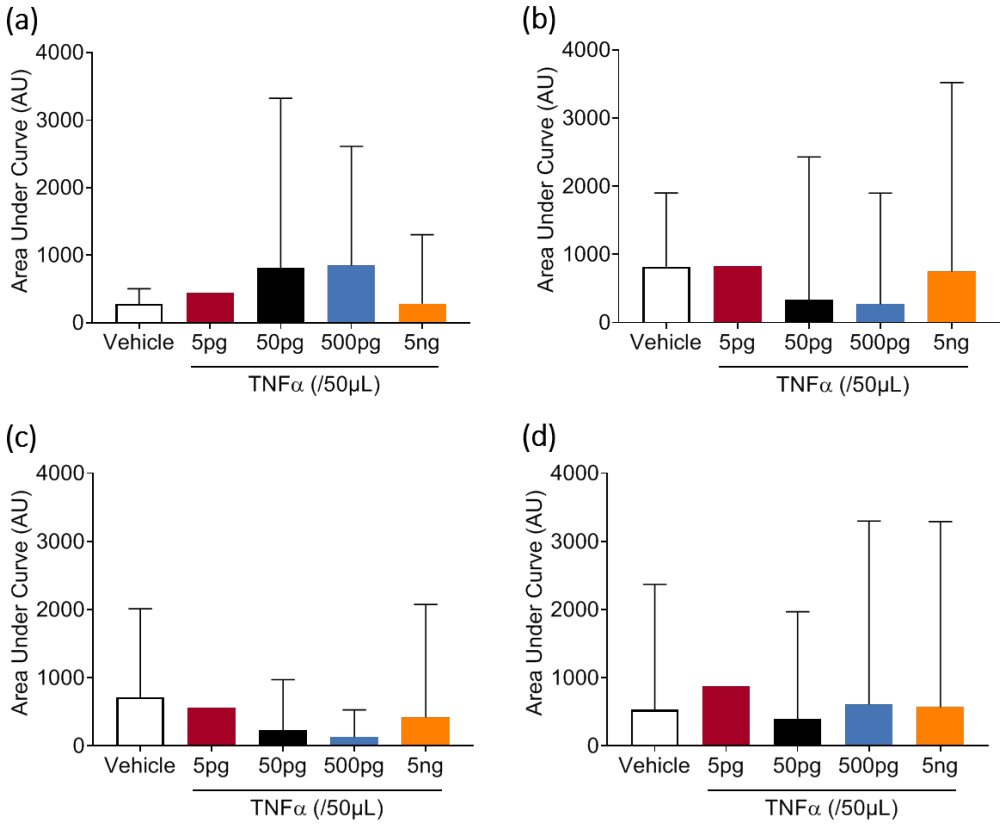


Figure 6.5: There was no statistical difference between area under the curve values of fibre-specific responses to intrathecal TNFα or vehicle. (a): Aβ fibres; (b): Aδ fibres; (c): C fibres; (d): post-discharge. Depth = 772.5±131.1μm, C fibre threshold = 1.81±0.7mA, C fibre latency = 175±55.16ms. One-way ANOVA. Vehicle: n = 4; 5pg: n = 1; 50pg: n = 13; 500pg: n = 9; 5ng: n = 11.

(Aδ, starting at 15min in the superficial and 25min in the deep; Aβ 75min in deep; PD at 75min in deep). This highlights the time needed for drugs to penetrate into the deep dorsal horn of the spinal cord, suggesting that here, TNFα may not have been able to penetrate deep into the spinal cord during the experiment time-frame, meaning its effects were not recorded.

Greenspon and colleagues (2019; 2018) used morphine, and as diffusion of drugs depends on the physical characteristics of the solute, the time for TNFα to penetrate the spinal cord is likely to be different. Using a diffusion time calculator (PhysiologyWeb 2020) and the diffusion coefficient value of TNFα from the Alzheimer's In Silico project from The University of British Columbia Mathematics Department (Alzheimer's In Silico 2001) the approximate diffusion time of TNFα over 772.5μm was calculated to be 165.77 minutes or 2.76 hours. Whilst this is an estimate, as diffusion depends on the temperature and physical properties of the medium, it suggests the experimental time-frame (60min per dose) may not have been long enough for TNFα to penetrate the spinal cord down to the WDR neurone being recorded and induce excitability. Effects of TNFα on WDR firing may therefore have been detected after a longer amount of time.

Additionally, saline was used to keep the surface of the cord wet between drug applications, meaning the TNFα may have been diluted when applied to the cord. The diluted TNFα also will have been able to distribute across the exposed surface of the cord, rather than being concentrated in the area just above the recorded WDR neurones, further diluting it. To avoid this, agarose could be used to cover the cord and a hole made to restrict the area that the drugs come into contact with the cord.

In contrast to these results, in the study by Reeve and colleagues (2000), there was a significant increase in late A fibre and PD firing with 5ng TNFα, and in acute C fibre firing with 50pg, 500pg and 5ng TNFα at the same depth of the spinal cord (739±51μm vs. 772.5±13μm here). In the Reeve's study, TNFα may have been acting at central terminals of primary afferent fibres through access at nerve root trunks. TNFα application here (on the L5 nerve root) at the lowest concentration used by Reeve et al. (0.01ng/mL) was able to increase WDR firing both spontaneously and in response to nociceptive stimuli (Onda et al. 2002). This significant increase in WDR firing was delayed, and measurable 1-2h post-TNFα application, again highlighting the lag in drug action from time of application. This finding by Onda et al. (2002) suggests the positive results from Reeve and colleagues (2000) may be from indirect action of TNFα diffusing and acting at the Dorsal Root Ganglion (DRG) or nerve root. Additionally, Reeve and colleagues gave the vehicle first and then gave cumulative doses of TNFα over a longer period of time (5h vs. 2h here), rather than using vehicle-specific animals. Spinal excitability may have increased over time due to repeated stimulation, and without a vehicle control to show the opposite this cannot be ruled out. Indeed, repeated peripheral stimulation does lead to functional plasticity in the spinal cord resulting in innocuous stimuli being processed as noxious (Woolf 1983), and was actually how Clif-

ford J. Woolf discovered central sensitisation (Li et al. 2007). Also, as discussed above, there is a delay between exogenous drug application and significant action, and the longer recording time in Reeve's study may have been long enough to measure TNFα's action whereas it was not here.

As well as TNFα having direct effects on primary afferents (Onda et al. 2002) and spinal dorsal horn neurones to modulate excitatory and inhibitory circuits (Zhang et al. 2010; Kawasaki et al. 2008b), it can also activate surrounding glial cells to increase spinal excitability therefore altering WDR transmission (Kanda et al. 2017). TNFR activation on glial cells can result in rapid kinase activation and release of cytokines/chemokines and excitatory neurotransmitters (Ji et al. 2019; Ji et al. 2013; Üçeyler et al. 2009). For example, TNFα-induced release of astrocytic C-C motif Chemokine Ligand 2 (CCL2) and C–X–C Chemokine Ligand 1 (CXCL1) can result in mechanical hypersensitivity through their binding to their receptors on neurones (Chen et al. 2014; Gao et al. 2010; Gao et al. 2009). These astrocyte expression changes can be fairly rapid, with protein expression evident within 15min (Gao et al. 2009) and behavioural hypersensitivity within 3h (Chen et al. 2014; Gao et al. 2010; Gao et al. 2009). This again suggests that the indirect effects of TNFα through glial activation were unlikely to be detected in this study as the time-frame here was too short. As well as glial activation directly altering spinal nociceptive signalling, endothelial activation can also impact nociception. Kanda et al. (2017) showed glial activation of endothelial cells via TNFα release contributed to neuropathic pain signalling via neuronal Prostaglandin I2 Receptor (IP), highlighting the three-way relationship between neurones, glia and endothelial cells that exists. More work is needed to fully understand this gliovascular-neuronal axis.

It should be noted that there is anaesthetic inhibition of spinal cord activity (Vahle-Hinz and Detsch 2002), although isoflurane inhibits activity to a lesser degree than some other anaesthetics, for example halothane (Cuellar et al. 2005). Additionally, WDR neurones are less susceptible to anaesthetic depression than nociceptive neurones in the dorsal horn (Barter et al. 2009), and so anaesthetic inhibition is unlikely to be the cause of the lack of effect seen with TNFα.

Due to the lack of changes with TNFα, this pilot study was halted. However, in conclusion, electrophysiology is a powerful technique that can uncover previously unknown neuronal signalling mechanisms, and is valuable in studying spinal nociceptive processing. Whilst the neuronal signalling effects of TNFα are well documented *in vitro*, it is necessary to measure spinal excitability in animals that have neuroinflammation and gliovascular alterations due to intra-articular CFA, and to investigate the role of TNFα and other locally released factors in these processes to fully understand their role in chronic pain development/maintenance. Additionally, to understand VEGF-A's role in chronic pain and how modulation of spinal endothelial cell VEGF receptor (VEGF-R) signalling can disrupt chronic pain development (Beazley-Long et al. 2018b), neuronal electrophysiology investigations will be required. To investigate this gliovascular-neuronal axis and how endothelial and glial cells contribute to neuronal sensitisation,

pharmacological interventions (either systemic or more concentrated intrathecal application to account for the limitations of exogenous intrathecal application highlighted above) or knockout mice could be employed. Additionally, using the more sophisticated MEA device to investigate these changes would give more information on whole dorsal horn responses to peripheral inflammation and spinal endothelial cell VEGF-R modulation, whilst allowing for temporal differences in intrathecal drug application.

7 | General Discussion and Conclusion

The aims of this thesis were to investigate the role of the gliovasculature in chronic pain development/maintenance, with particular emphasis on the contribution of endothelial cells and two inflammatory mediators, Vascular Endothelial Growth Factor (VEGF)-A and Tumour Necrosis Factor α (TNFα). Through both *in vivo* and *in vitro* techniques, the gliovasculature was shown to be activated in chronic pain and neuroinflammatory conditions, and contributed to chronic pain development and maintenance: knocking out endothelial-specific Vascular Endothelial Growth Factor Receptor (VEGF-R)2 prevented the development of vessel-associated glial activation (as well as secondary pain development); and concurrent disruption of VEGF-R2 and TNFα signalling partially reversed established inflammatory-induced secondary pain. Additionally, TNFα induced increased monocyte-like cell binding to Human Brain Microvascular Endothelial Cells (HBMECs) and HBMEC expression of adhesion molecules.

The findings in this thesis and the literature support my hypothesis that neural endothelial cells can be activated by inflammatory molecules (for example VEGF-A and TNFα) to increase permeability to blood-borne cells and molecules in chronic pain. These inflammatory molecules [that activate neural endothelial cells] may originate from the periphery and access neural endothelial cells through the blood (Totoson et al. 2016; Wei et al. 2015; Steyers and Miller 2014; Nakahara et al. 2003), or from chronic pain-associated neuroinflammation in the Central Nervous System (CNS) (Flores Bjurström et al. 2020; Jung et al. 2020; Albrecht et al. 2018). Additionally, endothelial cells can release inflammatory molecules (Ludewig et al. 2019; Smyth et al. 2018; Varatharaj and Galea 2016), including VEGF-A and TNFα, that can go on to further activate glial cells and exacerbate/contribute to neuroinflammation, increased Blood Spinal Cord Barrier (BSCB) permeability and central sensitisation (Varatharaj and Galea 2016; Grace et al. 2014). My hypothesised summary of acute inflammatory pain signalling (Figures 7.1 and 7.2) leading to central sensitisation and the contribution of endothelial cells and glia (Figures 7.3 and 7.4) are below. In short, during acute inflammatory pain (Figures 7.1 and 7.2), nociceptors are activated in the periphery and activate projection neurones in the dorsal horn of the spinal cord through release of neurotransmitters such as glutamate and substance P. These neurotransmitters can activate glial cells through Nuclear Factor Kappa-Light-Chain-Enhancer of Activated B Cells (NF-κB) activation (Milligan and Watkins 2009) in addition to causing projection neurones to relay nociceptive signals to supra-spinal centres in the brain for further processing. Innocuous touch detected by low threshold mechanoreceptors, for example some A fibres, is not normally perceived as noxious (Djouhri and Lawson 2004), but inflammatory conditions can result in tactile allodynia through central sensitisation (Schaible 2006). Astrocytes, microglia and endothelial cells maintain the BSCB to prevent extravasation of blood-borne cells and molecules, which could sensitise and

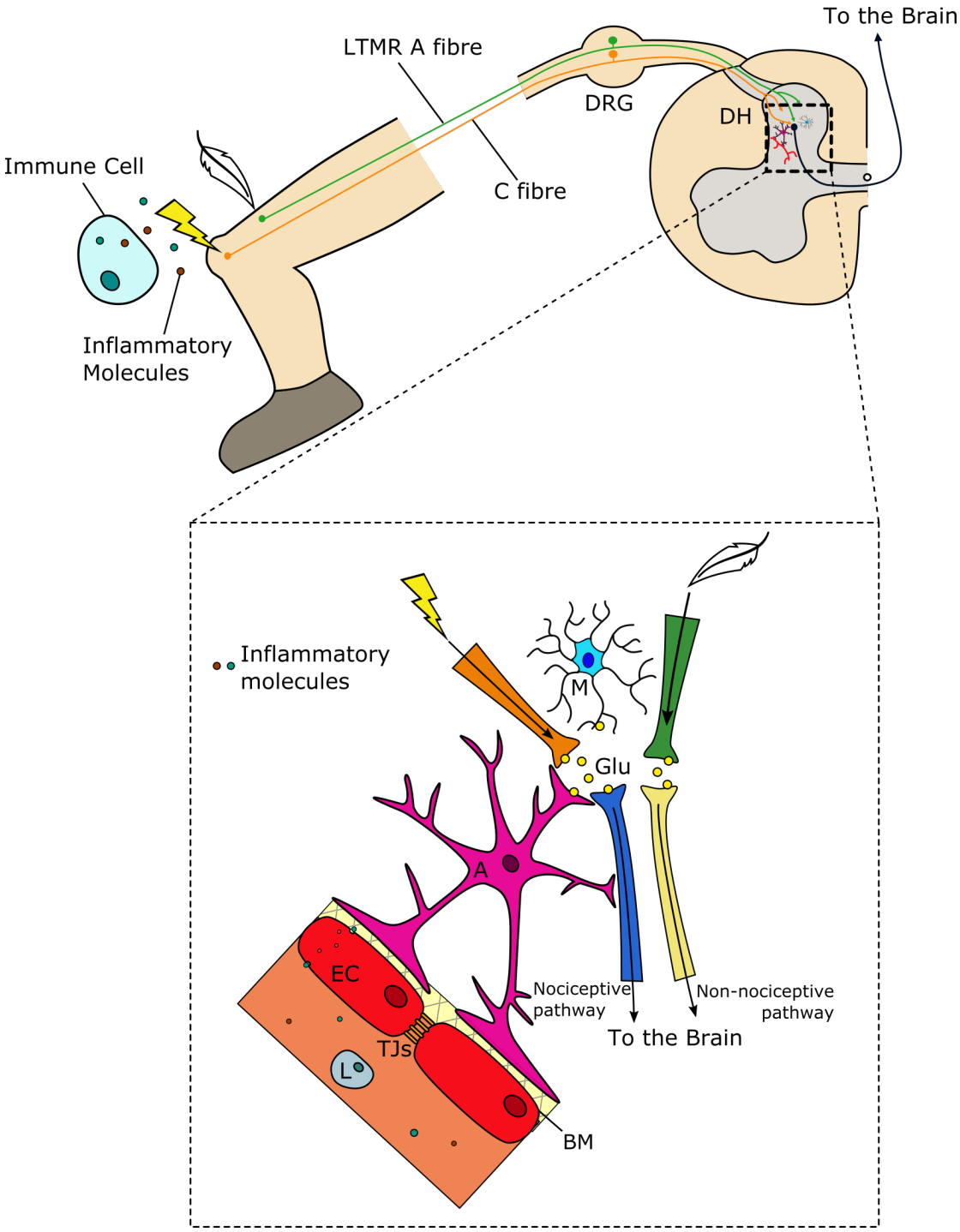


Figure 7.1: Acute inflammatory pain signalling in the periphery and spinal cord. Immune cells produce inflammatory molecules that activate nociceptors in the periphery (for example C fibres), which causes release of excitatory neurotransmitters (for example glutamate, Glu) in the dorsal horn (DH) of the spinal cord. These transmitters activate projection neurones to send nociceptive signals to supra-spinal centres in the brain for further nociceptive processing, and activate astrocytes (A) and microglia (M). Innocuous touch (represented by the feather) detected by low threshold mechanoreceptors (LTMR), for example some A fibres, is not normally perceived or interpreted in the brain as noxious (although peripheral sensitisation can occur resulting in tactile allodynia). The blood-spinal cord barrier is maintained by astrocytes and endothelial cells (EC). BM: basement membrane; L: leukocytes; TJs: tight junctions.

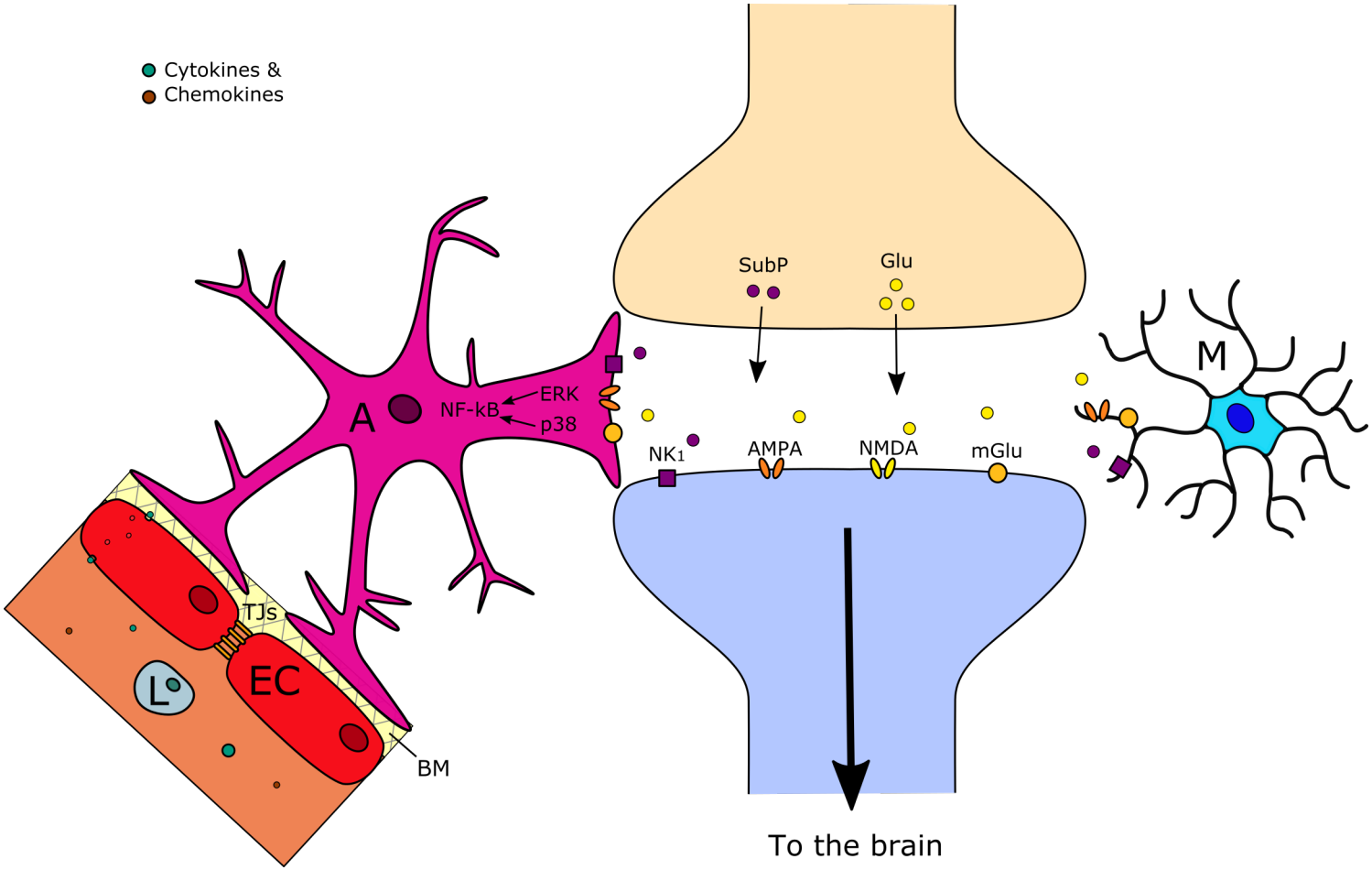


Figure 7.2: Receptors and transmitters in acute inflammatory pain signalling in the spinal cord. Upon activation, primary afferent fibres release excitatory neurotransmitters, such as glutamate (**Glu**) and substance P (**SubP**), in the dorsal horn of the spinal cord. These neurotransmitters activate receptors (mGlu, NMDA, AMPA, NK_1) on nociceptive projection neurones to relay nociceptive signals to supra-spinal centres in the brain for further nociceptive processing. Glutamate and substance P can also activate astrocytes (**A**) and microglia (**M**) through activation of NF-kB via ERK and p38 MAPK (**p38**) signalling. Astrocytes and endothelial cells (**EC**) maintain the blood spinal cord barrier through tight junctions (**TJs**), preventing extravasation of blood-borne cells (for example Leukocytes, **L**) and molecules. **AMPA**: α-amino-3-hydroxy-5-methylisoxazole-4-propionate receptors; **BM**: basement membrane; **ERK**: extracellular-regulated kinase; **MAPK**: mitogen-activated protein kinase; **mGlu**: metabotropic glutamate receptors; **NF-kB**: nuclear factor kappa-light-chain-enhancer of activated B cells; **NMDA**: N-methyl-D-aspartate receptors.

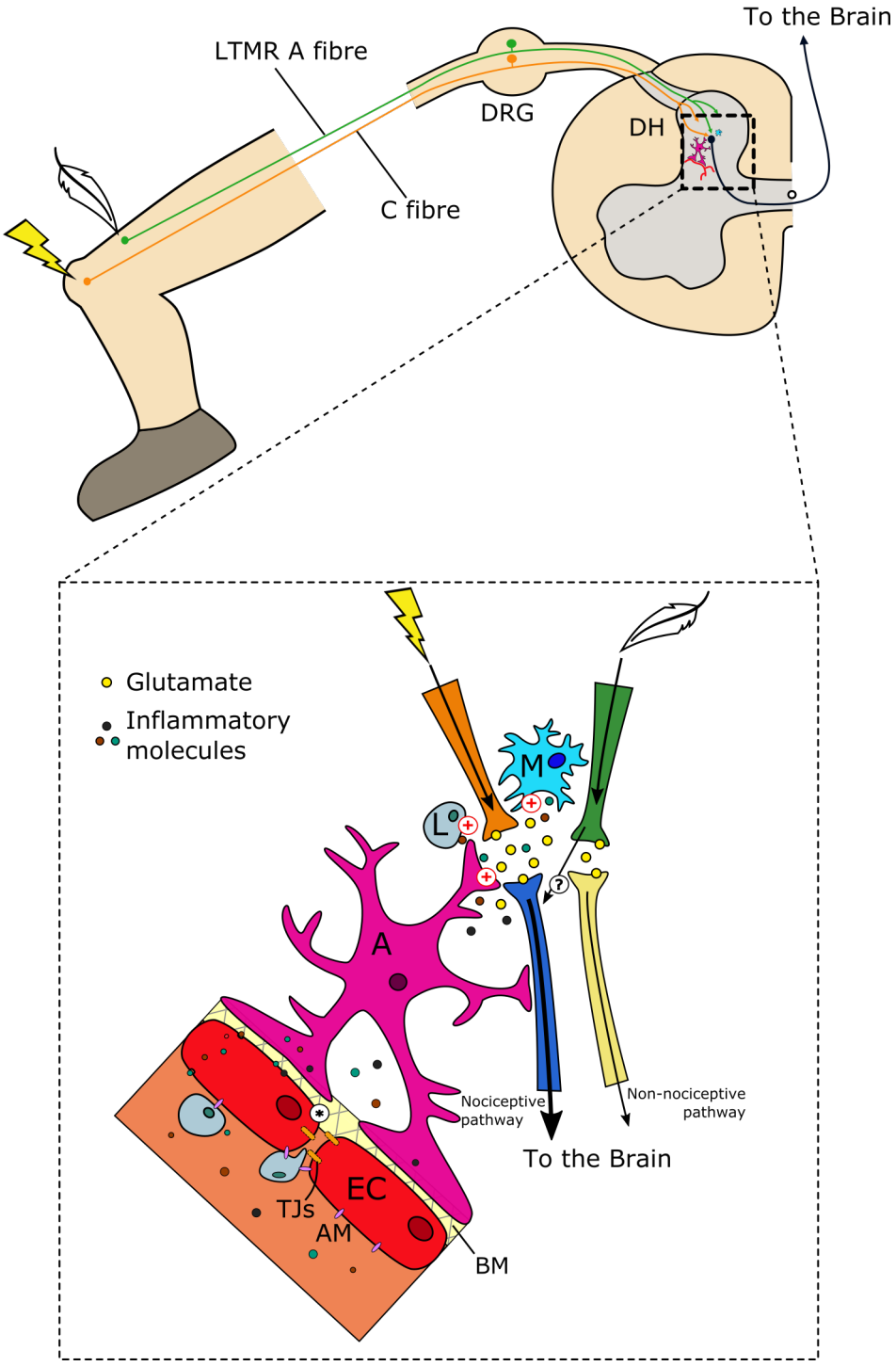


Figure 7.3: The contribution of neural endothelial cells and the gliovasculature to chronic inflammatory pain signalling in the periphery and spinal cord. Central sensitisation in the dorsal horn (DH) of the spinal cord, due to prolonged nociceptor (for example C fibre) firing, sensitises projection neurones to amplify nociceptive signals to the brain. Activated astrocytes (A) and microglia (M) can release inflammatory molecules to also sensitise DH neurones (+). I hypothesised that endothelial cells (EC) can be activated by reactive glial cells or circulating inflammatory molecules, and can contribute to central sensitisation and neuroinflammation through modulation of the blood-spinal cord barrier and release of inflammatory molecules (*). During chronic pain, projection neurones may be sensitised to non-nociceptive primary afferent fibres, for example low threshold mechanoreceptors (LTMR) A fibres, meaning innocuous touch (represented by the feather) can now activate the nociceptive pathway, although this is not fully understood (?). Hyperactive projection neurones send nociceptive signals to supra-spinal centres in the brain for further nociceptive processing. AM: adhesion molecules; BM: basement membrane; Glu: glutamate; L: leukocytes; TJs: tight junctions.

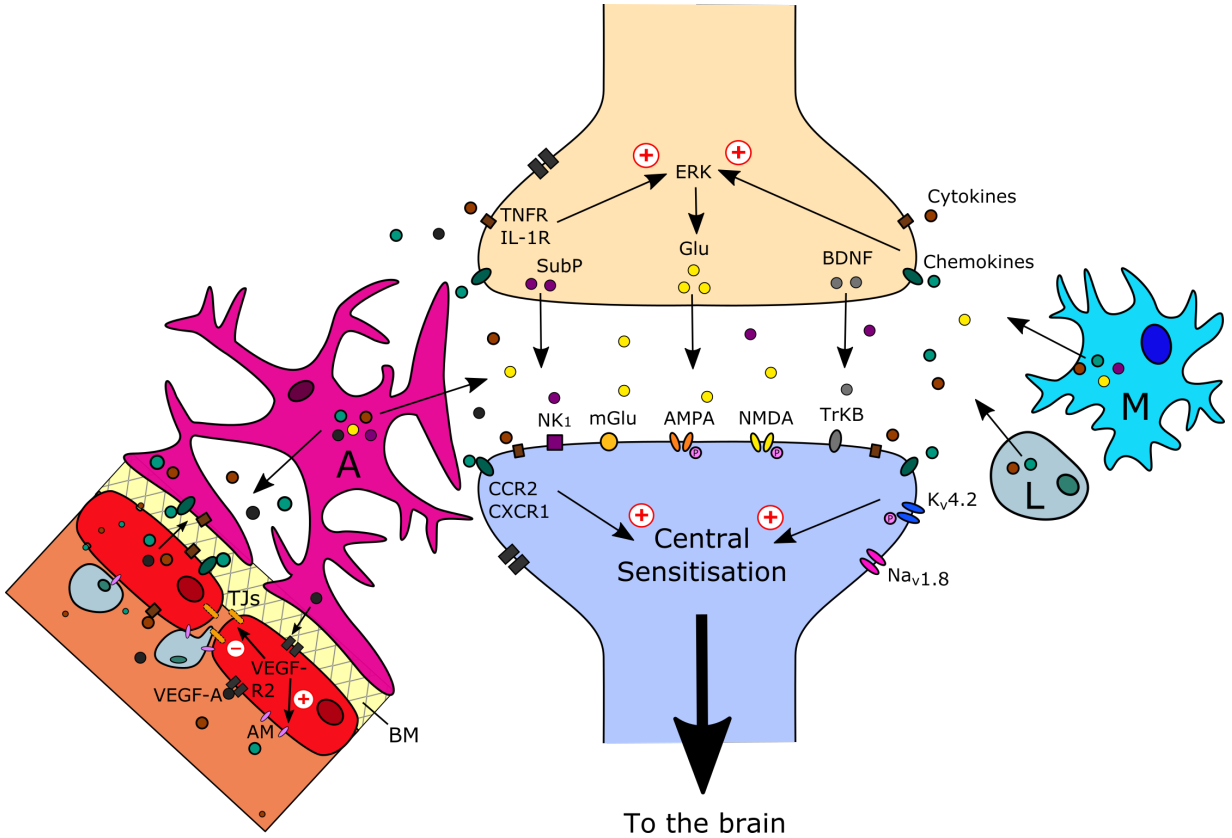


Figure 7.4: Receptors and Transmitters involved in neural endothelial cells and the gliovasculature's contribution to chronic inflammatory pain signalling in the spinal cord. Central sensitisation in the dorsal horn of the spinal cord due to prolonged primary afferent firing results in increased neurotransmitter release from pre-synaptic terminals and increased receptor and channel expression on post-synaptic dorsal horn neurones. Activated astrocytes (**A**) and microglia (**M**) can release excitatory gliotransmitters, for example glutamate (**Glu**) and substance P (**SubP**) to increase dorsal horn neurone sensitivity and central sensitisation (**+**). Additionally, activated glial cells can release inflammatory molecules, including cytokines and chemokines, to further sensitise dorsal horn neurones. I have suggested that endothelial cells (**EC**) can be activated by inflammatory molecules (including VEGF-A and TNFα) derived from activated glial cells or circulating in the blood. These activated endothelial cells can release pro-inflammatory molecules, increase extravasation of immune cells (for example leukocytes, **L**) and blood-borne molecules, increase production of adhesion molecules (**AM**), and down-regulate expression of tight junctions (**TJs**, **-**). Infiltrating leukocytes and endothelial cells can further activate glial cells, contribute to neuroinflammation, and sensitise neurones through release of pro-inflammatory molecules (for example VEGF-A and TNFα). Hyperactive projection neurones send nociceptive signals to supra-spinal centres in the brain for further nociceptive processing. **AMPA**: α-amino-3-hydroxy-5-methylisoxazole-4-propionate receptors; **BDNF**: brain-derived neurotrophic factor; **BM**: basement membrane; **CaMKII**: Ca2+/calmodulin-dependent protein kinase II; **CCR2**: C-C motif chemokine receptor 2; **CXCR1**: C-X-C motif chemokine receptor 1 (interleukin-8 receptor); **ERK**: extracellular-regulated kinase; **Glu**: glutamate; **IL-1R**: interleukin-1 receptor; **Kv4.2**: voltage-gated potassium ion channel subunit 4.2; **mGlu**: metabotropic glutamate receptors; **Nav1.8**: voltage-gated sodium ion channel subunit; **NK1**: Neurokinin 1 receptor; **NMDA**: N-methyl-D-aspartate receptors; **SubP**: substance P; **TNFR**: tumour necrosis factor receptor; **TrKB**: tyrosine kinase receptor B; **VEGF-A**; vascular endothelial growth factor-A; **VEGF-R2**: vascular endothelial growth factor receptor 2.

damage spinal neurones (Haruwaka et al. 2019; Abbott et al. 2010).

During prolonged inflammatory pain (Figures 7.3 and 7.4), such as in Rheumatoid Arthritis (RA), central sensitisation can occur in the dorsal horn of the spinal cord due to sustained primary afferent firing (Boyden et al. 2016; Walsh and McWilliams 2014). I have hypothesised and demonstrated a role of endothelial cells and the gliovasculature in contributing to this central sensitisation. It is known that activated astrocytes and microglia can release inflammatory molecules, for example TNFα and VEGF-A, and gliotransmitters, that can sensitise dorsal horn neurones (Ji et al. 2019; Tsuda et al. 2013; Ji et al. 2013; Argaw et al. 2012; Cuellar et al. 2004; Onda et al. 2002), resulting in hyperactive projection neurones. I have suggested that endothelial cells can be activated by VEGF-A and TNFα (and other inflammatory mediators) released by these reactive glial cells (Ji et al. 2019; Argaw et al. 2012) and/or by circulating inflammatory molecules, including by VEGF-A and TNFα, that are elevated in RA (Totoson et al. 2016; Wei et al. 2015; Nakahara et al. 2003), to: release pro-inflammatory molecules (Ludewig et al. 2019; Smyth et al. 2018; Varatharaj and Galea 2016; O'Carroll et al. 2015); increase extravasation of immune cells and blood-borne molecules (Yao and Tsirka 2014; Didier et al. 2003; Mark and Miller 1999); increase production of adhesion molecules (Radisavljevic et al. 2000); and down-regulate expression of tight junctions (Zhang et al. 2019; Argaw et al. 2012; Förster et al. 2008). Furthermore, infiltrating leukocytes and activated endothelial cells can further activate glial cells, contribute to neuroinflammation, and directly sensitise neurones through release of pro-inflammatory molecules (including VEGF-A and TNFα) (Varatharaj and Galea 2016; Grace et al. 2014). Under these neuroinflammatory conditions, normally silent nociceptors or non-nociceptive primary afferent fibres may begin to access spinal nociceptive circuitry and this can result in allodynia from innocuous stimuli being interpreted as noxious, possibly through disinhibition of excitatory interneurones (Torsney 2019).

I have demonstrated activation of astrocytes at spinal dorsal horn vessels during chronic inflammatory pain, which was prevented with VEGF-R2 knockdown, and activation of endothelial cells through increased adhesion molecule expression and monocyte-like cell binding in the presence of inflammatory mediators. Additionally, I demonstrated that chronic inflammatory pain could be partially reversed with anti-VEGF-R2 and TNFα treatment, and coupled with the previous results, this supports my theory that endothelial cells and their signalling with astrocytes through VEGF-A and TNFα may be key in central sensitisation and chronic pain.

While the contribution of glial cells and neuroinflammation to central sensitisation have been extensively reviewed (for example in Li et al. 2019; Ji et al. 2018; Ji et al. 2013; Tsuda et al. 2013; Milligan and Watkins 2009; Wieseler-Frank et al. 2005), the contribution of endothelial cells has been largely overlooked (for recent perspective see Beazley-Long 2019). It is the role of the gliovasculature that has been studied in this thesis to try to expand our knowledge of endothelial-glial-neuronal signalling in the context of pain.

7.1 Human Translation

There is substantial evidence for both glial activation and neuroinflammation in animal models of chronic pain (reviewed in Ji et al. 2019; Li et al. 2019; Tsuda 2019; Chen et al. 2018b; Inoue and Tsuda 2018; Ji et al. 2013; Ji and Suter 2007), and *in vitro* models of the Neurovascular Unit (NVU) have supported the crosstalk that exists between endothelial cells and glia in neuroinflammation (Osipova et al. 2018; Liebner et al. 2018; O'Carroll et al. 2015; Carvalho da Fonseca et al. 2014). As mentioned previously, glial cell activation/neuroinflammation has been detected in painful conditions in humans (Flores Bjurström et al. 2020; Jung et al. 2020; Albrecht et al. 2018), but although there is evidence for neuroinflammation in RA (Kosek et al. 2018; Kosek et al. 2015), glial activation is yet to be detected in RA (Forsberg et al. 2019).

BSCB disruption has been demonstrated in human neurodegenerative diseases such as motorneurone disease (Winkler et al. 2013; Zlokovic 2011), Alzheimer's disease (Zenaro et al. 2017), Multiple Sclerosis (MS) (Taheri et al. 2011), and chronic traumatic encephalopathy (Doherty et al. 2016), reviewed in Sweeney et al. (2018) and Varatharaj and Galea (2016). There is less direct evidence for Blood Brain Barrier (BBB)/BSCB breakdown in human RA, but this could be because it has not been a main research focus. There is some indirect evidence, however. Patients with RA have increased levels of S100 Calcium-Binding Protein (S100)A4 in synovial fluid and plasma (Klingelhöfer et al. 2007), which has been linked to BBB breakdown in Collagen-Induced Arthritis (CIA) via occludin down-regulation (Nishioku et al. 2011) and is positively correlated with disease activity (Ošlejšková et al. 2009). Similarly, Matrix Metalloproteinases (MMPs), notably MMP9 (Giannelli et al. 2004; Tchetverikov et al. 2004), Interleukin (IL)17 (Al-Saadany et al. 2016), and a multitude of other inflammatory markers (Altobelli et al. 2017) are elevated in RA serum, and these can degrade the BBB/BSCB (Becher et al. 2016; Patel and Frey 2015; Huppert et al. 2010; Ji et al. 2009). Increased levels of circulating Intracellular Adhesion Molecule-1 (ICAM-1) have also been demonstrated in RA (Cush et al. 1993): ICAM-1 is involved in immune cell infiltration into the CNS parenchyma and BBB/BSCB function (Clark et al. 2007). S100B is also increased in RA patient serum (Austermann et al. 2018) and can be used as a marker of BBB breakdown (Koh and Lee 2014; Yardan et al. 2011). However, S100B (like ICAM-1) is not restricted to the CNS (Donato et al. 2009), but increases in RA serum of S100B and ICAM-1 in combination with the other factors mentioned here indicate BBB/BSCB disruption. Additionally, patients show signs and markers of endothelial dysfunction (Chimenti et al. 2015; Steyers and Miller 2014), supporting the idea that endothelial cells and the BBB/BSCB could contribute to neuroinflammation/glial activation and central sensitisation.

7.2 Future Studies

There is an emerging role of pericytes in the regulation of the BBB/BSCB in neuroinflammation (Persidsky et al. 2016; Jansson et al. 2014; Takata et al. 2011; Machida et al. 2017), and a suggestion that they contribute to chronic pain development (reviewed in Durrant et al. 2018; Beazley-Long et al. 2018a). There is evidence from our lab that spinal cord pericytes are activated and express ICAM-1 in inflammatory arthritis (Durrant et al. 2018; Beazley-Long, unpublished), and considering pericytes express Platelet Derived Growth Factor Receptor-β (PDGFR-β) which is mildly inhibited by PTK787 (Wood et al. 2000), it is necessary to investigate their contribution to a) chronic pain development and b) the PTK787-mediated prevention of this secondary pain (as seen in Beazley-Long et al. 2018b) to follow up this theory.

In order to fully understand the role of the gliovasculature on chronic inflammatory pain/development and dorsal horn neuronal signalling, modulating NVU component function in inflammatory pain is needed. There are *in vitro* experiments that can be carried out using co-cultures of HBMECs and astrocytes or pericytes to probe mechanics of their relationship, but *in vivo* techniques can provide information in inflammatory pain conditions. As described in this thesis, inducible endothelial-cell VEGF-R2 knockout mice were used to investigate the contribution of VEGF-A and endothelial cells, but by knocking out astrocytes using an inducible astrocyte cell knockout mouse line (The Jackson Laboratory 2020; Hu et al. 2020; Davila et al. 2013; Casper et al. 2007), their contribution could be more closely investigated. Astrocytes can be inhibited using pharmacological agents such as fluorocitrate (Watkins et al. 2007; Swanson and Graham 1994; Meller et al. 1994), but this is not specific for astrocytes as it can also inhibit microgliosis (Sung et al. 2012), and so astrocyte knockout mice lines would be superior. Neuronal VEGF-R2 knockout mice could be used to investigate the contribution of neuronal-specific VEGF-R2 (for example in Okabe et al. 2014).

Coupled with NVU knockout mice, functional assays such as *in vivo* electrophysiology would provide information on the contribution of the gliovasculature on neuronal signalling during inflammatory pain. Additionally, using a more sophisticated Multi Electrode Array (MEA) device would allow for more informative investigations into both lamina-specific and neural population responses to peripheral-/neuro- inflammation.

7.3 Conclusion

In conclusion, these results indicate the gliovasculature, in particular astrocytes and endothelial cells, undergoes activation in chronic inflammatory pain and central sensitisation. They also support the hypothesis that endothelial cells are involved in maintaining chronic pain through their activation by inflammatory mediators and subsequent downstream signalling on glial cells and neurones. However, the specific mechanisms of the relationship of neurovasculature activation and neuronal signalling in central sensitisation are still unknown and require further investigation.

Bibliography

Abbott, N. J., A. A. Patabendige, D. E. Dolman, S. R. Yusof, and D. J. Begley (2010). "Structure and function of the blood–brain barrier". In: *Neurobiology of Disease* 37.1, pp. 13–25.

Abbott, N. J., L. Rönnbäck, and E. Hansson (2006). "Astrocyte–endothelial interactions at the blood–brain barrier". In: *Nature Reviews Neuroscience* 7.1, pp. 41–53.

Acharya, A., S. T. Baek, S. Banfi, B. Eskiocak, and M. D. Tallquist (2011). "Efficient inducible Cre-mediated recombination in Tcf21cell lineages in the heart and kidney". In: *Genesis* 49.11, pp. 870–877.

Adrian, E. D. and K. Umrath (1929). "The impulse discharge from the pacinian corpuscle". In: *The Journal of Physiology* 68.2, pp. 139–154.

Albrecht, D. S., S. U. Ahmed, N. W. Kettner, R. J. Borra, J. Cohen-Adad, H. Deng, T. T. Houle, A. Opalacz, S. A. Roth, M. F. Melo, L. Chen, J. Mao, J. M. Hooker, M. L. Loggia, and Y. Zhang (2018). "Neuroinflammation of the spinal cord and nerve roots in chronic radicular pain patients". In: *Pain* 159.5, pp. 968–977.

Albuquerque, R. J. et al. (2009). "Alternatively spliced vascular endothelial growth factor receptor-2 is an essential endogenous inhibitor of lymphatic vessel growth". In: *Nature Medicine* 15.9, pp. 1023–1030.

Alston-Roberts, C. et al. (2010). *Cell line misidentification: The beginning of the end*.

Altobelli, E., P. M. Angeletti, D. Piccolo, and R. De Angelis (2017). "Synovial Fluid and Serum Concentrations of Inflammatory Markers in Rheumatoid Arthritis, Psoriatic Arthritis and Osteoarthitis: A Systematic Review". In: *Current Rheumatology Reviews* 13.3.

Alvarez, J. I., A. Dodelet-Devillers, H. Kebir, I. Ifergan, P. J. Fabre, S. Terouz, M. Sabbagh, K. Wosik, L. Bourbonnière, M. Bernard, J. van Horssen, H. E. de Vries, F. Charron, and A. Prat (2011). "The Hedgehog pathway promotes blood-brain barrier integrity and CNS immune quiescence." In: *Science* 334.6063, pp. 1727–31.

Alzheimer's In Silico (2001). *Diffusion of molecules and cytokines*.

Argaw, A. T., L. Asp, J. Zhang, K. Navrazhina, T. Pham, J. N. Mariani, S. Mahase, D. J. Dutta, J. Seto, E. G. Kramer, N. Ferrara, M. V. Sofroniew, and G. R. John (2012). "Astrocyte-derived VEGF-A drives blood-brain barrier disruption in CNS inflammatory disease". In: *Journal of Clinical Investigation* 122.7, pp. 2454–2468.

Argaw, A. T., B. T. Gurfein, Y. Zhang, A. Zameer, and G. R. John (2009). "VEGF-mediated disruption of endothelial CLN-5 promotes blood-brain barrier breakdown." In: *Proceedings of the National Academy of Sciences* 106.6, pp. 1977–1982.

Argaw, A. T., Y. Zhang, B. J. Snyder, M.-L. Zhao, N. Kopp, S. C. Lee, C. S. Raine, C. F. Brosnan, and G. R. John (2006). "IL-1β Regulates Blood-Brain Barrier Permeability via Reactivation of the Hypoxia-Angiogenesis Program". In: *The Journal of Immunology* 177.8, pp. 5574–5584.

Ashburn, M. A. and P. S. Staats (1999). "Management of chronic pain". In: *The Lancet* 353.9167, pp. 1865–1869.

Asquith, D. L., A. M. Miller, I. B. McInnes, and F. Y. Liew (2009). "Animal models of rheumatoid arthritis". In: *European Journal of Immunology* 39.8, pp. 2040–2044.

Attwell, D., A. M. Buchan, S. Charpak, M. Lauritzen, B. A. MacVicar, and E. A. Newman (2010). *Glial and neuronal control of brain blood flow*.

Austermann, J., C. Spiekermann, and J. Roth (2018). "S100 proteins in rheumatic diseases". In: *Nature Reviews Rheumatology* 14.9, pp. 528–541.

Avraham, H. K., T. H. Lee, Y. Koh, T. A. Kim, S. Jiang, M. Sussman, A. M. Samarel, and S. Avraham (2003). "Vascular endothelial growth factor regulates focal adhesion assembly in human brain microvascular endothelial cells through activation of the focal adhesion kinase and related adhesion focal tyrosine kinase". In: *Journal of Biological Chemistry* 278.38, pp. 36661–36668.

Bajrović, F. and J. Sketelj (1998). "Extent of nociceptive dermatomes in adult rats is not primarily maintained by axonal competition". In: *Experimental Neurology* 150.1, pp. 115–121.

Banks, W. (2015). "The blood-brain barrier in neuroimmunology: Tales of separation and assimilation". In: *Brain, Behavior, and Immunity* 44, pp. 1–8.

Banks, W. A. et al. (2015). "Lipopolysaccharide-induced blood-brain barrier disruption: roles of cyclooxygenase, oxidative stress, neuroinflammation, and elements of the neurovascular unit". In: *Journal of Neuroinflammation* 12.1, p. 223.

Barros, L. F., A. Brown, and R. A. Swanson (2018). "Glia in brain energy metabolism: A perspective". In: *GLIA* 66.6, pp. 1134–1137.

Barter, L. S., E. E. Carstens, S. L. Jinks, and J. F. Antognini (2009). "Rat dorsal horn nociceptive-specific neurons are more sensitive than wide dynamic range neurons to depression by immobilizing doses of volatile anesthetics: An effect partially reversed by the opioid receptor antagonist naloxone". In: *Anesthesia and Analgesia* 109.2, pp. 641–647.

Bartoli, M., D. Platt, T. Lemtalsi, X. Gu, S. E. Brooks, M. B. Marrero, and R. B. Caldwell (2003). "VEGF differentially activates STAT3 in microvascular endothelial cells." In: *FASEB Journal* 17.11, pp. 1562–4.

Basbaum, A. I., D. M. Bautista, G. Scherrer, and D. Julius (2009). "Cellular and Molecular Mechanisms of Pain". In: *Cell* 139.2, pp. 267–284.

Bates, D. O. (2010). "Vascular endothelial growth factors and vascular permeability". In: *Cardiovascular Research* 87.2, pp. 262–271.

Bates, D. O., T. G. Cui, J. M. Doughty, M. Winkler, M. Sugiono, J. D. Shields, D. Peat, D. Gillatt, and S. J. Harper (2002). "VEGF165b, an inhibitory splice variant of vascular endothelial growth factor, is down-regulated in renal cell carcinoma". In: *Cancer Research* 62.14, pp. 4123–4131.

Beazley-Long, N. (2019). "Do neuronal microvascular activation and resultant dysfunction in rheumatoid arthritis contribute to chronic pain?" In: *Neural Regeneration Research* 14.1, pp. 79–81.

Beazley-Long, N., A. M. Durrant, M. N. Swift, and L. F. Donaldson (2018a). "The physiological functions of central nervous system pericytes and a potential role in pain". In: *F1000Research* 7, p. 341.

Beazley-Long, N., C. E. Moss, W. R. Ashby, S. M. Bestall, F. Almahasneh, A. M. Durrant, A. V. Benest, Z. Blackley, K. Ballmer-Hofer, M. Hirashima, R. P. Hulse, D. O. Bates, and L. F. Donaldson (2018b). "VEGFR2 promotes central endothelial activation and the spread of pain in inflammatory arthritis". In: *Brain, Behavior, and Immunity* 74, pp. 49–67.

Becher, B., S. Spath, and J. Goverman (2016). "Cytokine networks in neuroinflammation". In: *Nature Reviews Immunology* 17, 49–59 (2017).

Becker, J. B., A. P. Arnold, K. J. Berkley, J. D. Blaustein, L. A. Eckel, E. Hampson, J. P. Herman, S. Marts, W. Sadee, M. Steiner, J. Taylor, and E. Young (2005a). "Strategies and methods for research on sex differences in brain and behavior". In: *Endocrinology* 146.4, pp. 1650–1673.

Becker, P. M., J. Waltenberger, R. Yachechko, T. Mirzapoiazova, J. S. Sham, C. G. Lee, J. A. Elias, and A. D. Verin (2005b). "Neuropilin-1 regulates vascular endothelial growth factor-mediated endothelial permeability". In: *Circulation Research* 96.12, pp. 1257–1265.

Beggs, S., X. J. Liu, C. Kwan, and M. W. Salter (2010). "Peripheral nerve injury and TRPV1-expressing primary afferent C-fibers cause opening of the blood-brain barrier". In: *Molecular Pain* 6.1, p. 74.

Benarroch, E. E. (2016). "Dorsal horn circuitry Complexity and implications for mechanisms of neuropathic pain". In: *Neurology* 86, pp. 1060–1069.

Bennett, J., J. Basivireddy, A. Kollar, K. E. Biron, P. Reickmann, W. A. Jefferies, and S. McQuaid (2010). "Blood-brain barrier disruption and enhanced vascular permeability in the multiple sclerosis model EAE". In: *Journal of Neuroimmunology* 229.1-2, pp. 180–191.

Berlin, B. S. (1962). "Tests for biologic safety of arlacel A." In: *Annals of allergy* 20, pp. 472–479.

Berlin, B. S. and R. Wyman (1971). "Fractionation of Arlacel A". In: *Proceedings of the Society for Experimental Biology and Medicine* 136.4, pp. 1363–1368.

Bernier, L. P., A. R. Ase, and P. Séguéla (2018). "P2X receptor channels in chronic pain pathways". In: *British Journal of Pharmacology* 175.12, pp. 2219–2230.

Biber, K., H. Neumann, K. Inoue, and H. W. G. M. Boddeke (2007). "Neuronal 'On' and 'Off' signals control microglia". In: *Trends in Neurosciences* 30.11, pp. 596–602.

Billiau, A. and P. Matthys (2001). "Modes of action of Freund's adjuvants in experimental models of autoimmune diseases". In: *Journal of Leukocyte Biology* 70.6, pp. 849–860.

Boettger, M. K., S. Hensellek, F. Richter, M. Gajda, R. Stöckigt, G. S. von Banchet, R. Bräuer, and H.-G. Schaible (2008). "Antinociceptive effects of tumor necrosis factor α neutralization in a rat model of antigen-induced arthritis: Evidence of a neuronal target". In: *Arthritis and Rheumatism* 58.8, pp. 2368–2378.

Borlongan, C. V. and D. F. Emerich (2003). "Facilitation of drug entry into the CNS via transient permeation of blood brain barrier: Laboratory and preliminary clinical ev-

idence from bradykinin receptor agonist, Cereport". In: *Brain Research Bulletin* 60.3, pp. 297–306.

Bosshart, H. and M. Heinzelmann (2016). *THP-1 cells as a model for human monocytes*.

Bouïs, D., G. A. Hospers, C. Meijer, G. Molema, and N. H. Mulder (2001). "Endothelium in vitro: A review of human vascular endothelial cell lines for blood vessel-related research". In: *Angiogenesis* 4.2, pp. 91–102.

Boyden, S. D., I. N. Hossain, A. Wohlfahrt, and Y. C. Lee (2016). "Non-inflammatory Causes of Pain in Patients with Rheumatoid Arthritis". In: *Current Rheumatology Reports* 18.6, p. 30.

Brake, R. L., P. J. Simmons, and C. G. Begley (2004). "Cross-contamination with tamoxifen induces transgene expression in non-exposed inducible transgenic mice". In: *Genetics and Molecular Research* 3.4, pp. 456–462.

Brenner, M., A. Messing, and M. L. Olsen (2019). "AP-1 and the injury response of the GFAP gene". In: *Journal of Neuroscience Research* 97.2, pp. 149–161.

Brockington, A., S. B. Wharton, M. Fernando, C. H. Gelsthorpe, L. Baxter, P. G. Ince, C. E. Lewis, and P. J. Shaw (2006). "Expression of vascular endothelial growth factor and its receptors in the central nervous system in amyotrophic lateral sclerosis". In: *Journal of Neuropathology and Experimental Neurology* 65.1, pp. 26–36.

Broeke, E. N. van den, C. Lenoir, and A. Mouraux (2016). "Secondary hyperalgesia is mediated by heat-insensitive A-fibre nociceptors". In: *Journal of Physiology* 594.22, pp. 6767–6776.

Broman, J., S. Anderson, and O. P. Ottersen (1993). "Enrichment of Glutamate-like Immunoreactivity in Primary Afferent Terminals Throughout the Spinal Cord Dorsal Horn". In: *European Journal of Neuroscience* 5.8, pp. 1050–1061.

Brooks, T. A., S. M. Ocheltree, M. J. Seelbach, R. A. Charles, N. Nametz, R. D. Egleton, and T. P. Davis (2006). "Biphasic cytoarchitecture and functional changes in the BBB induced by chronic inflammatory pain". In: *Brain Research* 1120.1, pp. 172–182.

Brooks, T. A., B. T. Hawkins, J. D. Huber, R. D. Egleton, T. P. Davis, T. A, and R. D (2005). "Chronic inflammatory pain leads to increased blood-brain barrier permeability and tight junction protein alterations". In: *American Journal of Physiology - Heart and Circulatory Physiology* 289.2, H738–43.

Bullock, D. C., A. R. Palmer, and A. Rees (1988). "Compact and easy-to-use tungsten-in-glass microelectrode manufacturing workstation". In: *Medical & Biological Engineering & Computing* 26.6, pp. 669–672.

Butler, S. H., F. Godefroy, J. M. Besson, and J. Weil-Fugazza (1992). "A limited arthritic model for chronic pain studies in the rat". In: *Pain* 48.1, pp. 73–81.

Cahoy, J. D., B. Emery, A. Kaushal, L. C. Foo, J. L. Zamanian, K. S. Christopherson, Y. Xing, J. L. Lubischer, P. A. Krieg, S. A. Krupenko, W. J. Thompson, and B. A. Barres (2008). "A transcriptome database for astrocytes, neurons, and oligodendrocytes: A new resource for understanding brain development and function". In: *Journal of Neuroscience* 28.1, pp. 264–278.

Calvo, M. and D. L. H. Bennett (2012). "The mechanisms of microgliosis and pain following peripheral nerve injury." In: *Experimental Neurology* 234.2, pp. 271–82.

Campos, C. R., S. M. Ocheltree, S. Hom, R. D. Egleton, and T. P. Davis (2008). "Nociceptive inhibition prevents inflammatory pain induced changes in the blood-brain barrier". In: *Brain Research* 1221, pp. 6–13.

Cao, L. and J. A. DeLeo (2008). "CNS-infiltrating CD4+ T lymphocytes contribute to murine spinal nerve transection-induced neuropathic pain". In: *European Journal of Immunology* 38.2, pp. 448–458.

Capes-Davis, A., G. Theodosopoulos, I. Atkin, H. G. Drexler, A. Kohara, R. A. MacLeod, J. R. Masters, Y. Nakamura, Y. A. Reid, R. R. Reddel, and R. I. Freshney (2010). "Check your cultures! A list of cross-contaminated or misidentified cell lines". In: *International Journal of Cancer* 127.1, pp. 1–8.

Carvalho da Fonseca, A. C., D. Matias, C. Garcia, R. Amaral, L. H. Geraldo, C. Freitas, and F. R. S. Lima (2014). "The impact of microglial activation on blood-brain barrier in brain diseases." In: *Frontiers in Cellular Neuroscience* 8, p. 362.

Casper, K. B., J. Kristin, and K. D. McCarthy (2007). "Characterisation of Astrocyte-Specific Conditional Knockouts". In: *Genesis* 45, pp. 292–299.

Caterina, M. J., M. A. Schumacher, M. Tominaga, T. A. Rosen, J. D. Levine, and D. Julius (1997). "The capsaicin receptor: a heat-activated ion channel in the pain pathway." In: *Nature* 389.6653, pp. 816–824.

Chakrabarty, A., K. E. McCarson, and P. G. Smith (2011). "Hypersensitivity and hyperinnervation of the rat hind paw following carrageenan-induced inflammation". In: *Neuroscience Letters* 495.1, pp. 67–71.

Chan, W. I., G. Zhang, X. Li, C. H. Leung, D. L. Ma, L. Dong, and C. Wang (2017). "Carrageenan activates monocytes via type-specific binding with interleukin-8: An implication for design of immuno-active biomaterials". In: *Biomaterials Science* 5.3, pp. 403–407.

Chanput, W., J. J. Mes, and H. J. Wichers (2014). "THP-1 cell line: An in vitro cell model for immune modulation approach". In: *International Immunopharmacology* 23.1, pp. 37–45.

Chaplan, S. R., F. W. Bach, J. W. Pogrel, J. M. Chung, and T. L. Yaksh (1994). "Quantitative assessment of tactile allodynia in the rat paw". In: *Journal of Neuroscience Methods* 53.1, pp. 55–63.

Chen, G., X. Luo, M. Y. Qadri, T. Berta, and R. R. Ji (2018a). "Sex-Dependent Glial Signaling in Pathological Pain: Distinct Roles of Spinal Microglia and Astrocytes". In: *Neuroscience Bulletin* 34.1, pp. 98–108.

Chen, G., C. K. Park, R. G. Xie, T. Berta, M. Nedergaard, and R. R. Ji (2014). "Connexin-43 induces chemokine release from spinal cord astrocytes to maintain late-phase neuropathic pain in mice". In: *Brain* 137.8, pp. 2193–2209.

Chen, G., Y. Q. Zhang, Y. J. Qadri, C. N. Serhan, and R. R. Ji (2018b). "Microglia in Pain: Detrimental and Protective Roles in Pathogenesis and Resolution of Pain". In: *Neuron* 100.6, pp. 1292–1311.

Chen, Q. L. and M. M. Heinricher (2019). "Descending Control Mechanisms and Chronic Pain". In: *Current Rheumatology Reports* 21.5, pp. 1–7.

Chen, S. C., M. H. Tsai, H. J. Wang, H. S. Yu, and L. W. Chang (2007). "Involvement of substance P and neurogenic inflammation in arsenic-induced early vascular dysfunction". In: *Toxicological Sciences* 95.1, pp. 82–88.

Chen, X., D. C. Du Bois, R. R. Almon, and W. J. Jusko (2015). "Biodistribution of etanercept to tissues and sites of inflammation in arthritic rats". In: *Drug Metabolism and Disposition* 43.6, pp. 898–907.

Chen, X., G. Sooch, I. S. Demaree, F. A. White, and A. G. Obukhov (2020). "Transient Receptor Potential Canonical (TRPC) Channels: Then and Now". In: *Cells* 9.9.

Chiang, C. Y., B. J. Sessle, and J. O. Dostrovsky (2012). *Role of astrocytes in pain*.

Chillingworth, N. L. and L. F. Donaldson (2003). "Characterisation of a Freund's complete adjuvant-induced model of chronic arthritis in mice". In: *Journal of Neuroscience Methods* 128.1-2, pp. 45–52.

Chimenti, M. S., P. Triggianese, P. Conigliaro, E. Candi, G. Melino, and R. Perricone (2015). "The interplay between inflammation and metabolism in rheumatoid arthritis". In: *Cell Death and Disease* 6.9, e1887.

Chow, Y. Y. and K. Y. Chin (2020). "The Role of Inflammation in the Pathogenesis of Osteoarthritis". In: *Mediators of Inflammation* 2020.

Clark, P. R., T. D. Manes, J. S. Pober, and M. S. Kluger (2007). "Increased ICAM-1 expression causes endothelial cell leakiness, cytoskeletal reorganization and junctional alterations". In: *Journal of Investigative Dermatology* 127.4, pp. 762–774.

Constantinides, C. and K. Murphy (2016). "Molecular and Integrative Physiological Effects of Isoflurane Anesthesia: The Paradigm of Cardiovascular Studies in Rodents using Magnetic Resonance Imaging". In: *Frontiers in Cardiovascular Medicine* 3.July.

Cook, C. D. and K. I. Moore (2006). "Effects of sex, hindpaw injection site and stimulus modality on nociceptive sensitivity in arthritic rats". In: *Physiology and Behavior* 87.3, pp. 552–562.

Coste, B., J. Mathur, M. Schmidt, T. J. Earley, S. Ranade, M. J. Petrus, A. E. Dubin, and A. Patapoutian (2010). "Piezo1 and Piezo2 are essential components of distinct mechanically activated cation channels". In: *Science* 330.6000, pp. 55–60.

Costigan, M., A. Moss, A. Latremoliere, C. Johnston, M. Verma-Gandhu, T. A. Herbert, L. Barrett, G. J. Brenner, D. Vardeh, C. J. Woolf, and M. Fitzgerald (2009a). "T-Cell Infiltration and Signaling in the Adult Dorsal Spinal Cord Is a Major Contributor to Neuropathic Pain-Like Hypersensitivity". In: *Journal of Neuroscience* 29.46, pp. 14415–14422.

Costigan, M., J. Scholz, and C. J. Woolf (2009b). "Neuropathic Pain: A Maladaptive Response of the Nervous System to Damage". In: *Annual Review of Neuroscience* 32.1, pp. 1–32.

Coulthard, P., S. U. Simjee, and B. J. Pleuvry (2003). "Gait analysis as a correlate of pain induced by carrageenan intraplantar injection". In: *Journal of Neuroscience Methods* 128.1-2, pp. 95–102.

Craft, R. M., J. S. Mogil, and A. Maria Aloisi (2004). "Sex differences in pain and analgesia: The role of gonadal hormones". In: *European Journal of Pain* 8.5, pp. 397–411.

Cridland, R. A., K. Yashpal, V. V. Romita, S. Gauthier, and J. L. Henry (1987). "Distribution of label after intrathecal administration of 125I-substance P in the rat". In: *Peptides* 8.2, pp. 213–221.

Croll, S. D., R. M. Ransohoff, N. Cai, Q. Zhang, F. J. Martin, T. Wei, L. J. Kasselman, J. Kintner, A. J. Murphy, G. D. Yancopoulos, and S. J. Wiegand (2004). "VEGF-mediated inflammation precedes angiogenesis in adult brain". In: *Experimental Neurology* 187.2, pp. 388–402.

Cuellar, J. M., R. C. Dutton, J. F. Antognini, and E. Carstens (2005). "Differential effects of halothane and isoflurane on lumbar dorsal horn neuronal windup and excitability | BJA: British Journal of Anaesthesia | Oxford Academic". In: *British Journal of Anaesthesia* 94.5, pp. 617–625.

Cuellar, J. M., P. X. Montesano, and E. Carstens (2004). "Role of TNF-alpha in sensitization of nociceptive dorsal horn neurons induced by application of nucleus pulposus to L5 dorsal root ganglion in rats". In: *Pain* 110.3, pp. 578–587.

Cullinane, C. and R. Montacute (2017). "Life lessons, Improving essential life skills for young people". In: *The Sutton Trust* October, pp. 1–28.

Cush, J. J., R. Rothlein, H. B. Lindsley, E. A. Mainolfi, and P. E. Lipsky (1993). "Increased levels of circulating intercellular adhesion molecule 1 in the sera of patients with rheumatoid arthritis". In: *Arthritis & Rheumatism* 36.8, pp. 1098–1102.

D'Mello, R. and A. H. Dickenson (2008). "Spinal cord mechanisms of pain". In: *British Journal of Anaesthesia* 101.1, pp. 8–16.

Daneman, R., L. Zhou, A. A. Kebede, and B. A. Barres (2010). "Pericytes are required for blood-brain barrier integrity during embryogenesis". In: *Nature* 468.7323, pp. 562–566.

Daniels, B. P., D. W. Holman, L. Cruz-Orengo, H. Jujjavarapu, D. M. Durrant, and R. S. Klein (2014). "Viral Pathogen-Associated Molecular Patterns Regulate Blood-Brain Barrier Integrity via Competing Innate Cytokine Signals". In: *mBio* 5.5, e01476–14–e01476–14.

Daniels, B. P., L. Cruz-Orengo, T. J. Pasieka, P. O. Couraud, I. A. Romero, B. Weksler, J. A. Cooper, T. L. Doering, and R. S. Klein (2013). "Immortalized human cerebral microvascular endothelial cells maintain the properties of primary cells in an in vitro model of immune migration across the blood brain barrier". In: *Journal of Neuroscience Methods* 212.1, pp. 173–179.

Davila, D., K. Thibault, T. A. Fiacco, and C. Agulhon (2013). "Recent molecular approaches to understanding astrocyte function in vivo". In: *Frontiers in Cellular Neuroscience* 7.DEC, pp. 1–20.

De Bandt, M., M. H. Ben Mahdi, V. Ollivier, M. Grossin, M. Dupuis, M. Gaudry, P. Bohlen, K. E. Lipson, A. Rice, Y. Wu, M.-A. Gougerot-Pocidalo, and C. Pasquier (2003). "Blockade of Vascular Endothelial Growth Factor Receptor I (VEGF-RI), but not VEGF-RII,

Suppresses Joint Destruction in the K/BxN Model of Rheumatoid Arthritis". In: *The Journal of Immunology* 171.9, pp. 4853–4859.
de Sousa Valente, J. (2019). "The Pharmacology of Pain Associated With the Monoiodoacetate Model of Osteoarthritis". In: *Frontiers in Pharmacology* 10, p. 974.
Decosterd, I. and C. J. Woolf (2000). "Spared nerve injury: An animal model of persistent peripheral neuropathic pain". In: *Pain* 87.2, pp. 149–158.
DeLeo, J. A. and R. P. Yezierski (2001). *The role of neuroinflammation and neuroimmune activation in persistent pain*.
DeLeo, J. A., M. D. Rutkowski, A. K. Stalder, and I. L. Campbell (2000). "Transgenic expression of TNF by astrocytes increases mechanical allodynia in a mouse neuropathy model". In: *NeuroReport* 11.3, pp. 599–602.
Denko, C. W. and M. Petricevic (1978). "Sympathetic or reflex footpad swelling due to crystal-induced inflammation in the opposite foot". In: *Inflammation* 3.1, pp. 81–86.
Destefano, J. G., J. J. Jamieson, R. M. Linville, and P. C. Searson (2018). "Benchmarking in vitro tissue-engineered blood-brain barrier models". In: *Fluids and Barriers of the CNS* 15.1, p. 32.
Deuis, J. R., L. S. Dvorakova, and I. Vetter (2017). "Methods used to evaluate pain behaviors in rodents". In: *Frontiers in Molecular Neuroscience* 10.September, pp. 1–17.
Didier, N., I. A. Romero, C. Créminon, A. Wijkhuisen, J. Grassi, and A. Mabondzo (2003). "Secretion of interleukin-1β by astrocytes mediates endothelin-1 and tumour necrosis factor-α effects on human brain microvascular endothelial cell permeability". In: *Journal of Neurochemistry* 86.1, pp. 246–254.
Djouhri, L. and S. N. Lawson (2004). "Aβ-fiber nociceptive primary afferent neurons: A review of incidence and properties in relation to other afferent A-fiber neurons in mammals". In: *Brain Research Reviews* 46.2, pp. 131–145.
Dobrogowska, D. H., A. S. Lossinsky, M. Tarnawski, and A. W. Vorbrodt (1998). "Increased blood-brain barrier permeability and endothelial abnormalities induced by vascular endothelial growth factor". In: *Journal of Neurocytology* 27.3, pp. 163–173.
Doherty, C. P., E. O'Keefe, E. Wallace, T. Loftus, J. Keaney, J. Kealy, M. M. Humphries, M. G. Molloy, J. F. Meaney, M. Farrell, and M. Campbell (2016). "Blood-Brain Barrier Dysfunction as a Hallmark Pathology in Chronic Traumatic Encephalopathy". In: *Journal of Neuropathology and Experimental Neurology* 75.7, pp. 656–662.
Donaldson, L. F. and L. J. Wiseman (2000). "Expression and regulation of vascular cell adhesion molecule-1 in rat central nervous system during acute peripheral inflammation". In: *Journal of Physiology*, 148P–149P.
Donaldson, L. F. and N. Beazley-Long (2016). "Alternative RNA splicing: contribution to pain and potential therapeutic strategy". In: *Drug Discovery Today* 21.11, pp. 1787–1798.
Donaldson, L. F., J. R. Seckl, and D. S. McQueen (1993). "A discrete adjuvant-induced monoarthritis in the rat: effects of adjuvant dose". In: *Journal of Neuroscience Methods* 49.1-2, pp. 5–10.

Donato, R., G. Sorci, F. Riuzzi, C. Arcuri, R. Bianchi, F. Brozzi, C. Tubaro, and I. Giambanco (2009). "S100B's double life: Intracellular regulator and extracellular signal". In: *Biochimica et Biophysica Acta - Molecular Cell Research* 1793.6, pp. 1008–1022.

DosSantos, M. F., R. C. Holanda-Afonso, R. L. Lima, A. F. DaSilva, and V. Moura-Neto (2014). "The role of the blood-brain barrier in the development and treatment of migraine and other pain disorders". In: *Frontiers in Cellular Neuroscience* 8, p. 302.

Dostrovsky, J. and A. Craig (2013). "Ascending Projection Systems". In: *Wall & Melzack's Textbook of Pain*. Ed. by S. B. McMahon, M. Koltzenburg, I. Tracey, and D. C. Turk. 6th. Philadelphia: Elsevier. Chap. 12, pp. 182–197.

Dray, A. and M. N. Perkins (1993). "Bradykinin and inflammatory pain". In: *Trends in Neurosciences* 16.3, pp. 99–104.

Du, X., H. Hao, Y. Yang, S. Huang, C. Wang, S. Gigout, R. Ramli, X. Li, E. Jaworska, I. Edwards, J. Deuchars, Y. Yanagawa, J. Qi, B. Guan, D. B. Jaffe, H. Zhang, and N. Gamper (2017). "Local GABAergic signaling within sensory ganglia controls peripheral nociceptive transmission". In: *Journal of Clinical Investigation* 127.5, pp. 1741–1756.

Durrant, A. M., M. N. Swift, and N. Beazley-Long (2018). "A role for pericytes in chronic pain?" In: *Current Opinion in Supportive and Palliative Care* 12.2, pp. 154–161.

Dustin, M., R. Rothlein, A. Bhan, C. Dinarello, and T. Springer (1986). "Induction by IL-1 and interferon-7: tissue distribution, biochemistry, and function of a natural adherence molecule (ICAM-1)". In: *Journal of Immunology* 137, pp. 245–254.

Echeverry, S., X. Q. Shi, S. Rivest, and J. Zhang (2011). "Peripheral nerve injury alters blood-spinal cord barrier functional and molecular integrity through a selective inflammatory pathway." In: *Journal of Neuroscience* 31.30, pp. 10819–28.

Echeverry, S., X. Q. Shi, M. Yang, H. Huang, Y. Wu, L.-E. Lorenzo, J. Perez-Sanchez, R. P. Bonin, Y. De Koninck, and J. Zhang (2017). "Spinal microglia are required for long-term maintenance of neuropathic pain". In: *Pain* 158, pp. 1792–1801.

Ellis, A. and D. L. H. Bennett (2013). "Neuroinflammation and the generation of neuropathic pain". In: *British Journal of Anaesthesia* 111.1, pp. 26–37.

Elsheemy, M. S., A. H. Hasanin, A. Mansour, S. I. Mehrez, and M. Abdel-Bary (2019). "Etanercept improved anemia and decreased hepcidin gene expression in a rat model of rheumatoid arthritis". In: *Biomedicine and Pharmacotherapy* 112.

Eng, L. F. and R. S. Ghirnikar (1994). "GFAP and Astrogliosis". In: *Brain Pathology*. Vol. 4. 3. Brain Pathol, pp. 229–237.

Enna, S. J. and K. E. McCarson (2006). "The Role of GABA in the Mediation and Perception of Pain". In: *Advances in Pharmacology* 54, pp. 1–27.

Ernsberger, U. (2009). "Role of neurotrophin signalling in the differentiation of neurons from dorsal root ganglia and sympathetic ganglia". In: *Cell and Tissue Research* 336.3, pp. 349–384.

Fang, X., L. Djouhri, S. McMullan, C. Berry, K. Okuse, S. G. Waxman, and S. N. Lawson (2005). "TrkA is expressed in nociceptive neurons and influences electrophysiological properties via Nav1.8 expression in rapidly conducting nociceptors." In: *Journal of Neuroscience* 25.19, pp. 4868–78.

Faridgohar, M. and H. Nikoueinejad (2017). "New findings of Toll-like receptors involved in Mycobacterium tuberculosis infection". In: *Pathogens and Global Health* 111.5, pp. 256–264.

Fernihough, J., C. Gentry, M. Malcangio, A. Fox, J. Rediske, T. Pellas, B. Kidd, S. Bevan, and J. Winter (2004). "Pain related behaviour in two models of osteoarthritis in the rat knee". In: *Pain* 112.1-2, pp. 83–93.

Ferreira-Gomes, J., S. Adães, R. M. Sousa, M. Mendonça, and J. M. Castro-Lopes (2012). "Dose-dependent expression of neuronal injury markers during experimental osteoarthritis induced by monoiodoacetate in the rat". In: *Molecular Pain* 8.

Fields, H. L., M. M. Heinricher, and P. Mason (1991). "Neurotransmitters in nociceptive modulatory circuits." In: *Annual Review of Neuroscience* 14, pp. 219–45.

Fitzgerald, M. (1985). "The post-natal development of cutaneous afferent fibre input and receptive field organization in the rat dorsal horn." In: *Journal of Physiology* 364, pp. 1–18.

Flores Bjurström, M., M. Bodelsson, A. Montgomery, A. Harsten, M. Waldén, S. Janelidze, S. Hall, O. Hansson, M. R. Irwin, and N. Mattsson-Carlgren (2020). "Differential expression of cerebrospinal fluid neuroinflammatory mediators depending on osteoarthritis pain phenotype". In: *Pain* 161.9, pp. 2142–2154.

Forde, A., R. Constien, H.-J. Gröne, G. Hämmerling, and B. Arnold (2002). "Temporal Cre-mediated recombination exclusively in endothelial cells using Tie2 regulatory elements". In: *genesis* 33.4, pp. 191–197.

Forsberg, A., J. Lampa, J. Estelius, S. Cervenka, L. Farde, C. Halldin, M. Lekander, C. Olgart Höglund, and E. Kosek (2019). "Disease activity in rheumatoid arthritis is inversely related to cerebral TSPO binding assessed by [11C]PBR28 positron emission tomography". In: *Journal of Neuroimmunology* 334.May.

Förster, C., M. Burek, I. A. Romero, B. Weksler, P. O. Couraud, and D. Drenckhahn (2008). "Differential effects of hydrocortisone and TNFα on tight junction proteins in an in vitro model of the human blood-brain barrier". In: *Journal of Physiology* 586.7, pp. 1937–1949.

Gangadharan, V. and R. Kuner (2013). "Pain hypersensitivity mechanisms at a glance". In: *DMM Disease Models and Mechanisms* 6.4, pp. 889–895.

Gao, P., N. Niu, T. Wei, H. Tozawa, X. Chen, C. Zhang, J. Zhang, Y. Wada, C. M. Kapron, and J. Liu (2017). "The roles of signal transducer and activator of transcription factor 3 in tumor angiogenesis". In: *Oncotarget* 8.40, pp. 69139–69161.

Gao, Y. J. and R. R. Ji (2010). "Targeting Astrocyte Signaling for Chronic Pain". In: *Neurotherapeutics* 7.4, pp. 482–493.

Gao, Y. J., L. Zhang, and R. R. Ji (2010). "Spinal injection of TNF-α-activated astrocytes produces persistent pain symptom mechanical allodynia by releasing monocyte chemoattractant protein-1". In: *GLIA* 58.15, pp. 1871–1880.

Gao, Y. J., L. Zhang, O. A. Samad, M. R. Suter, K. Yasuhiko, Z. Z. Xu, J. Y. Park, A. L. Lind, Q. Ma, and R. R. Ji (2009). "JNK-induced MCP-1 production in spinal cord astrocytes

contributes to central sensitization and neuropathic pain". In: *Journal of Neuroscience* 29.13, pp. 4096–4108.

Garrison, C. J., P. M. Dougherty, K. C. Kajander, and S. M. Carlton (1991). "Staining of glial fibrillary acidic protein (GFAP) in lumbar spinal cord increases following a sciatic nerve constriction injury". In: *Brain Research* 565.1, pp. 1–7.

Gavard, J. and J. S. Gutkind (2006). "VEGF Controls endothelial-cell permeability promoting β-arrestin-dependent Endocytosis VE-cadherin". In: *Nature Cell Biology* 8.11, pp. 1223–1234.

Ge, S. and J. S. Pachter (2006). "Isolation and culture of microvascular endothelial cells from murine spinal cord". In: *Journal of Neuroimmunology* 177.1-2, pp. 209–214.

Gee, J. R. and J. N. Keller (2005). "Astrocytes: Regulation of brain homeostasis via apolipoprotein E". In: *International Journal of Biochemistry and Cell Biology* 37.6, pp. 1145–1150.

Giannelli, G., R. Erriquez, F. Iannone, F. Marinosci, G. Lapadula, S. Antonaci, G. Giannelli, R. Erriquez, F. Iannone, F. Marinosci, G. Lapadula, and S. Antonaci (2004). "MMP-2, MMP-9, T I M P-1 and TIMP-2 levels in patients with rheumatoid arthritis and psoriatic arthritis". In: *BRIEFPAPER Clinical and Experimental Rheumatology* 22, pp. 335–338.

Giovannoni, F. and F. J. Quintana (2020). "The Role of Astrocytes in CNS Inflammation". In: *Trends in Immunology* 41.9, pp. 805–819.

Glyn-Jones, S., A. J. Palmer, R. Agricola, A. J. Price, T. L. Vincent, H. Weinans, and A. J. Carr (2015). "Osteoarthritis". In: *The Lancet* 386.9991, pp. 376–387.

Goldberg, D. S. and S. J. McGee (2011). "Pain as a global public health priority". In: *BMC Public Health* 11.

Gordh, T., H. Chu, and H. S. Sharma (2006). "Spinal nerve lesion alters blood-spinal cord barrier function and activates astrocytes in the rat". In: *Pain* 124.1-2, pp. 211–221.

Gosselin, R.-D., M. R. Suter, R.-R. Ji, and I. Decosterd (2010). "Glial cells and chronic pain." In: *The Neuroscientist* 16.5, pp. 519–31.

Gözel, N., M. Çakirer, A. Karataş, M. Tuzcu, F. A. Özdemir, A. F. Dağli, K. Şahin, and S. S. Koca (2018). "Sorafenib reveals anti-arthritic potentials in collagen induced experimental arthritis model". In: *Archives of Rheumatology* 33.3, pp. 309–315.

Grace, P. M., M. R. Hutchinson, S. F. Maier, and L. R. Watkins (2014). "Pathological pain and the neuroimmune interface". In: *Nature Reviews Immunology* 14.4, pp. 217–231.

Greenspon, C. (2018). "Linear multi-electrode arrays for recording population data from the spinal dorsal horn". PhD thesis. University of Nottingham.

Greenspon, C. M., E. E. Battell, I. M. Devonshire, L. F. Donaldson, V. Chapman, and G. J. Hathway (2019). "Lamina-specific population encoding of cutaneous signals in the spinal dorsal horn using multi-electrode arrays". In: *Journal of Physiology* 597.2, pp. 377–397.

Grosios, K., J. Wood, R. Esser, A. Raychaudhuri, and J. Dawson (2004). "Angiogenesis inhibition by the novel VEGF receptor tyrosine kinase inhibitor, PTK787/ZK222584, causes significant anti-arthritic effects in models of rheumatoid arthritis". In: *Inflammation Research* 53.4, pp. 133–142.

Grubb, B. D., D. S. McQueen, A. Iggo, G. J. Birrell, and M. B. Dutia (1988). "A study of 5-HT-receptors associated with afferent nerves located in normal and inflamed rat ankle joints". In: *Agents and Actions* 25.3-4, pp. 216–218.

Gu, Y., G. Li, and L. Y. M. Huang (2018). "Inflammation induces Epac-protein kinase C alpha and epsilon signaling in TRPV1-mediated hyperalgesia". In: *Pain* 159.11, pp. 2383–2393.

Guimarães, R. M., M. Davoli-Ferreira, M. M. Fonseca, L. E. A. Damasceno, F. V. Santa-Cecilia, R. Kusuda, G. B. Menezes, F. Q. Cunha, J. C. Alves-Filho, and T. M. Cunha (2019). "Frontline Science: Blood-circulating leukocytes fail to infiltrate the spinal cord parenchyma after spared nerve injury". In: *Journal of Leukocyte Biology* 106.3, pp. 541–551.

Gursoy-Ozdemir, Y., J. Qiu, N. Matsuoka, H. Bolay, D. Bermpohl, H. Jin, X. Wang, G. A. Rosenberg, E. H. Lo, and M. A. Moskowitz (2004). "Cortical spreading depression activates and upregulates MMP-9". In: *Journal of Clinical Investigation* 113.10, pp. 1447–1455.

Hamilton, J. L., M. Nagao, B. R. Levine, D. Chen, B. R. Olsen, and H. J. Im (2016). "Targeting VEGF and Its Receptors for the Treatment of Osteoarthritis and Associated Pain". In: *Journal of Bone and Mineral Research* 31.5, pp. 911–924.

Hammond, T. R., C. Dufort, L. Dissing-Olesen, S. Giera, A. Young, A. Wysoker, A. J. Walker, F. Gergits, M. Segel, J. Nemesh, S. E. Marsh, A. Saunders, E. Macosko, F. Ginhoux, J. Chen, R. J. Franklin, X. Piao, S. A. McCarroll, and B. Stevens (2019). "Single-Cell RNA Sequencing of Microglia throughout the Mouse Lifespan and in the Injured Brain Reveals Complex Cell-State Changes". In: *Immunity* 50.1, 253–271.e6.

Hansen, R. R. and M. Malcangio (2013). "Astrocytes - multitaskers in chronic pain." In: *European Journal of Pharmacology* 716.1-3, pp. 120–8.

Haraoui, B. and V. Bykerk (2007). "Etanercept in the treatment of rheumatoid arthritis". In: *Therapeutics and Clinical Risk Management* 3.1, pp. 99–105.

Hargreaves, K., R. Dubner, F. Brown, C. Flores, and J. Joris (1988). "A new and sensitive method for measuring thermal nociception in cutaneous hyperalgesia". In: *Pain* 32.1, pp. 77–88.

Haruwaka, K., A. Ikegami, Y. Tachibana, N. Ohno, H. Konishi, A. Hashimoto, M. Matsumoto, D. Kato, R. Ono, H. Kiyama, A. J. Moorhouse, J. Nabekura, and H. Wake (2019). "Dual microglia effects on blood brain barrier permeability induced by systemic inflammation". In: *Nature Communications* 10.1, pp. 1–17.

Havelin, J., I. Imbert, J. Cormier, J. Allen, F. Porreca, and T. King (2016). "Central sensitization and neuropathic features of ongoing pain in a rat model of advanced osteoarthritis". In: *Journal of Pain* 17.3, pp. 374–382.

HEFCE (2010). *Trends in Young Participation in Higher Education: Core Results for England*. Tech. rep. Bristol, UK, pp. 1–38.

Heil, M., M. Clauss, K. Suzuki, I. R. Buschmann, A. Willuweit, S. Fischer, and W. Schaper (2000). "Vascular endothelial growth factor (VEGF) stimulates monocyte migration

through endothelial monolayers via increased integrin expression." In: *European journal of cell biology* 79.11, pp. 850–7.

Heinricher, M. M., J. J. Maire, D. Lee, J. W. Nalwalk, and L. B. Hough (2010). "Physiological basis for inhibition of morphine and improgan antinociception by CC12, a P450 epoxygenase inhibitor". In: *Journal of Neurophysiology* 104.6, pp. 3222–3230.

Heinricher, M. and H. Fields (2013). "Central nervous system mechanisms of pain modulation". In: *Wall and Melzack's Textbook of Pain*. Ed. by S. McMahon, M. Koltzenburg, I. Tracey, and D. Turk. 6th. London, pp. 129–142.

Hentall, I., G. Zorman, S. Kansky, and H. Fields (1984). "An estimate of minimum number of brain stem neurons required for inhibition of a flexion reflex". In: *Journal of neurophysiology* 51.5.

Herland, A., A. D. Van Der Meer, E. A. FitzGerald, T. E. Park, J. J. Sleeboom, and D. E. Ingber (2016). "Distinct contributions of astrocytes and pericytes to neuroinflammation identified in a 3D human blood-brain barrier on a chip". In: *PLoS ONE* 11.3. Ed. by M. A. Deli, e0150360.

Holmes, K., O. L. Roberts, A. M. Thomas, and M. J. Cross (2007). "Vascular endothelial growth factor receptor-2: Structure, function, intracellular signalling and therapeutic inhibition". In: *Cellular Signalling* 19.10, pp. 2003–2012.

Hu, N. Y., Y. T. Chen, Q. Wang, W. Jie, Y. S. Liu, Q. L. You, Z. L. Li, X. W. Li, S. Reibel, F. W. Pfrieger, J. M. Yang, and T. M. Gao (2020). "Expression Patterns of Inducible Cre Recombinase Driven by Differential Astrocyte-Specific Promoters in Transgenic Mouse Lines". In: *Neuroscience Bulletin* 36.5, pp. 530–544.

Hua, X. Y., C. I. Svensson, T. Matsui, B. Fitzsimmons, T. L. Yaksh, and M. Webb (2005). "Intrathecal minocycline attenuates peripheral inflammation-induced hyperalgesia by inhibiting p38 MAPK in spinal microglia". In: *European Journal of Neuroscience* 22.10, pp. 2431–2440.

Huang, T. Y., V. Belzer, and M. Hanani (2010). "Gap junctions in dorsal root ganglia: Possible contribution to visceral pain". In: *European Journal of Pain* 14.1, 49.e1–49.e9.

Huber, J. D., C. R. Campos, K. S. Mark, and T. P. Davis (2005). "Alterations in blood-brain barrier ICAM-1 expression and brain microglial activation after lambda-carrageenan-induced inflammatory pain." In: *American Journal of Physiology - Heart and Circulatory Physiology* 290.2, H732–40.

Huber, J. D., K. A. Witt, S. Hom, R. D. Egleton, K. S. Mark, and T. P. Davis (2001). "Inflammatory pain alters blood-brain barrier permeability and tight junctional protein expression." In: *American Journal of Physiology - Heart and Circulatory Physiology* 280.3, H1241–H1248.

Huber, J. D., V. S. Hau, L. Borg, C. R. Campos, R. D. Egleton, and T. P. Davis (2002). "Blood-brain barrier tight junctions are altered during a 72-h exposure to λ-carrageenan-induced inflammatory pain". In: *American Journal of Physiology-Heart and Circulatory Physiology* 283.4, H1531–H1537.

Huber, J. D., R. L. VanGilder, and K. A. Houser (2006). "Streptozotocin-induced diabetes progressively increases blood-brain barrier permeability in specific brain regions in

rats". In: *American Journal of Physiology - Heart and Circulatory Physiology* 291.6, H2660–H2668.

Hulse, R. P., N. Beazley-Long, J. Hua, H. Kennedy, J. Prager, H. Bevan, Y. Qiu, E. S. Fernandes, M. V. Gammons, K. Ballmer-Hofer, A. C. Gittenberger de Groot, A. J. Churchill, S. J. Harper, S. D. Brain, D. O. Bates, and L. F. Donaldson (2014). "Regulation of alternative VEGF-A mRNA splicing is a therapeutic target for analgesia". In: *Neurobiology of Disease* 71, pp. 245–259.

Hulse, R. P., N. Beazley-Long, N. Ved, S. M. Bestall, H. Riaz, P. Singhal, K. B. Hofer, S. J. Harper, D. O. Bates, and L. F. Donaldson (2015). "Vascular endothelial growth factor-A165b prevents diabetic neuropathic pain and sensory neuronal degeneration". In: *Clinical Science* 129.8, pp. 741–756.

Hulse, R. P., R. A. R. Drake, D. O. Bates, and L. F. Donaldson (2016). "The control of alternative splicing by SRSF1 in myelinated afferents contributes to the development of neuropathic pain". In: *Neurobiology of Disease* 96, pp. 186–200.

Hunt, S. P. and P. W. Mantyh (2001). "The molecular dynamics of pain control." In: *Nature Reviews Neuroscience* 2.2, pp. 83–91.

Huppert, J., D. Closhen, A. Croxford, R. White, P. Kulig, E. Pietrowski, I. Bechmann, B. Becher, H. J. Luhmann, A. Waisman, and C. R. W. Kuhlmann (2010). "Cellular mechanisms of IL-17-induced blood-brain barrier disruption". In: *The FASEB Journal* 24.4, pp. 1023–1034.

Hwang, H. J., H. J. Lee, C. J. Kim, I. Shim, and D. H. Hahm (2008). "Inhibitory effect of amygdalin on lipopolysaccharide-inducible TNF-α and IL-1β mRNA expression and carrageenan-induced rat arthritis". In: *Journal of Microbiology and Biotechnology* 18.10, pp. 1641–1647.

Ikeda, H., T. Kiritoshi, and K. Murase (2012). "Contribution of microglia and astrocytes to the central sensitization, inflammatory and neuropathic pain in the juvenile rat". In: *Molecular Pain* 8.1, p. 43.

Inglis, J. J., A. Nissim, D. M. Lees, S. P. Hunt, Y. Chernajovsky, and B. L. Kidd (2005). "The differential contribution of tumour necrosis factor to thermal and mechanical hyperalgesia during chronic inflammation". In: *Arthritis Research & Therapy* 7.4, R807.

Inoue, K. and M. Tsuda (2018). "Microglia in neuropathic pain: Cellular and molecular mechanisms and therapeutic potential". In: *Nature Reviews Neuroscience* 19.3, pp. 138–152.

IntoUniversity (2017). *Impact Report 2017*. Tech. rep. London.

Ivanavicius, S. P., D. R. Blake, I. P. Chessell, and P. I. Mapp (2004). "Isolectin B4 binding neurons are not present in the rat knee joint". In: *Neuroscience* 128.3, pp. 555–560.

Jansson, D., J. Rustenhoven, S. Feng, D. Hurley, R. L. Oldfield, P. S. Bergin, E. W. Mee, R. L. Faull, and M. Dragunow (2014). "A role for human brain pericytes in neuroinflammation". In: *Journal of Neuroinflammation* 11.1, p. 104.

Jensen, K. T., D. P. Rabago, T. M. Best, J. J. Patterson, and R. Vanderby (2008). "Early Inflammatory Response of Knee Ligaments to Prolotherapy in a Rat Model". In: *Journal of Orthopaedic Research* 26, pp. 816–823.

Jerrim, J. (2013). *The Reading Gap: The socio-economic gap in children's reading skills: A cross-national comparison using PISA 2009*. Tech. rep. July. London, pp. 1–11.

Ji, R.-R., T. Berta, and M. Nedergaard (2013). "Glia and pain: Is chronic pain a gliopathy?" In: *Pain* 154.SUPPL. 1, S10–S28.

Ji, R.-r., A. Chamessian, and Y.-q. Zhang (2016). "Pain regulation by non-neuronal cells and inflammation". In: *Pain Research* 354.6312, pp. 572–577.

Ji, R.-R. and M. R. Suter (2007). "p38 MAPK, microglial signaling, and neuropathic pain." In: *Molecular pain* 3, p. 33.

Ji, R.-R., Z. Z. Xu, X. Wang, and E. H. Lo (2009). "Matrix metalloprotease regulation of neuropathic pain". In: *Trends in Pharmacological Sciences* 30.7, pp. 336–340.

Ji, R. R., C. R. Donnelly, and M. Nedergaard (2019). "Astrocytes in chronic pain and itch". In: *Nature Reviews Neuroscience* 20.11, pp. 667–685.

Ji, R. R., T. Kohno, K. A. Moore, and C. J. Woolf (2003). "Central sensitization and LTP: Do pain and memory share similar mechanisms?" In: *Trends in Neurosciences* 26.12, pp. 696–705.

Ji, R. R., A. Nackley, Y. Huh, N. Terrando, and W. Maixner (2018). "Neuroinflammation and central sensitization in chronic and widespread pain". In: *Anesthesiology* 129.2, pp. 343–366.

Ji, R. R., T. A. Samad, S. X. Jin, R. Schmoll, and C. J. Woolf (2002). "p38 MAPK activation by NGF in primary sensory neurons after inflammation increases TRPV1 levels and maintains heat hyperalgesia". In: *Neuron* 36.1, pp. 57–68.

Jochmann, E., M. K. Boettger, P. Anand, and H. G. Schaible (2015). "Antigen-induced arthritis in rats is associated with increased growth-associated protein 43-positive intraepidermal nerve fibres remote from the joint". In: *Arthritis Research and Therapy* 17.1.

Julius, D. (2001). "Molecular mechanisms of nociception ". In: *Nature* 413.September, pp. 203–210.

Jung, C., E. Ichesco, E. M. Ratai, R. G. Gonzalez, T. Burdo, M. L. Loggia, R. E. Harris, and V. Napadow (2020). "Magnetic resonance imaging of neuroinflammation in chronic pain: a role for astrogliosis?" In: *Pain* 161.7, pp. 1555–1564.

Kalucka, J. et al. (2020). "Single-Cell Transcriptome Atlas of Murine Endothelial Cells". In: *Cell* 180.4, 764–779.e20.

Kanda, H., K. Kobayashi, H. Yamanaka, M. Okubo, and K. Noguchi (2017). "Microglial TNFα Induces COX2 and PGI2 Synthase Expression in Spinal Endothelial Cells during Neuropathic Pain". In: *eneuro* 4.2, ENEURO.0064–17.2017–46.

Kapałczyńska, M., T. Kolenda, W. Przybyła, M. Zajaczkowska, A. Teresiak, V. Filas, M. Ibbs, R. Bliźniak, Ł. Łuczewski, and K. Lamperska (2018). "2D and 3D cell cultures – a comparison of different types of cancer cell cultures". In: *Archives of Medical Science* 14.4, pp. 910–919.

Kawarai, Y., S. Orita, J. Nakamura, S. Miyamoto, M. Suzuki, K. Inage, S. Hagiwara, T. Suzuki, T. Nakajima, T. Akazawa, and S. Ohtori (2018). "Changes in proinflammatory cytokines,

neuropeptides, and microglia in an animal model of monosodium iodoacetate-induced hip osteoarthritis". In: *Journal of Orthopaedic Research* 36.11, pp. 2978–2986.

Kawasaki, Y., Z.-Z. Xu, X. Wang, J. Y. Park, Z.-Y. Zhuang, P.-H. Tan, Y.-J. Gao, K. Roy, G. Corfas, E. H. Lo, and R.-R. Ji (2008a). "Distinct roles of matrix metalloproteases in the early- and late-phase development of neuropathic pain." In: *Nature medicine* 14.3, pp. 331–6.

Kawasaki, Y., L. Zhang, J. K. Cheng, and R. R. Ji (2008b). "Cytokine mechanisms of central sensitization: Distinct and overlapping role of interleukin-1β, interleukin-6, and tumor necrosis factor-α in regulating synaptic and neuronal activity in the superficial spinal cord". In: *Journal of Neuroscience* 28.20, pp. 5189–5194.

Kerstein, P. C., D. del Camino, M. M. Moran, and C. L. Stucky (2009). "Pharmacological blockade of TRPA1 inhibits mechanical firing in nociceptors". In: *Molecular Pain* 5, pp. 1–13.

Kettenmann, H., U.-K. Hanisch, M. Noda, and A. Verkhratsky (2011). "Physiology of microglia." In: *Physiological Reviews* 91.2, pp. 461–553.

Khan, A., J. Calinas Correia, and D. Walsh (2021). "Arthritis Pain; Rheumatoid Arthritis, Osteoarthritis, and Fibromyalgia". In: *Chronic Pain Management in General and Hospital Practice*. Ed. by K. Shimoji, A. Nader, and W. Hamann. Singapore: Singapore.

Kiguchi, N., Y. Kobayashi, Y. Kadowaki, Y. Fukazawa, F. Saika, and S. Kishioka (2014). "Vascular endothelial growth factor signaling in injured nerves underlies peripheral sensitization in neuropathic pain". In: *Journal of Neurochemistry* 129.1, pp. 169–178.

Kim, D. sik, K. W. Figueroa, K. W. Li, A. Boroujerdi, T. Yolo, and Z. David Luo (2009). "Profiling of dynamically changed gene expression in dorsal root ganglia post peripheral nerve injury and a critical role of injury-induced glial fibrillary acetic protein in maintenance of pain behaviors". In: *Pain* 143.1-2, pp. 114–122.

Kirk, S. L. and S. J. Karlik (2003). "VEGF and vascular changes in chronic neuroinflammation". In: *Journal of Autoimmunity* 21.4, pp. 353–363.

Klingelhöfer, J., L. Šenolt, B. Baslund, G. H. Nielsen, I. Skibshøj, K. Pavelka, M. Neidhart, S. Gay, N. Ambartsumian, B. S. Hansen, J. Petersen, E. Lukanidin, and M. Grigorian (2007). "Up-regulation of metastasis-promoting S100A4 (Mts-1) in rheumatoid arthritis: Putative involvement in the pathogenesis of rheumatoid arthritis". In: *Arthritis and Rheumatism* 56.3, pp. 779–789.

Koch, S. C., D. Acton, and M. Goulding (2018). "Spinal Circuits for Touch, Pain, and Itch". In: *Annual Review of Physiology* 80.1, pp. 189–217.

Koh, S. X. and J. K. Lee (2014). "S100B as a marker for brain damage and blood-brain barrier disruption following exercise". In: *Sports Medicine* 44.3, pp. 369–385.

Kokkonen, H., I. Söderström, J. Rocklöv, G. Hallmans, K. Lejon, and S. R. Dahlqvist (2010). "Up-regulation of cytokines and chemokines predates the onset of rheumatoid arthritis". In: *Arthritis and Rheumatism* 62.2, pp. 383–391.

Kosek, E., A. Finn, C. Ultenius, A. Hugo, C. Svensson, and A. S. Ahmed (2018). "Differences in neuroimmune signalling between male and female patients suffering from knee osteoarthritis". In: *Journal of Neuroimmunology* 321.April, pp. 49–60.

Kosek, E., R. Altawil, D. Kadetoff, A. Finn, M. Westman, E. Le Maître, M. Andersson, M. Jensen-Urstad, and J. Lampa (2015). "Evidence of different mediators of central inflammation in dysfunctional and inflammatory pain - Interleukin-8 in fibromyalgia and interleukin-1β in rheumatoid arthritis". In: *Journal of Neuroimmunology* 280, pp. 49–55.

Koyama, Y. (2014). "Signaling molecules regulating phenotypic conversions of astrocytes and glial scar formation in damaged nerve tissues". In: *Neurochemistry International* 78, pp. 35–42.

Kroenke, K., E. E. Krebs, and M. J. Bair (2009). "Pharmacotherapy of chronic pain: a synthesis of recommendations from systematic reviews". In: *General Hospital Psychiatry* 31.3, pp. 206–219.

Krukowski, K., N. Eijkelkamp, G. Laumet, C. E. Hack, Y. Li, P. M. Dougherty, C. J. Heijnen, and A. Kavelaars (2016). "CD8+ T Cells and Endogenous IL-10 Are Required for Resolution of Chemotherapy-Induced Neuropathic Pain". In: *Journal of Neuroscience* 36.43, pp. 11074–11083.

Kubotera, H., H. Ikeshima-Kataoka, Y. Hatashita, A. L. Allegra Mascaro, F. S. Pavone, and T. Inoue (2019). "Astrocytic endfeet re-cover blood vessels after removal by laser ablation". In: *Scientific Reports* 9.1, pp. 1–10.

Kumar, V. and B. A. Mahal (2012). "NGF - The TrkA to successful pain treatment". In: *Journal of Pain Research* 5, pp. 279–287.

Lallemend, F. and P. Ernfors (2012). "Molecular interactions underlying the specification of sensory neurons". In: *Trends in Neurosciences* 35.6, pp. 373–381.

Latremoliere, A. and C. J. Woolf (2009). "Central Sensitization: A Generator of Pain Hypersensitivity by Central Neural Plasticity". In: *Journal of Pain* 10.9, pp. 895–926.

Lawson, C. and S. Wolf (2009). "ICAM-1 signaling in endothelial cells". In: *Pharmacological Reports*. Vol. 61. 1, pp. 22–32.

Lawson, S. N., B. A. Crepps, and E. R. Perl (1997). "Relationship of substance P to afferent characteristics of dorsal root ganglion neurones in guinea-pig". In: *Journal of Physiology* 505.1, pp. 177–191.

Lee, G. W., J. Y. Son, A. R. Lee, J. S. Ju, Y. C. Bae, and D. K. Ahn (2019). "Central VEGF-A pathway plays a key role in the development of trigeminal neuropathic pain in rats". In: *Molecular Pain* 15, p. 174480691987260.

Lee, J., S. Lee, H. Zhang, M. A. Hill, C. Zhang, and Y. Park (2017). "Interaction of IL-6 and TNF-α contributes to endothelial dysfunction in type 2 diabetic mouse hearts". In: *PLoS ONE* 12.11.

Lengfeld, J., T. Cutforth, and D. Agalliu (2014). "The role of angiogenesis in the pathology of multiple sclerosis". In: *Vascular Cell* 6.1.

Leopold, B., J. Strutz, E. Weiß, J. Gindlhuber, R. Birner-Gruenberger, H. Hackl, H. M. Appel, S. Cvitic, and U. Hiden (2019). "Outgrowth, proliferation, viability, angiogenesis and phenotype of primary human endothelial cells in different purchasable endothelial culture media: feed wisely". In: *Histochemistry and Cell Biology* 152.5, pp. 377–390.

Lertkiatmongkol, P., D. Liao, H. Mei, and P. J. Newman (2016). "Endothelial functions of PECAM-1 (CD31)". In: *Current Opinion in Hematology* 23.3, pp. 253–259.

Leung, L. and C. M. Cahill (2010). "TNFα and neuropathic pain - a review". In: *Journal of Neuroinflammation* 7.1, p. 27.

Levine, J. D., S. J. Dardick, A. I. Basbaum, and E. Scipio (1985). "Reflex neurogenic inflammation. I. Contribution of the peripheral nervous system to spatially remote inflammatory responses that follow injury". In: *Journal of Neuroscience* 5.5, pp. 1380–1386.

Levy, D. and D. W. Zochodne (2000). "Increased mRNA expression of the B1 and B2 bradykinin receptors and antinociceptive effects of their antagonists in an animal model of neuropathic pain". In: *Pain* 86.3, pp. 265–271.

Li, C. and M. J. Poznansky (1990). "Characterization of the ZO-1 protein in endothelial and other cell lines". In: *Journal of Cell Science* 97.2, pp. 231–237.

Li, L., R. Nohara, S. Ono, K. Okuda, M. Tanaka, H. Fujiwara, Y. Matoba, A. Matsumori, M. Fujita, S. Sasayama, N. Tamaki, and J. Konishi (2007). "Central Sensitization - Uncovering the Relation between Pain and Plasticity". In: *Anesthesiology* 106, pp. 867–867.

Li, L., M. Zhu, W. Wu, B. Qin, J. Gu, Y. Tu, J. Chen, D. Liu, Y. Shi, X. Liu, A. Sang, and D. Ding (2020). "Brivanib, a multitargeted small-molecule tyrosine kinase inhibitor, suppresses laser-induced CNV in a mouse model of neovascular AMD". In: *Journal of Cellular Physiology* 235.2, pp. 1259–1273.

Li, M., Y. Wang, M. Liu, and X. Lan (2018a). "Multimodality reporter gene imaging: Construction strategies and application". In: *Theranostics* 8.11, pp. 2954–2973.

Li, S., L.-x. Chen, X.-h. Peng, C. Wang, B.-y. Qin, D. Tan, C.-x. Han, H. Yang, X.-n. Ren, F. Liu, C.-h. Xu, and X.-h. Zhou (2018b). "Overview of the reporter genes and reporter mouse models". In: *Anim Models Exp Med* 1, pp. 29–35.

Li, T., X. Chen, C. Zhang, Y. Zhang, and W. Yao (2019). "An update on reactive astrocytes in chronic pain". In: *Journal of Neuroinflammation* 16.1, pp. 1–13.

Li, Y. N., R. Pan, X. J. Qin, W. L. Yang, Z. Qi, W. Liu, and K. J. Liu (2014). "Ischemic neurons activate astrocytes to disrupt endothelial barrier via increasing VEGF expression". In: *Journal of Neurochemistry* 129.1, pp. 120–129.

Liao, J. K. (2013). "Linking endothelial dysfunction with endothelial cell activation". In: *Journal of Clinical Investigation* 123.2, pp. 540–541.

Liddelow, S. A. et al. (2017). "Neurotoxic reactive astrocytes are induced by activated microglia". In: *Nature* 541, pp. 481–487.

Liebner, S., R. M. Dijkhuizen, Y. Reiss, K. H. Plate, D. Agalliu, and G. Constantin (2018). "Functional morphology of the blood–brain barrier in health and disease". In: *Acta Neuropathologica* 135.3, pp. 311–336.

Liem, L., E. Van Dongen, F. J. Huygen, P. Staats, and J. Kramer (2016). "The dorsal root ganglion as a therapeutic target for chronic pain". In: *Regional Anesthesia and Pain Medicine* 41.4, pp. 511–519.

Lim, T. K., X. Q. Shi, H. C. Martin, H. Huang, G. Luheshi, S. Rivest, and J. Zhang (2014). "Blood-nerve barrier dysfunction contributes to the generation of neuropathic pain and allows targeting of injured nerves for pain relief". In: *Pain* 155.5, pp. 954–967.

Lin, C. R., F. Amaya, L. Barrett, H. Wang, J. Takada, T. A. Samad, and C. J. Woolf (2006). "Prostaglandin E2 receptor EP4 contributes to inflammatory pain hypersensitivity". In: *Journal of Pharmacology and Experimental Therapeutics* 319.3, pp. 1096–1103.

Lin, J., G. Li, X. Den, C. Xu, S. Liu, Y. Gao, H. Liu, J. Zhang, X. Li, and S. Liang (2010). "VEGF and its receptor-2 involved in neuropathic pain transmission mediated by P2X2/3 receptor of primary sensory neurons". In: *Brain Research Bulletin* 83.5, pp. 284–291.

Liu, G., A. T. Place, Z. Chen, V. M. Brovkovych, S. M. Vogel, W. A. Muller, R. A. Skidgel, A. B. Malik, and R. D. Minshall (2012). "ICAM-1-activated Src and eNOS signaling increase endothelial cell surface PECAM-1 adhesivity and neutrophil transmigration". In: *Blood* 120.9, pp. 1942–1952.

Llorián-Salvador, M. and S. González-Rodríguez (2018). "Painful Understanding of VEGF". In: *Frontiers in Pharmacology* 9.November, pp. 2014–2018.

Lon, H. K., D. Liu, Q. Zhang, D. C. Dubois, R. R. Almon, and W. J. Jusko (2011). "Pharmacokinetic-pharmacodynamic disease progression model for effect of etanercept in lewis rats with collagen-induced arthritis". In: *Pharmaceutical Research* 28.7, pp. 1622–1630.

Loram, L. C., A. Fuller, L. G. Fick, T. Cartmell, S. Poole, and D. Mitchell (2007). "Cytokine Profiles During Carrageenan-Induced Inflammatory Hyperalgesia in Rat Muscle and Hind Paw". In: *Journal of Pain* 8.2, pp. 127–136.

Lu, M., V. L. Perez, N. Ma, K. Miyamoto, H. B. Peng, J. K. Liao, and A. P. Adamis (1999). "VEGF increases retinal vascular ICAM-1 expression in vivo". In: *Investigative Ophthalmology and Visual Science* 40.8, pp. 1808–1812.

Lucifora, S., H. H. Willcockson, C. R. Lu, M. Darstein, K. D. Phend, J. G. Valtschanoff, and A. Rustioni (2006). "Presynaptic low- and high-affinity kainate receptors in nociceptive spinal afferents". In: *Pain* 120.1-2, pp. 97–105.

Ludewig, P., J. Winneberger, and T. Magnus (2019). "The cerebral endothelial cell as a key regulator of inflammatory processes in sterile inflammation". In: *Journal of Neuroimmunology* 326, pp. 38–44.

Luo, X., B. Fitzsimmons, A. Mohan, L. Zhang, N. Terrando, H. Kordasiewicz, and R. R. Ji (2018). "Intrathecal administration of antisense oligonucleotide against p38α but not p38β MAP kinase isoform reduces neuropathic and postoperative pain and TLR4-induced pain in male mice". In: *Brain, Behavior, and Immunity* 72, pp. 34–44.

Machida, T., S. Dohgu, F. Takata, J. Matsumoto, I. Kimura, M. Koga, K. Nakamoto, A. Yamauchi, and Y. Kataoka (2017). "Role of thrombin-PAR1-PKCθ/δ axis in brain pericytes in thrombin-induced MMP-9 production and blood–brain barrier dysfunction in vitro". In: *Neuroscience* 350, pp. 146–157.

Maggi, A., L. Ottobrini, A. Biserni, G. Lucignani, and P. Ciana (2004). *Techniques: Reporter mice - A new way to look at drug action*.

Malfait, A. M., C. B. Little, and J. J. McDougall (2013). "A commentary on modelling osteoarthritis pain in small animals". In: *Osteoarthritis and Cartilage* 21.9, pp. 1316–1326.

Mapplebeck, J. C. S., S. Beggs, and M. W. Salter (2016). "Sex differences in pain: a tale of two immune cells." In: *Pain* 157 Suppl, S2–6.

Marchand, F., C. Tsantoulas, D. Singh, J. Grist, A. K. Clark, E. J. Bradbury, and S. B. McMahon (2009). "Effects of Etanercept and Minocycline in a rat model of spinal cord injury". In: *European Journal of Pain* 13.7, pp. 673–681.

Mark, K. S. and D. W. Miller (1999). "Increased permeability of primary cultured brain microvessel endothelial cell monolayers following TNF-alpha exposure." In: *Life Sciences* 64.21, pp. 1941–53.

Martínez-Estrada, O. M., E. Rodríguez-Millán, E. González-de Vicente, M. Reina, S. Vilaró, and M. Fabre (2003). "Erythropoietin protects the in vitro blood-brain barrier against VEGF-induced permeability". In: *European Journal of Neuroscience* 18.9, pp. 2538–2544.

McCoy, J. M., J. R. Wicks, and L. P. Audoly (2002). "The role of prostaglandin E2 receptors in the pathogenesis of rheumatoid arthritis". In: *Journal of Clinical Investigation* 110.5, pp. 651–658.

McGlone, F. and D. Reilly (2010). "The cutaneous sensory system". In: *Neuroscience and Biobehavioral Reviews* 34.2, pp. 148–159.

McKemy, D. D. (2007). "TRPM8: The Cold and Menthol Receptor". In: *TRP Ion Channel Function in Sensory Transduction and Cellular Signaling Cascades.* Ed. by W. Liedtke and S. Heller. Boca Raton, Florida: CRC Press/Taylor & Francis. Chap. 13.

McQuay, H. J., A. F. Sullivan, K. Smallman, and A. H. Dickenson (1989). "Intrathecal opioids, potency and lipophilicity". In: *Pain* 36.1, pp. 111–115.

McWilliams, D. F. and D. A. Walsh (2017). "Pain mechanisms in rheumatoid arthritis". In: *Clinical and Experimental Rheumatology* 35.5, S94–S101.

– (2016). "Factors predicting pain and early discontinuation of tumour necrosis factor-α-inhibitors in people with rheumatoid arthritis: results from the British society for rheumatology biologics register." In: *BMC Musculoskeletal Disorders* 17, p. 337.

Medina-Leyte, D. J., M. Domínguez-Pérez, I. Mercado, M. T. Villarreal-Molina, and L. Jacobo-Albavera (2020). "Use of human umbilical vein endothelial cells (HUVEC) as a model to study cardiovascular disease: A review". In: *Applied Sciences (Switzerland)* 10.3, p. 938.

Meents, J. E., C. I. Ciotu, and M. J. Fischer (2019). "Trpa1: A molecular view". In: *Journal of Neurophysiology* 121.2, pp. 427–443.

Meller, S. T., C. Dykstra, D. Grzybycki, S. Murphy, and G. F. Gebhart (1994). "The possible role of glia in nociceptive processing and hyperalgesia in the spinal cord of the rat". In: *Neuropharmacology* 33.11, pp. 1471–1478.

Mendell, L. M. and P. D. Wall (1965). "Responses of Single Dorsal Cord Cells To Peripheral Cutaneous Unmyelinated Fibres." In: *Nature* 206.January, pp. 97–99.

Menetski, J., S. Mistry, M. Lu, J. S. Mudgett, R. M. Ransohoff, J. A. DeMartino, D. E. MacIntyre, and C. Abbadie (2007). "Mice overexpressing chemokine ligand 2 (CCL2) in as-

trocytes display enhanced nociceptive responses". In: *Neuroscience* 149.3, pp. 706–714.

Millan, M. J. (1999). "The induction of pain: an integrative review". In: *Progress in Neurobiology* 57, pp. 1–164.

Miller, S. J. (2018). "Astrocyte Heterogeneity in the Adult Central Nervous System". In: *Frontiers in Cellular Neuroscience* 12, p. 15.

Milligan, E. D. and L. R. Watkins (2009). "Pathological and protective roles of glia in chronic pain." In: *Nature Reviews Neuroscience* 10.1, pp. 23–36.

Montague-Cardoso, K., T. Pitcher, K. Chisolm, G. Salera, E. Lindstrom, E. Hewitt, E. Solito, and M. Malcangio (2020). "Changes in vascular permeability in the spinal cord contribute to chemotherapy-induced neuropathic pain". In: *Brain, Behavior, and Immunity* 83, pp. 248–259.

Morioka, N., S. Fujii, S. Kondo, F. F. Zhang, K. Miyauchi, Y. Nakamura, K. Hisaoka-Nakashima, and Y. Nakata (2018). "Downregulation of spinal astrocytic connexin43 leads to upregulation of interleukin-6 and cyclooxygenase-2 and mechanical hypersensitivity in mice". In: *Glia* 66.2, pp. 428–444.

Muramatsu, R., M. Kuroda, K. Matoba, H. Lin, C. Takahashi, Y. Koyama, and T. Yamashita (2015). "Prostacyclin prevents pericyte loss and demyelination induced by lysophosphatidylcholine in the central nervous system." In: *The Journal of biological chemistry* 290.18, pp. 11515–25.

Naeini, R. S., C. M. Cahill, A. Ribeiro-Da-Silva, H. A. Ménard, and J. L. Henry (2005). "Remodelling of spinal nociceptive mechanisms in an animal model of monoarthritis". In: *European Journal of Neuroscience* 22.8, pp. 2005–2015.

Nagao, M., J. L. Hamilton, R. Kc, A. D. Berendsen, X. Duan, C. W. Cheong, X. Li, H. J. Im, and B. R. Olsen (2017). "Vascular Endothelial Growth Factor in Cartilage Development and Osteoarthritis". In: *Scientific Reports* 7.1.

Nakahara, H., J. Song, M. Sugimoto, K. Hagihara, T. Kishimoto, K. Yoshizaki, and N. Nishimoto (2003). "Anti-interleukin-6 receptor antibody therapy reduces vascular endothelial growth factor production in rheumatoid arthritis". In: *Arthritis and Rheumatism* 48.6, pp. 1521–1529.

Nam, Y., J. H. Kim, J. H. Kim, M. K. Jha, J. Y. Jung, M. G. Lee, I. S. Choi, I. S. Jang, D. G. Lim, S. H. Hwang, H. J. Cho, and K. Suk (2016). "Reversible Induction of Pain Hypersensitivity following Optogenetic Stimulation of Spinal Astrocytes". In: *Cell Reports* 17.11, pp. 3049–3061.

National Institute for Health and Care Excellence (2018). *Rheumatoid arthritis in adults: management*. Tech. rep.

Nestor, C. E., R. Ottaviano, D. Reinhardt, H. A. Cruickshanks, H. K. Mjoseng, R. C. McPherson, A. Lentini, J. P. Thomson, D. S. Dunican, S. Pennings, S. M. Anderton, M. Benson, and R. R. Meehan (2015). "Rapid reprogramming of epigenetic and transcriptional profiles in mammalian culture systems". In: *Genome Biology* 16.1, pp. 1–17.

Neubert, M. J., W. Kincaid, and M. M. Heinricher (2004). "Nociceptive facilitating neurons in the rostral ventromedial medulla". In: *Pain* 110, pp. 158–165.

Neugebauer, V., J. S. Han, H. Adwanikar, Y. Fu, and G. Ji (2007). "Techniques for assessing knee joint pain in arthritis". In: *Molecular Pain* 3.8, pp. 1–13.

Neugebauer, V., W. Li, G. C. Bird, and J. S. Han (2004). "The Neuroscientist The Amygdala and Persistent Pain". In: *The Neuroscientist* 10.3, pp. 221–234.

Newton, V. L., J. D. Guck, M. A. Cotter, N. E. Cameron, and N. J. Gardiner (2017). "Neutrophils Infiltrate the Spinal Cord Parenchyma of Rats with Experimental Diabetic Neuropathy". In: *Journal of Diabetes Research* 2017, pp. 1–10.

Nishioku, T., K. Furusho, A. Tomita, H. Ohishi, S. Dohgu, H. Shuto, A. Yamauchi, and Y. Kataoka (2011). "Potential role for S100A4 in the disruption of the blood-brain barrier in collagen-induced arthritic mice, an animal model of rheumatoid arthritis". In: *Neuroscience* 189, pp. 286–292.

Nitta, T., M. Hata, S. Gotoh, Y. Seo, H. Sasaki, N. Hashimoto, M. Furuse, and S. Tsukita (2003). "Size-selective loosening of the blood-brain barrier in claudin-5–deficient mice". In: *Journal of Cell Biology* 161.3, pp. 653–660.

Nordal, R. A. and C. S. Wong (2004). "Intercellular adhesion molecule-1 and blood-spinal cord barrier disruption in central nervous system radiation injury". In: *Journal of Neuropathology and Experimental Neurology* 63.5, pp. 474–483.

Norden, D. M., P. J. Trojanowski, E. Villanueva, E. Navarro, and J. P. Godbout (2016). "Sequential activation of microglia and astrocyte cytokine expression precedes increased iba-1 or GFAP immunoreactivity following systemic immune challenge". In: *GLIA* 64.2, pp. 300–316.

North, R. A. (2004). "P2X3 receptors and peripheral pain mechanisms." In: *Journal of Physiology* 554.Pt 2, pp. 301–308.

Nowak, D. G., J. Woolard, E. M. Amin, O. Konopatskaya, M. A. Saleem, A. J. Churchill, M. R. Ladomery, S. J. Harper, and D. O. Bates (2008). "Expression of pro- and anti-angiogenic isoforms of VEGF is differentially regulated by splicing and growth factors". In: *Journal of Cell Science* 121.20, pp. 3487–3495.

O'Brien, M., H. T. Philpott, and J. J. McDougall (2017). "Understanding osteoarthritis pain through animal models". In: *Clinical and Experimental Rheumatology* 35.5, S47–S52.

O'Carroll, S. J., D. T. Kho, R. Wiltshire, V. Nelson, O. Rotimi, R. Johnson, C. E. Angel, and E. S. Graham (2015). "Pro-inflammatory TNFα and IL-1β differentially regulate the inflammatory phenotype of brain microvascular endothelial cells". In: *Journal of Neuroinflammation* 12.1, pp. 1–18.

Obermeier, B., R. Daneman, and R. M. Ransohoff (2013). "Development, maintenance and disruption of the blood-brain barrier". In: *Nature Medicine* 19.12, pp. 1584–1596.

Ohara, P. T., J. P. Vit, A. Bhargava, and L. Jasmin (2008). "Evidence for a role of connexin 43 in trigeminal pain using RNA interference in vivo". In: *Journal of Neurophysiology* 100.6, pp. 3064–3073.

Okabe, K., S. Kobayashi, T. Yamada, T. Kurihara, I. Tai-Nagara, T. Miyamoto, Y. S. Mukouyama, T. N. Sato, T. Suda, M. Ema, and Y. Kubota (2014). "Neurons limit angiogenesis by titrating VEGF in retina". In: *Cell* 159.3, pp. 584–596.

Onda, A., M. Hamba, S. Yabuki, and S. Kikuchi (2002). "Exogenous tumor necrosis factor-α induces abnormal discharges in rat dorsal horn neurons". In: *Spine* 27.15, pp. 1618–1624.

Orita, S., T. Ishikawa, M. Miyagi, N. Ochiai, G. Inoue, Y. Eguchi, H. Kamoda, G. Arai, T. Toyone, Y. Aoki, T. Kubo, K. Takahashi, and S. Ohtori (2011). "Pain-related sensory innervation in monoiodoacetate-induced osteoarthritis in rat knees that gradually develops neuronal injury in addition to inflammatory pain". In: *BMC Musculoskeletal Disorders* 12.

Osada, T., Y. H. Gu, M. Kanazawa, Y. Tsubota, B. T. Hawkins, M. Spatz, R. Milner, and G. J. Del Zoppo (2011). "Interendothelial claudin-5 expression depends on cerebral endothelial cell-matrix adhesion by B 1-integrins". In: *Journal of Cerebral Blood Flow and Metabolism* 31.10, pp. 1972–1985.

Osipova, E. D., O. V. Semyachkina-Glushkovskaya, A. V. Morgun, N. V. Pisareva, N. A. Malinovskaya, E. B. Boitsova, E. A. Pozhilenkova, O. A. Belova, V. V. Salmin, T. E. Taranushenko, M. Noda, and A. B. Salmina (2018). "Gliotransmitters and cytokines in the control of blood-brain barrier permeability". In: *Reviews in the Neurosciences*.

Ošlejšková, L., M. Grigorian, H. Hulejová, J. Vencovský, K. Pavelka, J. Klingelhöfer, S. Gay, M. Neidhart, H. Brabcová, D. Suchý, and L. Šenolt (2009). "Metastasis-inducing S100A4 protein is associated with the disease activity of rheumatoid arthritis". In: *Rheumatology* 48.12, pp. 1590–1594.

Parry, D. M., F. M. Semenenko, R. K. Conley, and B. M. Lumb (2002). "Noxious somatic inputs to hypothalamic-midbrain projection neurones: a comparison of the columnar organisation of somatic and visceral inputs to the periaqueductal grey in the rat." In: *Experimental Physiology* 87.2, pp. 117–22.

Patel, J. P. and B. N. Frey (2015). "Disruption in the blood-brain barrier: The missing link between brain and body inflammation in bipolar disorder?" In: *Neural Plasticity* 2015.

Patwardhan, A. M., A. N. Akopian, N. B. Ruparel, A. Diogenes, S. T. Weintraub, C. Uhlson, R. C. Murphy, and K. M. Hargreaves (2010). "Heat generates oxidized linoleic acid metabolites that activate TRPV1 and produce pain in rodents". In: *Journal of Clinical Investigation* 120.5, pp. 1617–1626.

Peach, C. J., V. W. Mignone, M. A. Arruda, D. C. Alcobia, S. J. Hill, L. E. Kilpatrick, and J. Woolard (2018). "Molecular pharmacology of VEGF-A isoforms: Binding and signalling at VEGFR2". In: *International Journal of Molecular Sciences* 19.4, p. 1264.

Peirs, C., R. Dallel, and A. J. Todd (2020). "Recent advances in our understanding of the organization of dorsal horn neuron populations and their contribution to cutaneous mechanical allodynia". In: *Journal of Neural Transmission* 127.4, pp. 505–525.

Peng, J., N. Gu, L. Zhou, U. B Eyo, M. Murugan, W. B. Gan, and L. J. Wu (2016). "Microglia and monocytes synergistically promote the transition from acute to chronic pain after nerve injury". In: *Nature Communications* 7.

Persidsky, Y., J. Hill, M. Zhang, H. Dykstra, M. Winfield, N. L. Reichenbach, R. Potula, A. Mukherjee, S. H. Ramirez, and S. Rom (2016). "Dysfunction of brain pericytes in

chronic neuroinflammation". In: *Journal of Cerebral Blood Flow & Metabolism* 36.4, pp. 794–807.

Petersen, M., A. S. Eckert, G. Segond von Banchet, B. Heppelmann, A. Klusch, and K. D. Kniffki (1998). "Plasticity in the expression of bradykinin binding sites in sensory neurons after mechanical nerve injury." In: *Neuroscience* 83.3, pp. 949–59.

PhysiologyWeb (2020). *Diffusion Time Calculator - PhysiologyWeb*.

Pitcher, T., J. Sousa-Valente, and M. Malcangio (2016). "The monoiodoacetate model of osteoarthritis pain in the mouse". In: *Journal of Visualized Experiments* 2016.111.

Praag, H. van and H. Frenk (1991). "The development of stimulation-produced analgesia (SPA) in the rat". In: *Developmental Brain Research* 64.1, pp. 71–76.

Prato, V., F. J. Taberner, J. R. Hockley, G. Callejo, A. Arcourt, B. Tazir, L. Hammer, P. Schad, P. A. Heppenstall, E. S. Smith, and S. G. Lechner (2017). "Functional and Molecular Characterization of Mechanoinsensitive "Silent" Nociceptors". In: *Cell Reports* 21.11, pp. 3102–3115.

Privratsky, J. R. and P. J. Newman (2014). "PECAM-1: Regulator of endothelial junctional integrity". In: *Cell and Tissue Research* 355.3, pp. 607–619.

Proescholdt, M. A., J. D. Heiss, S. Walbridge, J. Mühlhauser, M. C. Capogrossi, E. H. Oldfield, and M. J. Merrill (1999). "Vascular endothelial growth factor (VEGF) modulates vascular permeability and inflammation in rat brain". In: *Journal of Neuropathology and Experimental Neurology* 58.6, pp. 613–627.

Qiu, S., C. Shi, A. N. Anbazhagan, V. Das, V. Arora, R. Kc, X. Li, I. S. O-Sullivan, A. van Wijnen, S. Chintharlapalli, G. Gott-Velis, R. Richard, F. Mwale, M. Shibuya, S. Min, and H. J. Im (2020). "Absence of VEGFR-1/Flt-1 signaling pathway in mice results in insensitivity to discogenic low back pain in an established disc injury mouse model". In: *Journal of Cellular Physiology* 235.6, pp. 5305–5317.

Radhakrishnan, R., S. A. Moore, and K. A. Sluka (2003). "Unilateral carrageenan injection into muscle or joint induces chronic bilateral hyperalgesia in rats". In: *Pain* 104.3, pp. 567–577.

Radisavljevic, Z., H. Avraham, and S. Avraham (2000). "Vascular endothelial growth factor up-regulates ICAM-1 expression via the phosphatidylinositol 3 OH-kinase/AKT/nitric oxide pathway and modulates migration of brain microvascular endothelial cells". In: *Journal of Biological Chemistry* 275.27, pp. 20770–20774.

Radu, B., P. Bramanti, F. Osculati, M.-L. Flonta, M. Radu, G. Bertini, and P. Fabene (2013). "Neurovascular unit in chronic pain". In: *Mediators of Inflammation* 2013.

Raghavendra, V., F. Y. Tanga, and J. A. DeLeo (2004). "Complete Freunds adjuvant-induced peripheral inflammation evokes glial activation and proinflammatory cytokine expression in the CNS". In: *European Journal of Neuroscience* 20.2, pp. 467–473.

Raja, S. N., D. B. Carr, M. Cohen, N. B. Finnerup, H. Flor, S. Gibson, F. J. Keefe, J. S. Mogil, M. Ringkamp, K. A. Sluka, X.-J. Song, B. Stevens, M. D. Sullivan, P. R. Tutelman, T. Ushida, and K. Vader (2020). "The revised International Association for the Study of Pain definition of pain: concepts, challenges, and compromises". In: *Pain* 161.9, pp. 1976–1982.

Ransohoff, R. M. (2016). "A polarizing question: Do M1 and M2 microglia exist". In: *Nature Neuroscience* 19.8, pp. 987–991.

Ransohoff, R. M. and M. A. Brown (2012). "Innate immunity in the central nervous system." In: *Journal of Clinical Investigation* 122.4, pp. 1164–71.

Raoof, R., H. Willemen, and N. Eijkelkamp (2018). "Divergent roles of immune cells and their mediators in pain". In: *Rheumatology (Oxford)* 57.3, pp. 429–440.

Raychaudhury, A., M. Elkins, D. Kozien, and M. T. Nakada (2001). "Regulation of PECAM-1 in endothelial cells during cell growth and migration". In: *Experimental Biology and Medicine* 226.7, pp. 686–691.

Reeve, A. J., S. Patel, A. Fox, K. Walker, and L. Urban (2000). "Intrathecally administered endotoxin or cytokines produce allodynia, hyperalgesia and changes in spinal cord neuronal responses to nociceptive stimuli in the rat." In: *European Journal of Pain* 4.3, pp. 247–57.

Reglero-Real, N., B. Marcos-Ramiro, and J. Millán (2012). "Endothelial membrane reorganization during leukocyte extravasation". In: *Cellular and Molecular Life Sciences* 69, pp. 3079–3099.

Reinhold, A. and H. Rittner (2017). "Barrier function in the peripheral and central nervous system—a review". In: *Pflügers Archiv - European Journal of Physiology* 469.1, pp. 123–134.

Remko, M., A. Boháč, and L. Kováčiková (2011). "Molecular structure, pKa, lipophilicity, solubility, absorption, polar surface area, and blood brain barrier penetration of some antiangiogenic agents". In: *Structural Chemistry* 22.3, pp. 635–648.

Richner, M., N. Ferreira, A. Dudele, T. S. Jensen, C. B. Vaegter, and N. P. Gonçalves (2019). "Functional and structural changes of the blood-nerve-barrier in diabetic neuropathy". In: *Frontiers in Neuroscience* 13.JAN, pp. 1–9.

Rosen, S., B. Ham, and J. S. Mogil (2017). *Sex differences in neuroimmunity and pain*.

Roudaut, Y., A. Lonigro, B. Coste, J. Hao, P. Delmas, and M. Crest (2012). "Touch sense: functional organization and molecular determinants of mechanosensitive receptors." In: *Channels (Austin, Tex.)* 6.4, pp. 234–245.

Rustenhoven, J., D. Jansson, L. C. Smyth, and M. Dragunow (2017). "Brain Pericytes As Mediators of Neuroinflammation". In: *Trends in Pharmacological Sciences* 38.3, pp. 291–304.

Al-Saadany, H. M., M. S. Hussein, R. A. Gaber, and H. A. Zaytoun (2016). "Th-17 cells and serum IL-17 in rheumatoid arthritis patients: Correlation with disease activity and severity". In: *Egyptian Rheumatologist* 38.1, pp. 1–7.

Salajegheh, A. and A. Salajegheh (2016). "Zinc Finger E-Box Binding Homeobox 1 (ZEB1)". In: *Angiogenesis in Health, Disease and Malignancy*. Springer International Publishing, pp. 387–391.

Salameh, T. S., G. N. Shah, T. O. Price, M. R. Hayden, and W. A. Banks (2016). "Blood-Brain Barrier Disruption and Neurovascular Unit Dysfunction in Diabetic Mice: Protection with the Mitochondrial Carbonic Anhydrase Inhibitor Topiramate." In: *The Journal of pharmacology and experimental therapeutics* 359.3, pp. 452–459.

Salter, M. W. and S. Beggs (2014). "Sublime microglia: expanding roles for the guardians of the CNS." In: *Cell* 158.1, pp. 15–24.

Sandkühler, J. (2013). "Spinal Cord Plasticity and Pain". In: *Wall & Melzack's Textbook of Pain*. Ed. by S. B. McMahon, M. Koltzenburg, I. Tracey, and D. Turk. 6th. Elsevier. Chap. 6, pp. 94–110.

Sauer, R. S., J. Kirchner, S. Yang, L. Hu, M. Leinders, C. Sommer, A. Brack, and H. L. Rittner (2017). "Blood–spinal cord barrier breakdown and pericyte deficiency in peripheral neuropathy". In: *Annals of the New York Academy of Sciences* 1405.1, pp. 71–88.

Saunders, N. R., K. M. Dziegielewska, K. Møllgård, and M. D. Habgood (2015). "Markers for blood-brain barrier integrity: how appropriate is Evans blue in the twenty-first century and what are the alternatives?" In: *Frontiers in Neuroscience* 9, p. 385.

Schäfers, M., C. I. Svensson, C. Sommer, and L. S. Sorkin (2003). "Tumor necrosis factor-α induces mechanical allodynia after spinal nerve ligation by activation of p38 MAPK in primary sensory neurons". In: *Journal of Neuroscience* 23.7, pp. 2517–2521.

Schaible, H.-G., G. Segond Von Banchet, M. K. Boettger, R. Bräuer, B. Bräuer, M. Gajda, F. Richter, S. Hensellek, D. Brenn, and G. Natura (2010). "The role of proinflammatory cytokines in the generation and maintenance of joint pain". In: *Ann. N.Y. Acad. Sci* 1193, pp. 60–69.

Schaible, H. G. (2014). "Nociceptive neurons detect cytokines in arthritis". In: *Arthritis Research and Therapy* 16.1, pp. 1–9.

Schaible, H. (2006). "Peripheral and Central Mechanisms of Pain Generation". In: *HEP* 177, pp. 3–28.

Schnitzer, T. J. and J. A. Marks (2015). "A systematic review of the efficacy and general safety of antibodies to NGF in the treatment of OA of the hip or knee". In: *Osteoarthritis and Cartilage* 23, S8–S17.

Schoenberger, J., D. Grimm, P. Kossmehl, M. Infanger, E. Kurth, and C. Eilles (2004). "Effects of PTK787/ZK222584, a Tyrosine Kinase Inhibitor, on the Growth of a Poorly Differentiated Thyroid Carcinoma: An Animal Study". In: *Endocrinology* 145.3, pp. 1031–1038.

Schreiber, K. L., A. J. Beitz, and G. L. Wilcox (2008). "Activation of spinal microglia in a murine model of peripheral inflammation-induced, long-lasting contralateral allodynia". In: *Neuroscience Letters* 440.1, pp. 63–67.

Schreiner, B., E. Romanelli, P. Liberski, B. Ingold-Heppner, B. Sobottka-Brillout, T. Hartwig, V. Chandrasekar, H. Johannssen, H. U. Zeilhofer, A. Aguzzi, F. Heppner, M. Kerschensteiner, and B. Becher (2015). "Astrocyte Depletion Impairs Redox Homeostasis and Triggers Neuronal Loss in the Adult CNS". In: *Cell Reports* 12.9, pp. 1377–1384.

Sedgwick, J. D., A. L. Ford, E. Foulcher, and R. Airriess (1998). "Central nervous system microglial cell activation and proliferation follows direct interaction with tissue-infiltrating T cell blasts." In: *Journal of Immunology* 160.11, pp. 5320–30.

Segond von Banchet, G., M. K. Boettger, N. Fischer, M. Gajda, R. Bräuer, and H. G. Schaible (2009). "Experimental arthritis causes tumor necrosis factor-α-dependent

infiltration of macrophages into rat dorsal root ganglia which correlates with pain-related behavior". In: *Pain* 145.1-2, pp. 151–159.

Selvaraj, D., V. Gangadharan, C. W. Michalski, M. Kurejova, S. Stösser, K. Srivastava, M. Schweizerhof, J. Waltenberger, N. Ferrara, P. Heppenstall, M. Shibuya, H. G. Augustin, and R. Kuner (2015). "A Functional Role for VEGFR1 Expressed in Peripheral Sensory Neurons in Cancer Pain". In: *Cancer Cell* 27.6, pp. 780–796.

Sharma, H. (2005). "Pathophysiology of Blood-Spinal Cord Barrier in Traumatic Injury and Repair". In: *Current Pharmaceutical Design* 11.11, pp. 1353–1389.

Shen, F., H. Zheng, L. Zhou, W. Li, Y. Zhang, and X. Xu (2019). "LINC00657 expedites neuropathic pain development by modulating miR-136/ZEB1 axis in a rat model". In: *Journal of Cellular Biochemistry* 120.1, pp. 1000–1010.

Smith, B. H. and N. Torrance (2012). "Epidemiology of neuropathic pain and its impact on quality of life". In: *Current Pain and Headache Reports* 16.3, pp. 191–198.

Smith, C. W., S. D. Marlin, R. Rothlein, C. Toman, and D. C. Anderson (1989). "Cooperative interactions of LFA-1 and Mac-1 with intracellular adhesion molecule-1 in facilitating adherence and transendothelial migration of human neutrophils in vitro". In: *Journal of Clinical Investigation* 83.6, pp. 2008–2017.

Smyth, L. C., J. Rustenhoven, T. I. Park, P. Schweder, D. Jansson, P. A. Heppner, S. J. O'Carroll, E. W. Mee, R. L. Faull, M. Curtis, and M. Dragunow (2018). "Unique and shared inflammatory profiles of human brain endothelia and pericytes". In: *Journal of Neuroinflammation* 15.1, pp. 1–18.

Sofroniew, M. V. and H. V. Vinters (2010). "Astrocytes: Biology and pathology". In: *Acta Neuropathologica* 119.1, pp. 7–35.

Soker, S., S. Takashima, H. Q. Miao, G. Neufeld, and M. Klagsbrun (1998). "Neuropilin-1 is expressed by endothelial and tumor cells as an isoform- specific receptor for vascular endothelial growth factor". In: *Cell* 92.6, pp. 735–745.

Sokolova, E. V., Y. Karetin, V. N. Davydova, A. O. Byankina, A. A. Kalitnik, L. N. Bogdanovich, and I. M. Yermak (2016). "Carrageenans effect on neutrophils alone and in combination with LPS in vitro". In: *Journal of Biomedical Materials Research - Part A* 104.7, pp. 1603–1609.

Sommer, C., M. Schäfers, M. Marziniak, and K. V. Toyka (2001). "Etanercept reduces hyperalgesia in experimental painful neuropathy". In: *Journal of the Peripheral Nervous System* 6.2, pp. 67–72.

Sorge, R. E., M. L. LaCroix-Fralish, a. H. Tuttle, S. G. Sotocinal, J.-S. Austin, J. Ritchie, M. L. Chanda, a. C. Graham, L. Topham, S. Beggs, M. W. Salter, and J. S. Mogil (2011). "Spinal Cord Toll-Like Receptor 4 Mediates Inflammatory and Neuropathic Hypersensitivity in Male But Not Female Mice". In: *Journal of Neuroscience* 31.43, pp. 15450–15454.

Sorge, R. E. et al. (2014). "Olfactory exposure to males, including men, causes stress and related analgesia in rodents". In: *Nature Methods* 11.6, pp. 629–632.

Sorge, R. E. et al. (2015). "Different immune cells mediate mechanical pain hypersensitivity in male and female mice". en. In: *Nature Neuroscience* 18.8, pp. 1081–1083.

Souza, G. R., J. Talbot, C. M. Lotufo, F. Q. Cunha, T. M. Cunha, and S. H. Ferreira (2013). "Fractalkine mediates inflammatory pain through activation of satellite glial cells". In: *Proceedings of the National Academy of Sciences* 110.27, pp. 11193–11198.

Speight, J. G. (2011). "Pharmaceuticals". In: *Handbook of Industrial Hydrocarbon Processes*. Elsevier, pp. 467–497.

Steyers, C. M. and F. J. Miller (2014). "Endothelial dysfunction in chronic inflammatory diseases". In: *International Journal of Molecular Sciences* 15.7, pp. 11324–11349.

Stils, H. F. (2005). "Adjuvants and Antibody Production: Dispelling the Myths Associated with Freund's Complete and Other Adjuvants". In: *ILAR Journal* 46.3, pp. 280–293.

Stone, N. L., T. J. England, and S. E. O'Sullivan (2019). "A novel transwell blood brain barrier model using primary human cells". In: *Frontiers in Cellular Neuroscience* 13, p. 230.

Sun, S., H. Cao, M. Han, T. T. Li, Z. Q. Zhao, and Y. Q. Zhang (2008). "Evidence for suppression of electroacupuncture on spinal glial activation and behavioral hypersensitivity in a rat model of monoarthritis". In: *Brain Research Bulletin* 75.1, pp. 83–93.

Sun, S., H. Cao, M. Han, T.-T. Li, H.-L. Pan, Z.-Q. Zhao, and Y.-Q. Zhang (2007). "New evidence for the involvement of spinal fractalkine receptor in pain facilitation and spinal glial activation in rat model of monoarthritis". In: *Pain* 129.1-2, pp. 64–75.

Sung, C. S., C. H. Cherng, Z. H. Wen, W. K. Chang, S. Y. Huang, S. L. Lin, K. H. Chan, and C. S. Wong (2012). "Minocycline and fluorocitrate suppress spinal nociceptive signaling in intrathecal IL-1β-induced thermal hyperalgesic rats". In: *GLIA* 60.12, pp. 2004–2017.

Suzumura, A., T. Marunouchi, and H. Yamamoto (1991). "Morphological transformation of microglia in vitro". In: *Brain Research* 545.1-2, pp. 301–306.

Swanson, R. A. and S. H. Graham (1994). "Fluorocitrate and fluoroacetate effects on astrocyte metabolism in vitro". In: *Brain Research* 664.1-2, pp. 94–100.

Sweeney, M. D., A. P. Sagare, and B. V. Zlokovic (2018). "Blood-brain barrier breakdown in Alzheimer disease and other neurodegenerative disorders". In: *Nature Reviews Neurology* 14.3, pp. 133–150.

Sweitzer, S. M., W. F. Hickey, M. D. Rutkowski, J. L. Pahl, and J. A. DeLeo (2002). "Focal peripheral nerve injury induces leukocyte trafficking into the central nervous system: Potential relationship to neuropathic pain". In: *Pain* 100.1-2, pp. 163–170.

Taheri, S., C. Gasparovic, N. J. Shah, and G. A. Rosenberg (2011). "Quantitative measurement of blood-brain barrier permeability in human using dynamic contrast-enhanced MRI with fast T1 mapping". In: *Magnetic Resonance in Medicine* 65.4, pp. 1036–1042.

Takahashi, Y., T. Chiba, H. Sameda, S. Ohtori, M. Kurokawa, and H. Moriya (2002). "Organization of cutaneous ventrodorsal and rostrocaudal axial lines in the rat hindlimb and trunk in the dorsal horn of the spinal cord". In: *Journal of Comparative Neurology* 445.2, pp. 133–144.

Takahashi, Y. and Y. Nakajima (1996). "Dermatomes in the rat limbs as determined by antidromic stimulation of sensory C-fibers in spinal nerves". In: *Pain* 67.1, pp. 197–202.

Takahashi, Y., Y. Nakajima, and T. Sakamoto (1994). "Dermatome mapping in the rat hindlimb by electrical stimulation of the spinal nerves". In: *Neuroscience Letters* 168.1-2, pp. 85–88.

Takata, F., S. Dohgu, J. Matsumoto, H. Takahashi, T. Machida, T. Wakigawa, E. Harada, H. Miyaji, M. Koga, T. Nishioku, A. Yamauchi, and Y. Kataoka (2011). "Brain pericytes among cells constituting the blood-brain barrier are highly sensitive to tumor necrosis factor-α, releasing matrix metalloproteinase-9 and migrating in vitro". In: *Journal of Neuroinflammation* 8.1, p. 106.

Tashima, R., S. Mikuriya, D. Tomiyama, M. Shiratori-Hayashi, T. Yamashita, Y. Kohro, H. Tozaki-Saitoh, K. Inoue, and M. Tsuda (2016). "Bone marrow-derived cells in the population of spinal microglia after peripheral nerve injury." In: *Scientific Reports* 6, p. 23701.

Taves, S., T. Berta, D.-l. Liu, S. Gan, G. Chen, Y. Ho, T. V. D. Ven, S. Laufer, and R.-r. Ji (2015). "Spinal inhibition of p38 MAP kinase reduces inflammatory and neuropathic pain in male but not female mice: Sex-dependent microglial signaling in the spinal cord". In: *Brain, Behavior, and Immunity*.

Tchetverikov, I., H. K. Ronday, B. Van El, G. H. Kiers, N. Verzijl, J. M. TeKoppele, T. W. Huizinga, J. DeGroot, and R. Hanemaaijer (2004). "MMP profile in paired serum and synovial fluid samples of patients with rheumatoid arthritis". In: *Annals of the Rheumatic Diseases* 63.7, pp. 881–883.

Thakur, M., A. H. Dickenson, and R. Baron (2014). "Osteoarthritis pain: Nociceptive or neuropathic?" In: *Nature Reviews Rheumatology* 10.6, pp. 374–380.

Thakur, M., W. Rahman, C. Hobbs, A. H. Dickenson, and D. L. H. Bennett (2012). "Characterisation of a peripheral neuropathic component of the rat monoiodoacetate model of osteoarthritis". In: *PLoS ONE* 7.3. Ed. by M. L. Baccei, e33730.

The Jackson Laboratory (2020). *004600 - FVB-Tg(GFAP-cre)25Mes/J*.

Thichanpiang, P., S. J. Harper, K. Wongprasert, and D. O. Bates (2014). "TNF-α-induced ICAM-1 expression and monocyte adhesion in human RPE cells is mediated in part through autocrine VEGF stimulation." In: *Molecular vision* 20.February, pp. 781–9.

Thompson, H. L. and K. Matsushima (1992). "Human polymorphonuclear leucocytes stimulated by tumour necrosis factor-alpha show increased adherence to extracellular matrix proteins which is mediated via the CD11b/18 complex". In: *Clinical and Experimental Immunology* 90.2, pp. 280–285.

Timpl, R., H. Rohde, P. Robey, S. Rennard, F. Foidart, and G. Martin (1979). "Laminin - a glycoprotein from basement membranes". In: *J Biol Chem* 254.19, pp. 9933–9937.

Todd, A. J. (2010). "Neuronal circuitry for pain processing in the dorsal horn". In: *Nature Reviews Neuroscience* 11.12, pp. 823–836.

– (2017). *Identifying functional populations among the interneurons in laminae I-III of the spinal dorsal horn*.

Torsney, C. (2019). "Inflammatory pain neural plasticity". In: *Current Opinion in Physiology* 11, pp. 51–57.

Totoson, P., K. Maguin-Gaté, M. Nappey, D. Wendling, and C. Demougeot (2016). "Endothelial dysfunction in rheumatoid arthritis: Mechanistic insights and correlation with circulating markers of systemic inflammation". In: *PLoS ONE* 11.1, e0146744.

Town, T., V. Nikolic, and J. Tan (2005). "The microglial "activation" continuum: from innate to adaptive responses." In: *Journal of Neuroinflammation* 2, p. 24.

Treede, R.-D. et al. (2019). "Chronic pain as a symptom or a disease: the IASP Classification of Chronic Pain for the International Classification of Diseases (ICD-11)". In: *Pain* 160.1, pp. 19–27.

Tsai, H. H., H. Li, L. C. Fuentealba, A. V. Molofsky, R. Taveira-Marques, H. Zhuang, A. Tenney, A. T. Murnen, S. P. Fancy, F. Merkle, N. Kessaris, A. Alvarez-Buylla, W. D. Richardson, and D. H. Rowitch (2012). "Regional astrocyte allocation regulates CNS synaptogenesis and repair". In: *Science* 337.6092, pp. 358–362.

Tsuchiya, S., M. Yamabe, Y. Yamaguchi, Y. Kobayashi, T. Konno, and K. Tada (1980). "Establishment and characterization of a human acute monocytic leukemia cell line (THP□1)". In: *International Journal of Cancer* 26.2, pp. 171–176.

Tsuda, M. (2019). "Microglia-Mediated Regulation of Neuropathic Pain: Molecular and Cellular Mechanisms". In: *Biological and Pharmaceutical Bulletin* 42.12, pp. 1959–1968.

Tsuda, M., S. Beggs, M. W. Salter, and K. Inoue (2013). "Microglia and intractable chronic pain". In: *Glia* 61.1, pp. 55–61.

Tsuda, M., Y. Kohro, T. Yano, T. Tsujikawa, J. Kitano, H. Tozaki-Saitoh, S. Koyanagi, S. Ohdo, R. R. Ji, M. W. Salter, and K. Inoue (2011). "JAK-STAT3 pathway regulates spinal astrocyte proliferation and neuropathic pain maintenance in rats". In: *Brain* 134.4, pp. 1127–1139.

Ubogu, E. E. (2020). "Biology of the human blood-nerve barrier in health and disease". In: *Experimental Neurology* 328, p. 113272.

Üçeyler, N., M. Schäfers, and C. Sommer (2009). "Mode of action of cytokines on nociceptive neurons". In: *Experimental Brain Research* 196.1, pp. 67–78.

Urch, C. and A. Dickenson (2003). "In vivo single unit extracellular recordings from spinal cord neurones of rats". In: *Brain Research Protocols* 12.1, pp. 26–34.

Vahle-Hinz, C. and O. Detsch (2002). "What can in vivo electrophysiology in animal models tell us about mechanisms of anaesthesia?" In: *British Journal of Anaesthesia* 89.1, pp. 123–142.

Van Doorn, E., H. Liu, A. Huckriede, and E. Hak (2016). *Safety and tolerability evaluation of the use of Montanide ISATM51 as vaccine adjuvant: A systematic review*.

Varatharaj, A. and I. Galea (2016). "The blood-brain barrier in systemic inflammation". In: *Brain, Behavior, and Immunity* 60, pp. 1–12.

Ved, N., M. E. Da Vitoria Lobo, S. M. Bestall, C. L. Vidueira, N. Beazley-Long, K. Ballmer-Hofer, M. Hirashima, D. O. Bates, L. F. Donaldson, and R. P. Hulse (2018). "Diabetes-induced microvascular complications at the level of the spinal cord: a contributing factor in diabetic neuropathic pain". In: *Journal of Physiology* 596.16, pp. 3675–3693.

Vollenhoven, R. F. van (2009). "Sex differences in rheumatoid arthritis: More than meets the eye..." In: *BMC Medicine* 7.1, pp. 1–4.

Wall, P. D. and M. Devor (1983). "Sensory afferent impulses originate from dorsal root ganglia as well as from the periphery in normal and nerve injured rats". In: *Pain* 17.4, pp. 321–339.

Walsh, D. A. and D. F. McWilliams (2014). "Mechanisms, impact and management of pain in rheumatoid arthritis". In: *Nature Reviews Rheumatology* 10.10, pp. 581–592.

Wang, Y., Y. Cao, A. K. Mangalam, Y. Guo, R. G. LaFrance-Corey, J. D. Gamez, P. A. Atanga, B. D. Clarkson, Y. Zhang, E. Wang, R. S. Angom, K. Dutta, B. Ji, I. Pirko, C. F. Lucchinetti, C. L. Howe, and D. Mukhopadhyay (2016). "Neuropilin-1 modulates interferon-γ-stimulated signaling in brain microvascular endothelial cells". In: *Journal of Cell Science* 129.20, pp. 3911–3921.

Watkins, L. R., M. R. Hutchinson, A. Ledeboer, J. Wieseler-Frank, E. D. Milligan, and S. F. Maier (2007). "Glia as the "bad guys": Implications for improving clinical pain control and the clinical utility of opioids". In: *Brain, Behavior, and Immunity* 21.2, pp. 131–146.

Watson, C., G. Paxinos, G. Kayalioglu, and C. Heise (2009). "Atlas of the Rat Spinal Cord". In: *The Spinal Cord*. Elsevier Ltd. Chap. 15, pp. 238–306.

Watson, P. M. D., J. C. Paterson, G. Thom, U. Ginman, S. Lundquist, and C. I. Webster (2013). "Modelling the endothelial blood-CNS barriers: A method for the production of robust in vitro models of the rat blood-brain barrier and blood-spinal cord barrier". In: *BMC Neuroscience* 14, p. 59.

Weddell, J. C., S. Chen, and P. I. Imoukhuede (2018). "VEGFR1 promotes cell migration and proliferation through PLCγ and PI3K pathways". In: *npj Systems Biology and Applications* 4.1, pp. 1–11.

Weerasuriya, A. and A. P. Mizisin (2011). "The Blood-Nerve Barrier: Structure and Functional Significance". In: *The Blood-Brain and Other Neural Barriers: Reviews and Protocols*. Ed. by S. Nag. Vol. 686. Chap. 6, pp. 149–173.

Wei, S. T., Y. H. Sun, S. H. Zong, and Y. B. Xiang (2015). "Serum levels of IL-6 and TNF-α may correlate with activity and severity of rheumatoid arthritis". In: *Medical Science Monitor* 21, pp. 4030–4038.

Weksler, B. B., E. A. Subileau, N. Perrière, P. Charneau, K. Holloway, M. Leveque, H. Tricoire□Leignel, A. Nicotra, S. Bourdoulous, P. Turowski, D. K. Male, F. Roux, J. Greenwood, I. A. Romero, and P. O. Couraud (2005). "Blood-brain barrier-specific properties of a human adult brain endothelial cell line". In: *The FASEB Journal* 19.13, pp. 1872–1874.

Wemmie, J. A., R. J. Taugher, and C. J. Kreple (2013). "Acid-sensing ion channels in pain and disease". In: *Nature Reviews Neuroscience* 14.7, pp. 461–471.

Wieseler-Frank, J., S. F. Maier, and L. R. Watkins (2005). "Central proinflammatory cytokines and pain enhancement." In: *Neuro-Signals* 14.4, pp. 166–74.

Wilhelm, I., C. Fazakas, and I. A. Krizbai (2011). "In Vitro Models of the Blood-Brain Barrier". In: *Acta Neurobiol Exp* 71.1, pp. 113–128.

Willis, C. L., T. a. Brooks, and T. P. Davis (2008). "Chronic inflammatory pain and the neurovascular unit: a central role for glia in maintaining BBB integrity?" In: *Current pharmaceutical design* 14.16, pp. 1625–43.

Wimmer, I., S. Tietz, H. Nishihara, U. Deutsch, F. Sallusto, F. Gosselet, R. Lyck, W. A. Muller, H. Lassmann, and B. Engelhardt (2019). "PECAM-1 stabilizes blood-brain barrier integrity and favors paracellular T-cell diapedesis across the blood-brain barrier during neuroinflammation". In: *Frontiers in Immunology* 10.APR, p. 711.

Winkler, E. A., J. D. Sengillo, J. S. Sullivan, J. S. Henkel, S. H. Appel, and B. V. Zlokovic (2013). "Blood-spinal cord barrier breakdown and pericyte reductions in amyotrophic lateral sclerosis". In: *Acta Neuropathologica* 125.1, pp. 111–120.

Winkler, E. A., R. D. Bell, and B. V. Zlokovic (2011). "Central nervous system pericytes in health and disease." In: *Nature neuroscience* 14.11, pp. 1398–1405.

Wittchen, E. S. (2009). "Endothelial signaling in paracellular and transcellular leukocyte transmigration." In: *Frontiers in Bioscience* 14, pp. 2522–45.

Wong, D. and K. Dorovini-Zis (1995). "Expression of vascular cell adhesion molecule-1 (VCAM-1) by human brain microvessel endothelial cells in primary culture". In: *Microvascular Research* 49.3, pp. 325–339.

Wong, D., R. Prameya, and K. Dorovini-Zis (1999). "In vitro adhesion and migration of T lymphocytes across monolayers of human brain microvessel endothelial cells: Regulation by ICAM-1, VCAM-1, E- selectin and PECAM-1". In: *Journal of Neuropathology and Experimental Neurology* 58.2, pp. 138–152.

Wood, J. M. et al. (2000). "PTK787/ZK 222584, a novel and potent inhibitor of vascular endothelial growth factor receptor tyrosine kinases, impairs vascular endothelial growth factor-induced responses and tumor growth after oral administration". In: *Cancer Research* 60.8, pp. 2178–2189.

Woodell-May, J. E. and S. D. Sommerfeld (2020). "Role of Inflammation and the Immune System in the Progression of Osteoarthritis". In: *Journal of Orthopaedic Research* 38.2, pp. 253–257.

Woolf, C. J. (1983). "Evidence for a central component of post-injury pain hypersensitivity". In: *Nature* 306, pp. 686–688.

– (2011). "Central sensitization: Implications for the diagnosis and treatment of pain". In: *Pain* 152.SUPPL.3, S2.

Wooten, M., H. J. Weng, T. V. Hartke, J. Borzan, A. H. Klein, B. Turnquist, X. Dong, R. A. Meyer, and M. Ringkamp (2014). "Three functionally distinct classes of C-fibre nociceptors in primates". In: *Nature Communications* 5.4122.

Wu, H., R. Deng, X. Chen, W. C. Wong, H. Chen, L. Gao, Y. Nie, W. Wu, and J. Shen (2016). "Caveolin-1 Is Critical for Lymphocyte Trafficking into Central Nervous System during Experimental Autoimmune Encephalomyelitis". In: *Journal of Neuroscience* 36.19, pp. 5193–5199.

Wuestefeld, R., J. Chen, K. Meller, B. Brand-Saberi, and C. Theiss (2012). "Impact of vegf on astrocytes: Analysis of gap junctional intercellular communication, proliferation, and motility". In: *GLIA* 60.6, pp. 936–947.

Xanthos, D. N., I. Püngel, G. Wunderbaldinger, and J. Sandkühler (2012). "Effects of peripheral inflammation on the blood-spinal cord barrier." In: *Molecular pain* 8, p. 44.

Xing, L. Y., T. Yang, S. S. Cui, and G. Chen (2019). "Connexin hemichannels in astrocytes: Role in CNS disorders". In: *Frontiers in Molecular Neuroscience* 12, p. 23.

Xu, F., Y. Li, S. Li, Y. Ma, N. Zhao, Y. Liu, N. Qian, H. Zhao, and Y. Li (2014). "Complete Freund's adjuvant-induced acute inflammatory pain could be attenuated by triptolide via inhibiting spinal glia activation in rats". In: *Journal of Surgical Research* 188.1, pp. 174–182.

Yamadera, M., H. Fujimura, K. Inoue, K. Toyooka, C. Mori, H. Hirano, and S. Sakoda (2015). "Microvascular disturbance with decreased pericyte coverage is prominent in the ventral horn of patients with amyotrophic lateral sclerosis". In: *Amyotrophic Lateral Sclerosis and Frontotemporal Degeneration* 16.5-6, pp. 393–401.

Yan, X. T., J. M. Lu, Y. Wang, X. L. Cheng, X. H. He, W. Z. Zheng, H. Chen, and Y. L. Wang (2018a). "XIST accelerates neuropathic pain progression through regulation of miR-150 and ZEB1 in CCI rat models". In: *Journal of Cellular Physiology* 233.8, pp. 6098–6106.

Yan, X. T., Y. Zhao, X. L. Cheng, X. H. He, Y. Wang, W. Z. Zheng, H. Chen, and Y. L. Wang (2018b). "Inhibition of miR-200b/miR-429 contributes to neuropathic pain development through targeting zinc finger E box binding protein-1". In: *Journal of Cellular Physiology* 233.6, pp. 4815–4824.

Yang, L., R. M. Froio, T. E. Sciuto, A. M. Dvorak, R. Alon, and F. W. Luscinskas (2005). "ICAM-1 regulates neutrophils adhesion and transcellular migration of TNF-alpha-activated vascular endothelium under flow". In: *Blood* 106.2, pp. 584–592.

Yang, X., Y. Chang, and W. Wei (2016). "Endothelial Dysfunction and Inflammation: Immunity in Rheumatoid Arthritis". In: *Mediators of Inflammation* 2016, pp. 1–9.

Yao, Y. and S. E. Tsirka (2014). "Monocyte chemoattractant protein-1 and the blood-brain barrier". In: *Cellular and Molecular Life Sciences* 71.4, pp. 683–697.

Yardan, T., A. K. Erenler, A. Baydin, K. Aydin, and C. Cokluk (2011). "Usefulness of S100B protein in neurological disorders". In: *Journal of the Pakistan Medical Association* 61.3, pp. 276–281.

Yu, X., H. Liu, K. A. Hamel, M. G. Morvan, S. Yu, J. Leff, Z. Guan, J. M. Braz, and A. I. Basbaum (2020). "Dorsal root ganglion macrophages contribute to both the initiation and persistence of neuropathic pain". In: *Nature Communications* 11.1.

Zamanian, J. L., L. Xu, L. C. Foo, N. Nouri, L. Zhou, R. G. Giffard, and B. A. Barres (2012). "Genomic analysis of reactive astrogliosis". In: *Journal of Neuroscience* 32.18, pp. 6391–6410.

Zeilhofer, H. U., H. Wildner, and G. E. Yévenes (2012). "Fast synaptic inhibition in spinal sensory processing and pain control". In: *Physiological Reviews* 92.1, pp. 193–235.

Zenaro, E., G. Piacentino, and G. Constantin (2017). "The blood-brain barrier in Alzheimer's disease". In: *Neurobiology of Disease* 107, pp. 41–56.

Zhang, E. Y., G. T. Knipp, S. Ekins, and P. W. Swaan (2002). "Structural biology and function of solute transporters: implications for identifying and designing substrates." In: *Drug Metabolism Reviews* 34.4, pp. 709–50.

Zhang, H., H. Nei, and P. M. Dougherty (2010). "A p38 mitogen-activated protein kinase-dependentmechanism of disinhibition in spinal synaptic transmission induced by tumor necrosis factor-α". In: *Journal of Neuroscience* 30.38, pp. 12844–12855.

Zhang, J., X. Q. Shi, S. Echeverry, J. S. Mogil, Y. De Koninck, and S. Rivest (2007). "Expression of CCR2 in Both Resident and Bone Marrow-Derived Microglia Plays a Critical Role in Neuropathic Pain". In: *Journal of Neuroscience* 27.45, pp. 12396–12406.

Zhang, R. X. and K. Ren (2011). "Animal models of inflammatory pain". In: *Animal Models of Pain, Neuromethods*. Vol. 49. Humana Press, Totowa, NJ, pp. 23–40.

Zhang, X., Y. Zhang, W. Cai, Y. Liu, H. Liu, Z. Zhang, and Z. Su (2020). "MicroRNA-128-3p Alleviates Neuropathic Pain Through Targeting ZEB1". In: *Neuroscience Letters* 729.134946.

Zhang, Y., X. Ding, C. Miao, and J. Chen (2019). "Propofol attenuated TNF-α-modulated occludin expression by inhibiting Hif-1α/ VEGF/ VEGFR-2/ ERK signaling pathway in hCMEC/D3 cells". In: *BMC Anesthesiology* 19.1, p. 127.

Zhao, X.-H., T. Zhang, and Y.-Q. Li (2015a). "The up-regulation of spinal Toll-like receptor 4 in rats with inflammatory pain induced by complete Freund's adjuvant." In: *Brain Research Bulletin* 111, pp. 97–103.

Zhao, Z., A. R. Nelson, C. Betsholtz, and B. V. Zlokovic (2015b). "Establishment and Dysfunction of the Blood-Brain Barrier". In: *Cell* 163.5, pp. 1064–1078.

Zhou, L. J., J. Peng, Y. N. Xu, W. J. Zeng, J. Zhang, X. Wei, C. L. Mai, Z. J. Lin, Y. Liu, M. Murugan, U. B. Eyo, A. D. Umpierre, W. J. Xin, T. Chen, M. Li, H. Wang, J. R. Richardson, Z. Tan, X. G. Liu, and L. J. Wu (2019). "Microglia Are Indispensable for Synaptic Plasticity in the Spinal Dorsal Horn and Chronic Pain". In: *Cell Reports* 27.13, 3844–3859.e6.

Zlokovic, B. V. (2011). "Neurovascular pathways to neurodegeneration in Alzheimer's disease and other disorders". In: *Nature Reviews Neuroscience* 12.12, pp. 723–738.

A | Appendices

A.1 PIP Reflective Statement

Note to Examiners

This statement is included as an appendix to the thesis in order that the thesis accurately captures the PhD training experienced by the candidate as a BBSRC Doctoral Training Partnership student.

The Professional Internship Placement (PIP) for PhD Students is a compulsory 3-month placement which must be undertaken by DTP students. It is usually centred on a specific project and must not be related to the PhD project. This reflective statement is designed to capture the skills development which has taken place during the student's placement and the impact on their career plans it has had.

Reflective Statement

I spent 3 months with the widening participation charity, IntoUniversity, working as an Education Worker. Pupils from disadvantaged and poorer backgrounds do less well at school and are less likely to go to university than their more advantaged peers (Jerrim 2013; HEFCE 2010). IntoUniversity was set up to help young people from these underrepresented backgrounds to achieve their potential and help them get into university. With their intervention, children who are eligible for Free School Meals have a university-progression rate of 75% compared to 22% nationally (IntoUniversity 2017). IntoUniversity deliver at least two in-school sessions with the same cohort of students in primary school in years 5 and 6, and in secondary school from year 7 to year 13. These sessions are designed to expose the students to university-life and the different career paths available, and to help them understand how to achieve their designed career. As well as these university-based workshops, IntoUniversity run skills-based workshops, such as leadership, problem-solving and team-work, and also run career-based workshops that allow students to experience a career that they may not have previously considered. One such career workshop was a law simulation at a local law firm where students took on different roles within a law team to work together and present in a simulated court case. My role within IntoUniversity was to help deliver these sessions, which meant that I was able to work with a wide range of pupils from age 7 to 18 and enhance my presentation and communication skills. I was also required to lease with schools and teachers and help to organise and create resources, and so my skills in both delivering and facilitating widening participation have been developed. IntoUniversity also run after-school sessions, Academic Support, for primary and secondary students to help with their homework and give them the oppor-

tunity to participate in additional curriculum and projects to help develop academic and soft-skills. Within secondary Academic Support, IntoUniversity have recently developed the Future Readiness Award, which allows pupils to complete projects that are designed to develop soft-skills, such as metacognition, resilience and autonomy. These skills are thought to contribute to learning, academic achievement and later-life success (Cullinane and Montacute 2017), and educators are recognising the importance of teaching these skills to pupils. During my placement I was tasked with assessing the practices used in secondary Academic Support and in the Future Readiness Award to determine whether best evidence-based practices shown to raise attainment were being used. Through performing a literature review and observations of Academic Support and the Future Readiness Award, I identified key areas where IntoUniversity used these practices effectively and opportunities for improvement. As a result of my report, IntoUniversity is incorporating practices that were identified as having the potential to encourage soft-skills and raise attainment such as self-reflection, formative feedback, and additional planning resources, meaning that my research has had a direct impact on the way the Future Readiness Award is run.

Through completing my placement with IntoUniversity I was able to experience both the delivery and organisation of widening participation, and get an understanding of what goes on behind-the-scenes in a national education charity. Before starting this placement, the delivery of widening participation workshops was a career that I was interested in pursuing, but after being involved with the assessment of their practices, I have found that I am more interested in a research-based role that looks at the impact of a charity's work.

A.2 COVID19 Impact Statement

COVID19 Impact Statement 2020
For use only by UKRI funded PGRs with funding end date between 1st March 2020 and 31st March 2021

The University of Nottingham aims to support all our PGRs to complete their degrees within their period of study, by meeting our Doctoral Outcomes. We recognise, and aim to take into account, personal circumstances that may affect a PGR's ability to achieve this.

This Impact Statement should be used to provide details and evidence of impact for:

- applications for an additional funded period of registered study;
- applications for a funded extension to Thesis Pending;
- the thesis examination.

It will also be used to determine both the case and length of a COVID extension to funding **up to a maximum of six months** (twelve for part time PGRs). **Please note that it is expected that most approved extensions will reflect the duration of enforced change in activity during lockdown, and that extensions of longer duration will be the exception rather than the rule.**

Please keep a completed copy of this form as you may want to refer to it as evidence of impact in your thesis examination. You will also need to use it copy/paste your responses for submission in the online version of the form which will be the format used to make your extension request. The online form will be made available during the week of 11 May.

Please carefully consider your case for any extension with reference to the University's online Policy on Circumstances Affecting Students' Ability to Study and Complete Assessments (under Exceptional Guidance to Extenuating Circumstances Panels) and section 16 of the PhD Regulations (see Appendix 2, section 1), relating to existing regulations on circumstances that may or may not be usual grounds for an extension, and the Exceptional Regulations for UKRI funded PGR extensions (which can be found on the same site as this form).

In accordance with UKRI guidance, **we strongly encourage you to discuss the completion of this form with your supervisors.** If you prefer, you can alternatively discuss the form with an appropriate member of PGR support staff such as your DTP/CDT Director or Manager, DTP/CDT Welfare Officer, School Postgraduate Student Advisor, School PGR Director or other member of the Welfare team, or the Researcher Academy Faculty Lead (formerly Associate Dean for the Graduate School).

To ensure that you cover the full impact of the COVID-19 pandemic on you and your research **since March 15th 2020**, please complete all relevant sections of the form. You can be very brief but please include all relevant information even in note or bullet form.

When applying for an extension to either your period of registered study (i.e. when active data collection is to be done) or to Thesis Pending, or both you should show, briefly how/whether your work to date already meets some of the University and QAA Doctoral Outcomes, and clarify which doctoral outcomes are not currently met and how your plan will enable you to meet these (Appendix 1).

Under the exceptional conditions of the COVID-19 pandemic, in addition to the usual circumstances that may be grounds for an extension, you can and should also consider, and evidence if asked to do so, the additional circumstances listed in Section 1. These include but are not limited to:

- your ability to work effectively now that you are not in your usual working environment;
- any change in access to research settings or facilities, such as archives, field-sites, laboratories, software, or databases;
- any changes in your personal circumstances or environment resulting from remote working, or national restrictions , including those related to:
    - caring responsibilities,
    - disability and/or being at higher risk from coronavirus

- impacts on your supervisory team that have affected your research progress
- your mental health, and whether you have access to mental health support if needed,

- any financial impacts, either personal or on the research in progress or planned.
- any other considerations that should be taken into account, whether these do or do not relate to any protected characteristics.

This form should capture the impact of the pandemic on you and your research progress, not solely any impact of the University closure itself.

For further information including addressing future impacts; privacy and confidentiality of information submitted, and additional notes and guidance please see Appendix 2.

The information collected in this form will be used for the purposes of assessing your case for a funded extension to your doctoral studies, to provide information to your funder; to inform the University of the range of impacts that our PGRs have experienced, and to inform policy decisions on how to support our PGRs in future. The document will also aid discussion and decision making, to ensure consistency in evaluation of the impacts for different people.

All information used for other than the stated purposes will be anonymised, and all personal information through which anyone could be identified removed. The information on this form will not be shared with anyone, including supervisory teams, for other than the stated purposes, without your permission.

Background Information – your details			
Family Name:	Durrant	First Name(s)	Alexandra Margaret
ID:	14259488	School:	Life Sciences
If this form is competed for an extension request: I am applying for: ☒ an additional period of registered study; ☐ extension to Thesis Pending; ☐ both			
Please identify your relevant funder(s)	~~AHRC~~/ BBSRC/ ~~ESRC/EPSRC/MRC/NERC/ STFC~~	Dates of impact: (the date from which the impact has had an effect).	1st May 2020
Start date	1st October 2015	Funding end date	30th September 2020
Length of extension requested: (up to a maximum of twenty four (26) weeks)	10weeks	Programme length (3, 3.5, 4 years) and full time or part time	4yrs (+1yr maternity) Full time

The primary areas of impact:

Please tick all that are relevant for the ways in which you have been affected by the COVID pandemic and the resulting effect(s) on you and/or your research progression. You can give more details on these impacts, if you wish, on the next page.

Note: We will ask you to explain whether and how you have been able to manage or reduce any of these impacts in Section 2, on p.5.

The ways in which you have been affected (choose all that apply)

☒ additional/new caring responsibilities
☐ specific impact resulting from remote working as a result of a disability*
☐ being at higher risk of coronavirus;
☐ personal financial impact;
☐ new illness, accident or hospitalisation, including any mental health problems
☐ lack of access to mental health support (if needed);
☐ death or illness of a partner/close relative*
☐ illness of a relative for whom you are a carer
☐ impacts related to any protected characteristics*
☐ an impact on your supervisory team that has affected your supervision or progress
☐ military or other service (e.g. NHS) that has not already been accommodated
☐ parental leave that has not already been accommodated
☐ redeployment to work in another area (e.g. COVID) where this has not already been accommodated.
☐ other events not on this list that are specifically related to the COVID pandemic (please describe below)

The ways in which your research activity has been affected
(for each that applies, please also indicate whether you have tried to mitigate the effect in this area).

	Was any mitigation possible?
☐ Disruption of planned activities	Yes/No
☐ Access to facilities/archives/lab/equipment/field sites etc	Yes/No
☐ Postponement of critical activities where alternatives are not available	Yes/No
☐ Access to other research resources including financial impact	Yes/No
☐ Ability to achieve a planned outcome/ milestone/deliverable	Yes/No
☐ Access a research partner, including research-related placements	Yes/No
☒ Inability to devote your usual time to research activity	~~Yes~~/No
☐ *Lack of usual supervisory support for thesis progression/writing	Yes/No
☐ *Lack of usual supervisory support to help manage risk and mitigate plans	Yes/No
☐ Other (please describe below)	Yes/No

*We are collecting this information in order to fully understand how you have been affected. Any information that you give here will only be used as information to inform us and will not be shared with anyone other than the teams considering the cases for extension and collating information for submission to UKRI.

1. DESCRIBING THE IMPACT

(Please complete this section to provide us with more detailed information)

For example you could write a short clear description of the nature of the impacts or problems that you face/have faced, make making this description as brief, and specific as possible. You could also give more detail on the nature of the impacts on your research progress.

We understand that personal and research impacts will be related, so if it helps you could structure the content in line with the impacts you identified in the tick boxes above.

Error! Reference source not found. additional guidance

The impact **on you**:

I returned from a year's maternity leave on 1st May and due to the COVID pandemic our nursery has been shut for non-keyworkers. As neither my husband nor I are keyworkers, we have not had access to planned childcare meaning we must share childcare whilst both working from home. I was due to return to work full time, and due to childcare, I am now unable to work for more than 3-4 hours a day, rather than my planned 8 hours. Additionally, as I could not have planned for the current situation when I left for maternity leave, I did not take all my physical lab/study records home with me and when I returned from maternity leave I did not have access to these files as I did not have access to the building. Organising access to the building and locating files took a couple of weeks to organise, delaying some of my work.

The impact **on your research**:

An initial delay in collecting lab/study files from work delayed analysing and writing up research by a couple of weeks.
I am unable to work effectively for as long as I would under normal circumstances due to sharing childcare responsibilities. This, along with the disruptive work environment as a result of my daughter being at home, is causing data analysis and writing to take longer than initially planned and I am concerned I will not complete my thesis before my September deadline.
Additionally, I had planned to do several more laboratory experiments to go into my thesis, but as I do not have access to the lab these cannot go ahead.

2. ACTIONS TAKEN TO MINIMISE THE IMPACT

a) How have you tried to mitigate the risk to your project?

Please **briefly** explain how you are trying to minimise the impact of the situation on your research activities and progress. **If you have not tried to alter your plans ,it's particularly important to explain here why you have taken this decision.**

For example,

- have you discussed how to do this with your supervisors?
- have you considered different ways to get the research done, such as changing your research plans to alter the order in which you do different elements?
- have you altered your research design, for example to conduct research online, or using other digital resources?
  what constraints or barriers did you have to try to remove, modify or overcome?
- **If you have not tried to alter your plans at all, why not?**

Try to show how/whether your work to date already meets some of the University and QAA Doctoral Outcomes, clarify which doctoral outcomes are not currently met and how your plan will enable you to meet these.
up to 200 words

Section 2 additional guidance

I have now collected everything I need from the office and lab, and now all my work can be done from home. I am continuing to analyse experiments and write my thesis, but at a slower pace than planned.
In terms of the cancelled experiments, they are not necessary for completion of my thesis, so I have now altered my writing to meet the needs of the doctoral outcomes.
I have organised with my partner to share childcare responsibilities during the day, and I am working every day and trying to work some evenings to maximise working time.
I have provisionally arranged for my daughter to start nursery at the beginning of July, subject to Government assessments and whether this is deemed safe by both the Government, the nursery, and myself and partner. However, this is also contingent upon the nursery actually opening, and being able to organise appropriate settling-in sessions.

b) List the aspects of your research plan that you have managed to achieve or progress during the period of impact.

I have been able to achieve/progress with the following aspects since returning from maternity leave on 1st May

- Collect necessary files and records from university
- Development of analysis macros
- Analysis of AD6 GFAP/RECA1/ZEB1 tissue
- Progression of Methods, Optimising Methods, and In Vivo chapters
- Begin ePhys chapter

3. NEXT STEPS

Please **list** what you have planned to do, in order to continue to lessen the impact on your research **once you are able to** resume the specific activities listed in Section 1

For example, what plans do you have to make sure that elements of your research that you have been unable to undertake due to the University closure restart quickly, or to efficiently complete the work you started during the closure?

up to 200 words

Section 3 additional guidance

I have provisionally organised my daughter to start nursery at the beginning of July, subject to Government assessments and whether this is deemed safe. I have planned the following milestones for the remainder of my time:

May
- Analyse and write-up AD6 GFAP/RECA1/ZEB1 tissue
- Re-analyse AD4 GFAP/laminin tissue with overlap macro
- Continue writing Methods and Optimising Methods chapters

June
- Analyse AD6 RECA1/ICAM1 tissue
- Send Methods and Optimising Methods chapters to supervisor
- Write ePhys Chapter
- Write In Vivo chapter
- Review recent literature

July
- Continued analysis of AD6 RECA1/ICAM1 tissue
- Analyse AD5 RECA1/CD68 tissue
- Method corrections
- Send ePhys chapter to supervisor
- Continue to write In Vivo chapter/send to supervisor
- Review recent literature

August
- Continue In Vivo chapter/send to supervisor
- Continue In Vitro chapter/send to supervisor
- ePhys corrections
- Review recent literature

September
- Begin Introduction
- Continue Discussion/send to supervisor
- In vivo corrections
- In Vitro corrections
- Review recent literature

October
- Write and send Introduction to supervisor
- Send Discussion to supervisor/Discussion corrections
- Previous chapter corrections

November
- Introduction/Discussion corrections
- Figure proofreading
- Check LaTeX compiling and Proofread thesis
- Potentially print thesis

4. EVIDENCE

List any evidence that you have to demonstrate the impact you have detailed in section 1.

Please do not provide the evidence with this form, we will request it from you if we need to see it.

Please also provide here:

- a brief bullet list of the doctoral work completed prior to COVID-19 impact
- a revised research plan **that shows how the requested length of extension is justified by the work that remains to be done to enable you to meet the Doctoral Outcomes**;
- only if available, a previous work plan for comparison

up to 200 words

Section 4 additional guidance

Thesis plan – highlighting cancelled further experiments due to COVID-19
Letter from husband

5. CONFIDENTIAL INFORMATION

Please use this section to provide any confidential information that you would like to be considered. Information given here will only be shared with the team assessing your case and returning the information to UKRI for their consideration of your application.

☒ **I confirm that I have completed this form after/in discussion with**:
(indicate all those that apply, discussion with only one person is required)

☒ Primary supervisor/other supervisor ☐ SPSA ☐ School PGR Director ☐ DTP/CDT Director
☐ DTP/CDT Manager ☐ DTP/CDT Welfare Officer ☐ other member of the Welfare Team
☐ Researcher Academy Faculty Lead (RAFL, aka Associate Dean of the Graduate School)

RAFLs are: Prof A Grabowska (MHS), Dr L Bradnock (Arts), Prof R Graham (Science) and Dr N Porter (Eng).

☒ **I confirm that the information provided in this form is true and request an extension for the reasons and purposes outlined above.**

A.3 Macros

A.3.1 CD31-associated GFAP

A.3.1.1 Overlay Method: ROI

Relevant to Section 3.3.3.

```
macro"Split, Thresh[1]"
{ imageTitle=getTitle();
run("Split Channels");
selectWindow(imageTitle+" (red)");
run("Threshold..."); setThreshold(48, 255);
setOption("BlackBackground", false); }
macro"Thresh Mask[2]"
{ run("Convert to Mask"); setTool("freehand");
}
//trace DH
macro"Trace and analyse CD31[3]"
{ run("Analyze Particles...", "size=25-3000 pixel show=[Overlay Masks] display clear include add in_situ slice"); run("Clear Results");
run("Images to Stack", "name=Stack title=[] use"); }
macro"Select and measure GFAP[4]"
{ roiManager("Measure"); }
```

A.3.1.2 Overlay Method (Selection) and Overlap Extraction

Relevant to Section 3.3.2.

```
macro"split channels + thresh GFAP[1]"
{
run("Set Scale...", "distance=151 known=100 pixel=1 unit=um global");
title1 =getTitle();
run("Split Channels");
selectWindow(title1+" (blue)");
```

```
rename("DAPI"); selectWindow(title1+" (red)"); rename("GFAP"); selectWindow(title1+" (green)"); rename("CD31");

selectWindow("GFAP"); run("Duplicate...", " "); selectWindow("GFAP"); run("Threshold...");

setThreshold(47, 255);

setOption("BlackBackground", false);

run("Convert to Mask"); run("Analyze Particles...", "size=5-Infinity pixel show=Masks clear add in_situ"); setOption("BlackBackground", false); roiManager("Show None"); run("Convert to Mask");

selectWindow("CD31"); run("Threshold...");

setThreshold(39, 255);

setOption("BlackBackground", false);

run("Convert to Mask");

run("Images to Stack", "name=percy title=[] use"); setTool("freehand"); }

Select DH, measure GFAP

macro"measure[2]"

{ run("Measure"); }

Select CD31 mask

macro"analyse[3]"

{ run("Analyze Particles...", "size=25-infinity pixel show=Masks clear add in_situ"); roiManager("Show All without labels"); run("Create Selection"); }

Measure ICAM/GFAP

macro"measure[2]"

{ run("Measure"); }

macro"GFAP particle analysis and extraction[4]" { run("Stack to Images"); selectWindow("CD31"); run("Convert to Mask"); selectWindow("GFAP"); run("Convert to Mask"); run("Binary Feature Extractor", "objects=[GFAP] selector=[CD31] object_overlap=0 count");

selectWindow("GFAP-1"); run("Invert LUT"); selectWindow("Extracted_GFAP-1"); run("Invert LUT");

run("Images to Stack", "name=woofy title=[] use"); }

macro"create selection[5]"

{ run("Create Selection"); }
```

```
Select GFAP and measure
macro"measure[2] { run("Measure"); }
```

A.3.1.3 Overlay Method: ROI

A.3.2 Laminin-associated GFAP

Relevant to Section 4.3.3

A.3.2.1 Vessel Overlay

```
macro"split channels[1]"
{
title1 =getTitle();
run("Split Channels");
selectWindow(title1+" (blue)"); close();
selectWindow(title1+" (red)"); close();
selectWindow(title1+" (green)"); rename("GFAP");
}
open laminin
macro"vessel[2]"
{
run("8-bit");
run("Threshold...");
setThreshold(30, 255);
setOption("BlackBackground", false);
run("Convert to Mask");
setTool("freehand");
}
select deep laminae
macro"analyse[3]"
{
```

```
run(”Analyze Particles...”, ”size=25-25000 pixel show=[Overlay Masks] display clear in-
clude add in_situ”);

run(”Images to Stack”, ”name=hedgehog title=[] use”);

roiManager(”Show All”);

}

Select GFAP and measure

macro”measure[4]

{

run(”Clear Results”);

roiManager(”Measure”);

}
```

A.3.2.2 Vessel Overlap

```
macro”split channels[1]”

{

run(”Set Scale...”, ”distance=100 known=100 pixel=1 unit=um global”);

title1 =getTitle();

run(”Split Channels”);

selectWindow(title1+” (blue)”); close();

selectWindow(title1+” (red)”); close();

selectWindow(title1+” (green)”); rename(”GFAP”);

selectWindow(”GFAP”);

run(”Duplicate...”, ” ”);

selectWindow(”GFAP”);

run(”Threshold...”);

setThreshold(49, 255);

setOption(”BlackBackground”, false);

run(”Convert to Mask”);

run(”Analyze Particles...”, ”size=5-Infinity pixel show=Masks clear add in_situ”);
```

```
setOption("BlackBackground", false);
roiManager("Show None");
run("Convert to Mask");
}
open laminin
macro"vessel[2]"
{
run("8-bit");
rename("laminin");
run("Threshold...");
setThreshold(30, 255);
setOption("BlackBackground", false);
run("Convert to Mask");
//setTool("freehand");
}
select deep laminae
macro"analyse[3]"
{
run("Analyze Particles...", "size=25-25000 pixel show=Masks clear add in_situ");
run("Create Selection");
roiManager("Show All without labels");
}
macro"GFAP particle analysis and extraction[4]"
{
selectWindow("laminin");
run("Convert to Mask");
selectWindow("GFAP");
run("Convert to Mask");
```

```
run(”Binary Feature Extractor”, ”objects=[GFAP] selector=[laminin] object_overlap=0 count”);
run(”Invert LUT”);
run(”Images to Stack”, ”name=woofy title=[] use”);
}
macro”create selection[5]”
{
run(”Create Selection”);
}
Select GFAP and measure
macro”measure[6]
{
run(”Measure”);
}
```

A.3.3 Laminin Overlay on GFAP or ICAM-1

Relevant to Sections 4.3.4.2 and 4.3.4.3

```
Open ICAM
macro”ICAM thresh + duplicate[1]”
{
run(”Set Scale...”, ”distance=93 known=50 pixel=1 unit=um global”);
run(”8-bit”);
rename(”ICAM”);
}
macro”split channels + thresh GFAP[2]”
{
title1 =getTitle();
run(”Split Channels”);
selectWindow(title1+” (blue)”); rename(”DAPI”);
selectWindow(title1+” (red)”); rename(”GFAP”);
```

```
selectWindow(title1+" (green)"); close();
}
open laminin
macro"laminin thresh[3]"
{ run("8-bit");
rename("laminin");
selectWindow("laminin");
run("Duplicate...", " ");
selectWindow("laminin-1");
run("Threshold...");
setThreshold(30, 255);
setOption("BlackBackground", false);
run("Convert to Mask");
run("Images to Stack", "name=barky title=[] use");
}
Select DH, measure ICAM
macro"measure[4]"
{
run("Measure");
}
Select laminin mask
macro"analyse[5]"
{
run("Analyze Particles...", "size=25-infinity pixel show=Masks clear add in_situ");
roiManager("Show All without labels");
run("Create Selection");
}
Measure ICAM
```

```
macro"measure[4]"
{
run("Measure");
}
macro"Merge channels for count[6]"
{
run("Stack to Images");
run("Color Balance...");
selectWindow("ICAM"); run("Cyan"); run("Color Balance..."); setMinAndMax(0, 30);
selectWindow("GFAP"); run("Green"); run("Color Balance..."); setMinAndMax(0, 104);
selectWindow("laminin"); run("Magenta"); run("Color Balance..."); setMinAndMax(10, 154);
selectWindow("DAPI"); run("Blue"); run("Color Balance..."); setMinAndMax(20, 240);
run("Merge Channels...", "c2=GFAP c3=DAPI c5=ICAM c6=laminin create");
run("Channels Tool..."); Stack.setActiveChannels("0011");
run("Cell Counter");
}
```

A.3.4 RECA-1-associated GFAP

Relevant to Section 4.3.4.2

```
macro"split + threshold[1]"
{
run("Set Scale...", "distance=102 known=100 pixel=1 unit=um global"); title1 =getTitle();
run("Split Channels");
selectWindow(title1+" (blue)"); rename("DAPI");
selectWindow(title1+" (red)"); rename("GFAP");
selectWindow(title1+" (green)"); rename("RECA1");
selectWindow("RECA1"); run("Threshold..."); setThreshold(54, 255);
setOption("BlackBackground", false); run("Convert to Mask");
selectWindow("GFAP"); run("Duplicate...", " ");
```

```
selectWindow("GFAP"); run("Threshold...");
setThreshold(45, 255); setOption("BlackBackground", false); run("Convert to Mask");
run("Analyze Particles...", "size=5-25000 pixel show=Masks clear add in_situ"); setOption("BlackBackground", false);
roiManager("Show None"); run("Convert to Mask");
run("Images to Stack", "name=daphne title=[] use");
setTool("freehand");
}
Select DH, measure GFAP
macro"measure[2]"
{
run("Measure");
}
Select RECA1 mask
macro"analyse[3]"
{
run("Analyze Particles...", "size=5-25000 pixel show=Masks clear add in_situ");
setOption("BlackBackground", false);
run("Create Selection");
roiManager("Show All without labels");
}
Create RECA1 Selection
macro"create selection[4]"
{
run("Create Selection");
}
measure GFAP
macro"measure[2]"
{
```

```
run(”Measure”);
}
macro”GFAP particle analysis and extraction[5]”
{
run(”Stack to Images”);
selectWindow(”RECA1”); run(”Convert to Mask”);
selectWindow(”GFAP”); run(”Convert to Mask”);
run(”Binary Feature Extractor”, ”objects=[GFAP] selector=[RECA1] object_overlap=0 count”);
run(”Invert LUT”);
run(”Images to Stack”, ”name=daphne title=[] use”);
}
macro”create selection[4]”
{
run(”Create Selection”);
}
macro”measure[2]”
{
run(”Measure”);
}
```

A.3.5 RECA-1-associated ZEB1

Relevant to Section 4.3.4.3

```
macro”threshold ZEB1[1]”
{
run(”Set Scale...”, ”distance=102 known=100 pixel=1 unit=um global”);
run(”8-bit”); rename(”ZEB1”);
run(”Duplicate...”, ” ”);
run(”Threshold...”); setThreshold(53, 255); setOption(”BlackBackground”, false);
run(”Convert to Mask”);
```

```
run(”Analyze Particles...”, ”size=5-25000 pixel show=Masks clear add in_situ”);
setOption(”BlackBackground”, false);
roiManager(”Show None”);
run(”Convert to Mask”);
}
macro”split + threshold[2]”
{
title1 =getTitle(); run(”Split Channels”);
selectWindow(title1+” (blue)”); rename(”DAPI”);
selectWindow(title1+” (red)”); rename(”GFAP”);
selectWindow(title1+” (green)”); rename(”RECA1”);
selectWindow(”GFAP”); close();
selectWindow(”RECA1”); run(”Threshold...”); setThreshold(54, 255);
setOption(”BlackBackground”, false); run(”Convert to Mask”);
run(”Images to Stack”, ”name=daphne title=[] use”);
setTool(”freehand”);
}
Select DH, measure ZEB1
macro”measure[3]”
{
run(”Measure”);
}
Select RECA1 mask
macro”analyse[4]”
{
run(”Analyze Particles...”, ”size=5-25000 pixel show=Masks clear add in_situ”);
setOption(”BlackBackground”, false);
run(”Create Selection”);
```

```
roiManager(”Show All without labels”);
}
Create RECA1 Selection
macro”create selection[6]”
{
run(”Create Selection”);
}
measure ZEB1 macro”measure[3]”
{
run(”Measure”);
}
macro”ZEB1-RECA1 particle analysis and extraction[5]”
{
run(”Stack to Images”); selectWindow(”RECA1”);
run(”Convert to Mask”); selectWindow(”ZEB1-1”); run(”Convert to Mask”);
run(”Binary Feature Extractor”, ”objects=[ZEB1-1] selector=[RECA1] object_overlap=0
count”);
run(”Images to Stack”, ”name=elly title=[] use”); run(”Invert LUT”);
}
macro”create selection[6]”
{ run(”Create Selection”); }
macro”measure[3]”
{
run(”Measure”);
}
```

A.3.6 RECA-1-associated ZEB1 Nuclei

Relevant to Section 4.3.4.3

```
macro”threshold ZEB1[1]”
```

```
{
run("Set Scale...", "distance=102 known=100 pixel=1 unit=um global");
run("8-bit"); rename("ZEB1"); run("Duplicate...", " ");
run("Threshold..."); setThreshold(53, 255);setOption("BlackBackground", false);
run("Convert to Mask");
run("Analyze Particles...", "size=5-25000 pixel show=Masks clear add in_situ");
setOption("BlackBackground", false);
roiManager("Show None"); run("Convert to Mask");
}
macro"split + threshold[2]"
{
title1 =getTitle();
run("Split Channels");
selectWindow(title1+" (blue)"); rename("DAPI");
selectWindow(title1+" (red)"); rename("GFAP");
selectWindow(title1+" (green)"); rename("RECA1");
selectWindow("GFAP"); close();
selectWindow("RECA1"); run("Threshold...");
setThreshold(54, 255);
setOption("BlackBackground", false);
run("Convert to Mask");
selectWindow("DAPI"); run("Threshold..."); setThreshold(121, 255);
run("Convert to Mask"); setTool("freehand");
selectWindow("DAPI");
run("Analyze Particles...", "size=25-infinity pixel show=Masks clear add in_situ");
roiManager("Show All without labels");
run("Binary Feature Extractor", "objects=[ZEB1-1] selector=[DAPI] object_overlap=30
count");
run("Invert LUT");
```

```
run(”Images to Stack”, ”name=daphne title=[] use”); setTool(”freehand”);
}
Select DH vessels
macro”analyse[3]”
{
run(”Analyze Particles...”, ”size=5-25000 pixel show=Masks clear add in_situ”);
setOption(”BlackBackground”, false);
run(”Create Selection”);
roiManager(”Show All without labels”);
run(”Stack to Images”);
selectWindow(”RECA1”); run(”Convert to Mask”);
selectWindow(”Extracted_ZEB1-1”); run(”Convert to Mask”);
run(”Binary Feature Extractor”, ”objects=[Extracted_ZEB1-1] selector=[RECA1] object_overlap=0
count”);
run(”Images to Stack”, ”name=elly title=[] use”);
run(”Invert LUT”);
}
macro”create selection[4]”
{
run(”Create Selection”);
}
macro”measure[5]”
{
run(”Measure”);
}
```

A.3.7 Cell Coverage

A.3.7.1 p4 HBMECs: Phalloidin-488

Relevant to Section 5.5

```
macro ”Split [1]” {

run(”Set Scale...”, ”distance=100 known=100 pixel=1 unit=um”);title1 =getTitle();

run(”RGB Split”);

selectWindow(title1+” (blue)”);

close();

selectWindow(title1+” (green)”);

run(”Threshold...”); setThreshold(21, 255); setOption(”BlackBackground”, false); run(”Convert to Mask”);selectWindow(title1+” (red)”); close();

}

macro ”Measure Area [2]”  run(”Set Measurements...”, ”area area_fraction redirect=None decimal=3”); run(”Measure”);
```